Petrology and Stratigraphy of the White Rock Formation, Yarmouth Area, Nova Scotia

by

Lisa A. MacDonald
B.A. (Hons.) Dalhousie University
B.Sc. Dalhousie University

Thesis
submitted in partial fulfillment of the requirements for
the Degree of Master of Science (Geology)

Acadia University
Fall Convocation 2000

Table of Contents

List of Figures.....ix

List of Tables.....xiii

List of Plates.....xiv

Acknowledgments.....xvi

Abstract.....xviii

Chapter 1 Introduction

Introduction.....1

Purpose of Study.....1

Location and Access.....3

Previous Work.....4

1.4.1. Lithology and Stratigraphy.....4

1.4.2. Structure and Metamorphism.....5

1.4.3. Geochemistry.....6

1.4.4. Age.....7

1.4.5. Brenton Pluton.....8

Chapter 2 Field Relations and Stratigraphy

2.1. Introduction.....9

2.2. Goldenville Formation.....11

2.3. Halifax Formation.....11

2.4. White Rock Formation.....12

2.4.1. Unit S_{WRss}.....12

2.4.2. Unit S_{WRqt}.....15

2.4.3. Unit S_{WRsv}.....15

2.4.4. Unit S_{WRmf}.....17

2.4.5. Unit S_{WRft}.....27

Bear Island Area.....31

Inner False Harbour.....33

Outer False Harbour.....34

Government Brook.....35

Sunday Point.....35

Other Outcrops of unit S_{WRft}.....40

2.4.6. Unit S_{WRmt}.....40

2.4.7. Unit S_{WRmv}.....55

2.5. Mafic Sills and Dykes.....56

2.6. Brenton Pluton.....57

Chapter 3 Petrography

3.1. Introduction.....60

3.2. White Rock Formation.....60

3.2.1. Metasedimentary Rocks.....60

3.2.2. Mafic Flows.....68

3.2.3. Mafic Tuff.....78

3.2.4. Mafic Lithic Tuff.....80

3.2.5. Amphibolite.....81

3.2.6. Intermediate Flows.....83

3.2.7. Mafic and Intermediate Crystal Tuff.....85

3.2.8. Felsic Crystal Tuff.....88

3.3. Mafic Dykes and Sills.....91

3.4. Brenton Pluton.....99

3.5. Metamorphism and Deformation.....101

Chapter 4 Geochemistry and Age

4.1. Introduction.....106

4.2. Effects of Alteration and Metamorphism.....107

4.3. Major Element Goechemistry.....112

4.3.1. Mafic Volcanic Rocks.....112

4.3.2. Intermediate and Felsic Volcanic Rocks.....115

4.3.3. Mafic Dykes and Sills.....116

4.3.4. Brenton Pluton.....116

4.4. Trace Element Geochemistry.....117

4.4.1. Mafic Volcanic Rocks.....117

4.4.2. Intermediate and Felsic Volcanic Rocks.....122

4.4.3. Mafic Dykes and Sills.....123

4.4.4. Brenton Pluton.....123

4.5. Rare Earth Element Geochemistry.....123

4.5.1. Mafic Volcanic Rocks.....123

4.5.2. Felsic Crystal Tuff.....125

4.5.3. Mafic Sills.....125

4.5.4. Brenton Pluton.....128

4.6. Chemical Affinity and Tectonic Setting.....128

4.6.1. Mafic Volcanic Rocks.....128

4.6.2. Intermediate and Felsic Volcanic Rocks.....136

4.6.3. Mafic Dykes and Sills.....136

4.6.4. Brenton Pluton.....140

4.7. U-Pb Age of Felsic Crystal Tuff in the White Rock Formation 140

4.8. Sm/Nd Isotopic Data.....143

4.9. Petrogenesis.....143

4.9.1. Mafic Volcanic Rocks.....143

4.9.2. Felsic Volcanic Rocks.....147

4.9.3. Mafic Dykes and Sills.....149

4.9.4. Brenton Pluton.....150

Chapter 5 Discussion

5.1. Introduction.....151

5.2. Comparison with Previous Work in Yarmouth Area.....151

5.2.1. Age of the White Rock Formation and Brenton Pluton.....151

5.2.2. Stratigraphic and Structural Interpretations.....152

5.2.3. Geochemistry of the White Rock Formation.....157

5.2.4. Geochemistry of the Brenton Pluton.....167

5.3. Comparison of the Yarmouth Area with Other Areas of the White Rock Formation.....169

5.3.1. Stratigraphy.....169

5.3.2. Comparison with Other Stratigraphic Interpretations.....173

5.3.3. Geochemical Comparisons.....176

5.4. Regional Comparisons.....188

5.4.1. Arisaig Group.....188

5.5. Regional Implications.....198

Chapter 6 Conclusions.....201

References.....205

Appendix A. Petrographic Descriptions.....211

Appendix B. Microprobe Analysis.....235

Appendix C. Major and Trace element Geochemistry.....252

Appendix D. Rare Earth Element Geochemistry.....262

Appendix E. Sm/Nd Isotopic Analysis.....264

List of Figures

1.1. Simplified geological map of the Meguma terrane.....2

1.2. Previous stratigraphic interpretations of the White Rock Formation.....(In pocket)

2.1. Geological map of the Yarmouth area.....(In pocket)

2.2. Second derivative aeromagnetic map with map units.....10

2.3. Generalized stratigraphic column.....(In pocket)

2.4. Distribution of lithologies on Cape Forchu West.....21

2.5. Distribution of lithologies on Sunday Point.....36

2.6. Distribution of lithologies on Cape Forchu.....43

3.1. Thin section and geochemical sample location map.....(In pocket)

3.2. Composition of garnet in slate and mafic dykes.....63

3.3. Composition of feldspar in metavolcanic samples.....69

3.4. Composition of amphibole in mafic volcanic rocks and dykes.....71

3.5. Composition of biotite in mafic samples.....73

4.1. Plots of SiO_2, CaO, Na_2O, and K_2O against Nb.....109

4.2. Plots of Rb, Sr, TiO_2 and Zr against Nb, V against TiO_2 and Y against Zr.....110

4.3. Samples from the study area plotted on the igneous spectrum.....111

4.4. Major element variation diagram.....113

4.5. Trace element variation diagram.....118

4.6. Chondrite-normalized REE diagram for mafic flow samples from the White Rock Formation and East African Rift.....124

4.7. Chondrite-normalized REE diagram for a felsic crystal tuff from the White Rock Formation, a granite sample from the Brenton Pluton and felsic samples from the East African Rift.....126

4.8. Chondrite-normalized REE diagram for mafic dyke samples from the White Rock Formation and mafic samples from the East African Rift.....127

4.9. Zr/TiO_2 vs. Nb/Y diagram showing chemical affinities.....129

4.10. Zr-Ti-Y ternary discrimination diagram for mafic samples.....131

4.11. Th-Hf-Ta ternary discrimination diagram for mafic flows and dykes.....132

4.12. Zr-Nb-Y ternary discrimination diagram for mafic samples.....133

4.13. V vs. Ti discrimination diagram for mafic samples.....134

4.14. N-MORB-normalized spider diagrams for mafic flow and sill samples compared to average within-plate alkalic and tholeiitic samples and with mafic samples from the East African Rift.....135

4.15. Rb vs. Y+Nb and Nb vs. Y discrimination diagrams for felsic rocks.....137

4.16. Zr vs. Ga/Al discrimination diagram for felsic rocks.....138

4.17. Y-Nb-Ga*3 ternary diagram for granitoid rocks.....139

4.18. ANK vs. ACNK discrimination diagram for felsic rocks.....141

4.19. Concordia diagram for felsic crystal tuff sample 4-1.....142

4.20. εNd diagram for felsic crystal tuff sample 4-1.....144

4.21. Plots of Ni, Cr, and TiO_2 against FeO^t/MgO for the mafic samples.....146

4.22. Incompatible element plots.....148

5.1. Major element variation diagrams for the White Rock Formation and the Brenton Pluton, comparing data from this study to those of Sarkar

(1978) and O'Reilly (1976).....160

5.2. Trace element variation diagrams for the White Rock Formation and the Brenton Pluton, comparing data from the present to those of Sarkar (1978) and O'Reilly (1976).....162

5.3. Discrimination diagrams for mafic samples from the White Rock Formation comparing data from the present study to those of Sarkar (1978).....164

5.4. Discrimination diagrams for felsic samples of the White Rock Formation and Brenton Pluton comparing data from the present study to those of Sarkar (1978).....165

5.5. Chondrite-normalized REE plots for mafic samples from the White Rock Formation comparing data from the present study to those of Sarkar (1978)....166

5.6. Chondrite-normalized REE plots for felsic samples from the White Rock Formation and Brenton Pluton comparing data from the present study to those of Sarkar (1978).....168

5.7. Correlation of the stratigraphy from the Yarmouth area to the Black River Area.....171

5.8. Geochemical comparison of volcanic rocks in the White Rock and New Canaan formations.....177

5.9. Plots of incompatible elements in samples from the White Rock and New Canaan formations.....178

5.10. Major element variation diagrams for samples from the Yarmouth, Cape St. Mary and Torbrook areas.....179

5.11. Trace element variation diagrams for samples from the Yarmouth area,

Cape St. Mary and Torbrook areas.....181

5.12. Chondrite-normalized REE diagrams for mafic and felsic samples from the Yarmouth, Cape St. Mary areas.....184

5.13. Chondrite-normalized REE diagrams for mafic and felsic samples from the Yarmouth, Cape St. Mary and Torbrook areas.....185

5.14. Incompatible element plots for samples from the Yarmouth, Cape St. Mary and Torbrook areas.....186

5.15. Major element variation diagrams for samples from the White Rock Formation and Arisaig Group.....189

5.16. Trace element variation diagrams for samples from the White Rock Formation and Arisaig Group.....192

5.17. Chondrite-normalized REE diagrams for mafic and felsic samples from the study area, Bear Brook Formation, Beechill Cove Formation, and Arisaig Group.....194

5.18. Incompatible element ratios in samples from the White Rock Formation and Arisaig Group.....196

List of Tables

5.1. Correlation of units of Hwang (1985) with units of this study.....158

5.2. Sm/Nd isotopic data for samples from the White Rock Formation and Arisaig Group.....197

List of Plates

2.1. Crenulation cleavage in the Halifax Formation.....13

2.2. Boudinaged metasedimentary and metavolcanic layers in unit S_{WRmf}.....19

2.3. Bomb and lapilli-size clasts in mafic tuff.....22

2.4. Banded amphibole-rich mafic tuff and tuffaceous sandstone.....23

2.5. Alteration of mafic tuff.....25

2.6. Flow-top brecciation in a mafic flow.....26

2.7. Comglomerate layer at Cape Forchu West.....28

2.8. Conglomerate clast with amphibole-rich rim.....29

2.9. Mafic tuff and tuffaceous sandstone.....30

2.10. Intermediate crystal tuff with basaltic inclusions.....38

2.11. Intermediate crystal tuff with a clast of tuffaceous sandstone.....39

2.12. Laminated mafic tuff at Cape Forchu.....45

2.13. Bombs in mafic tuff at Cape Forchu.....46

2.14. Pseudotachylite in mafic tuff at Cape Forchu.....47

2.15a. Possible basalt pillows at Cape Forchu.....48

2.15b. Possible basalt pillows at Cape Forchu.....49

2.16a. Interbedded tuffaceous sandstone, amphibole-rich mafic tuff and mafic lapilli tuff.....52

2.16b. Interbedded tuffaceous sandstone, amphibole-rich mafic tuff and mafic lapilli tuff.....53

2.17. Amphibole-rich rim and core of a mafic bomb.....54

2.18. Mafic dyke intruding laminated mafic tuff.....58

3.1. Photomicrograph of chloritoid porphyroblasts in slate.....62

3.2. Photomicrograph of poikiloblastic garnet with aligned inclusions in schist.....64

3.3. Photomicrograph of staurolite porphyroblast with aligned inclusions.....66

3.4. Photomicrograph of biotite-epidote rich layer between quartz-feldspar-epidote layers in tuffaceous sandstone.....67

3.5. Photomicrograph of acicular amphibole texture and relict plagioclase grain.....74

3.6. Photomicrograph of bladed amphibole texture in mafic flow sample 84-1.....76

3.7. Photomicrograph of sheaf amphibole texture in mafic flow sample 75-4.....77

3.8. Photomicrograph of amphibole-rich lithic fragments.....82

3.9. Photomicrograph of intermediate flow sample 125-1.....84

3.10. Photomicrograph of fine-grained matrix deflected around a relict plagioclase grain in intermediate crystal tuff sample 11-1.....86

3.11. Photomicrograph of a relict grain with embayed grain boundaries and subidioblastic bladed amphibole.....87

3.12. Photomicrograph of felsic crystal tuff.....89

3.13. Photomicrograph of felsic crystal tuff sample 4-1.....90

3.14. Photomicrograph of granophyric texture in sample 209-1.....92

3.15. Photomicrograph of bladed amphibole in dyke sample 198-1.....93

3.16. Photomicrograph of sheaf texture of amphibole in dyke sample 200-1.....94

3.17. Photomicrograph of tabular texture of amphibole in dyke sample 202-1.....95

3.18. Photomicrograph of acicular amphibole texture in dyke sample 94-1.....96

3.19. Photomicrograph showing sutured texture in granite sample 161D-1.....100

ACKNOWLEDGMENTS

Many people have contributed to this project in invaluable ways and I wish to thank them for their efforts. I am grateful to Dr. Sandra Barr for her patient guidance, encouragement and support during the last two years. Thank you to Dr. Chris White and the Nova Scotia Department of Natural Resources for their interest and partial funding of this project. Many thanks to Jo Price for assistance in preparing the samples, her friendly advice and warm empathy. Special thanks to Miranda Huskins for her constant support and friendship, and her time and effort in assisting with the production of this thesis. Lastly, I would like to thank my parents and Pradeep. Without their love, patience and unwavering support this thesis would not have been completed.

To Dr. Paul Schenk
who always encouraged me to see "the big picture"

Abstract

The White Rock Formation in the Yarmouth area occurs in a faulted synclinal structure underlain by the Halifax Formation. The formation is divided into 7 stratigraphic units based on field mapping, petrographic study and published geophysical maps. All units are commonly intruded by mafic dykes and/or sills that also occur in the adjacent Halifax Formation. Metamorphic grade is greenschist to amphibolite facies. The Brenton Pluton occurs on the eastern limb of the syncline and appears to be in faulted contact with the basal unit of the White Rock Formation on the west and slate of the Halifax Formation on the east.

The chemistry of mafic volcanic rocks indicates an alkalic affinity and a within plate tectonic setting. The felsic volcanic rocks are chemically similar to the Brenton Pluton and both have characteristics of within-plate A-type granites. The mafic volcanic rocks are comagmatic with the mafic dykes and sills and with the felsic rocks, but Sm-Nd data (εNd +1.37) indicate a crustal influence in the felsic rocks. Volcanic rocks in the Yarmouth area are chemically similar to those elsewhere in the White Rock Formation.

A felsic tuff from near the top of the formation yields a U-Pb age of 438 +3/-2 Ma, which supports an Early Silurian age for the formation and provides a constraint for stratigraphic correlation with other areas in western Nova Scotia. A regional geochemical comparison with the Arisaig Group indicates similar tectonic settings but chemically different sources.

The geochemistry of the White Rock Formation and Brenton Pluton indicate a continental extensional environment in the Meguma terrane during the Silurian.

Chapter 1 Introduction

1.1. Introduction

Igneous activity was widespread in the northern Appalachian orogen during the Silurian (e.g. Dunning et al., 1990; Barr and Jamieson, 1991; Bevier and Whalen, 1990). Both volcanic and plutonic activity occurred, as well as deposition of associated sedimentary rocks, as exemplified by the White Rock Formation and the spatially associated Brenton Pluton of southern Nova Scotia. These units are components of the Meguma terrane (Fig. 1.1).

The White Rock Formation consists of metasedimentary and metavolcanic rocks preserved in northeast-trending synclines from the Wolfville area southwest to Yarmouth. The formation is underlain by the Cambrian-Ordovician Goldenville and Halifax formations and overlain by the Silurian-Devonian Kentville, New Canaan and Torbrook formations (Taylor, 1965; Taylor, 1967; Keppie, 2000). The Brenton Pluton is in contact with the White Rock and Halifax formations on the eastern limb of the Yarmouth syncline (Fig.1.1).

1.2. Purpose of Study

Previous work on the White Rock Formation showed the complexity of the stratigraphy and wide variety of lithologies present (Taylor, 1965; Lane, 1979; Schenk, 1995). However many aspects of the formation in the Yarmouth area required further study. The stratigraphy was uncertain, and the nature of contacts with adjacent units was

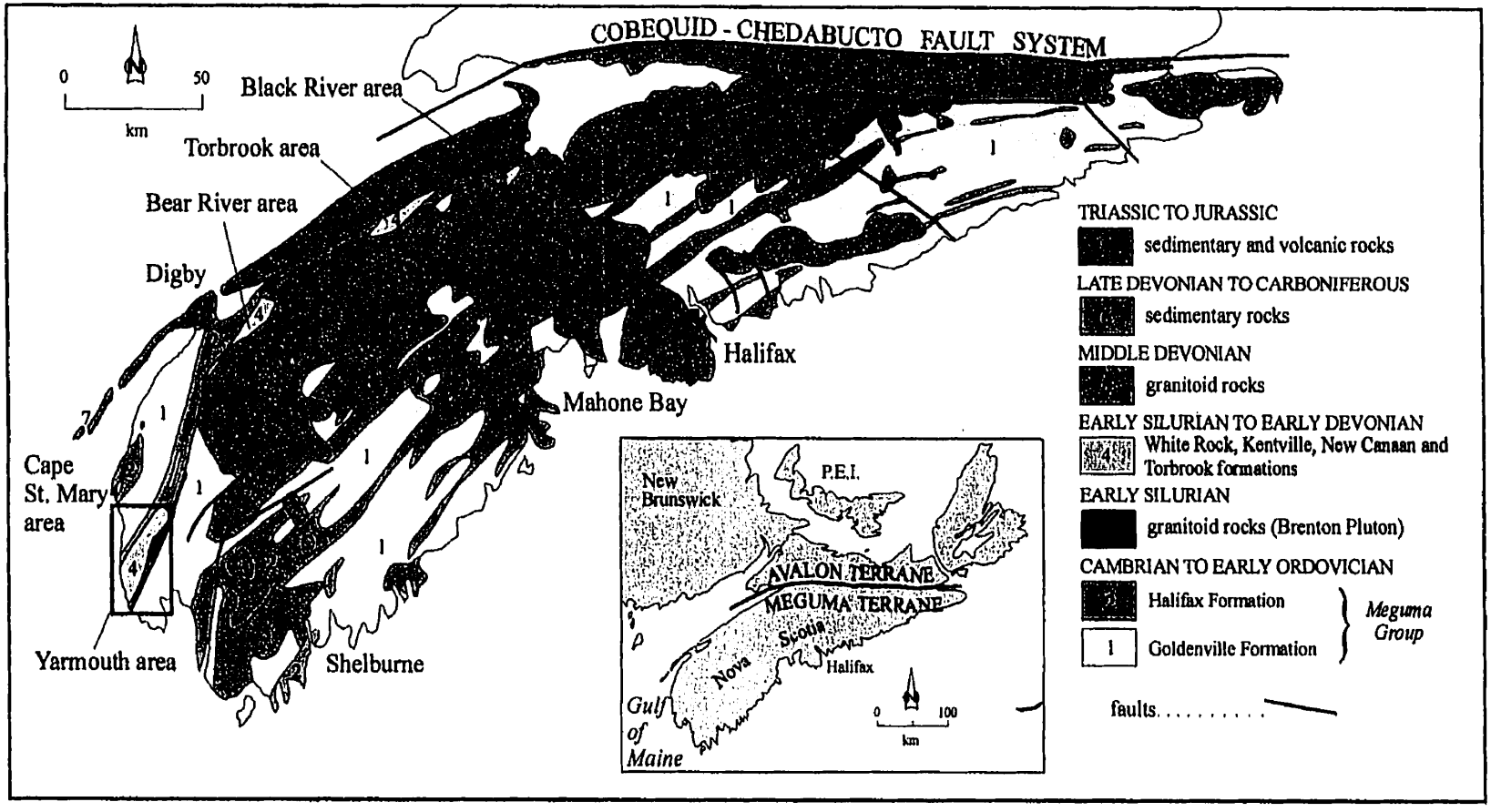

Figure 1.1. Simplified geological map of the Meguma terrane showing the location of the study area (box) and other areas of the White Rock Formation.

not well defined (Taylor, 1965; Taylor, 1967; Lane, 1979; Hwang, 1985; Schenk, 1995). Petrochemical studies of the volcanic rocks which dominate the formation in the Yarmouth area yielded inconclusive results (Sarkar, 1978) and the age of the volcanic rocks had not been constrained by reliable radiometric dating. The relationship of the spatially associated Brenton Pluton to the volcanic components of the White Rock Formation had not been assessed.

Hence, the present study was undertaken to provide new information about the White Rock Formation in the Yarmouth area through mapping and petrological investigations. It was the purpose of this project to (1) re-evaluate field relations and stratigraphy of the White Rock Formation in the Yarmouth area, (2) perform detailed petrological studies with emphasis on the volcanic rocks of the formation, (3) assess the petrogenetic relationship between the volcanic rocks and the granitic rocks of the Brenton Pluton, and (4) interpret the paleotectonic environment in which the White Rock Formation and Brenton Pluton originated.

1.3. Location and Access

The White Rock Formation in the Yarmouth area extends northeastward from the coast of the Gulf of Maine for a distance of approximately 35 km (Taylor, 1967; 1969), spanning NTS sheet 20O/16 and the southern part of 21B/1. An extensive network of roads and streams provide excellent access to the area. Exposure is generally good along the coast but is limited inland due to low topography and till cover.

1.4. Previous Work

1.4.1. Lithology and Stratigraphy

Previous maps which included parts of the White Rock Formation were produced by Crosby (1962), Smitheringale (1960; 1973), and Taylor (1965; 1967; 1969) as part of a series of Geological Survey of Canada papers and memoirs. These maps show the distribution of the White Rock Formation and preliminary lithological subdivisions (Fig. 1.2, in pocket). More detailed investigations of the White Rock Formation include Trapasso (1979) who studied the geology in the Torbrook area, Cullen et al. (1996) who also mapped the Torbrook area and subdivided the formation into units (Fig. 1.2, in pocket), White et al. (1998) who re-mapped the Bear River area, and Lane (1979) who interpreted the stratigraphy from the Black River area to Yarmouth (Fig. 1.1) (Fig. 1.2, in pocket). Lane (1979) subdivided the White Rock Formation into units and numerous lithostratigraphic facies. He also contributed to the understanding of the environment of deposition by interpreting the facies present as indicative of a shallow marine shelf.

Hwang (1985), as part of a dominantly structural study, re-interpreted the stratigraphy in the Yarmouth area. His interpretation inverted the stratigraphy compared to earlier studies by showing metavolcanic rocks overlain by metasedimentary rocks (Fig. 1.2, in pocket). Schenk (1995; 1997) elevated the White Rock Formation to group status and included it as part of the Annapolis Supergroup. The term White Rock Formation is retained in this study as the name White Rock Group is not broadly used. Schenk (1995) divided the White Rock Group into three formations, (from bottom to top) termed the Nictaux Volcanics, Fales River Formation and Deep Hollow Formation. He interpreted the White Rock Group as a predominantly metasedimentary package with a minor

Yarmouth area

Taylor, 1965
Chegoggin-Overton

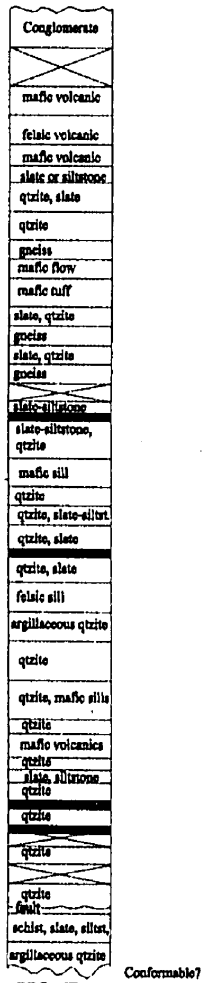

Hfx Fm

Cape St. Mary area

Taylor, 1965

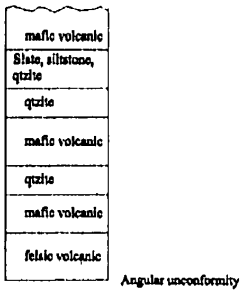

Hfx Fm

Bear River area

Taylor, 1965

Kentville Fm

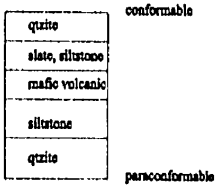

Hfx Fm

Torbrook area

Taylor, 1965

Kentville Fm

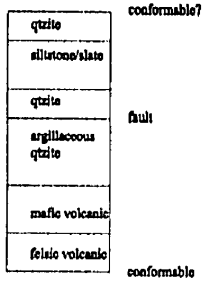

Hfx Fm

Black River area

Crosby, 1962
Kentville Fm

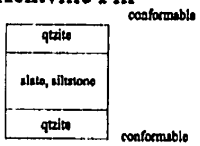

Hfx Fm

Taylor, 1965
same as Crosby

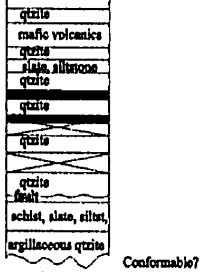

Hfx Fm

Lane, 1979

generalized section

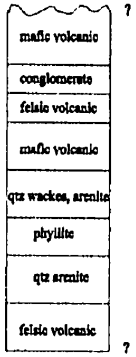

Hfx Fm

Lane, 1979

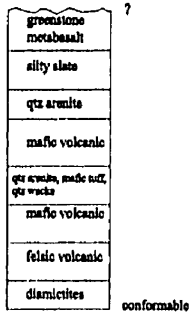

Hfx Fm

Lane, 1979

Kentville Fm ?

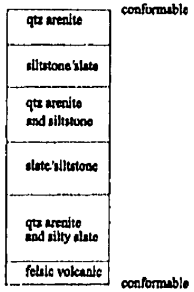

Hfx Fm

Lane, 1979

Kentville Fm

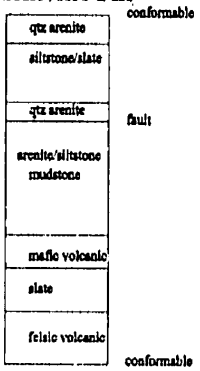

Hfx Fm

Lane, 1979

Kentville Fm

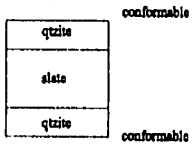

Hfx Fm

Hwang, 1985

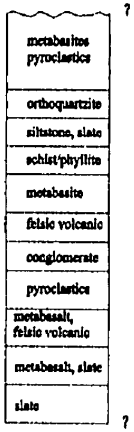

Hfx Fm

Sarkar, 1978

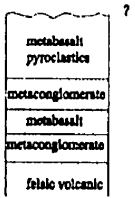

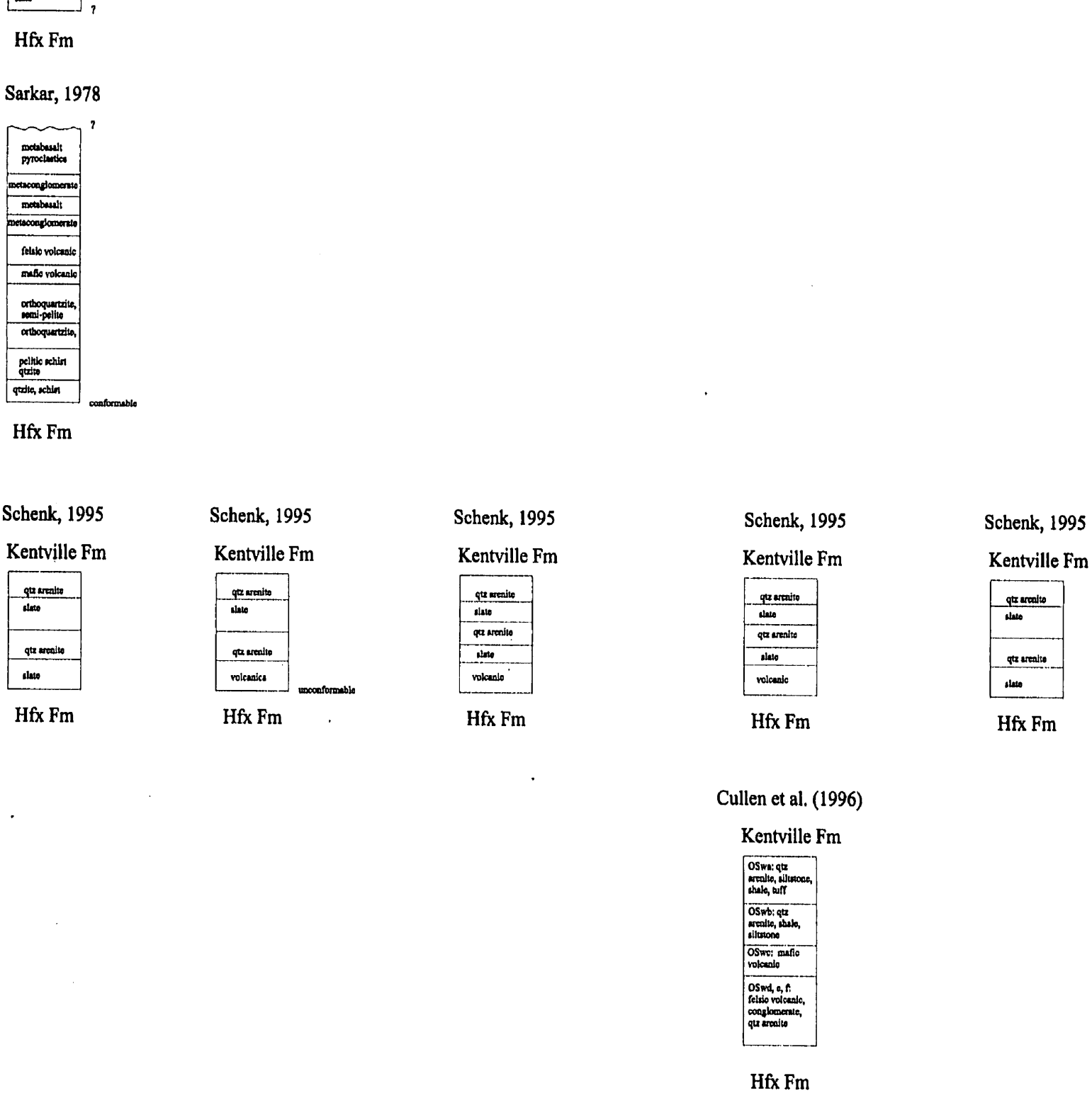

Figure 1.2. Previous interpretations of the stratigraphy of the White Rock Formation.

volcanic component near the base which could be correlated from the Black River area to the Yarmouth area (Fig. 1.2, in pocket).

1.4.2. Structure and Metamorphism

Hwang (1985) studied the structure in the Yarmouth area and reported mesoscale and minor scale asymmetric folds. He proposed that the main synclinal structure consists of two minor synclines separated by an anticline. According to Hwang (1985), deformation and metamorphism began with isoclinal folding during the Acadian orogeny. Superimposed on Acadian structures are dextral kink bands, indicating a post-Acadian (possibly Carboniferous) disturbance. This event was followed by the development of major, NNE-trending faults during the early Jurassic. Culshaw and Liesa (1997) interpreted the structure as a single syncline with shallow south-southwest plunge and northwest vergence. On the basis of deformational structures, they reported that shear zones lie along the limbs of the folds in the Yarmouth and Cape St. Mary areas and exhibit dip-slip displacement with local strike-slip movement. A shear zone on the west side of the core of the syncline was also reported and attributed to Acadian deformation. Culshaw and Liesa (1997) attributed the development of the shear zones on the limbs to a D2 deformational event that reactivated Acadian structures. Culshaw and Reynolds (1997), using the $^{40}Ar/^{39}Ar$ dating technique, suggested a Mid-Carboniferous (ca. 320 Ma) age for the D2 event.

Crosby (1962), Taylor (1967), Trapasso (1979), and White et al. (1998) described regional greenschist facies metamorphism in eastern parts of the White Rock Formation, and Culshaw and Liesa (1997) reported chlorite and biotite metamorphic zones in the

Cape St. Mary area. However, grade increases to garnet zone in the Yarmouth area (Culshaw and Liesa, 1997). Sarkar (1978) determined greenschist facies conditions on the southeastern limb of the Yarmouth syncline, increasing to amphibolite facies on the northwestern limb with pressures less than 3.5 kb and temperatures between 480-580°C. Hwang (1985) found that the metamorphic grade in the Yarmouth area ranges from lower greenschist facies to the transition zone between greenschist and amphibolite facies.

1.4.3. Geochemistry

Sarkar (1978) investigated the chemical character of the metavolcanic rocks in the Yarmouth area. He recognized two series, a mildly alkaline basalt-trachyte series, which is strongly differentiated, and a less voluminous olivine tholeiite-rhyolite series. Sarkar (1978) determined that the "parental" magmas for these series possibly evolved at different times from a non-depleted mantle source and involved fractionation of garnet. From the results of his geochemical study, Sarkar (1978) suggested that the volcanic rocks were erupted through a sialic basement in a failed continental rift and/or a distant back-arc setting related to subduction. Kendall (1981) analyzed the volcanic components of the White Rock Formation in the Cape St. Mary section and interpreted a similar chemical affinity and tectonic setting as Sarkar (1978). Keppie et al. (1997) confirmed alkalic-to-tholeiitic magmatic affinity and a within-plate, continental setting for volcanic components of the White Rock Formation in the Torbrook area.

1.4.4. Age

Taylor (1967) based the age of the White Rock Formation on stratigraphic position between the Lower Ordovician Halifax Formation and the Upper Silurian (Ludlow) Kentville and Pridolian New Canaan formations. Lane (1979) interpreted the formation to be approximately Late Ordovician (Ashgill) to Late Silurian in age, on the basis of underlying Late Ordovician glaciomarine deposits and Late Silurian and Early Devonian fossils found in the overlying New Canaan and Torbrook formations, respectively.

Schenk (1995) indicated that the age of the White Rock Group ranges from Early Ordovician to Middle Silurian, according to its stratigraphic position between the Tremodoc Halifax Group and Ludlow Kentville Group, but narrowed the estimate to Late Ordovician on the basis of event stratigraphy. Blaise et al. (1991) found upper Ludlow and lower Pridolian fauna in the upper part of the White Rock Formation in the Bear River area and Bouyx et al. (1997) found Wenlock-to- Pridolian fauna in the Kentville Formation (the lateral equivalent of the upper part of the White Rock Formation). Bouyx et al. (1997) placed the age of graptolites from the White Rock Formation in the Torbrook area between Llandovery and Wenlock. A U-Pb (zircon) age from rhyolite in the lower volcanic layer of the White Rock Formation in the Torbrook area is 442 +/- 4 Ma (J.D. Keppie, written comm. to Nova Scotia Department of Natural Resources, 1999), or latest Ordovician to earliest Silurian (Okulitch, 1999). The volcanic rocks in the White Rock Formation in the Yarmouth area have been presumed to be Upper Silurian (Lane, 1979).

1.4.5. Brenton Pluton

O'Reilly (1976) described the Brenton Pluton as lens-shaped with well-developed foliation parallel to the regional northeasterly structural trends. He showed that the composition is homogeneous and transitional between monzogranite and syenogranite. He also demonstrated that the pluton is chemically distinct from the South Mountain Batholith, highly silicic and potassic, and formed by crustal melting. He assumed that the pluton is Devonian and was emplaced syntectonically during the Acadian orogeny.

The cooling age of the Brenton Pluton was reported to be 325 +/- 9 Ma based on $^{40}Ar/^{39}Ar$ dating, and the age of emplacement was between 400 and 445 Ma (O'Reilly, 1976). Recent U-Pb dating of zircon showed that the igneous crystallization age of the pluton is 439 +4/-3 Ma, and U-Pb dating of monazite indicates a metamorphic age of 380 +/- 3 Ma (J.D. Keppie, written comm. to NSDNR, 1999).

1.4.5. Brenton Pluton

O'Reilly (1976) described the Brenton Pluton as lens-shaped with well-developed foliation parallel to the regional northeasterly structural trends. He showed that the composition is homogeneous and transitional between monzogranite and syenogranite. He also demonstrated that the pluton is chemically distinct from the South Mountain Batholith, highly silicic and potassic, and formed by crustal melting. He assumed that the pluton is Devonian and was emplaced syntectonically during the Acadian orogeny.

The cooling age of the Brenton Pluton was reported to be 325 +/- 9 Ma based on $^{40}Ar/^{39}Ar$ dating, and the age of emplacement was between 400 and 445 Ma (O'Reilly, 1976). Recent U-Pb dating of zircon showed that the igneous crystallization age of the pluton is 439 +4/-3 Ma, and U-Pb dating of monazite indicates a metamorphic age of 380 +/- 3 Ma (J.D. Keppie, written comm. to NSDNR, 1999).

Chapter 2 Field Relations and Stratigraphy

2.1. Introduction

The purpose of this chapter is to describe the rock types and their field relations observed in the Yarmouth area (Fig.2.1, in pocket), with emphasis on the White Rock Formation.

A wide range of lithologies is present in the White Rock Formation in the study area, and most, especially metavolcanic rock types, occur throughout the area and are not confined to specific units. Therefore, division of the formation into map units relied in part on characteristics displayed on second vertical derivative aeromagnetic maps (Fig. 2.2), as well as on field observations and petrographic features. The stratigraphically lowest units are predominantly metasedimentary (slate, metasandstone and quartzite). Mafic volcanic rocks including tuff and flows generally increase in abundance upward and become the dominant rock type in the formation. Felsic and intermediate volcanic rocks occur in the middle part of the formation and mafic tuff and flows with minor metasedimentary rocks occur near the top. Mafic dykes and sills are abundant throughout the stratigraphy. Lithological variations are summarized in a generalized stratigraphic column in Figure 2.3 (in pocket).

Original rock type is difficult to determine in some places due to the effects of greenschist- to amphibolite-facies metamorphism and deformation which have obliterated many of the sedimentary and volcanic features. Some macroscopic features such as layering, bombs and lapilli, clasts, and basalt pillows are still faintly apparent,

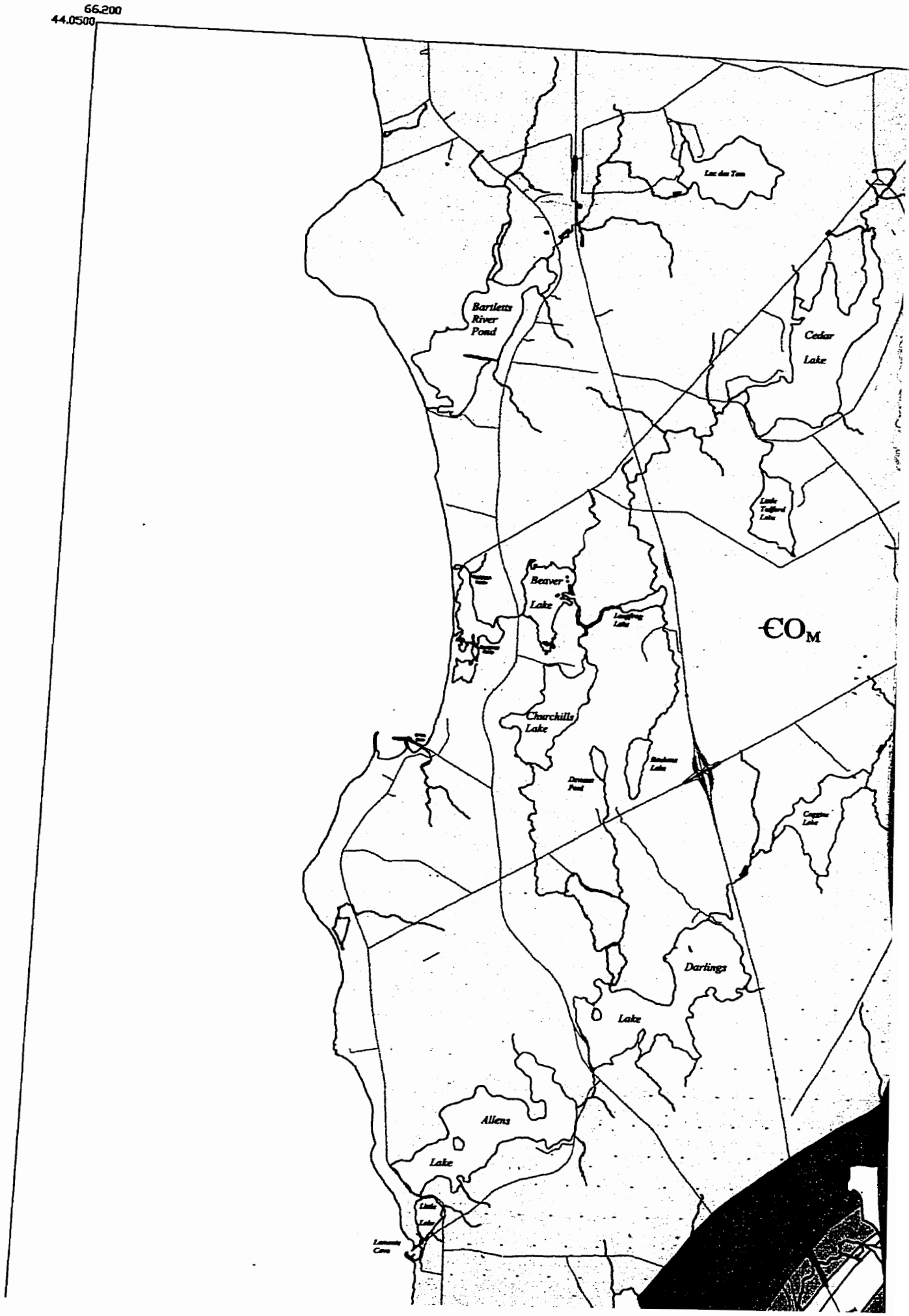
66.200
44.0500
Bartletts River Pond
Cedar Lake
Beaver Lake
Churchills Lake
Darlings Lake
Allens Lake

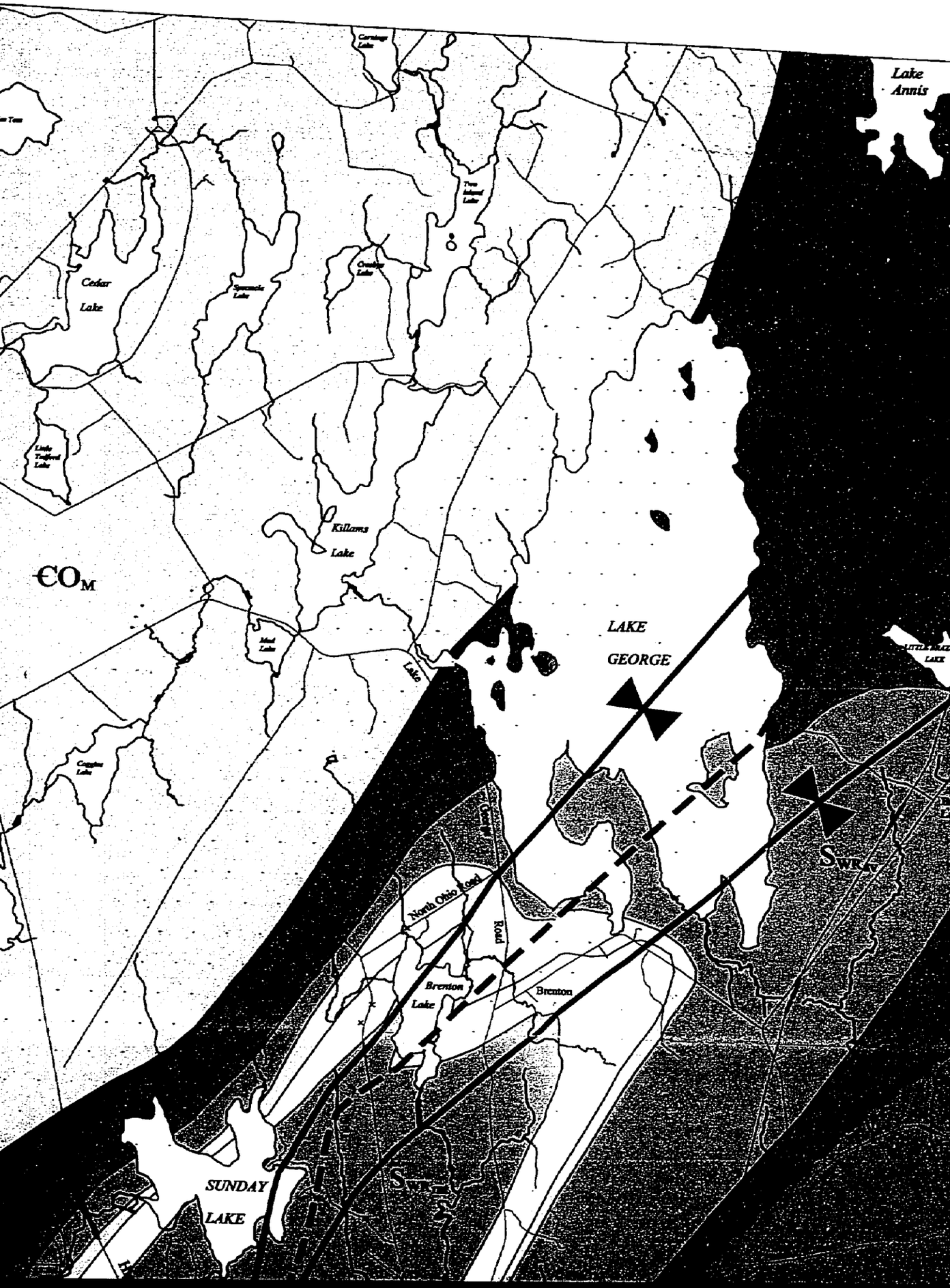
Lake
Annis
Cedar
Lake
Killams
Lake
LAKE
GEORGE
North Ohio Road
Brenton
Lake
Brenton
SUNDAY
LAKE


65.900
44.0500
Ogden Lake
Rounding Lake
Pickle Bay
Lake Fanning
BRAZIL LAKE
Pleasant Valley
Sloans
Lake
Raynards Lake
Hoopers Lake
Deerfield
Dam
88

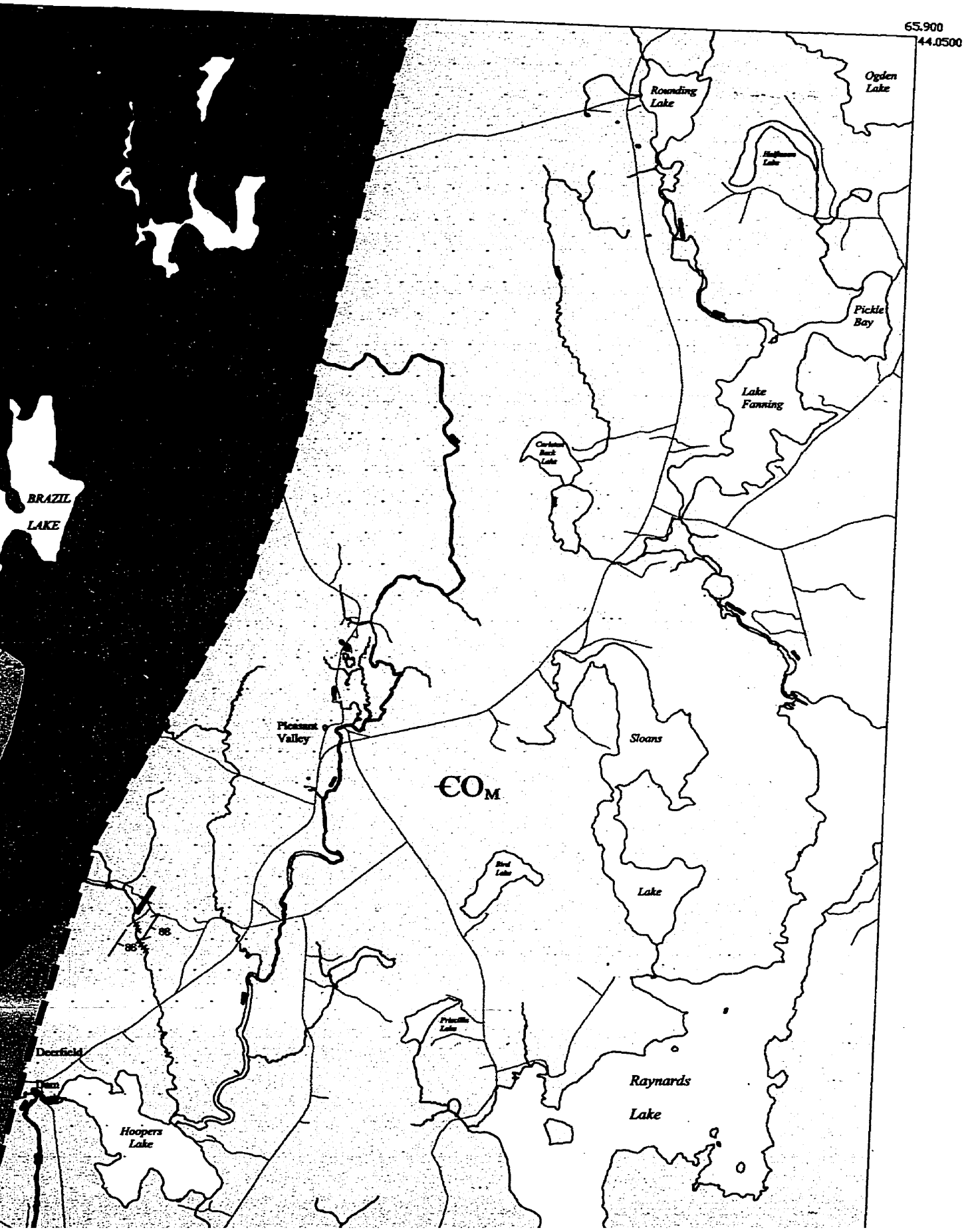
65.900
44.0500
Rounding Lake
Ogden Lake
Pickle Bay
Lake Fanning
BRAZIL LAKE
Pleasant Valley
Sloans
Lake
Raynards Lake
Hoopers Lake
Deerfield
Dam
88
88

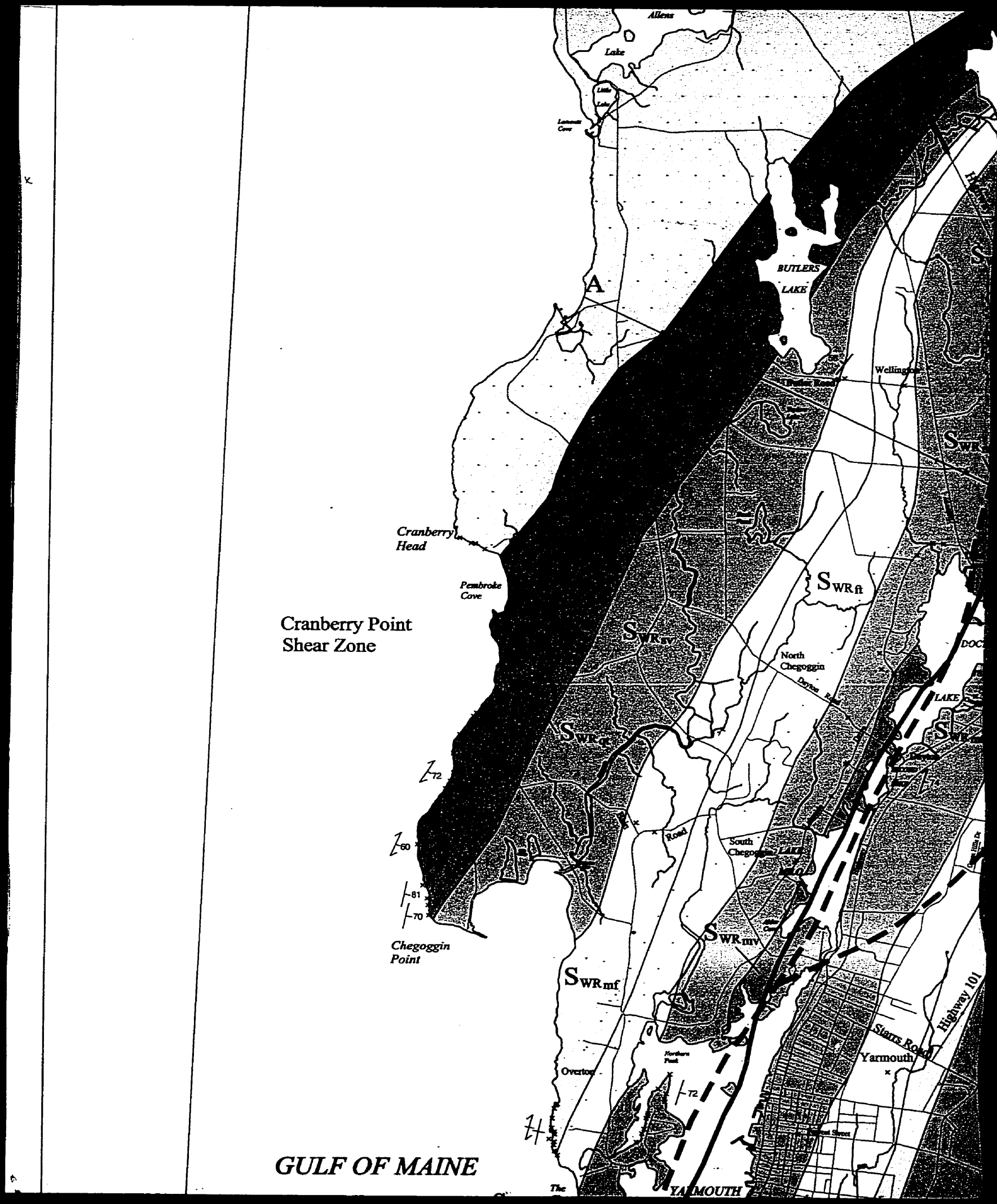
Allens
Lake
Little
Lake
Lennox
Cove
BUTLERS
LAKE
A
Wellington
Public Road
Cranberry
Head
Pembroke
Cove
Cranberry Point
Shear Zone
SWRtv
SWRft
SWRmv
SWRmf
North
Chegoggin
Dayton Rd
LAKE
72
60
81
70
Road
South
Chegoggin
LAKE
Chegoggin
Point
Highway 101
Stans Road
Yarmouth
Overton
Northern
Point
72
YARMOUTH
GULF OF MAINE


South Otto
BUNKERS LAKE
Exit 34
Highway 340
Agard Lake
Salmon
Lake
Greenville
Churchills Mill Lake
Trefry Lake

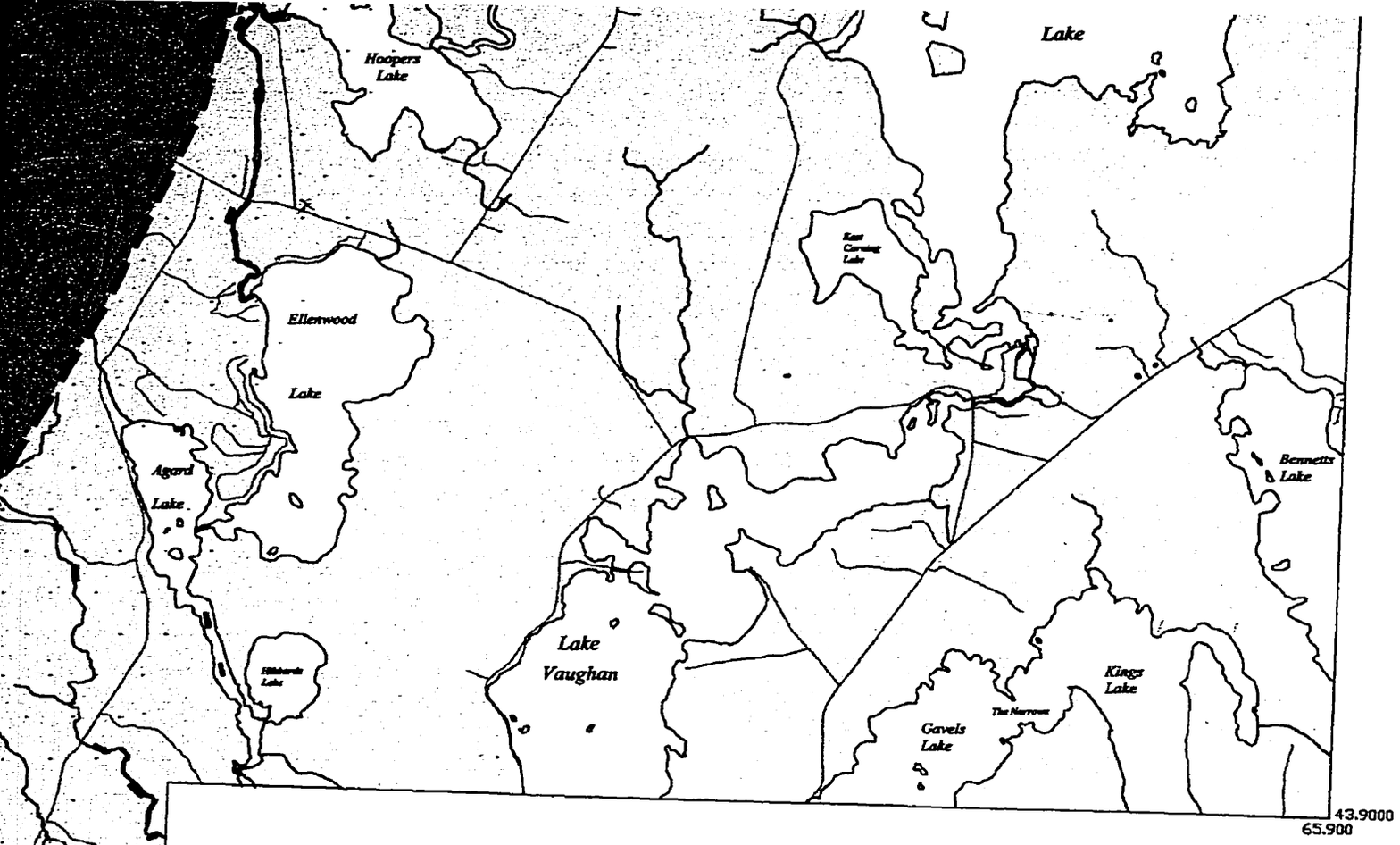

Figure 2.1. Geological map of the Yarmouth area.

LEGEND

SILURIAN

Brenton Pluton

Medium grained, foliated syenogranite to monzogranite.

White Rock Formation

Predominantly mafic tuff and mafic flows.

Mafic tuff interbedded with mafic lithic tuff, conglomerate and tuffaceous sandston

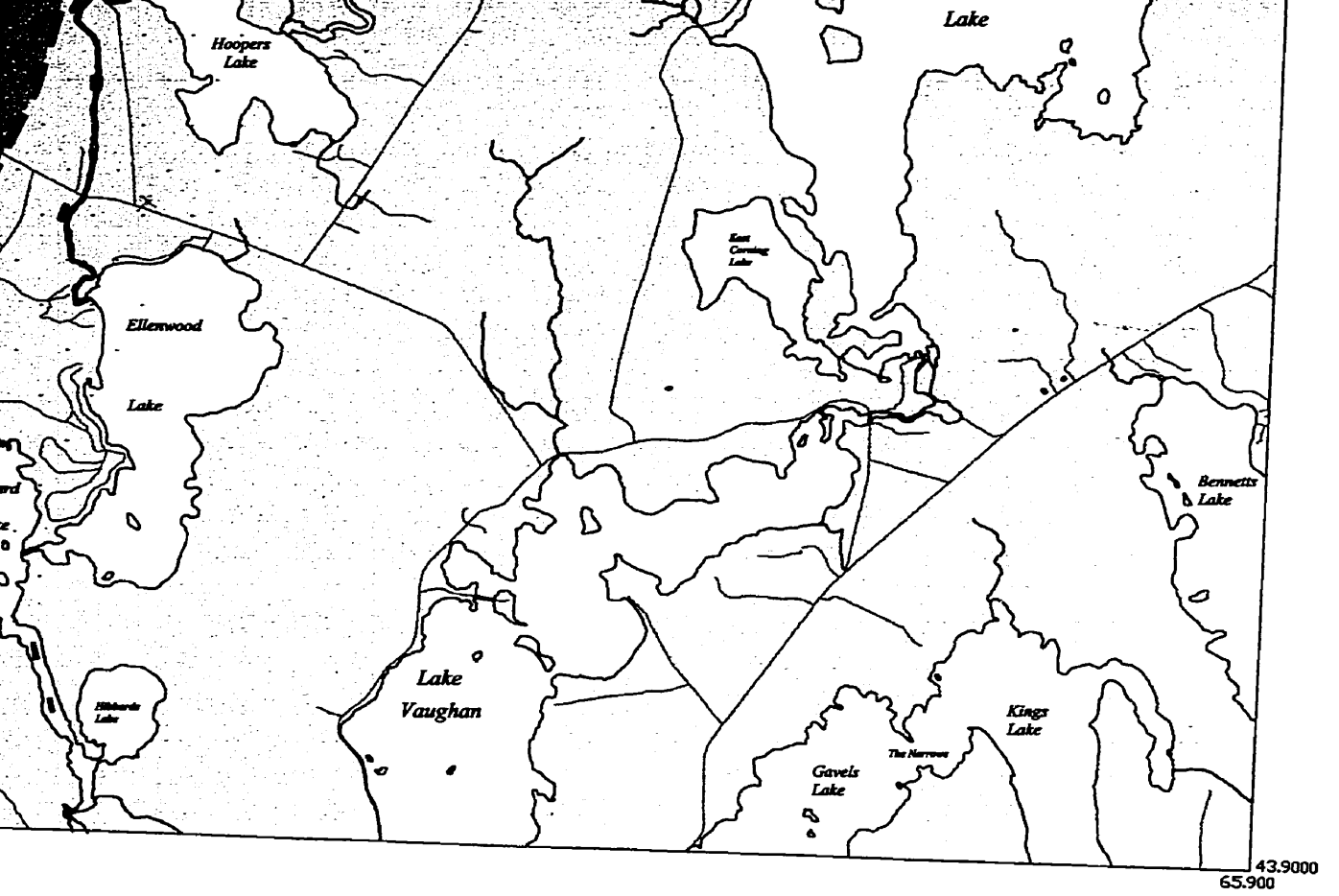

Figure 2.1. Geological map of the Yarmouth area.

LEGEND

SILURIAN

Brenton Pluton

Medium grained, foliated syenogranite to monzogranite.

White Rock Formation

Predominantly mafic tuff and mafic flows.

Mafic tuff interbedded with mafic lithic tuff, conglomerate and tuffaceous sandstone near the base with pillows higher in the sequence and black slate near the top

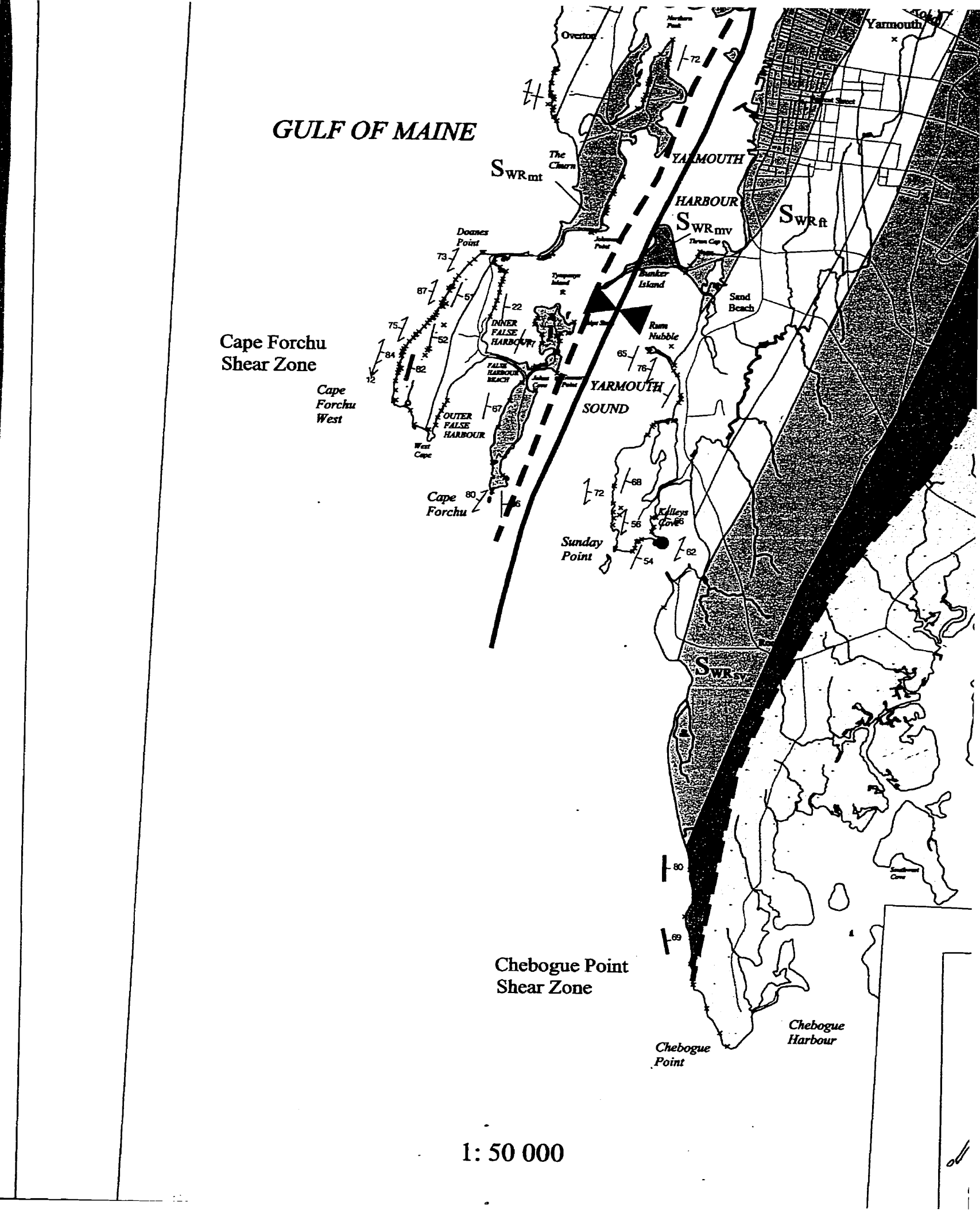
GULF OF MAINE
Cape Forchu
Shear Zone
Chebogue Point
Shear Zone
Overton
Yarmouth
The Cleam
YARMOUTH
HARBOUR
Doanes Point
Bunker Island
Sand Beach
INNER FALSE HARBOUR
Rum Nubble
FALSE HARBOUR BEACH
YARMOUTH SOUND
Cape Forchu West
OUTER FALSE HARBOUR
West Cape
Cape Forchu
Killeys Cove
Sunday Point
Chebogue Harbour
Chebogue Point
1: 50 000

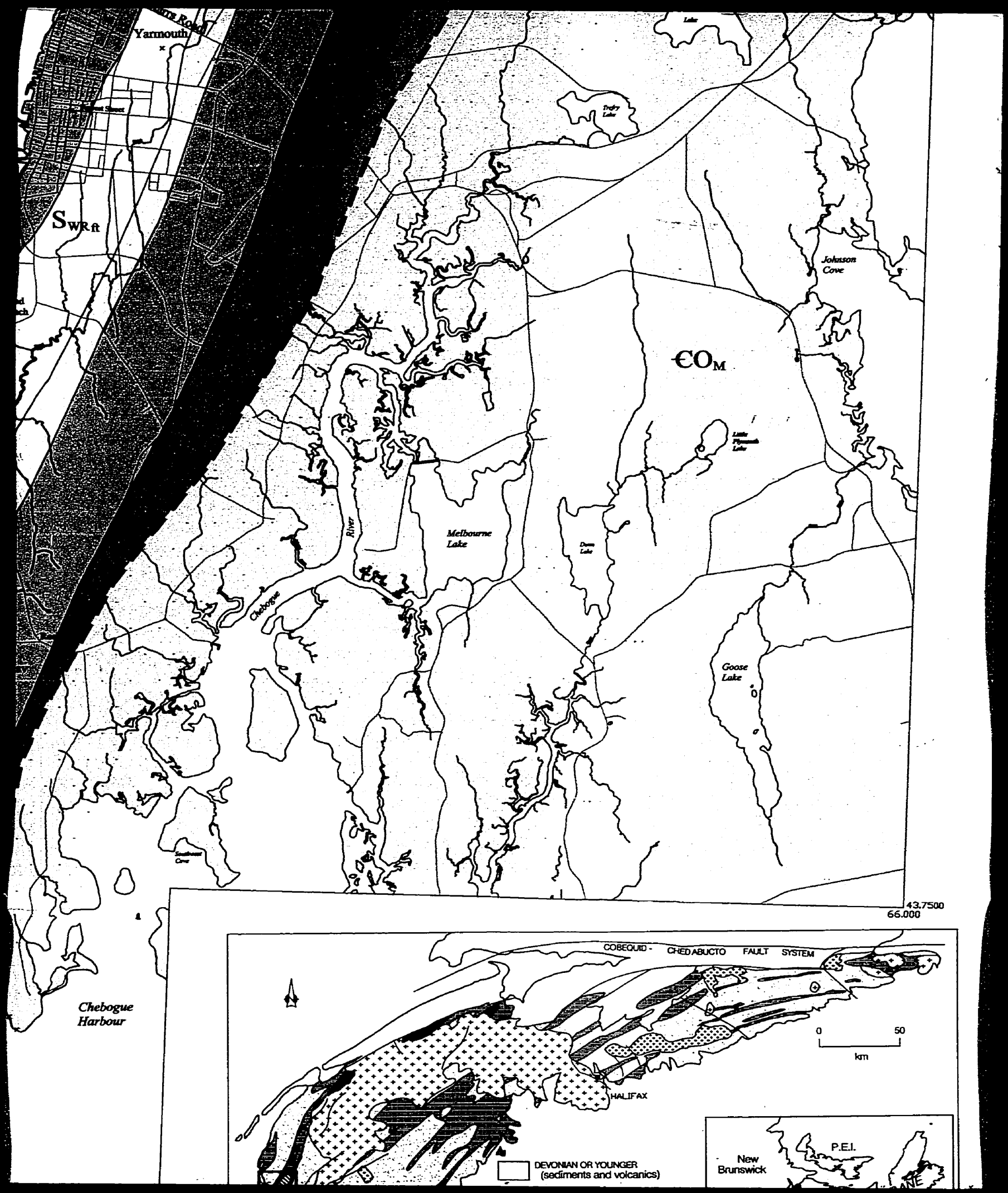
Yarnouth
Swrft
Trefry Lake
Johnson Cove
CO M
Little Pleasant Lake
Melbourne Lake
River
Chebogue
Dunn Lake
Goose Lake
43.7500
66.000
Chebogue Harbour
COBEQUID - CHEDABUCTO FAULT SYSTEM
0
50
km
HALIFAX
DEVONIAN OR YOUNGER
(sediments and volcanics)
New Brunswick
P.E.I.
NE

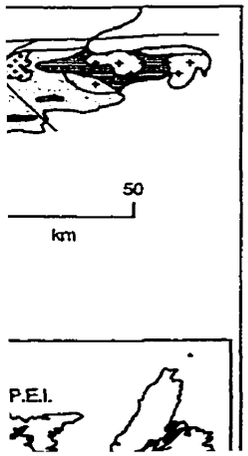

White Rock Formation

Predominantly mafic tuff and mafic flows.

$S_{WR_{mt}}$ Mafic tuff interbedded with mafic lithic tuff, conglomerate and tuffaceous sand near the base with pillows higher in the sequence and black slate near the top.

$S_{WR_{ft}}$ Mafic flows, tuff and amphibolite overlain by conglomerate, mafic tuff and pos pillows on the western limb. Interbedded mafic flows, mafic tuff, felsic crystal tuffaceous sandstone on the eastern limb.

$S_{WR_{mf}}$ Mafic tuff and metasiltstone grading into mafic tuff, mafic flows and tuffaceou sandstone with rare quartzite. Overlain by conglomerate, felsic crystal tuff, maf and mafic flows.

$S_{WR_{cv}}$ Mafic tuff interbedded with tuffaceous sandstone and quartzite becoming mafic mafic tuff, felsic crystal tuff, and mafic crystal tuff.

Predominantly quartzite with finely interbedded phyllite grading into massive quartzite.

Finely interbedded metasandstone and metasiltstone/slate with common quartzi lenses becoming phyllite on the western limb and staurolite, biotite and garnet s on the eastern limb.

CAMBRIAN-ORDOVICIAN

Undivided Meguma Group

ϵO_M Metasandstone, metasiltstone and slate.

SYMBOLS

- Outcrop Location
- U-Pb Dating Sample Location
- Inclined and Vertical Bedding
- Inclined and Vertical Cleavage
- Bedding-Cleavage Intersection Lineation
- Inclined and Vertical Sill or Dyke
- Fault
- Trace of Syncline

White Rock Formation

Predominantly mafic tuff and mafic flows.

$S_{WR_{mf}}$ Mafic tuff interbedded with mafic lithic tuff, conglomerate and tuffaceous sandstone near the base with pillows higher in the sequence and black slate near the top.

$S_{WR_{ft}}$ Mafic flows, tuff and amphibolite overlain by conglomerate, mafic tuff and possible pillows on the western limb. Interbedded mafic flows, mafic tuff, felsic crystal tuff and tuffaceous sandstone on the eastern limb.

$S_{WR_{mf}}$ Mafic tuff and metasiltstone grading into mafic tuff, mafic flows and tuffaceous sandstone with rare quartzite. Overlain by conglomerate, felsic crystal tuff, mafic tuff and mafic flows.

$S_{WR_{sv}}$ Mafic tuff interbedded with tuffaceous sandstone and quartzite becoming mafic flows, mafic tuff, felsic crystal tuff, and mafic crystal tuff.

Predominantly quartzite with finely interbedded phyllite grading into massive quartzite.

Finely interbedded metasandstone and metasiltstone/slate with common quartzite lenses becoming phyllite on the western limb and staurolite, biotite and garnet schist on the eastern limb.

CAMBRIAN-ORDOVICIAN

Undivided Meguma Group

$\in O_M$ Metasandstone, metasiltstone and slate.

SYMBOLS

- Outcrop Location
- U-Pb Dating Sample Location
- Inclined and Vertical Bedding
- Inclined and Vertical Cleavage
- Bedding-Cleavage Intersection Lineation
- Inclined and Vertical Sill or Dyke
- Fault
- Trace of Syncline

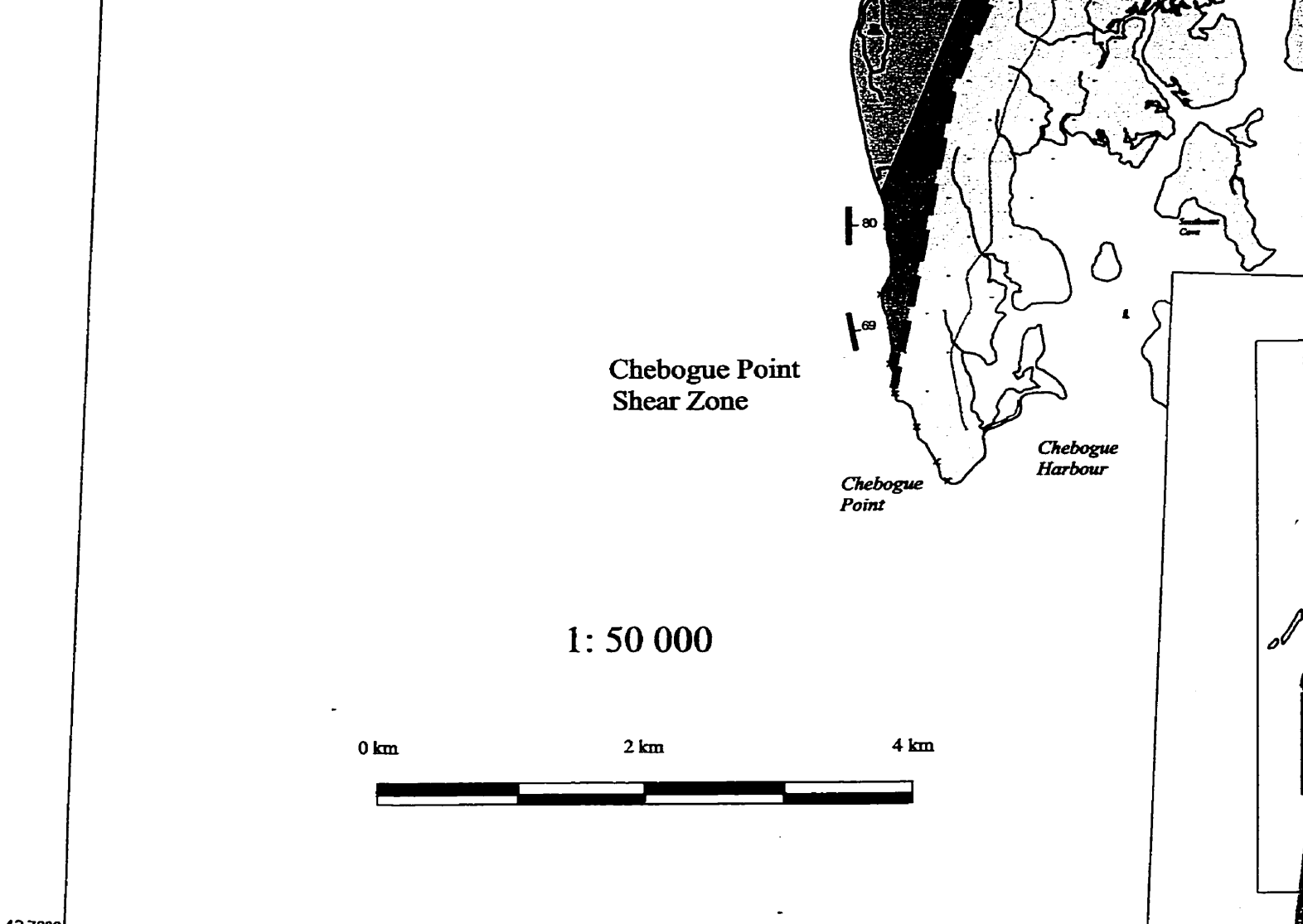

Fig. 2.1. Geological map of the Yarmouth area

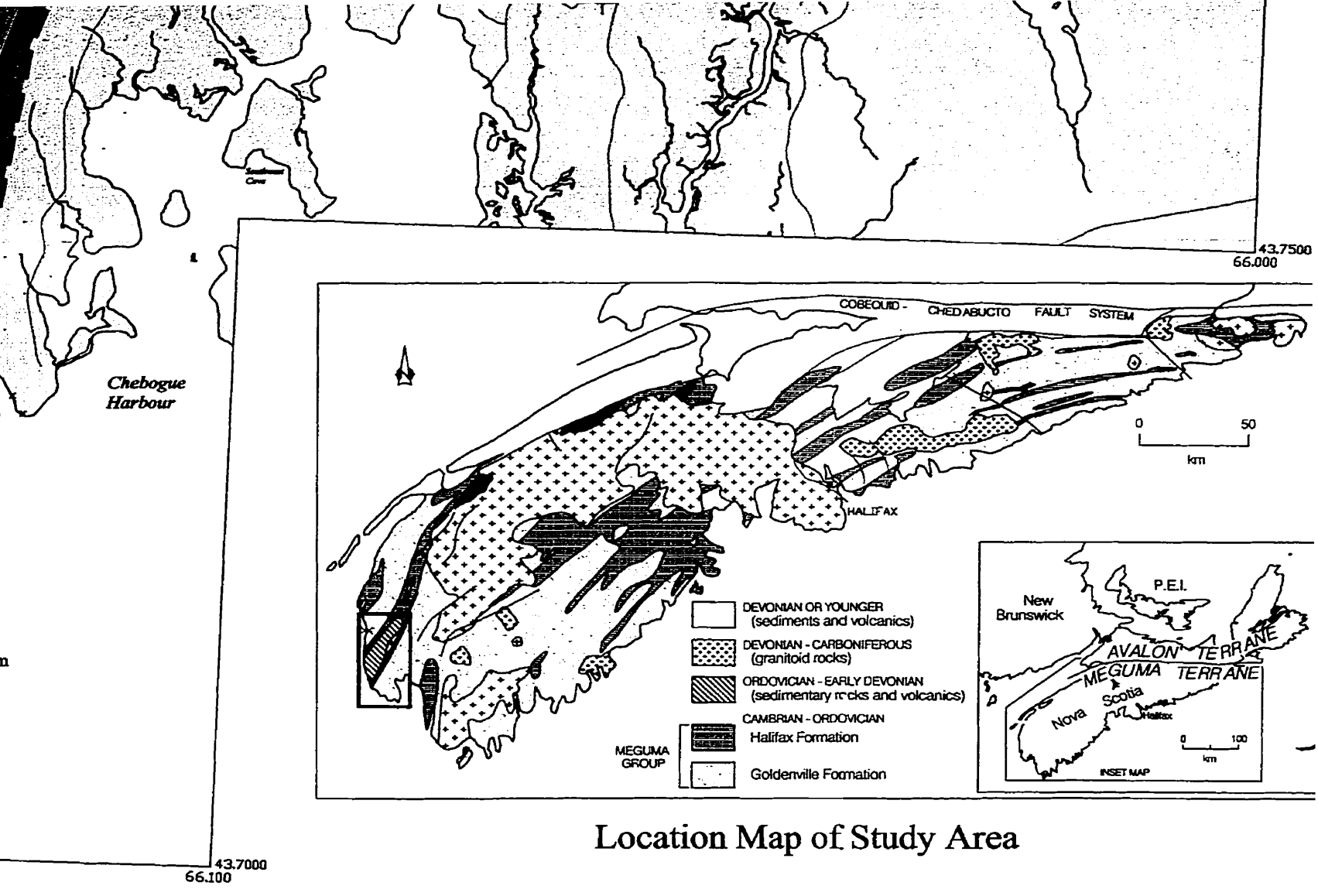

Location Map of Study Area

Cross- sectic

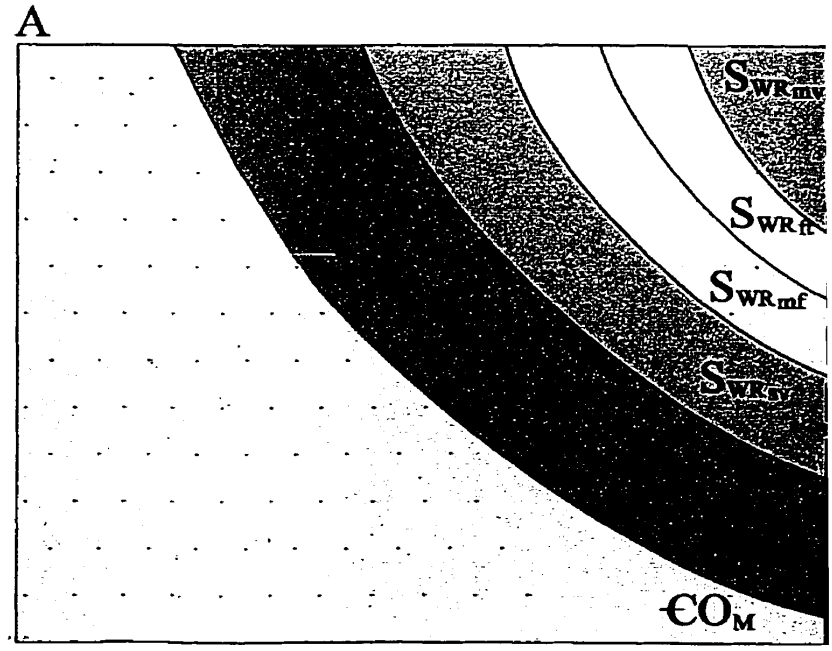

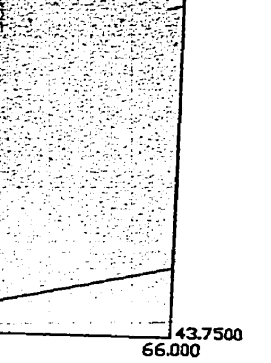

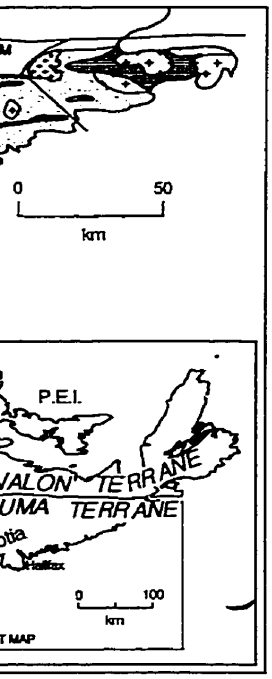

Undivided Meguma Group

ϵO_M Metasandstone, metasiltstone and slate.

SYMBOLS

- Outcrop Location
- U-Pb Dating Sample Location
- Inclined and Vertical Bedding
- Inclined and Vertical Cleavage
- Bedding-Cleavage Intersection Lineation
- Inclined and Vertical Sill or Dyke
- Fault
- Trace of Syncline
- Geological Contact
- Shear zone (interpreted from Culshaw and Liesa, 1997)

Cross- section of the Yarmouth Syncline

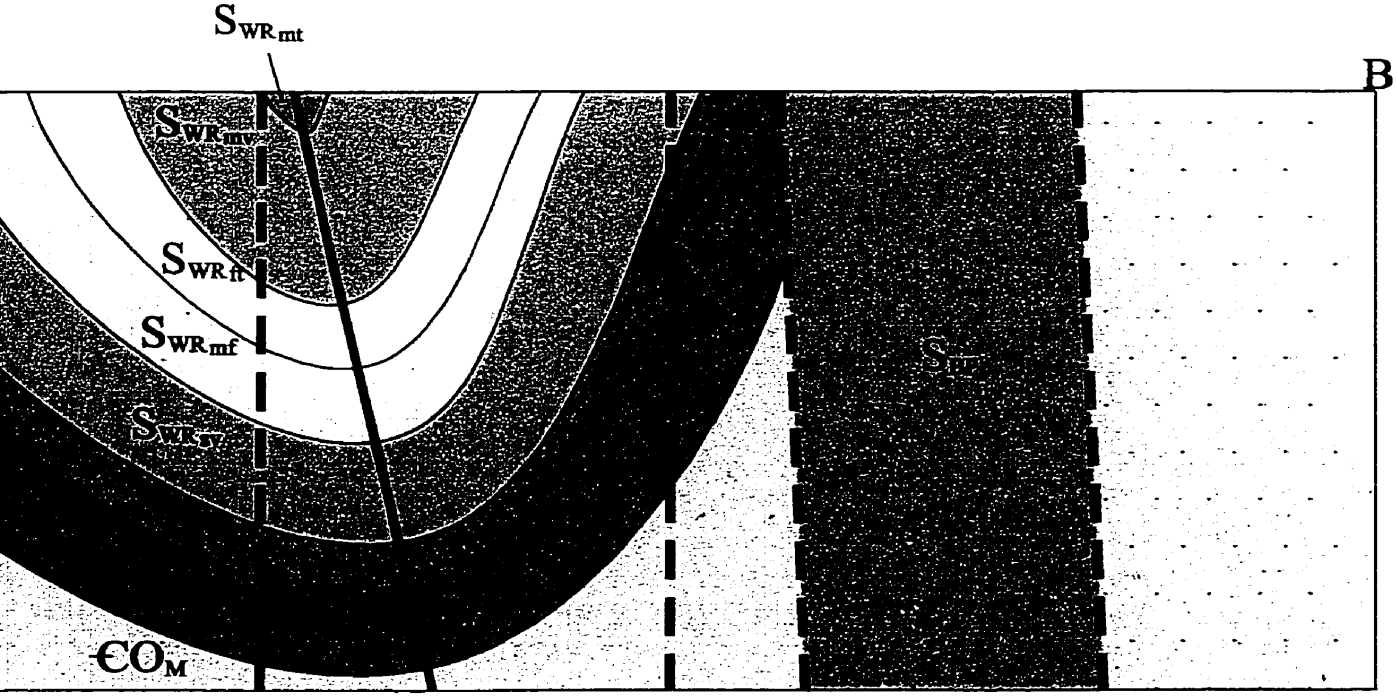

Undivided Meguma Group

ϵO_M Metasandstone, metasiltstone and slate.

SYMBOLS

- Outcrop Location
- U-Pb Dating Sample Location
- Inclined and Vertical Bedding
- Inclined and Vertical Cleavage
- Bedding-Cleavage Intersection Lineation
- Inclined and Vertical Sill or Dyke
- Fault
- Trace of Syncline
- Geological Contact
- Shear zone (interpreted from Culshaw and Liesa, 1997)

of the Yarmouth Syncline

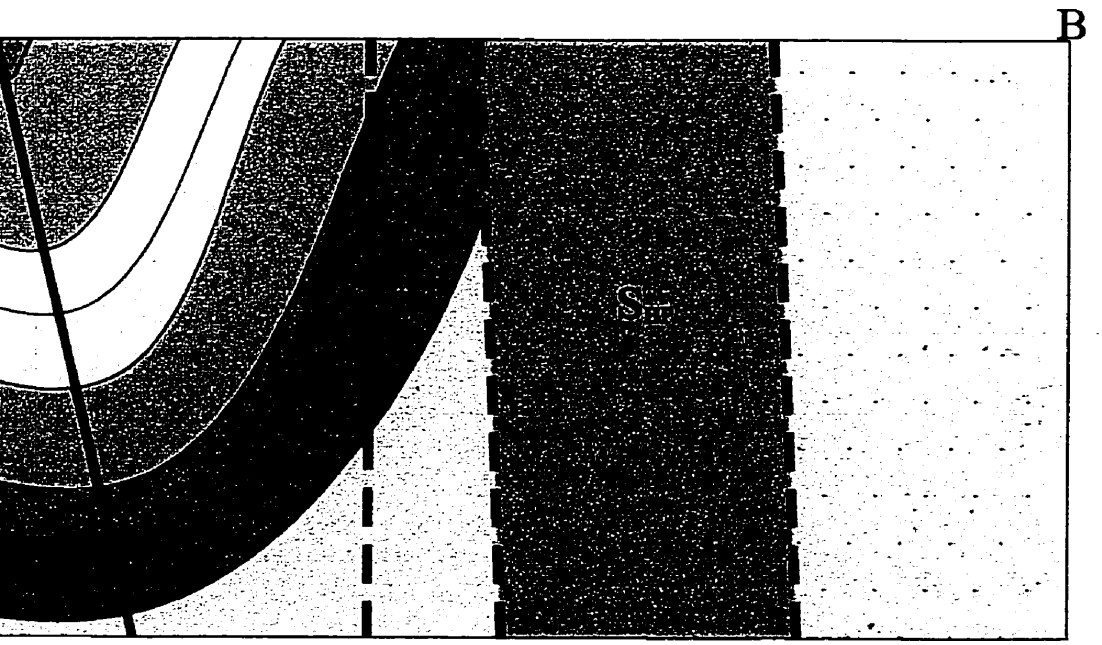

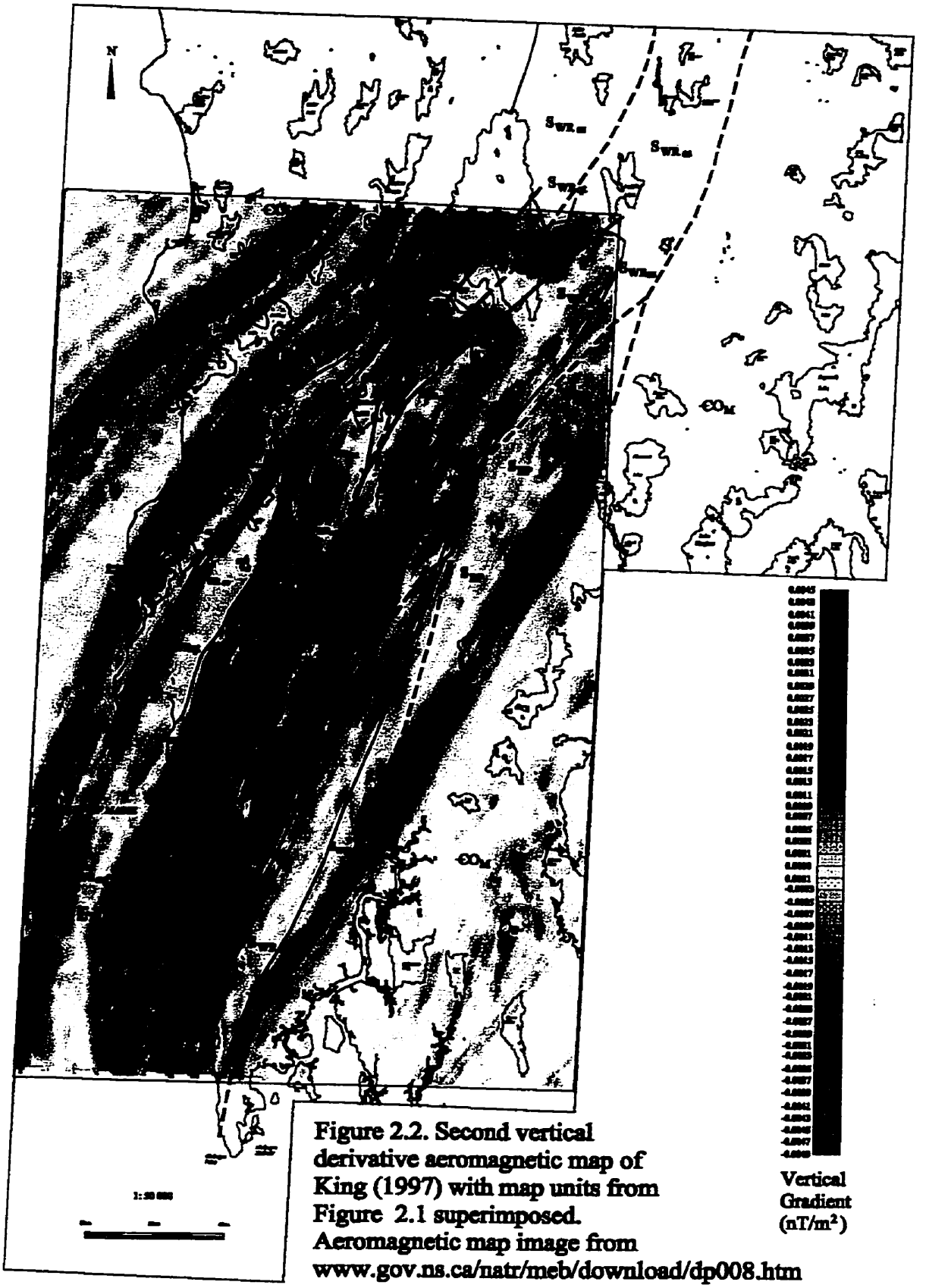

Figure 2.2. Second vertical derivative aeromagnetic map of King (1997) with map units from Figure 2.1 superimposed. Aeromagnetic map image from www.gov.ns.ca/natr/meb/download/dp008.htm

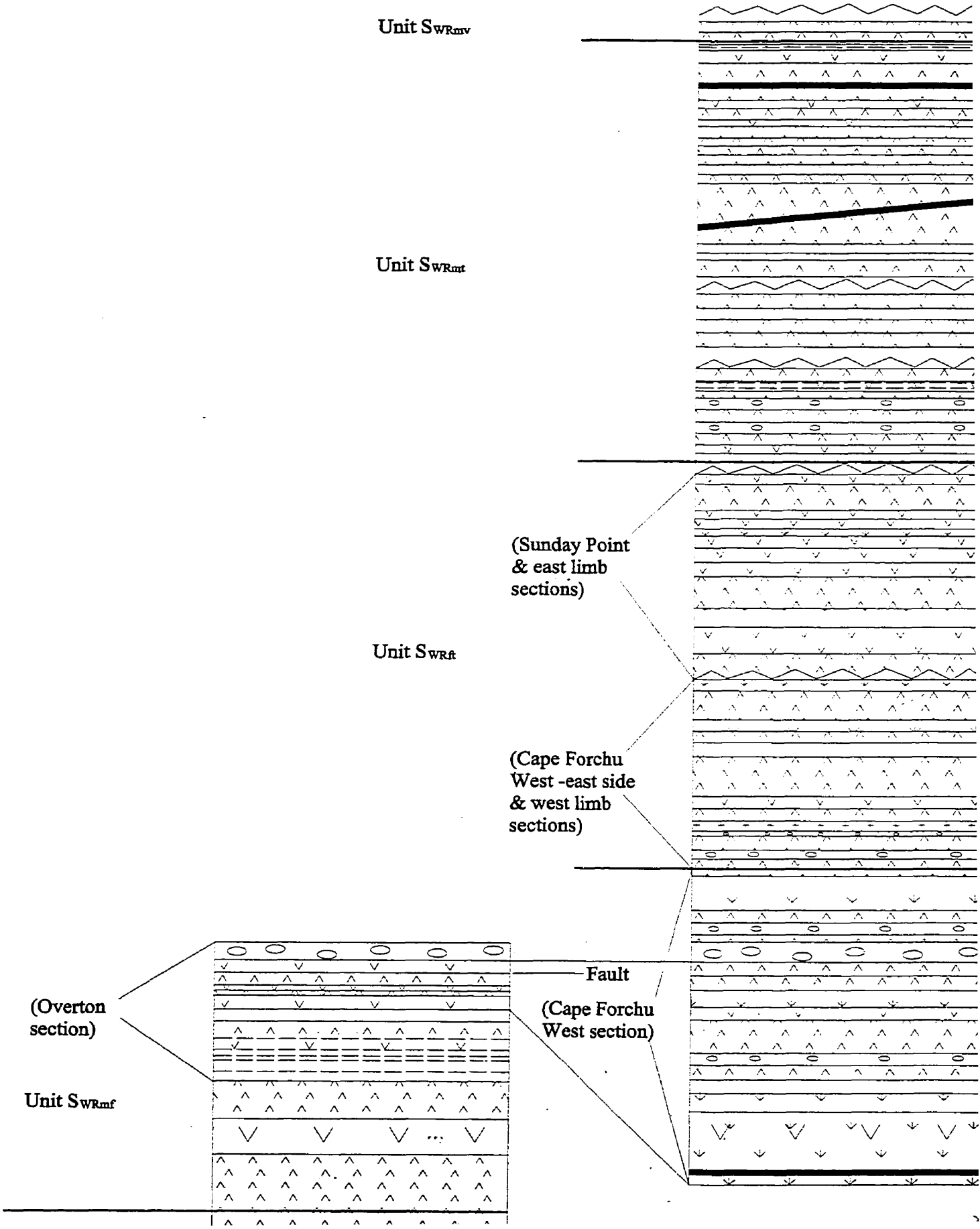
Unit S_{WRmv}
Unit S_{WRmt}
(Sunday Point & east limb sections)
Unit S_{WRft}
(Cape Forchu West -east side & west limb sections)
Fault
(Overton section)
(Cape Forchu West section)
Unit S_{WRmf}

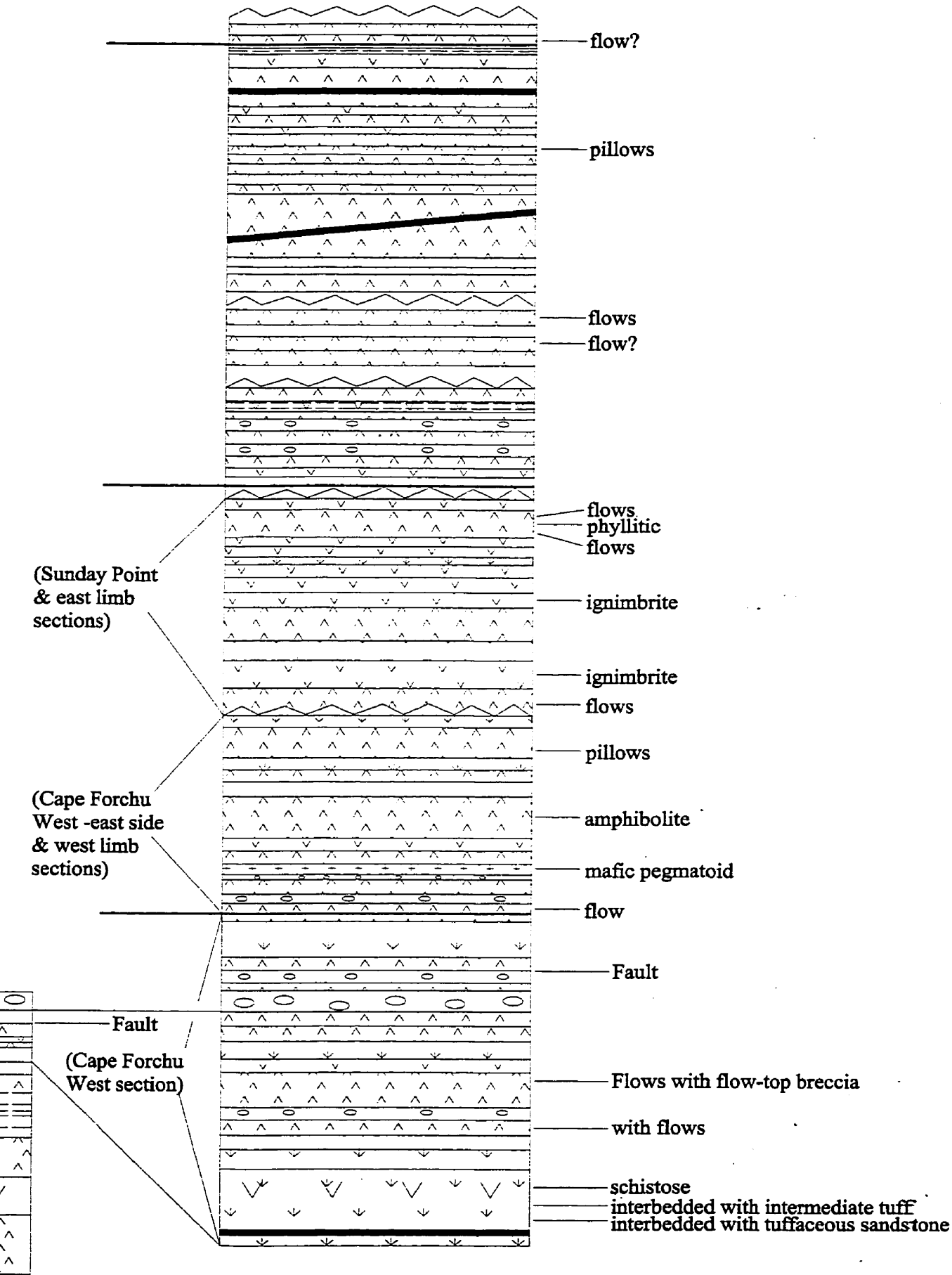
flow?
pillows
flows
flow?
flows
phyllitic
flows
ignimbrite
ignimbrite
flows
pillows
amphibolite
mafic pegmatoid
flow
Fault
Fault
Flows with flow-top breccia
with flows
schistose
interbedded with intermediate tuff
interbedded with tuffaceous sandstone
(Sunday Point & east limb sections)
(Cape Forchu West -east side & west limb sections)
(Cape Forchu West section)

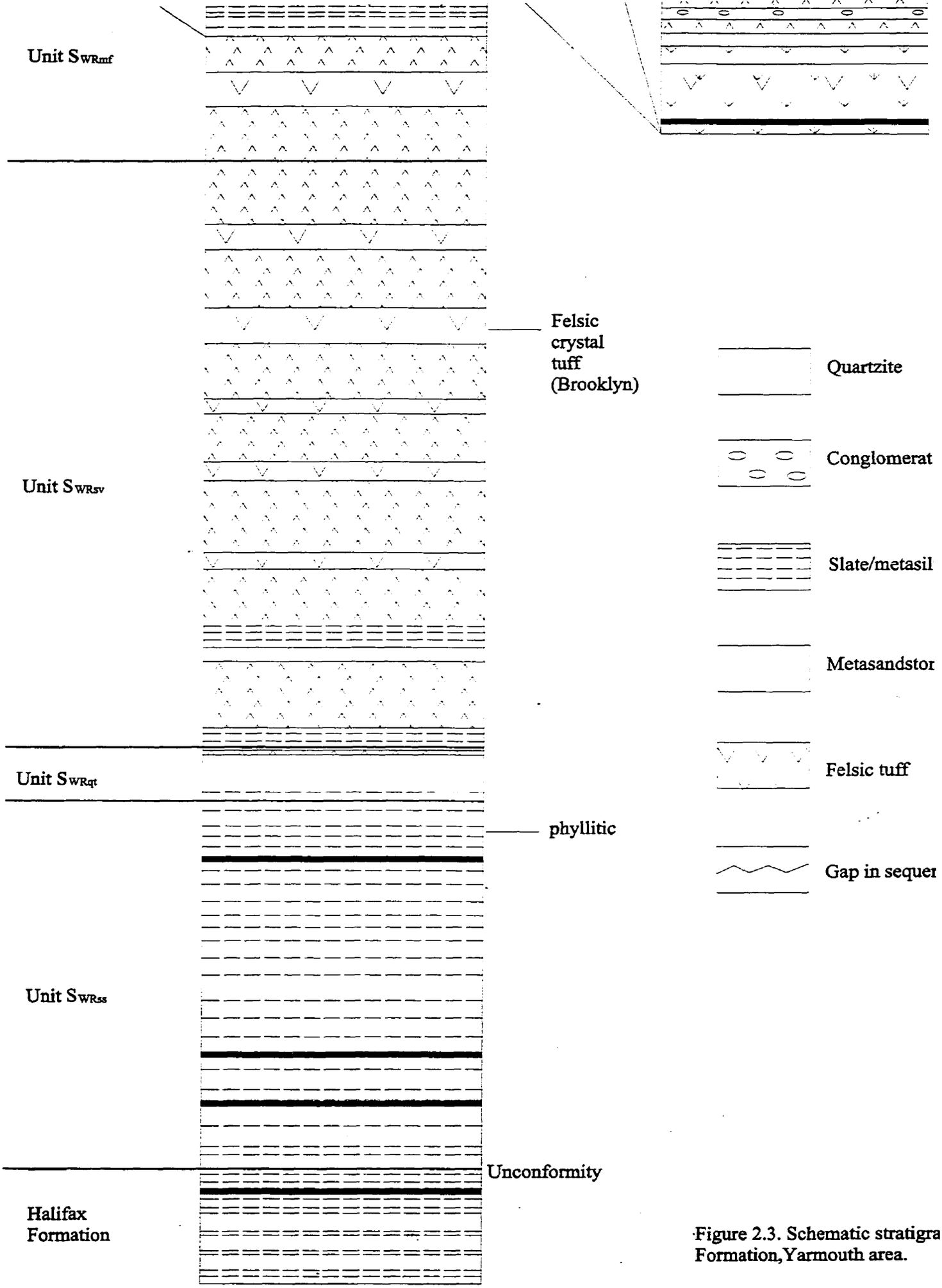

Figure 2.3. Schematic stratigra
Formation, Yarmouth area.

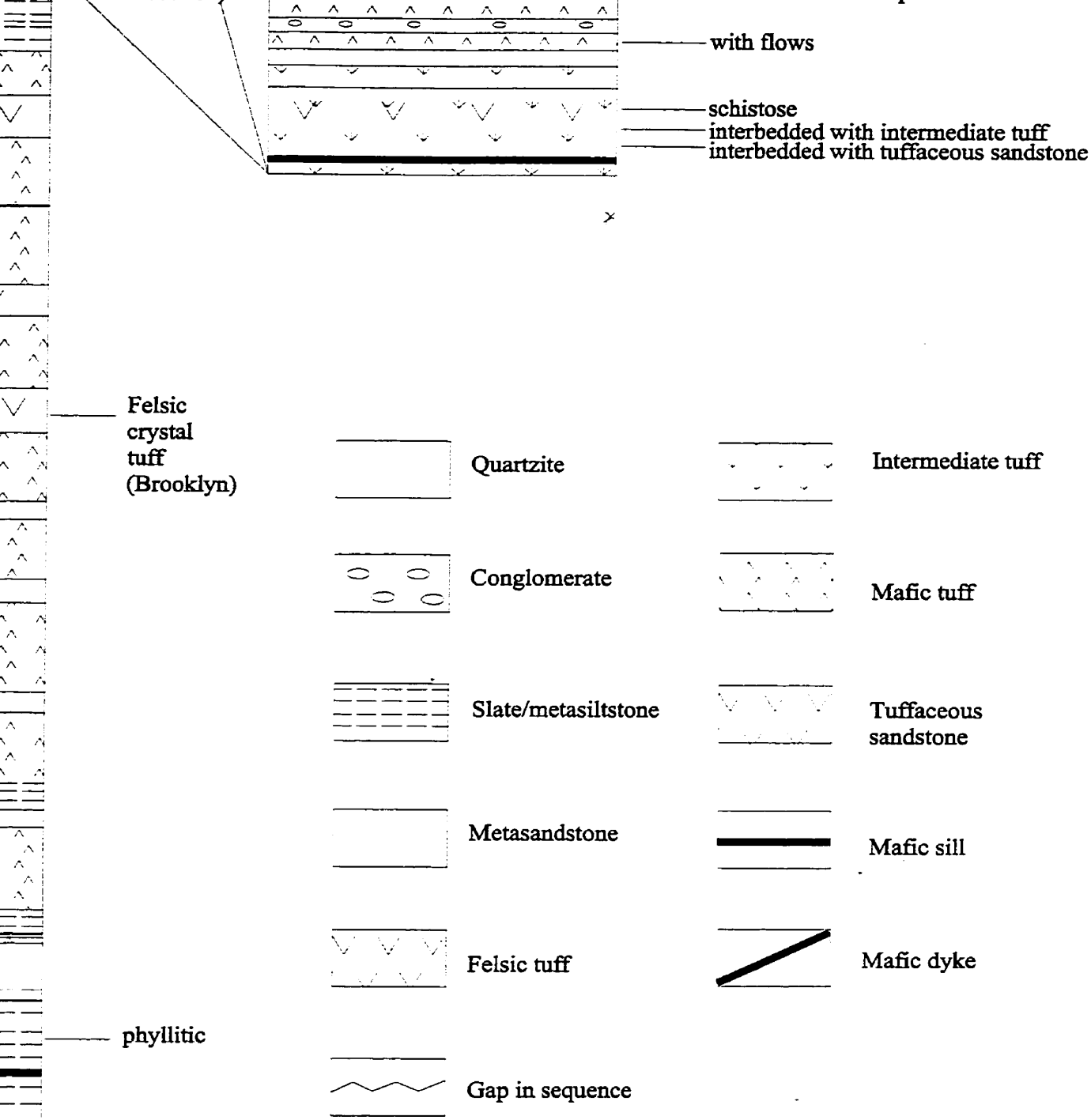

Figure 2.3. Schematic stratigraphic column for the White Rock Formation, Yarmouth area.

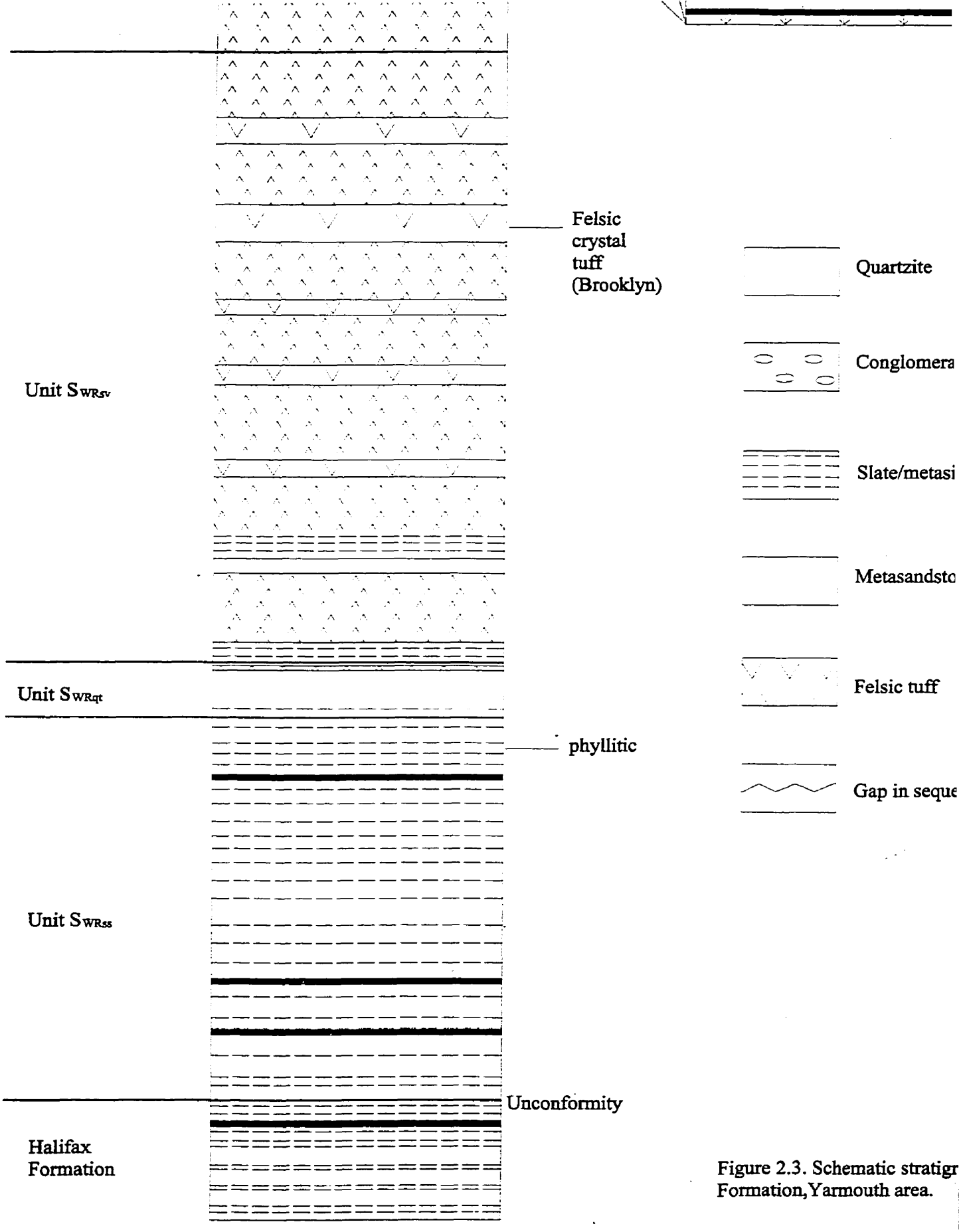

Figure 2.3. Schematic stratigr
Formation, Yarmouth area.

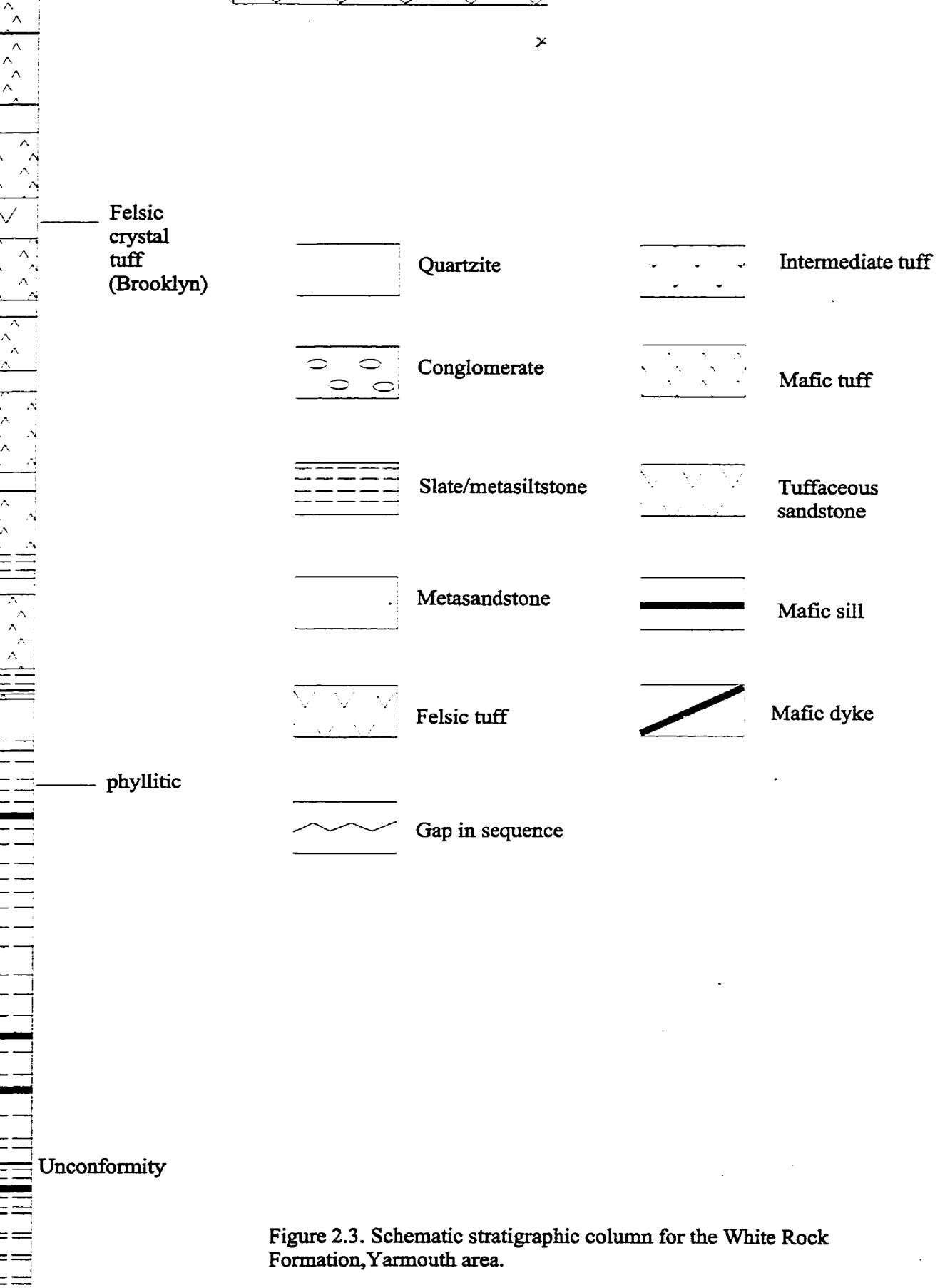

Figure 2.3. Schematic stratigraphic column for the White Rock Formation, Yarmouth area.

but the mineralogy is dominantly metamorphic. Wherever identifiable, the protolith name is used in order to give a representation of the original rock assemblage.

Rocks in the Yarmouth area occur in a synclinal structure and are generally steeply dipping. Minor faults are common and major faults offset the outer eastern limb and the core of the syncline. Shear zones occur on the outer limbs and core of the syncline as well (Fig. 2.1). Coastal exposures provide extensive stratigraphic sections, in contrast to most inland outcrops which are typically only a few meters in extent. Limited inland exposure also causes difficulties in determining the nature of the contacts between units. In some cases, outcrops are continuous enough to infer the relationship, but such exposures are rare, especially for units near the core of the syncline.

2.2. Goldenville Formation

Within the study area, the Goldenville Formation outcrops only at the southern tip of Chebogue Point (Fig. 2.1) where it is exposed in gradational contact with the overlying Halifax Formation. Away from the contact, the Goldenville Formation consists of massive metasandstone with minor, thin interbeds of metasiltstone. The sequence fines upward to the northwest toward the contact with the Halifax Formation, becoming finely interbedded metasiltstone and metasandstone.

2.3. Halifax Formation

The Halifax Formation is exposed at Cranberry Head, Chebogue Point and Deerfield dam, and in brooks north of Hoopers Lake and south of Churchills Mill Lake.

These areas correspond with areas of high positive amplitude aeromagnetic signature (Fig. 2.2). At the inland outcrops and Chebogue Point, the formation consists of grey and dark green to grey, finely interbedded slate and metasiltstone/metasandstone. However, at Cranberry Head the rocks are phyllite and appear to be at higher metamorphic grade than at other locations. At both Cranberry Head and Chebogue Point, the rocks are within shear zones proposed by Culshaw and Liesa (1997) (Fig. 2.1) and are strongly crenulated (Plate 2.1). A narrow zone of slate adjacent to the contact with the overlying White Rock Formation at Chebogue Point is brecciated, indicating the presence of a brittle fault at the contact. As noted above, the contact with the underlying Goldenville Formation at Chebogue Point appears gradational as metasandstone beds of the Goldenville Formation fine upward into interbedded metasandstone and metasiltstone then into interbedded metasiltstone and slate of the Halifax Formation.

2.4. White Rock Formation

2.4.1. Unit S_{WRss}

The stratigraphically lowest unit in the White Rock Formation consists of metasedimentary rocks and is exposed along the coast from south of Cranberry Head to Chegoggin Point, and at Chebogue Point, and inland near Rodneys Lake, in a stream north of Deerfield dam and in the eastern portion of Government Brook (Fig. 2.1). The extent of the unit in areas of little or no outcrop is based on the magnetic signature, which ranges from negative amplitude near the base to moderately high positive

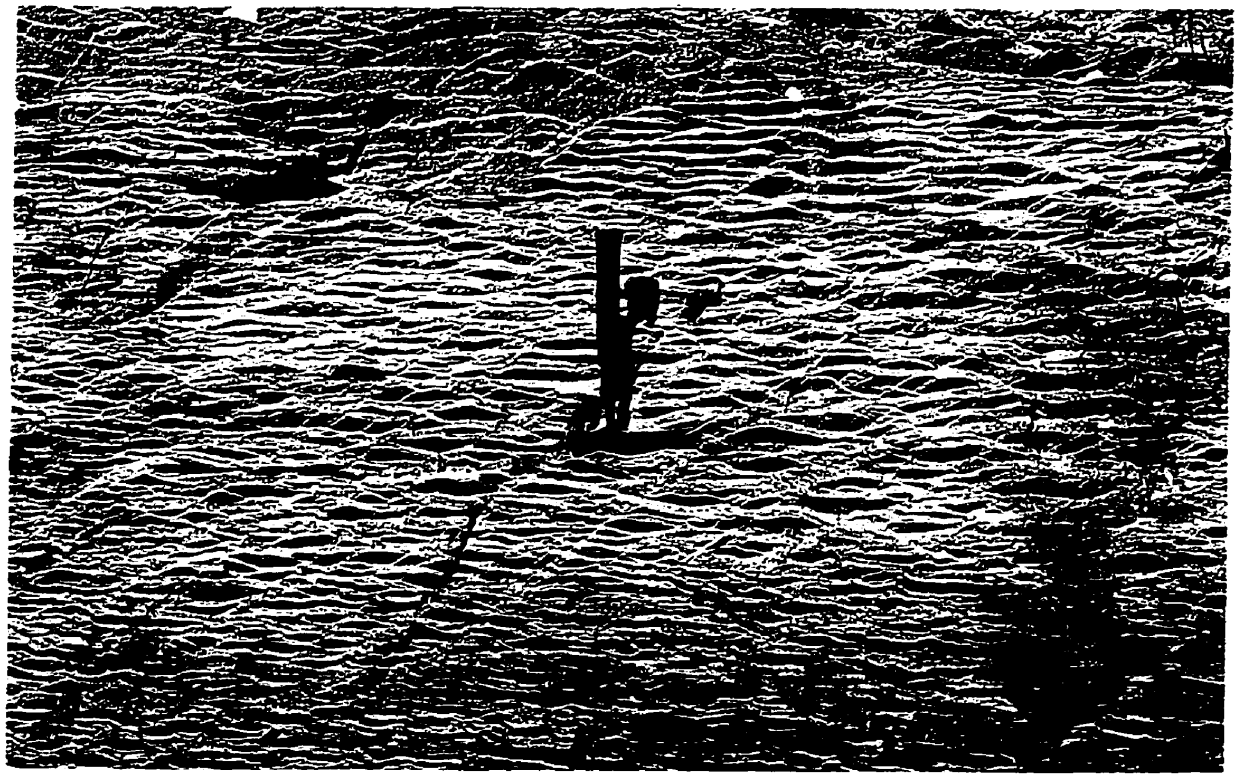

Plate 2.1. Crenulation cleavage in the Halifax Formation within the Cranberry Point Shear Zone (Culshaw and Liesa, 1997) at Cranberry Head. Camera faces northwest.

amplitude near the top (Fig. 2.2). The unit has an estimated thickness range of 0.5 to 1 km.

The lowest part of the unit consists of cm-scale interbeds of buff-coloured metasandstone and light grey metasiltstone/slate. Metasandstone lenses approximately 30 cm wide are common in the sequence at Chegoggin Point and contain coarse-grained amphibole porphyroblasts. Upward, the unit gradually becomes finer and consists of finely interbedded metasiltstone and slate. In the Chegoggin Point section, the unit gradually becomes phyllitic upward with rare garnet-bearing layers. Idiomorphic garnet porphyroblasts become increasingly abundant upward in the unit. Near Chegoggin Point, numerous amphibole-rich mafic dykes and sills are present and quartz veins are abundant. At Chebogue Point, unit S_{WRss} consists of finely laminated black slate with abundant porphyroblasts of pyrite. Interbedded with the black slate are dark grey metasiltstone layers which decrease in abundance up-section. Near the base, the slate is crenulated and strongly brecciated. Boudinaged, coarse-grained, amphibole-rich dykes cross cut the unit and increase in abundance up-section.

Inland exposures appear similar to those along the coast, except in Government Brook where the unit consists of staurolite schist near the base and grades upward into biotite schist and garnet schist.

The contact with the underlying Halifax Formation at Chebogue Point appears to be a fault as both formations are strongly brecciated. The location of the contact at the fault coincides with a colour change in the slate and metasiltstone beds from grey and green in the Halifax Formation to black in unit S_{WRss}. The contact between unit S_{WRss} and the Halifax Formation is not exposed at Cranberry Head but coincides with

the location of the Cranberry Point Shear Zone proposed by Culshaw and Liesa (1997). The contact at both Cranberry Head and Chebogue Point also coincides with an abrupt change in aeromagnetic signature from high positive amplitude in the Halifax Formation to negative amplitude in unit S_{WRss}.

2.4.2. Unit S_{WRqt}

Unit S_{WRqt} is exposed only at Chegoggin Point and is predominantly massive quartzite with an estimated thickness of 250 m. The unit appears to coincide with a negative amplitude magnetic signature on Figure 2.2 and on that basis can be traced inland to the trough of the syncline but does not appear to be present on the eastern limb. At Chegoggin Point, the contact with underlying unit S_{WRss} appears gradational, with phyllite of unit S_{WRss} becoming interbedded with quartzite. Near the base, unit S_{WRqt} appears cherty with interbedded grey, arenaceous layers. Upwards, the unit becomes pure, massive quartzite which is slightly orange. It appears quite fractured and is cross cut by abundant quartz veins. Near the top of the unit, the quartzite contains fine interbeds of mafic tuff.

2.4.3. Unit S_{WRsv}

Unit S_{WRsv} consists mainly of metavolcanic rocks with minor metasedimentary rocks near the base. Excellent exposure occurs in Government Brook and less extensive outcrops occur at Chegoggin Point, at Lake George, north of Brazil Lake, and south of Brooklyn (Fig. 2.1). The unit has a maximum thickness of 1250 m and is characterized

by high, positive amplitude aeromagnetic gradient in lower parts and a zero amplitude gradient in the remainder of the unit.

Lower parts of the unit are exposed at Chegoggin Point and in the eastern part of Government Brook, and poorly exposed on the Holley Road near Brazil Lake (Fig. 2.1). At Chegoggin Point, the unit consists of mainly mafic metavolcanic rocks, including fine-grained, green, phyllitic tuff with porphyroblasts of amphibole interbedded with buff-to-grey tuffaceous metasandstone and quartzite. At Chegoggin Point, the fine interbeds of mafic tuff near the top of unit S_{WRqt} are similar to those in unit S_{WRsv}, indicating a gradational contact. Above the quartzite and tuff beds is a possible mafic flow which is green and vesicular and contains abundant biotite porphyroblasts. Intruding both the flow and quartzite is a massive, vesicular sill with abundant amphibole and biotite porphyroblasts. On Holley Road, the lower part of the unit also contains volcanic rocks but at this location the tuff consists of alternating coarse-grained amphibole-rich layers and quartz- and plagioclase-rich layers. The eastern section of Government Brook contains intermediate-to-mafic crystal tuff and tuffaceous sandstone, interbedded with mafic tuff with plagioclase crystals. In Government Brook, the upper beds of S_{WRss} are schistose and it is difficult to determine whether they were originally similar to the tuffaceous layers at the base of unit S_{WRsv}.

Upper portions of unit S_{WRsv} are exposed on Lake George, in the western part of Government Brook and on Hardscratch Road (Fig. 2.1). On Lake George, the outcrops consist of layers of coarse-grained amphibole-rich and amphibole-poor mafic tuff. Exposures on Government Brook consist of a wide variety of lithologies including medium- to coarse-grained amphibole-rich mafic tuff and laminated tuffaceous

sandstone overlain by fine-grained, laminated, phyllitic tuff with porphyroblasts of amphibole. Exposures in a brook near Hardscratch Road (Fig. 2.1) appear to consist of foliated felsic crystal tuff with porphyroblasts of mica and phenocrysts of K-feldspar and plagioclase.

2.4.4. Unit S_{WRmf}

Exposure of unit S_{WRmf} is excellent along the coast near Overton and Cape Forchu West but limited in inland areas. The unit is traced inland on the basis of its distinctive magnetic gradient signature which has for the most part strongly negative amplitude. The unit is predominantly composed of mafic and felsic volcanic rocks and reaches a maximum thickness of approximately 750 m.

On Bain Road near South Chegoggin, the lower part of the unit is exposed and consists of fine-grained, grey-green tuff with crystals of plagioclase less than 0.5 cm long. Approximately 250 m up-section (further along Bain Road), the unit appears massive, medium grained and crystalline, with large grains of amphibole. The base of the unit also appears to contain metasedimentary layers; for example, an outcrop of grey, laminated metasiltstone/metasandstone with possible cross laminations is exposed on Butler Road near Wellington (Fig. 2.1).

A nearly continuous cross-section of unit S_{WRmf} is exposed on the eastern limb of the Yarmouth syncline in Government Brook. Outcrops near the base of the unit are phyllitic with medium-grained porphyroblasts of biotite and pyrite and probably have a gradational contact with the phyllitic tuff at the top of (underlying) unit S_{WRsv}. Upward, the unit becomes less phyllitic and contains garnet porphyroblasts. Near the top,

exposures are of fine-grained, green to grey tuff (or possibly a flow) with biotite porphyroblasts.

Isolated outcrops inland near the middle of the unit contain possible metavolcanic layers. North of Brenton Lake on the North Ohio Road the rocks are laminated, with alternating feldspar-rich and amphibole-rich layers, and may be tuffaceous. Both types of layers contain abundant biotite. An exposure on the C.P. Railway line near South Ohio is possibly a tuffaceous sandstone, appearing grey, massive, and crystalline with grains of plagioclase and amphibole.

Exposures of the middle and upper parts of unit S_{WRmf} occur along the coast at Overton and Cape Forchu West. At both of these locations, the lower part of the unit is not exposed. The northernmost exposures at Overton consist of finely laminated phyllitic metasiltstone with thin layers of tuffaceous sandstone. Upward in the section, the layers of tuffaceous sandstone become thicker and the interbeds of phyllitic metasiltstone and tuffaceous sandstone are in places interrupted by layers of amphibole-rich mafic tuff. These layers are locally boudinaged (Plate 2.2). Amphibole-rich mafic tuff with coarse grains of plagioclase and amphibole is more common up-section and the abundance of phyllitic beds decreases. The abundance of tuffaceous sandstone layers also decreases and amphibole-rich layers become coarser grained and also contain plagioclase grains approximately 1 cm in length. Up-section from the amphibole-rich mafic tuff layers is a massive, approximately 10 m wide red to brown quartzite bed in sharp contact with overlying light green/grey tuffaceous sandstone. The quartzite contains fine-grained garnet porphyroblasts and trace fossils of chondrites.

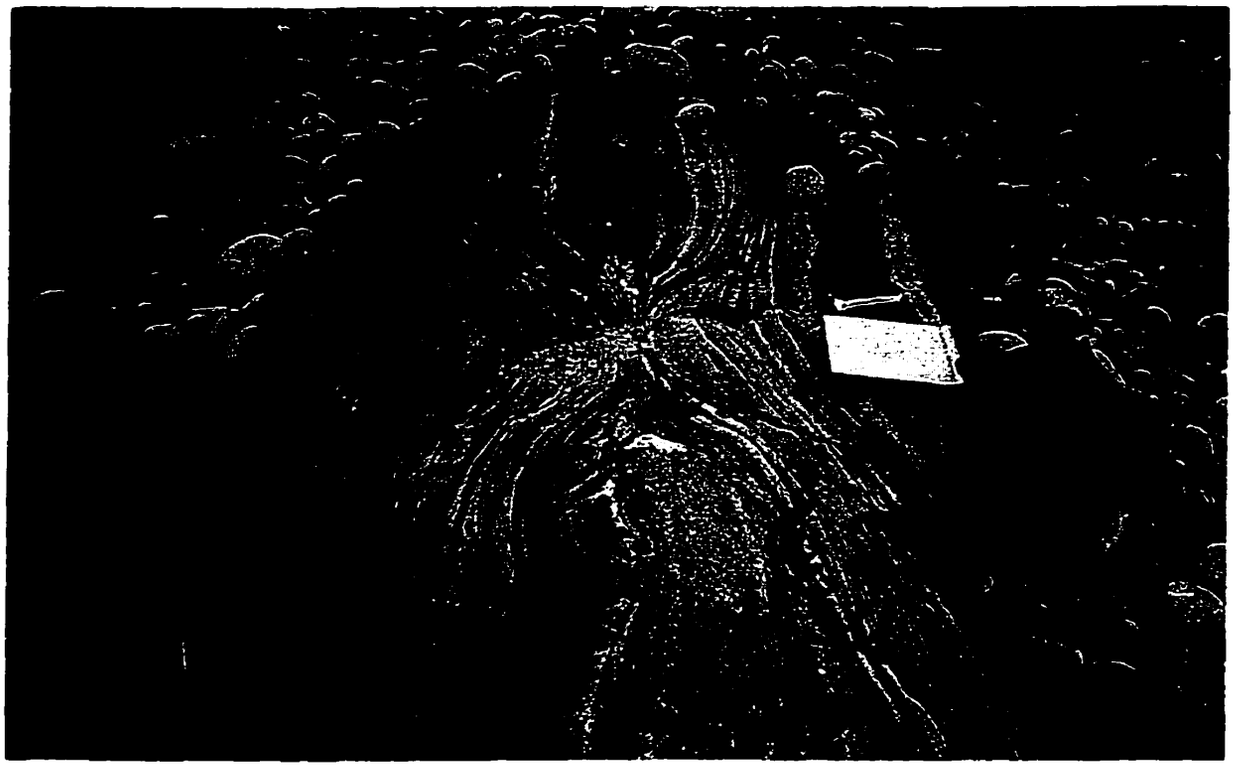

Plate 2.2. Boudinaged phyllitic metasiltstone, tuffaceous sandstone and amphibole-rich mafic tuff from unit $S_{WR_{mf}}$, Overton.

Some areas of the quartzite appear brecciated. The tuffaceous sandstone beds are fine grained and well laminated near the contact with the quartzite. Up-section, they become coarser grained and interbedded with amphibole-rich mafic tuff. Tuffaceous sandstone interbeds gradually disappear from the unit, leaving a section of well banded, medium- to coarse-grained amphibole-rich mafic tuff, with plagioclase grains less than 0.5 cm long. A fault separates the amphibole-rich mafic tuff from another grey tuffaceous sandstone bed. Above the tuffaceous sandstone is a distinctive marker bed (< 10 m thick) which also occurs at Cape Forchu West. This bed is a conglomerate with flattened, elongate clasts up to 50 cm in length near the top. The clasts consist of felsic and mafic crystal tuff and mafic and andesitic tuff. Some clasts appear more crystalline and possess a fine-to medium-grained, light grey matrix and abundant amphibole porphyroblasts. Many of the clasts have amphibole-rich rims.

At Cape Forchu West (Fig. 2.4), middle and upper parts of unit S_{WRmf} contain a variety of rocks types and abundant mafic sills. The middle part (Fig. 2.4, location a) consists of mafic lithic tuff with both bomb- and lapilli-size clasts (Plate 2.3). The tuff has a fine-grained green/grey matrix and biotite and amphibole porphyroblasts. The bombs and lapilli are flattened and also contain biotite and amphibole porphyroblasts. Also present is laminated tuffaceous sandstone with abundant biotite. Up-section from these beds, the unit contains mafic tuff and amphibole-rich mafic tuff interlayered with intermediate tuff. The intermediate tuff is schistose with porphyroblasts of biotite and amphibole. Banded amphibole-rich mafic tuff and tuffaceous sandstone (Plate 2.4) overlie the schistose layer. These lithologies grade into interbedded, slaty, intermediate

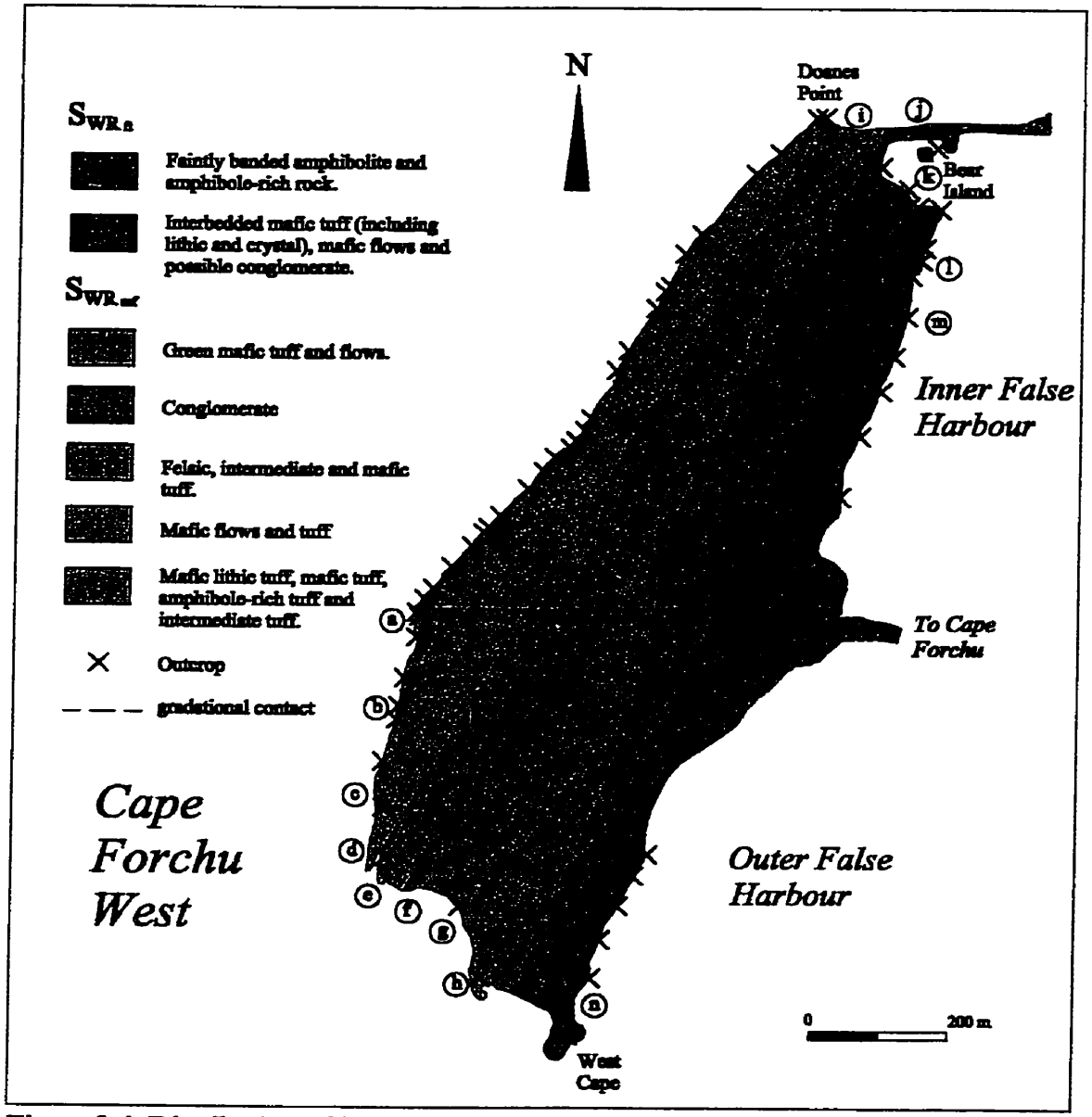

Figure 2.4. Distribution of lithologies in units SWRmf and SWRft on Cape Forchu West from Figure 2.1. Letters a-n are keyed to text.

Plate 2.3. Bomb and lapilli-size clasts in mafic tuff, unit Swr_{mf}, Cape Forchu West.

Plate 2.4. Banded amphibole-rich mafic tuff and tuffaceous sandstone, unit Swr_{mf}, Cape Forchu West.

tuff with amphibole porphyroblasts and fine-grained, light brown lapilli, and amphibole-rich mafic tuff. Southward along strike, mafic flows are interbedded with mafic tuff (Fig. 2.4, location b). Flows are massive and dark grey with abundant amphibole and biotite porphyroblasts. Flattened amygdules also occur and increase in abundance to the east, indicating the direction of the top of the unit. Some layers of the mafic tuff are amphibole-rich and contain bombs up to 0.5 m long. Alteration (epidotization) is particularly strong in the mafic tuffs in this part of the unit (Plate 2.5) (Fig. 2.4, location c). Upward, unit S_{WRmf} contains a massive dark grey tuff or flow with biotite porphyroblasts, interbedded, fine-grained tuff with amphibole and plagioclase crystals, and possible conglomerate. The matrix of the conglomerate is fine grained and contains abundant amphibole and plagioclase. Two types of clasts occur: wacke-like clasts with biotite clusters, and medium-grained, crystalline clasts with fine-grained amphibole. More mafic tuff and flows overlie the conglomerate layer. Flow-top brecciation (Plate 2.6) occurs in some flows and both tuff and flows have strong, local epidotization.

Farther up in the sequence, mafic tuff with plagioclase, biotite and amphibole grains is overlain by coarse-grained, massive, crystalline tuff interbedded with silty, well-cleaved layers containing pyrite porphyroblasts. Fine-grained, grey to green mafic tuff with bombs occurs above green to grey, banded tuff with abundant biotite and amphibole porphyroblasts. Stratigraphically higher, mafic tuff, mafic crystal tuff and mafic flows are exposed (Fig. 2.4, location d). At the southwestern tip of Cape Forchu West, tuffaceous sandstone underlies a sequence of interbedded felsic crystal tuff and

Plate 2.5. Extensive alteration of mafic tuff and flows, unit Swr_{mf}, Cape Forchu West.

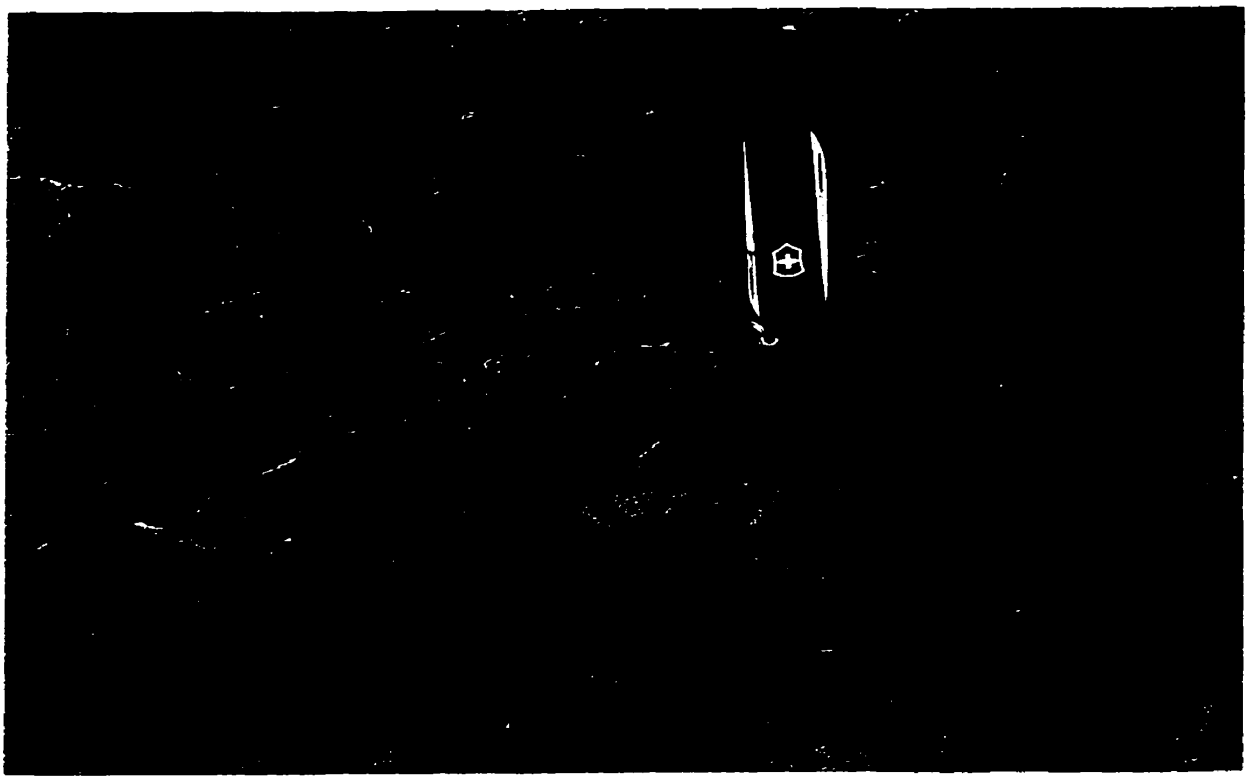

Plate 2.6. Flow-top brecciation in mafic flow from unit Sw_{Rmf}, Cape Forchu West.

felsic to intermediate lithic tuff (Fig. 2.4, location e). Above these layers are mafic and lithic tuff. The clasts in the lithic tuff are cm-scale, flattened fine-to medium-grained and dark to light grey mafic tuff or flow. The tuff is overlain by a conglomerate layer (Plate 2.7) (Fig. 2.4, location f) similar to the conglomerate exposed near the top of the unit in the Overton section. Clasts in the conglomerate increase in size to approximately 0.5 m to the east and clast types include crystal tuff and mafic tuff, both with well-developed amphibole rims (Plate 2.8). Upward, conglomerate or lithic tuff (with clasts/bombs less than 20 cm long) is interlayered with mafic tuff that contains rare bombs with phenocrysts of plagioclase. These beds are in faulted contact with grey-green mafic tuff with amphibole porphyroblasts. The tuff layers host rare beds of conglomerate with clasts of tuffaceous sandstone, mafic tuff and crystal tuff (Fig. 2.4, location g).

Up-section, unit S_{WRmf} contains green, mafic tuff and possible flows (Fig. 2.4, location h). The tuff contains phenocrysts of plagioclase and the flows become more amygdaloidal to the east and show autobrecciation. Along strike to the north (at Doanes Point) (Fig. 2.4, location i), uppermost rocks of the unit are interbedded, medium-grained mafic tuff (with abundant biotite porphyroblasts) and mafic crystal tuff. Also present are finely layered (less than 10 cm thick) beds of mafic tuff and tuffaceous sandstone (Plate 2.9).

2.4.5. Unit S_{WRft}

Unit S_{WRft} consists of mafic and felsic metavolcanic and minor metasedimentary rocks. The unit has a maximum thickness of approximately 1 km and is characterized

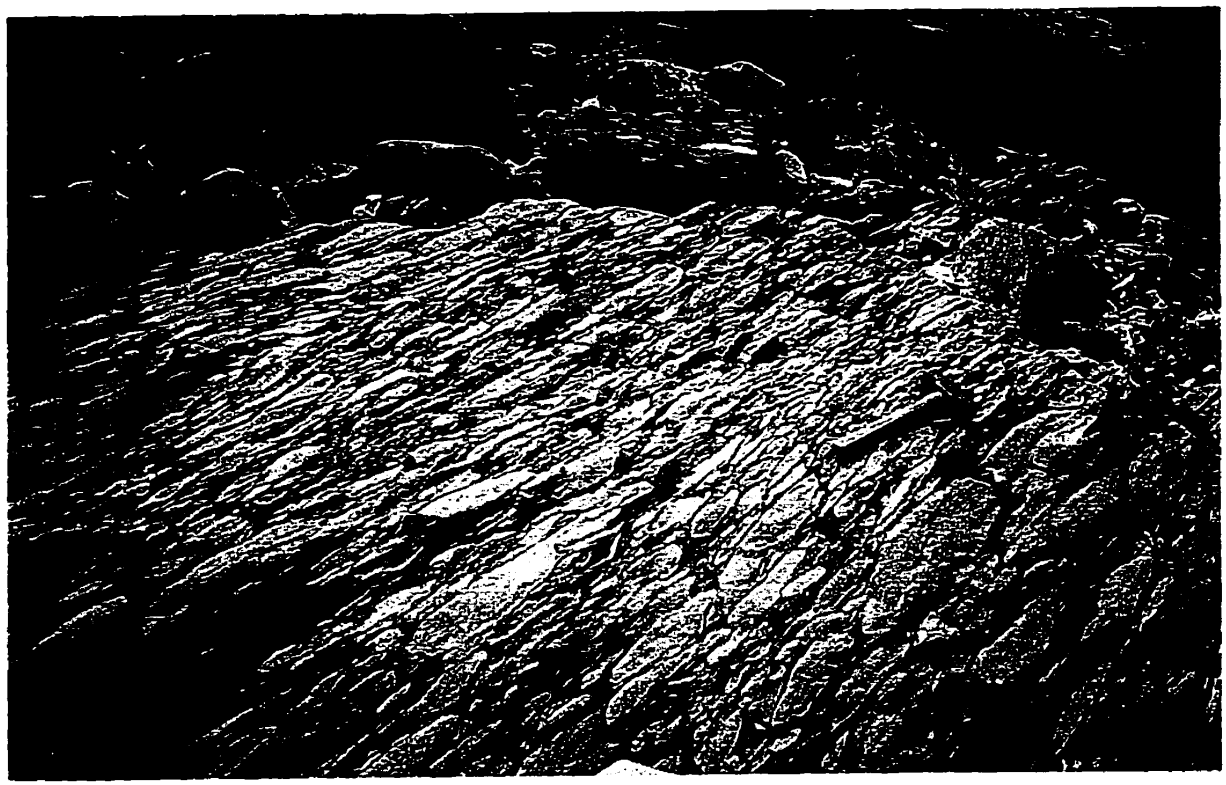

Plate 2.7. Conglomerate layer, unit $Sw_{R_{mf}}$, Cape Forchu West.

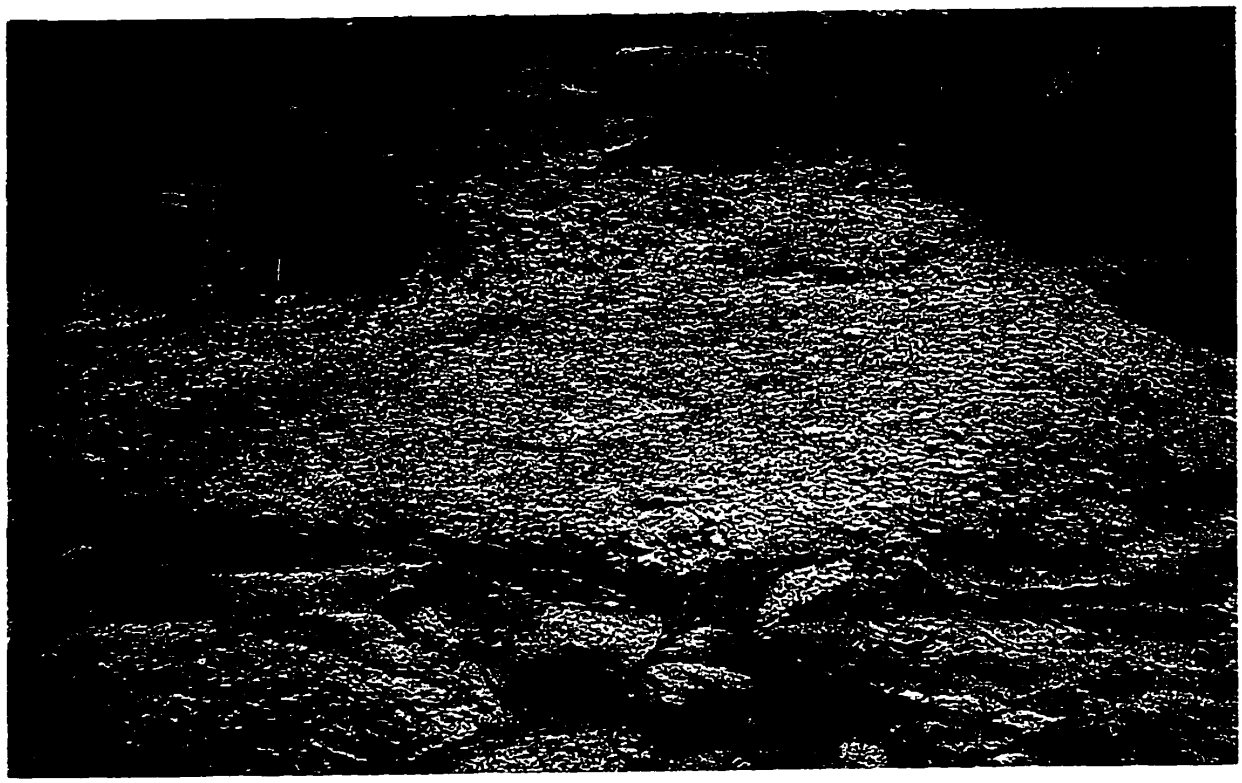

Plate 2.8. Conglomerate clast with amphibole-rich rim, unit Swr_{mf}, Cape Forchu West.

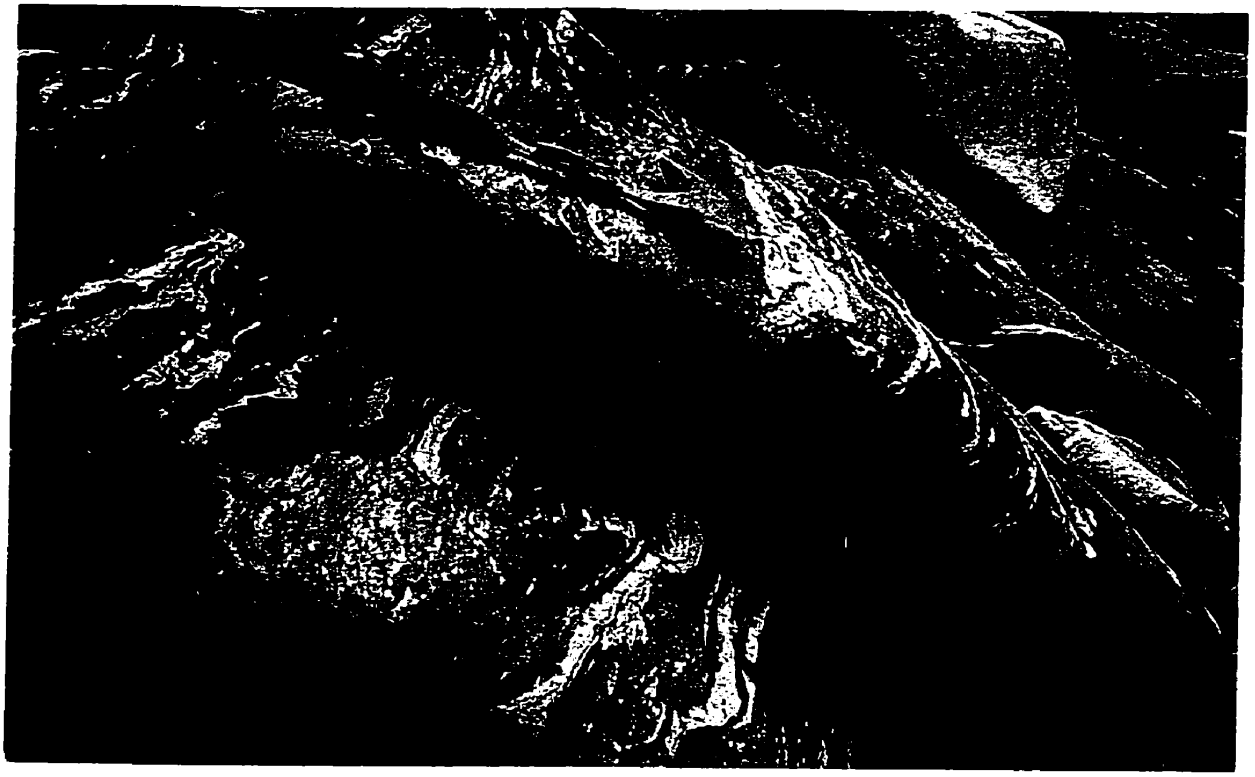

Plate 2.9. Mafic tuff and tuffaceous sandstone, unit Swr_{mf}, Doanes Point.

by a high positive amplitude aeromagnetic signature. As is the case with previous units, inland exposures are typically isolated outcrops with only a few meters of exposed stratigraphy, whereas coastal exposures are almost continuous. The lower part of the unit is exposed at Inner and Outer False Harbour (Cape Forchu West; Fig. 2.4), Sunday Point and Government Brook (Fig. 2.1) and consists predominantly of mafic metavolcanic rocks. The upper part of the unit occurs mainly in scattered outcrops and is less well known.

Bear Island area

At Bear Island in Inner False Harbour, unit S_{WRft} displays a wide range of lithologies over a short distance (< 100 m). The most prominent rock types are lithic tuff, amphibole-rich mafic tuff and basaltic flows. Roadside exposures a few meters north of Bear Island (Fig. 2.4, location j) include fine-grained, dark grey, vesicular basaltic flows with calcite-filled amygdules and abundant, millimeter-scale amphibole porphyroblasts. In contact with the flow is a paler grey, fine-grained layer with much less amphibole and calcite but abundant 1-5 mm clusters of amphibole.

Bear Island is one of only two areas where the nature of the contact with underlying unit S_{WRmf} may be inferred. As was described previously, the mafic tuff and flows at the top of unit S_{WRmf} as seen at Doanes Point are similar to the rock types near Bear Island, indicating a gradational contact. Overall, rocks east of the contact in unit S_{WRft} contain more amphibole and larger amphibole porphyroblasts than rocks west of the contact in unit S_{WRmf}. This location also marks an abrupt change in aeromagnetic

gradient from the low positive to negative amplitude characteristic of unit S_{WRmf} to a high positive signature typical of S_{WRft} (Fig. 2.2).

Also present in the Bear Island area is conglomerate or agglomerate with clasts up to 10 cm long. Some clasts are medium grained and crystalline with fine-grained amphibole porphyroblasts, and others are very fine grained and dark grey. The matrix is also fine grained, grey and contains millimeter-scale amphibole grains. The most easterly part of the outcrop is coarse grained with porphyroblasts of amphibole grading into a finer grained, vesicular rock with small amphibole porphyroblasts and millimeter-scale clusters of amphibole. This rock type grades into lithic tuff which has a very fine-grained, vesicular greenish-grey matrix with bombs. The tuff grades into a fine-grained, green-grey rock with abundant vesicles, which is in contact with a possible conglomerate. The conglomerate has a fine-grained, grey, crystalline matrix with amphibole porphyroblasts and clasts which are very fine grained and dark grey or coarser grained and lighter grey. The coarser grained clasts appear to be composed of lithic tuff as they contain very fine-grained, amphibole-rich, flattened bombs with long "tails" (ends of the bomb appear elongated). The conglomerate grades into a finer grained, grey mafic tuff. The tuff contains medium-grained amphibole porphyroblasts and a clast of crystal tuff approximately 20 cm long. The mafic tuff is interrupted by convoluted bands of medium-grained, light grey rock with amphibole porphyroblasts which hosts angular clasts similar to the mafic tuff bed. The angular clasts may be rip-up clasts as they appear to be fragments of the underlying bed. Also observed are medium-grained, grey-green crystalline beds with abundant millimeter-scale amphibole porphyroblasts which appear to be cross-cut by the convoluted bands. Amphibole

abundance varies greatly across this area, as does grain size. Variation does not appear gradational but in random patches which may juxtapose medium-grained and extremely coarse-grained (up to 3-4 cm) amphibole grains. Veins of quartz and feldspar are abundant in this area.

Also present on Bear Island is an unusual coarse-grained mafic rock of uncertain protolith. The overall appearance is very inhomogeneous, with patches that vary in grain size, crystal form and abundance of amphibole. Grain size of amphibole varies over short distances from medium grained to very coarse grained (2-3 cm). Crystal form ranges from needles to feathers to "stacks". The amount of fine-grained, grey matrix also varies over short distances from approximately <10 % to ~ 30%. Other areas of Bear Island appear tuffaceous with mafic lithic tuff which contains flattened, millimeter-scale, amphibole-rich bombs and a mica-rich (phyllitic), well-cleaved, grey-green layer.

Inner False Harbour

In contrast to the complexity of Bear Island, the coast of Inner False Harbour shows very little variation in lithology because the amount of stratigraphic section exposed is limited due to the closeness of the strike of bedding and trend of the shoreline. The exposed rocks in the area are generally mafic tuffs and flows. On the northwestern shore of Inner False Harbour, medium-grained, green-grey, micaceous tuff with amphibole porphyroblasts grades into green, fine-grained lithic tuff with lighter grey bombs (similar to lithic tuff near Bear Island) (Fig. 2.4, location k). Eastward, the matrix becomes grey and grains in bombs increase in size. Farther east, the tuff grades

into a wacke-like (tuffaceous sandstone?) layer with common, millimeter-scale amphibole porphyroblasts and amygdules (filled with calcite). To the south, mafic-andesitic, fine-grained, green tuff is exposed, interbedded with fine-grained, amphibole-rich layers and lithic tuff with a wacke-like matrix and amygdaloidal bombs (Fig. 2.4, location l). Farther south, the lithic tuff is interbedded with a mafic flow which contains abundant amygdules near the top and fewer amygdules toward the bottom.

Locally along the shore, the flow contains pillow-like structures (Fig. 2.4, location m). They appear flattened, contain amygdules and phenocrysts of plagioclase, and are rimmed by darker, finer-grained micaceous material. The "pillowed" rocks are interbedded with amphibole-rich mafic tuff. More amphibole-rich tuff is exposed to the south but appears coarser grained and has a feldspar-rich matrix. Farther south, lithic tuff appears together again with the coarse-grained, amphibole-rich tuff and a finer grained, green/grey mafic tuff containing biotite clusters and amphibole porphyroblasts. The most southerly outcrops along Inner False Harbour consist of well-bedded layers of fine and medium-grained vesicular, green andesitic tuff above coarse-grained, amphibole-rich layers with calcite-filled amygdules. The coarse-grained, amygdaloidal, amphibole-rich layer grades into medium-grained, micaceous tuff which has abundant centimeter-scale amygdules (filled with feldspar and epidote).

Outer False Harbour

Rocks observed on Cape Forchu West along West Cape and Outer False Harbour are more homogeneous than those exposed near Bear Island. They consist of medium-to coarse-grained, dark grey-green amphibolite with grains of amphibole and

plagioclase. For the most part, the rocks show little variation except for slight differences in amphibole abundance which causes faint banding. Small, centimeter-wide veins of feldspar cut the amphibolite, and green epidote clusters and veins occur in eastern portions of the section (Fig. 2.4, location n).

Government Brook

Government Brook is the location is the second exposure where the nature of the contact between unit S_{WRft} and the underlying unit S_{WRmf} may be inferred. As was the case at Bear Island, the rocks in the upper part of S_{WRmf} and those at the base of unit S_{WRft} are very similar, indicating a gradational contact between the units. This location also coincides with an abrupt change in aeromagnetic amplitude from negative (characteristic of unit S_{WRmf}) to high positive (characteristic of S_{WRft}). The rock type observed near the base of unit S_{WRft} in the western part of Government Brook is fine-grained, green-grey, well-cleaved tuff (?).

Sunday Point

Sunday Point offers an almost complete section of unit S_{WRft} on the eastern limb of the Yarmouth Syncline (Fig. 2.5). In this area, all but the lowest and highest stratigraphic levels are exposed. The easternmost exposure on the point consists of felsic crystal tuff (Fig. 2.5, location a). A series of basalt flows and fine-grained, grey mafic tuff occurs to the west (Fig. 2.5, location b). The felsic rocks appear more foliated than the mafic rocks and have a crystalline matrix with coarse-grained, euhedral plagioclase and K-feldspar porphyroclasts, some of which appear fractured.

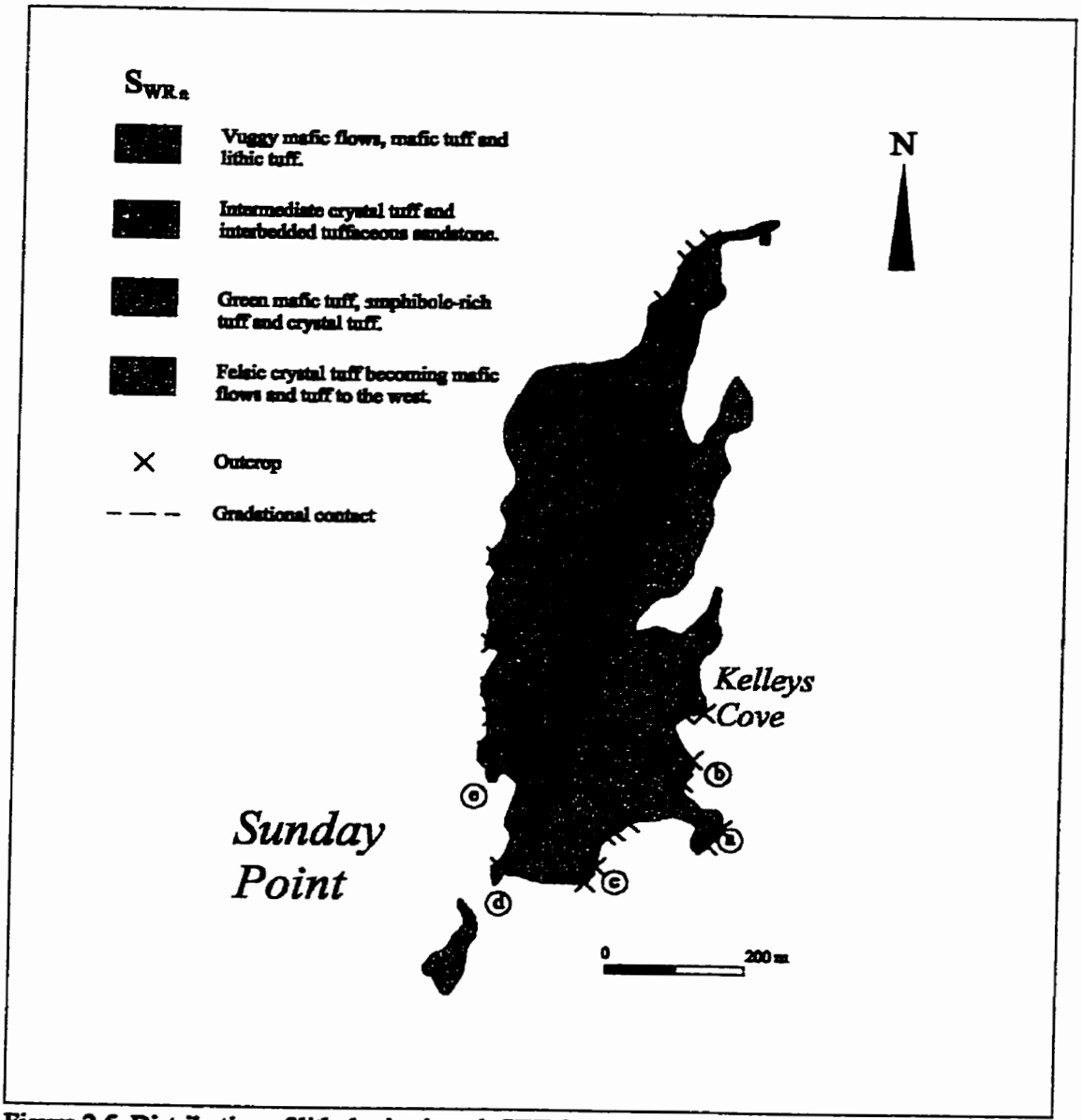

Figure 2.5. Distribution of lithologies in unit SWRft on Sunday Point. Letters a-e are keyed to text.

Approximately 100 m to the west the crystal tuff is intermediate and the plagioclase crystals are larger. Flattened amygdules, euhedral plagioclase phenocrysts up to 1 cm in length, and fine-to medium- grained amphibole porphyroblasts are typical characteristics of the mafic flows. To the west, in sharp contact with the intermediate crystal tuff, is a fine-grained, green mafic tuff overlain by a coarser, amphibole-rich mafic tuff (Fig. 2.5, location c). Westward, the outcrop consists of very fine-grained, laminated (parallel and convolute), well cleaved tuff, interbedded with layers of crystal tuff and amphibole-rich mafic tuff. These layers are in sharp contact with a bed of intermediate crystal tuff (Fig. 2.5, location d). This intermediate crystal layer differs from previous layers in that it contains patches of black, very fine-grained material in sharp but convoluted contact with the crystal tuff (Plate 2.10). The black material may be inclusions of basalt. Within the crystal tuff is a clast of laminated tuffaceous sandstone with irregular contacts (Plate 2.11), as well as clasts of a medium-grained, amphibole-rich rock. The crystal tuff is interbedded with fine-grained, green, laminated tuff and medium-grained, grey, laminated and cross-laminated tuffaceous sandstone.

Westward, vuggy mafic flows with brecciated tops (indicating that the top is to the west) are interbedded with fine-grained, laminated, phyllitic tuff and lithic tuff (Fig. 2.5, location e). Some beds host coarse-grained (<0.5 cm) plagioclase phenocrysts or epidote porphyroblasts. The beds become alternately amphibole-rich and amphibole-poor to the west. Grain size increases and the beds become tuffaceous with laminations and cross-bedding indicating way-up to the west. Approximately 2 km to the north along the coast between Rum Nubble and Sunday Point, medium-grained, grey,

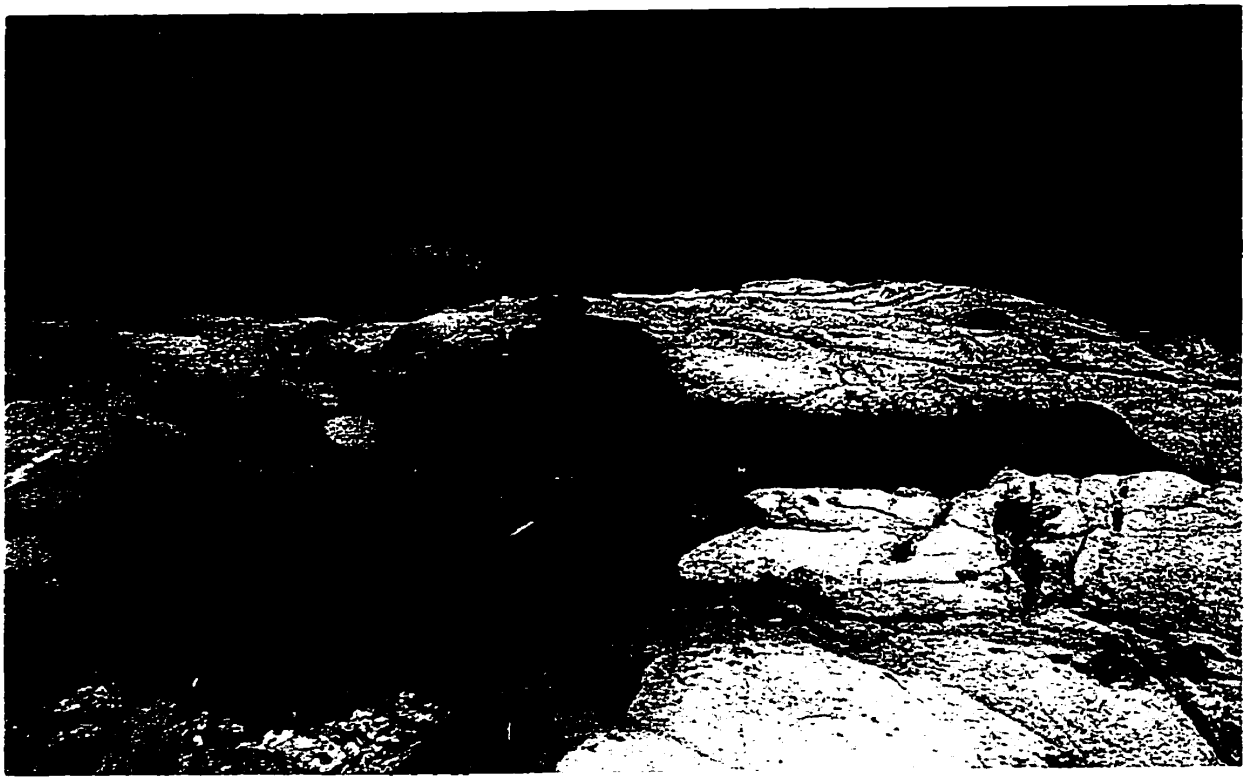

Plate 2.10. Intermediate crystal tuff with basaltic inclusion, unit Swr_{ft}, Sunday Point.

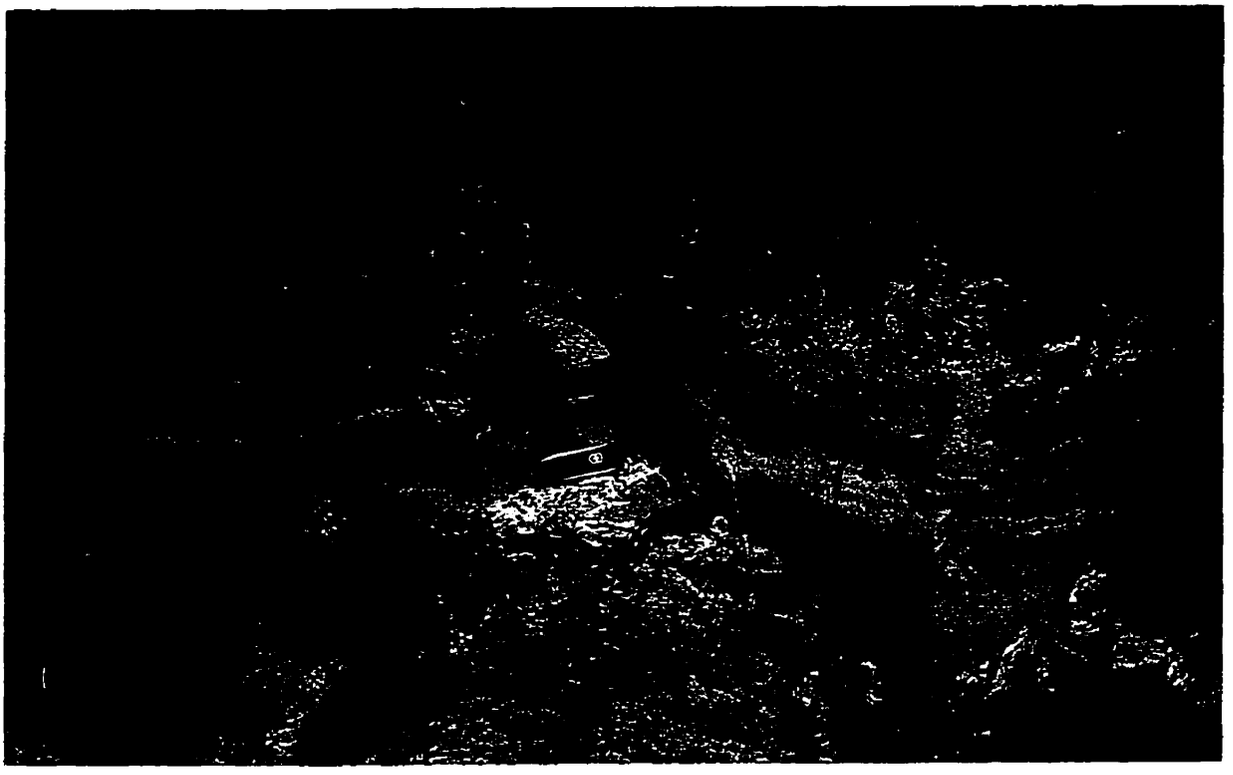

Plate 2.11. Intermediate crystal tuff with clast of laminated tuffaceous sandstone, unit Swr_{ft}, Sunday Point. Coarse-grained crystals in the felsic crystal tuff are plagioclase.

crystalline tuffaceous sandstone occurs, with parallel and cross-laminations marked by mica-rich layers.

Other outcrops of unit S_{WRft}

Outcrops interpreted to be in the middle part of unit S_{WRft} include a location west of Brooklyn on Green Hills Drive (Fig. 2.1) that consists of dark grey, crystalline rock with fine-grained amphibole, and may be a flow. Other lithologies in the middle of unit S_{WRft} include a dark grey phyllite, a mafic flow, and amphibole-rich mafic tuff exposed near the North Ohio Road west of Brenton Lake. It is possible that the rocks interpreted to be the flow and tuff represent a dyke with an amphibole-rich chilled margin, as exposure is limited. On Butler Road near Wellington, an outcrop of dark grey, crystalline tuffaceous sandstone is exposed in contact with a dark grey, crystalline, amphibole-rich mafic tuff.

Outcrops interpreted to be in the upper part of unit S_{WRft} include: (i) an outcrop of mafic tuff on Highway 101 north of Exit 34 which contains biotite porphyroblasts and an amygdaloidal bed with abundant plagioclase, (ii) an outcrop on Highway 340 near Hebron of silty, grey-green tuff with <1 mm scale grains of plagioclase, and (iii) a short section off Starrs Road in Yarmouth that consists of green, mafic tuff with biotite and epidote porphyroblasts.

2.4.6. Unit S_{WRmt}

As in the case of stratigraphically lower units, unit S_{WRmt} is best exposed along the coast, with extensive outcrops at Cape Forchu, Ships Stern, Northern Peak and

Thrum Cap (Fig. 2.1). Most outcrops (especially those along the coast) are in the upper part of the unit and the lower part is poorly represented. The estimated thickness of unit S_{WRmt} is approximately 750 m.

The unit consists predominantly of mafic volcanic rocks with minor sedimentary beds in the upper part. Second derivative aeromagnetic maps show a composite magnetic signature, a background with negative amplitude and local areas of high positive amplitude (Fig. 2.2). Areas of high positive amplitude appear to differ slightly in lithology from areas of low negative amplitude in that they have less varied rock types and lack metasedimentary layers.

Lower parts of unit S_{WRmt}, such as those which outcrop on Rum Nubble, contain possible conglomerate as well as mafic tuff. Fine-grained, green, slaty rocks are interlayered with coarser, crystalline beds containing feldspar porphyroclasts, and conglomerate with fine-grained, green matrix containing abundant amphibole porphyroblasts. The conglomerate contains medium-grained, laminated clasts and fine-grained, dark grey clasts with amphibole porphyroblasts and feldspar phenocrysts. Laminated tuff with crystals of plagioclase is in contact with medium-grained, green, crystalline tuff with porphyroblasts of amphibole. In contact with the crystalline tuff is another layer of conglomerate. Also present is a bed of fine-grained, fissile rock (tuff?) with abundant pyrite and feldspar grains.

Outcrop on Thrum Cap also contains a combination of metavolcanic rocks (lithic tuff) and metasedimentary rocks (tuffaceous sandstone and conglomerate). The lithic tuff has a silty matrix with porphyroblasts of amphibole which are 1-2 mm long, as well as (mafic?) clasts with phenocrysts of plagioclase. The tuffaceous sandstone is

medium grained, with fine bands containing abundant amphibole and biotite. The conglomerate has a well-cleaved, silty, green matrix with amphibole porphyroblasts, and contains three types of clasts: (i) very fine-grained clasts with abundant amphibole and biotite; (ii) crystalline clasts with abundant plagioclase; and (iii) coarser grained clasts which contain abundant amphibole.

Inland outcrops in the lower parts of unit S_{WRmt} have slightly different lithologies than those on the coast. They are predominantly composed of metavolcanic tuff such as the massive, amphibole-rich mafic tuff outcrops on Lake George Road south of Brenton, but also contain mafic tuff (with a medium-grained matrix and plagioclase crystals) with silty laminations such as outcrop on Forest Street in Yarmouth. Outcrop on Highway 1 near Wellington at the base of the unit appears to be a mafic lithic lapilli tuff. Farther up in the sequence on Lakeside Drive near North Chegoggin, the lithic tuff is fine grained, green and contains bombs that are slightly coarser grained and contain euhedral plagioclase phenocrysts. A similar mafic lithic lapilli tuff occurs on the Dayton Road northwest of Dayton but at this location it is paired with a massive, medium-grained mafic tuff. The mafic lithic lapilli tuff is also exposed on Lakeside Drive near South Chegoggin and farther north on this road, the medium-grained, massive mafic tuff is repeated. A massive, medium-grained, crystalline tuff is exposed in an old pit east of Wellington but contains biotite and amphibole porphyroblasts and possible lapilli. Two hundred meters east of the pit the lithology changes to amphibole-rich, micaceous tuff.

Rock in the middle to upper sections of the unit are well exposed at Cape Forchu (Fig. 2.6). The west side of Cape Forchu consists of fine-grained, green mafic tuff with

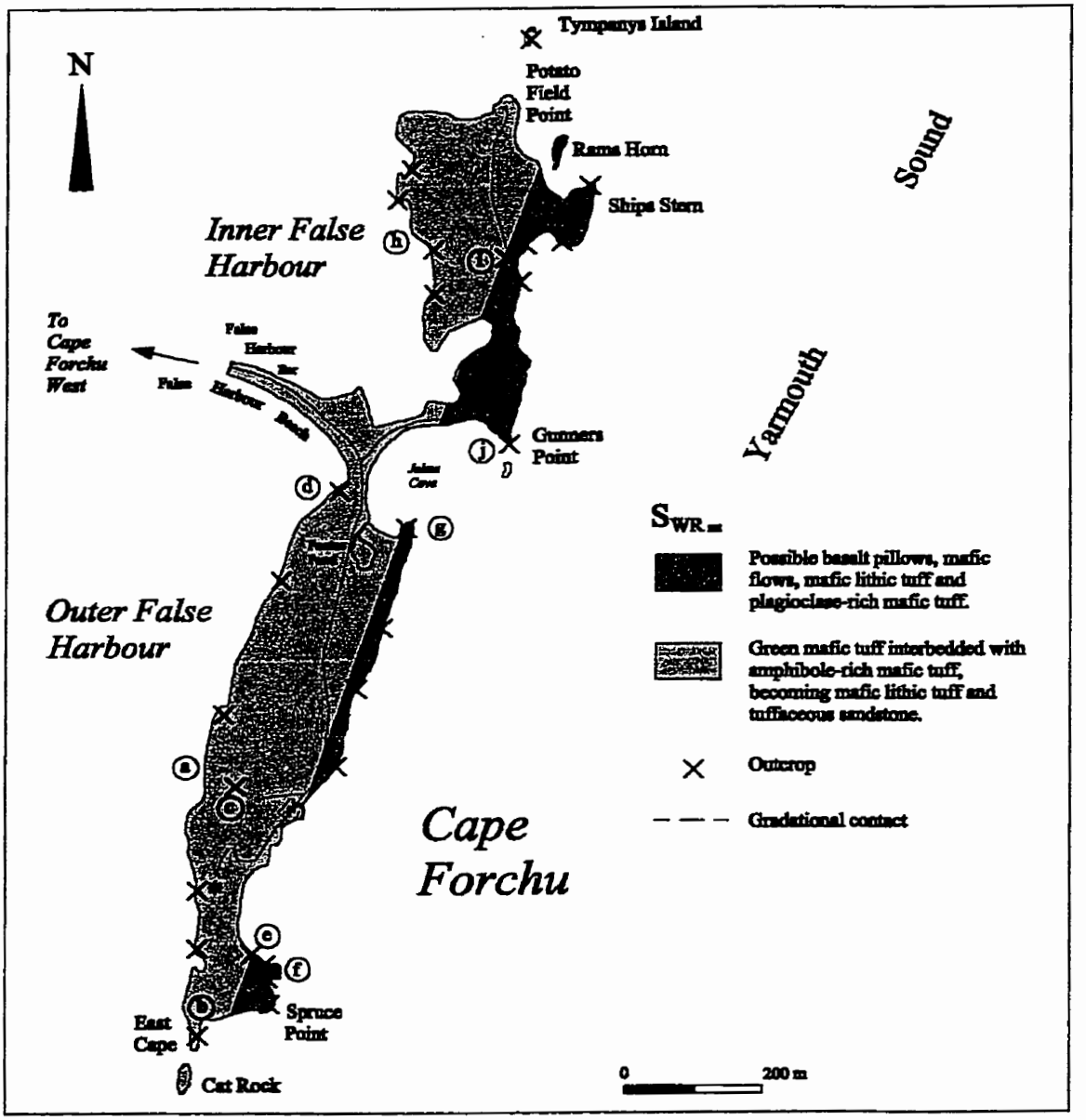

Figure 2.6. Distribution of lithologies in the middle and upper parts of unit SWRmt on Cape Forchu. Letters a-j are keyed to text.

thin amphibole-rich laminae (Plate 2.12) (Fig. 2.6, location a). Fine-grained, grey bombs and lapilli occur in some of the layers (Plate 2.13) (Fig. 2.6, location b) and very fine-grained, grey ash beds are also present. Some bombs provide way-up indicators and show that the top is to the east. Glassy, centimeter-scale, black, pseudotachylite layers also occur within the tuff (Plate 2.14) (Fig. 2.6, location c). Near False Harbour Beach, medium-grained, amphibole-rich mafic tuff layers are interbedded with tuffaceous sandstone and green mafic tuff (Fig. 2.6, location d).

On the east side of Cape Forchu (stratigraphically higher) (Fig. 2.6, location e) the green mafic tuff becomes massive, grey and crystalline, with abundant vesicles and amphibole porphyroblasts, and is possibly a flow. Eastward, the outcrop becomes banded by amphibole-rich mafic tuff layers, followed by a mafic lithic lapilli tuff with a fine-grained matrix. Bombs in the lithic tuff are fine-grained, have abundant calcite amygdules and porphyroblasts of biotite and epidote. Farther east the outcrop appears to be of a mafic tuff or tuffaceous sandstone. It is fine to medium grained and crystalline, with porphyroblasts of amphibole and biotite, and becomes vuggy to the east. It contains calcite-filled amygdules and fine-grained grey bombs. Possible pillows occur east of the tuff (Plate 2.15) (Fig. 2.6, location f). The rocks appear porphyritic with coarse-grained plagioclase phenocrysts and a fine grained crystalline matrix. The pillows are elongate and surrounded by fine-grained, chlorite-rich rims.

Near Johns Cove, the upper part of the unit contains fine-grained, crystalline mafic tuff with biotite and epidote porphyroblasts and with unusually abundant feldspar grains. It is interbedded with layers (approximately 5 cm wide) of tuffaceous sandstone

Plate 2.12. Laminated mafic tuff, unit Swr_{mt}, Cape Forchu.

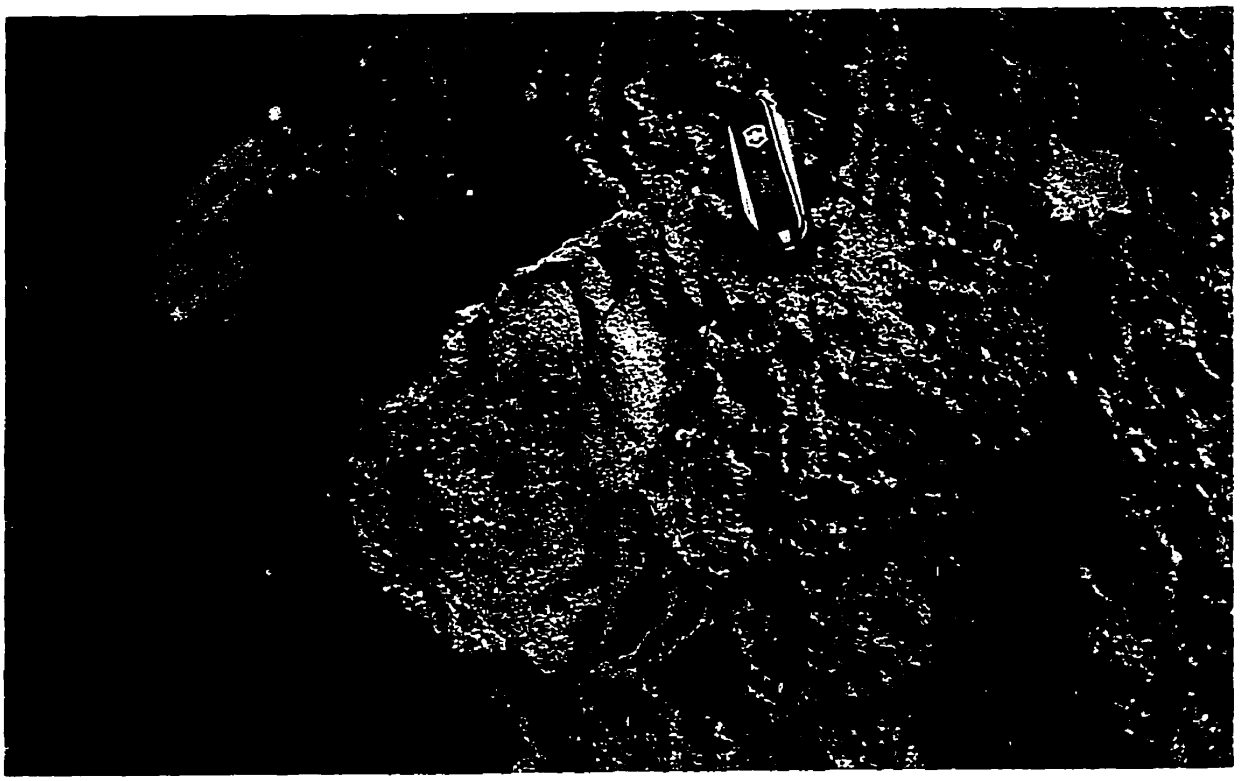

Plate 2.13. Bombs in mafic tuff, unit Swr_{mt}, Cape Forchu. Way up is to the left (east).

Plate 2.14. Pseudotachylite in mafic tuff, unit Swr_{mt}, Cape Forchu.

(a)

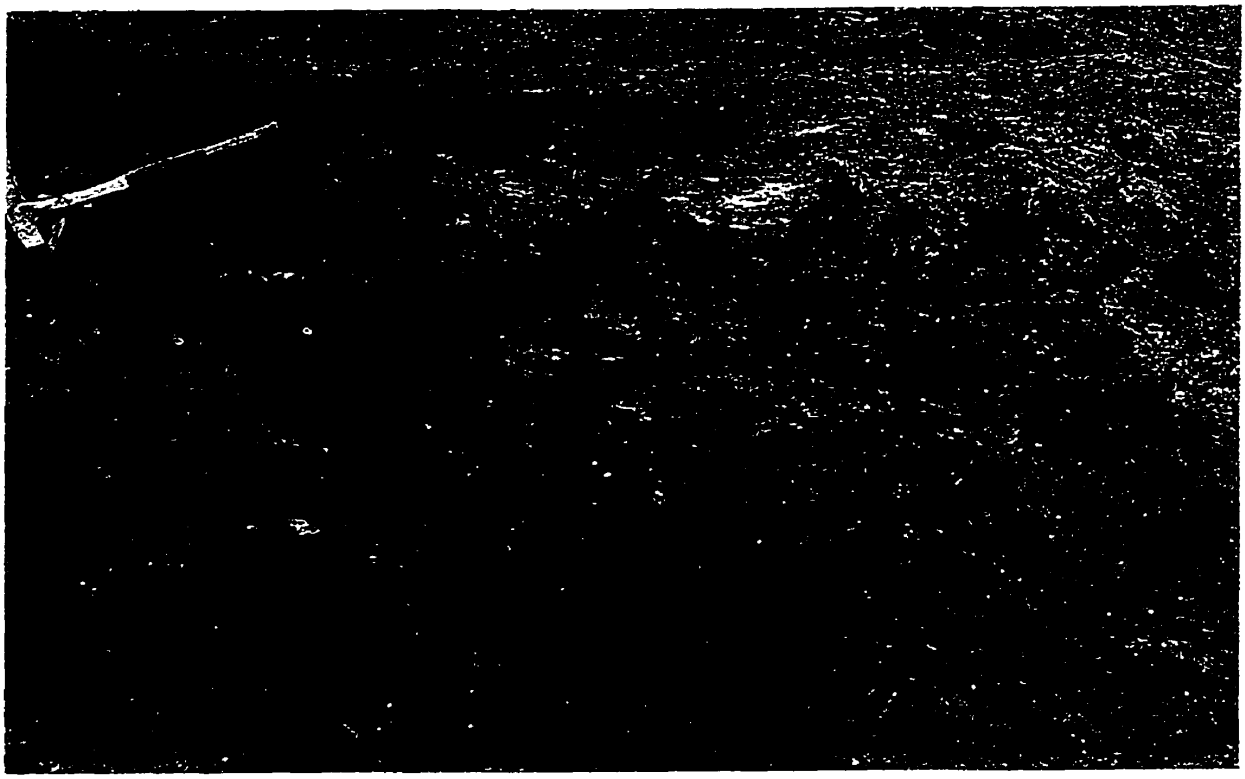

Plate 2.15a. Possible basalt pillows, unit Swr_{mf}, Cape Forchu.

(b)

Plate 2.15b. Possible basalt pillows, unit Swr_{mf}, Cape Forchu.

and mafic lithic tuff (Fig. 2.6, location g). The mafic lithic tuff has a fine-to medium-grained, micaceous matrix and flattened, epidote-rich bombs.

The northern peninsula of Cape Forchu contains rocks similar to those on the southern peninsula, except for the absence of green mafic tuff. Interbedded mafic tuff, mafic lithic tuff, flows and tuffaceous sandstone are typical. The lower sections exposed on the west side are mainly mafic, biotite and amphibole-rich, massive flows and banded tuff (Fig. 2.6, location h), overlain by interbedded medium-to coarse-grained, amphibole-rich mafic tuff, medium-grained, grey, massive tuffaceous sandstone and lithic tuff (as seen on Tympanys Island). Outcrops on Lobster Pound Road expose medium-grained mafic flows with amphibole porphyroblasts and euhedral plagioclase phenocrysts (Fig. 2.6, location i). The upper section of the unit, as seen at Gunners Point and Ships Stern, consists of mafic tuff, lithic tuff, plagioclase-rich mafic tuff (like that at Footes Pond) and tuffaceous sandstone (Fig. 2.6, location j).

Northward, the unit contains only tuffaceous lithologies. Near Johnsons Point, it consists of bands of medium-to coarse-grained, amphibole-rich mafic tuff interbedded with medium-grained, grey, crystalline tuff, and mafic tuff with very large crystals of plagioclase and finer grained biotite-rich interbeds. Also present is mafic lithic lapilli tuff with a coarse-grained, grey, crystalline matrix and amphibole and biotite porphyroblasts, as well as fine-grained, grey, flattened lapilli. Farther north, mafic lithic tuff beds contain light grey bombs up to 30 cm long with fine-grained phenocrysts of plagioclase. The matrix of the lithic tuff contains coarse-grained (approximately 1 cm long) amphibole porphyroblasts. Farther north, two types of lithic tuff are exposed. Both have a fine-grained matrix but the first contains fine-grained amphibole

porphyroblasts whereas the second has plagioclase phenocrysts and coarse amphibole. Both types of tuff contain flattened bombs, 3-5 cm in length, which are slightly more abundant in the coarse-grained tuff. The tuffs also contain rare megacrysts (up to 10 cm long) of plagioclase. Continuing north, the outcrop is grey to black, crystalline rock which hosts very abundant coarse-grained amphibole porphyroblasts. Western portions of the outcrop contain mafic lithic tuff with unusual "pods" of plagioclase which are up to 40 cm long.

Similar lithologies occur farther north near Northern Peak. At Northern Peak the outcrop is comprised of grey, crystalline tuffaceous sandstone, interbedded with amphibole-rich mafic tuff and mafic lapilli tuff layers (Plate 2.16). Bombs in the lithic tuff are typically fine grained, grey-green and reach 5 cm in length. The amphibole-rich tuff layers range from medium to coarse grained, and amphibole abundance varies significantly between beds. The lithic tuff matrix is amphibole-rich and the bombs have amphibole-rich rims and cores with an intervening feldspar-rich layer (Plate 2.17). Southwest of the peak the exposures are of medium-grained, finely laminated tuffaceous sandstone that become interbedded with amphibole-rich mafic tuff in the south.

The upper part of unit S_{WRmt} contains metasedimentary as well as metavolcanic rocks. Near the central fault of the Yarmouth Syncline at the waterfall by the dam at the north end of Doctors Lake, the unit contains metasandstone or tuffaceous sandstone. The rocks are massive, medium grained, and contain abundant mica. Laminations can be seen on the weathered surface and millimeter-scale grains of feldspar (or quartz?) are also present. Not all outcrops contain both metasedimentary and metavolcanic rocks.

(a)

Plate 2.16a. Interbedded tuffaceous sandstone, amphibole-rich mafic tuff and mafic lapilli tuff, unit Swr_{mt}, Northern Peak.

(b)

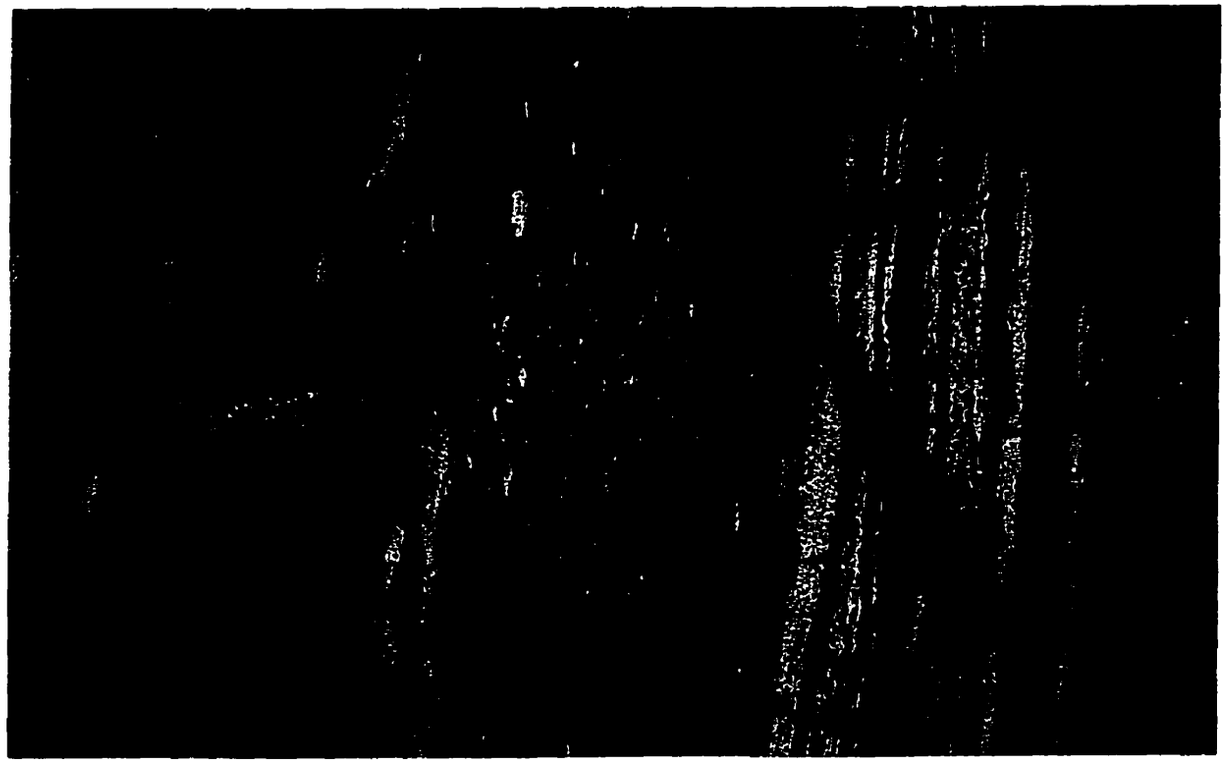

Plate 2.16b. Interbedded tuffaceous sandstone, amphibole-rich mafic tuff and mafic lapilli tuff, unit Swr_{mt}, Northern Peak.

Plate 2.17. Amphibole-rich rim and core of a mafic bomb, unit Swr_{mt}, Northern Peak.

On Crosby Court east of Doctors Lake, the exposure is fine grained, grey-green, well-cleaved rock with porphyroblasts of amphibole. A massive, medium-grained, micaceous tuff or flow is exposed along a private road north of Bunkers Lake. Mafic lithic tuff with a green-grey, fine-grained, micaceous matrix and amphibole needles and lapilli-to bomb-sized clasts with abundant plagioclase occur at many locations, including along a road west of Bunkers Lake, and along Highway 101 (north of Exit 34). An outcrop of black slate with millimeter-sized porphyroblasts of chloritoid is located beside Highway 1, east of Second Lake.

Areas of unit S_{WRmt} with high positive amplitude aeromagnetic signatures appear to coincide with mafic tuff and flows. Mafic lithic tuff southwest of Northern Peak has centimeter-scale beds of fine-and coarse-grained amphibole with centimeter-scale, fine-grained bombs. Outcrop on Lakeside Drive west of Doctors Lake are green-grey, massive, tuff or flows at the west end and fine-grained tuff with coarse-grained amphibole porphyroblasts in the east. A ridge on the road to Sunday Lake is fine grained and strongly foliated, with medium-grained porphyroblasts of sulphide minerals (pyrite?). North of Bunkers Lake on Meadowbrook Road, the unit contains beds of amphibole-rich and amphibole-poor mafic tuff. Grey-green, fine-grained, cleaved tuff or flow with amphibole porphyroblasts and < 0.5 cm crystals of plagioclase occurs on the Cemetery Road, north of Hebron.

2.4.7. Unit S_{WRmv}

Unit S_{WRmv} is the uppermost unit in the White Rock Formation in the Yarmouth area. It is not well exposed and its extent is largely defined by geophysical

characteristics. Second vertical derivative aeromagnetic data show a distinct region with high magnetic signature at the core of the syncline (Fig. 2.2). Mapping showed that this area is underlain by mafic tuff and flows. At Bunker Island, outcrop is mafic lithic tuff with a fine-grained, light grey matrix with coarse-grained amphibole porphyroblasts. The bombs appear flattened and contain a very fine-grained matrix and fine-grained amphibole. Some bombs have medium-grained amphibole in their cores and others contain phenocrysts of plagioclase. Outcrop on the west side of Lake Milo includes a fine-grained possible flow-type rock with abundant biotite porphyroblasts and rare amygdules, and fine grained, well-cleaved tuff with vesicles, biotite porphyroblasts and laminations. The unit also contains massive, green-grey, medium-grained possible flows with coarse-grained, euhedral plagioclase phenocrysts as seen on Lakeside Drive.

2.5. Mafic Sills and Dykes

Mafic sills and dykes occur in both the Halifax and White Rock formations in the Yarmouth area. In this study, the term sill describes an intrusion which is bedding or layering parallel, and dyke describes an intrusion which cuts bedding or layering. Both dykes and sills were observed at Cranberry Head, Chegoggin Point, Overton, Cape Forchu West, Cape Forchu, and Chebogue Point. They are difficult to recognize in the generally smaller inland exposures, but were observed near exit 34 on Highway 101 in unit S_{WRmv} and in a brook south of Pleasant Valley in the Halifax Formation.

Like other rocks in the study area, the mafic dykes and sills have been affected by metamorphism and deformation. The rocks have been recrystallized and are typically medium to coarse grained and contain abundant amphibole, although some retain coarse

grained plagioclase grains (relict phenocrysts). Most sills and dykes are between 0.5 and 3 m wide. At Cape Forchu West, Chegoggin Point, Overton, and Chebogue Point dykes are boudinaged and extensively cross-cut by quartz and feldspar veins. Some dykes and sills (Cape Forchu and Highway 101) are finer grained and less amphibole-rich and have abundant sulphide porphyroblasts. Many of the dykes have chilled margins which are marked by finer grain size and colour change. Beneath the Cape Forchu lighthouse the green tuff is cross-cut by a mafic (basaltic) dyke (Plate 2.18) which is medium grained and contains abundant amphibole and feldspar grains near the centre. Chilled margins are indicated by increasing abundance of amygdules, finer grain size and colour change from grey to green.

An unusual dyke occurs in unit S_{WRss} north of Chegoggin Point. The dyke has a narrow chilled margin (< 15 cm wide) which, at the contact with the country rock, consists almost completely of garnet. A few centimeters away from the contact, the dyke contains abundant, 1-1.5 cm long idioblastic garnet porphyroblasts. The centre of the dyke is coarser grained that the margin and contains medium-to coarse-grained garnet in a matrix with abundant biotite.

2.6. Brenton Pluton

The extent of the Brenton Pluton is difficult to establish as it is not well exposed and shows no distinct signature on the second vertical derivative aeromagnetic maps (Fig. 2.2). The area of the pluton is estimated from sparse outcrop and compilation of data from earlier maps (O'Reilly, 1976; Hwang, 1985). Outcrops of the Brenton Pluton occur in a quarry and on logging/access roads off Hardscratch Road, as well as in

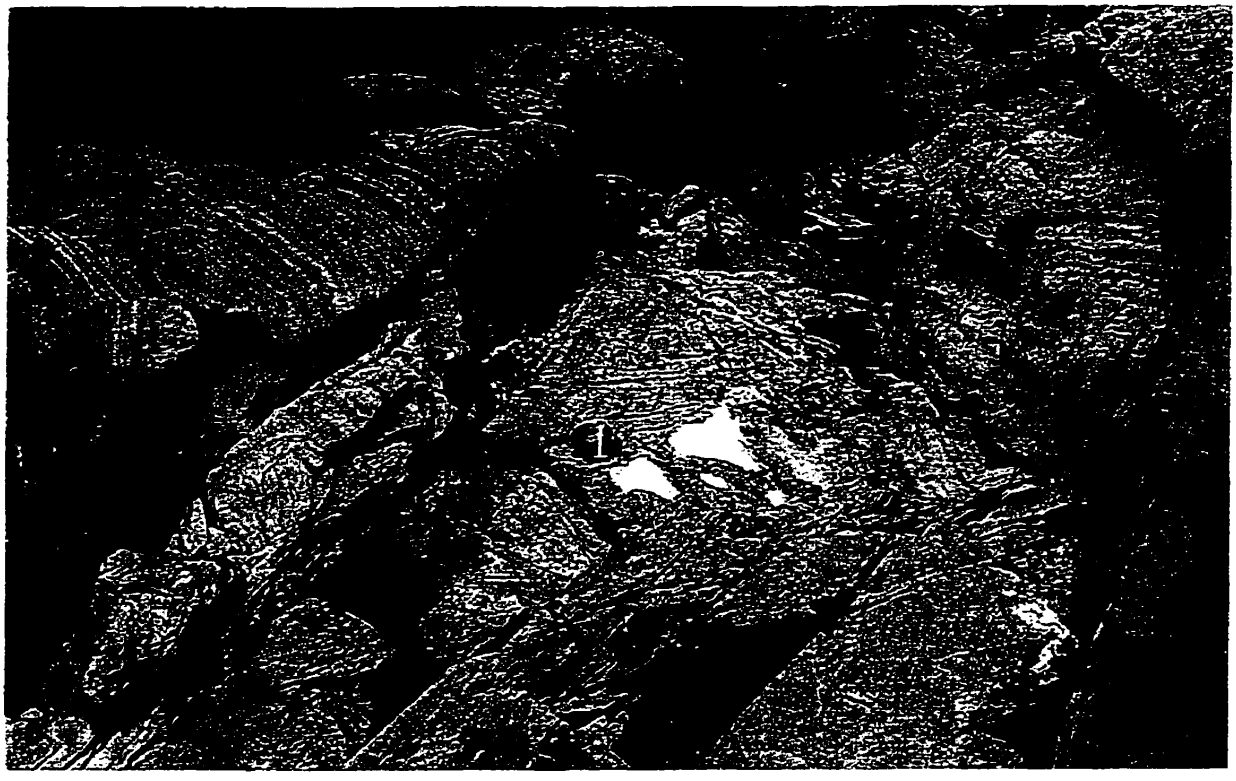

Plate 2.18. Mafic dyke intruding interbedded mafic tuff, unit Swr_{mt}, Cape Forchu.

private yards on Pitman Road. O'Reilly (1976) reported an outcrop near Churchills Mill Lake but this outcrop was not found in 1998.

The pluton appears to be in faulted contact with both the White Rock and Halifax formations, as interpreted from the schistose nature of the rocks in Government Brook and observed brecciation and shearing of metasedimentary rocks at Churchills Mill Lake and Deerfield dam. No evidence of contact metamorphism was observed in the outcrop of unit S_{WRss} adjacent to the pluton in Government Brook. O'Reilly (1976) reported a narrow thermal aureole at the southern tip of the pluton, marked by a decrease in metamorphic grade of the country rock from garnet and/or staurolite schist near the contact to chlorite schist approximately 50 m away from the contact. These outcrops were not found during the present study.

In all outcrops, the pluton consists of strongly foliated monzogranite with no difference between exposures except for varying degree of weathering. Only the quarry contains fresh, white outcrop; all others are weathered and slightly hematitized. The foliation trends northeast, parallel to the inferred faulted margins of the pluton and regional foliation observed in the adjacent White Rock Formation.

Chapter 3 Petrography

3.1. Introduction

The purpose of this chapter is to describe the petrography of the White Rock Formation, associated mafic sills and dykes and the Brenton Pluton. Metamorphism and deformation have generally changed the original igneous or sedimentary minerals and textures of the rocks and replaced them with metamorphic minerals and textures. Nevertheless, it is generally possible to infer the original protolith based on field observations combined with examination of slabbed hand specimen and thin section. For the purposes of petrographic description and to avoid repetition, the samples are grouped according to the probable protolith, rather than by map unit.

The petrographic descriptions are based on examination of 79 thin sections; petrographic features of individual samples are tabulated in Appendix A. Microprobe analyses of minerals in representative samples are presented in Appendix B. Sample locations are shown on Figure 3.1 (in pocket).

3.2. White Rock Formation

3.2.1. Metasedimentary Rocks

Metasedimentary rocks in the White Rock Formation in the study area include quartzite, metaconglomerate, slate, metasiltstone, schist, and tuffaceous metasandstone. Typical samples of slate, schist and tuffaceous metasandstone were collected for petrographic study and described here.

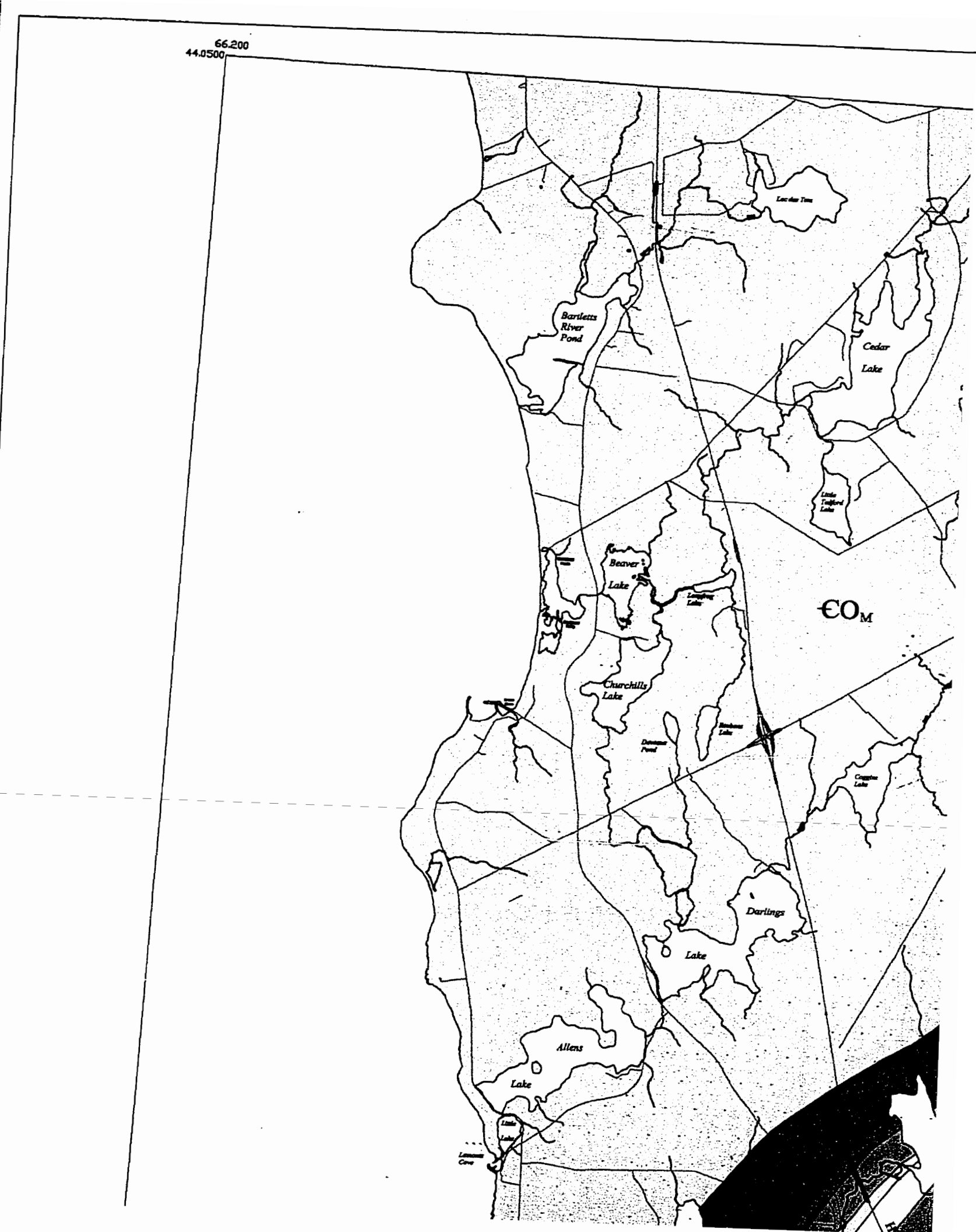
66.200
44.0500
Bartletts River Pond
Cedar Lake
Beaver Lake
Churchills Lake
Darlings Lake
Allens Lake

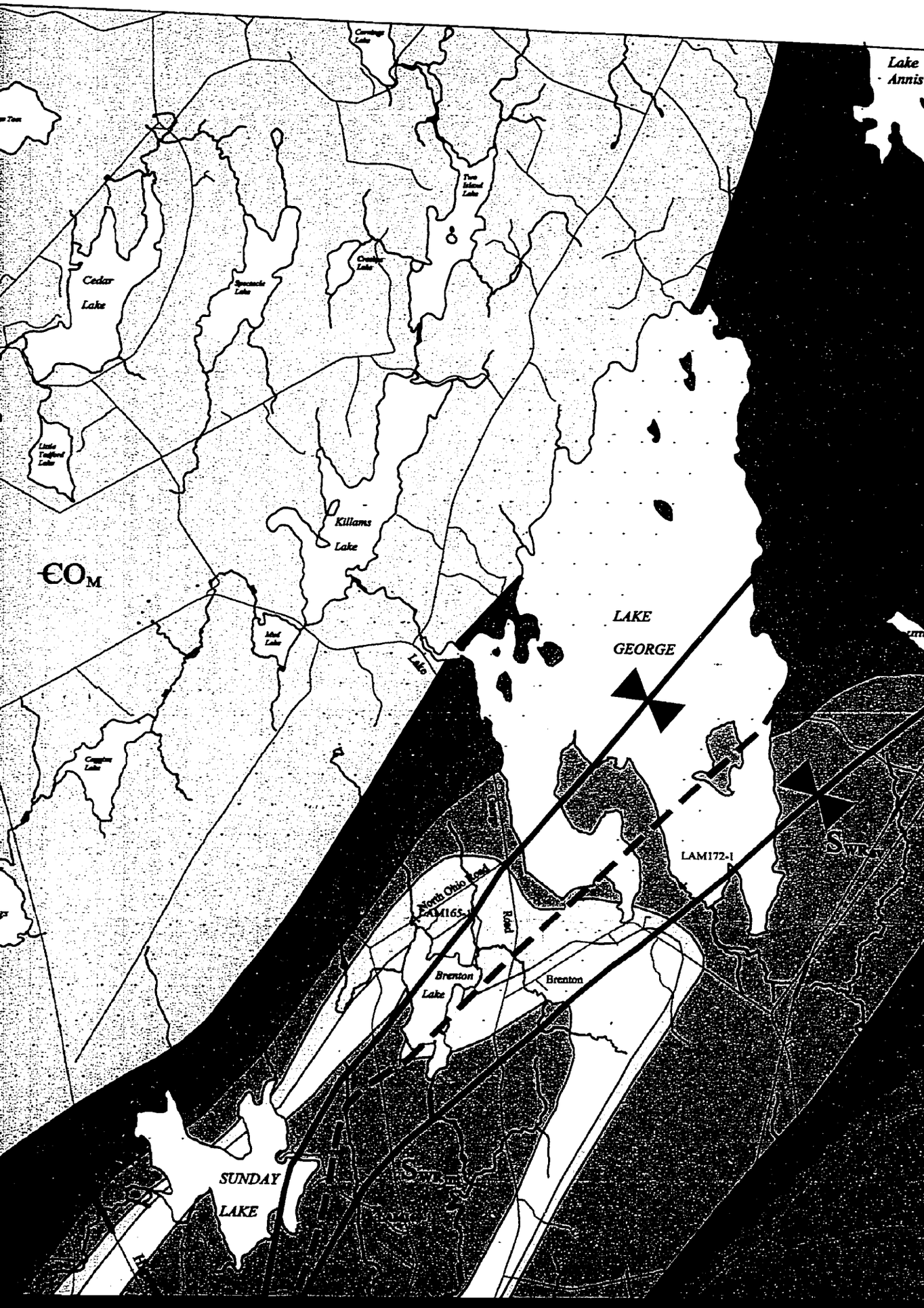
Cedar
Lake
Killams
Lake
LAKE
GEORGE
LAM172-1
North Ohio Road
LAM165-1
Brenton
Lake
Brenton
SUNDAY
LAKE

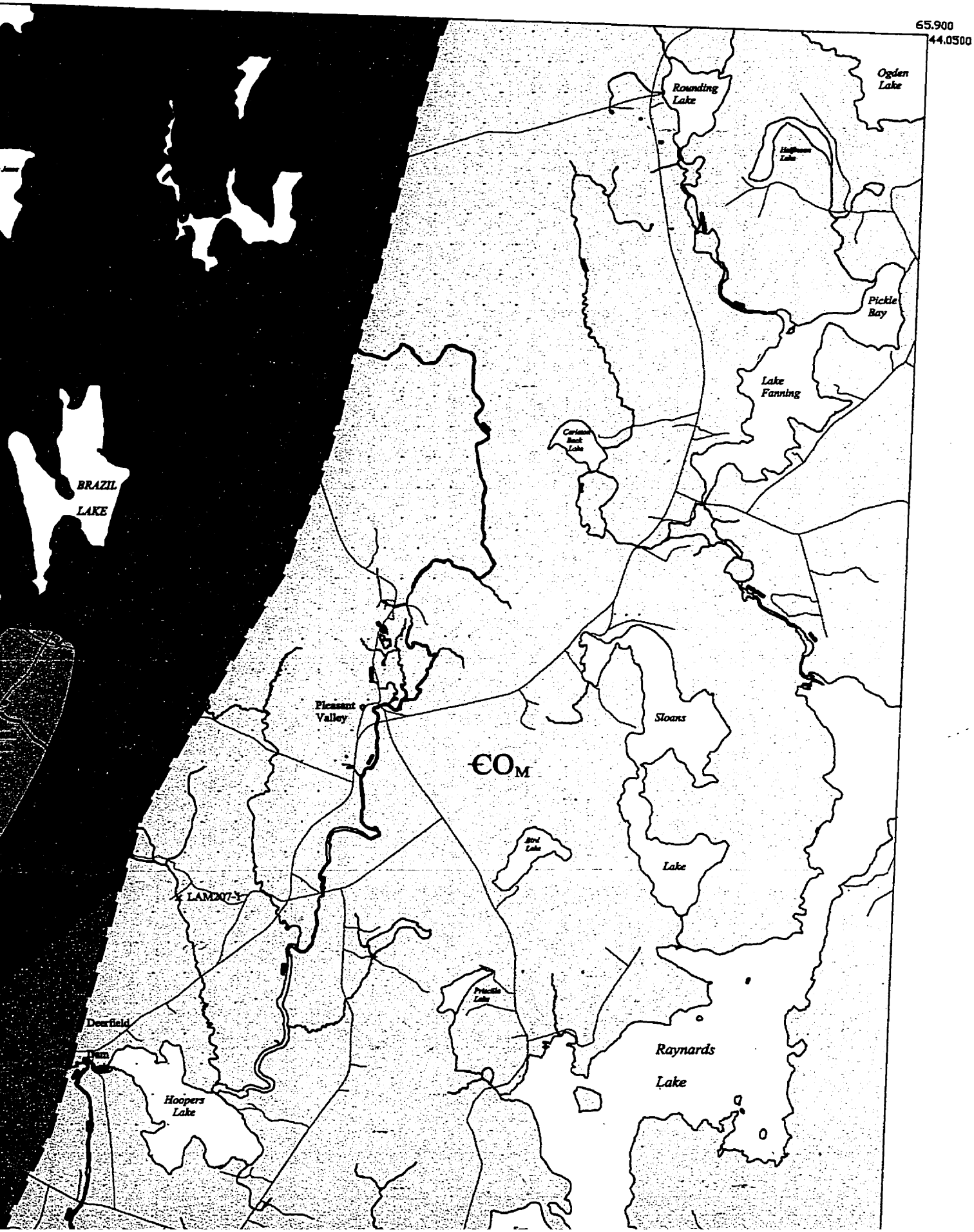
65.900
44.0500
Rounding Lake
Ogden Lake
Pickle Bay
Lake Fanning
BRAZIL LAKE
Pleasant Valley
Sloans
Lake
LAM207-1
Deerfield
Dam
Hoopers Lake
Raynards Lake

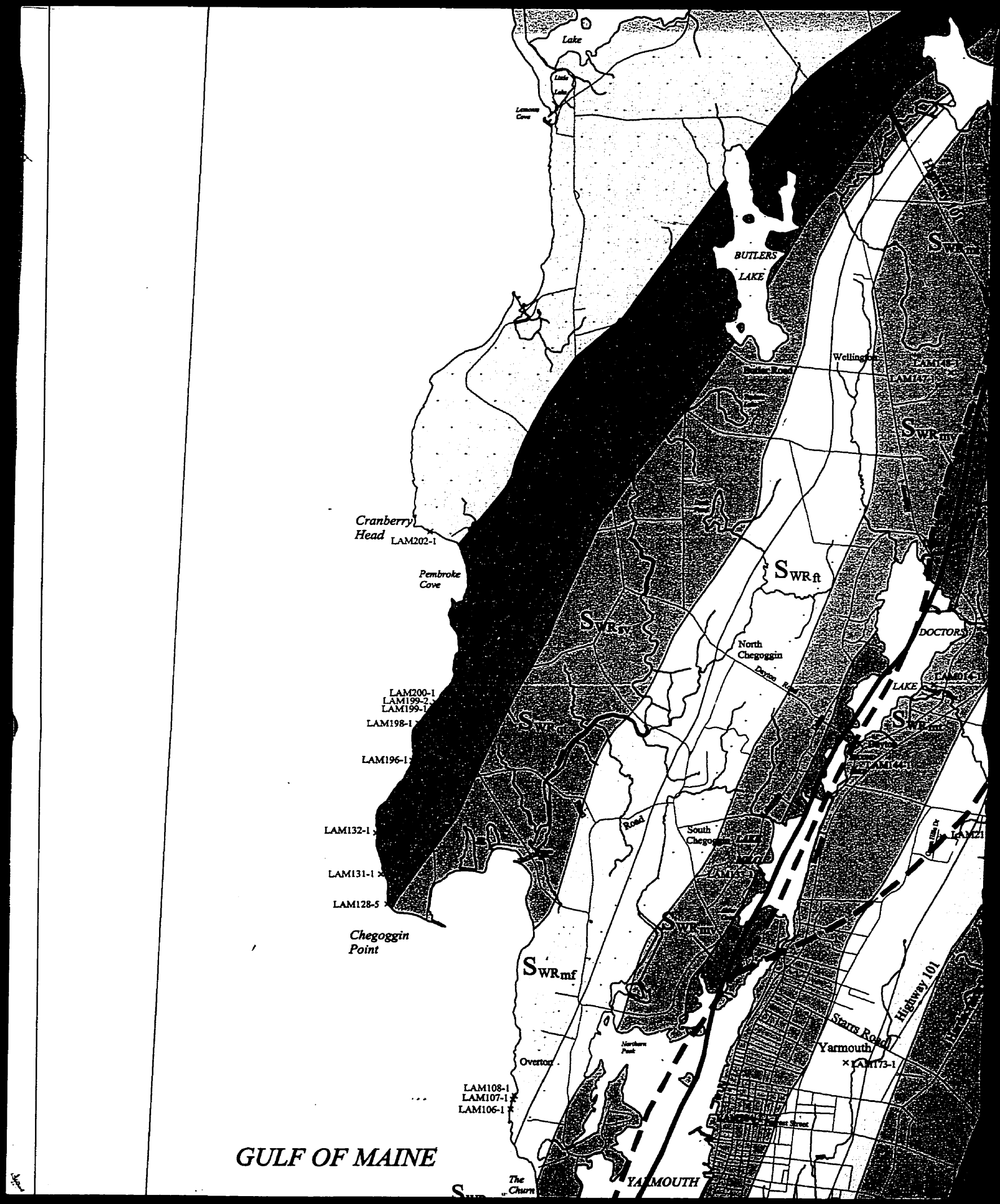
Lake
Lemons Cove
BUTLERS
LAKE
Wellington
Cranberry
Head
LAM202-1
Pembroke
Cove
North
Chegoggin
DOCTORS
LAM200-1
LAM199-2
LAM199-1
LAM198-1
LAM196-1
LAM132-1
LAM131-1
LAM128-5
Chegoggin
Point
South
Chegoggin
Overton
LAM108-1
LAM107-1
LAM106-1
Yarmouth
LAM173-1
Highway 101
Starrs Road
GULF OF MAINE
YARMOUTH
The
Churn

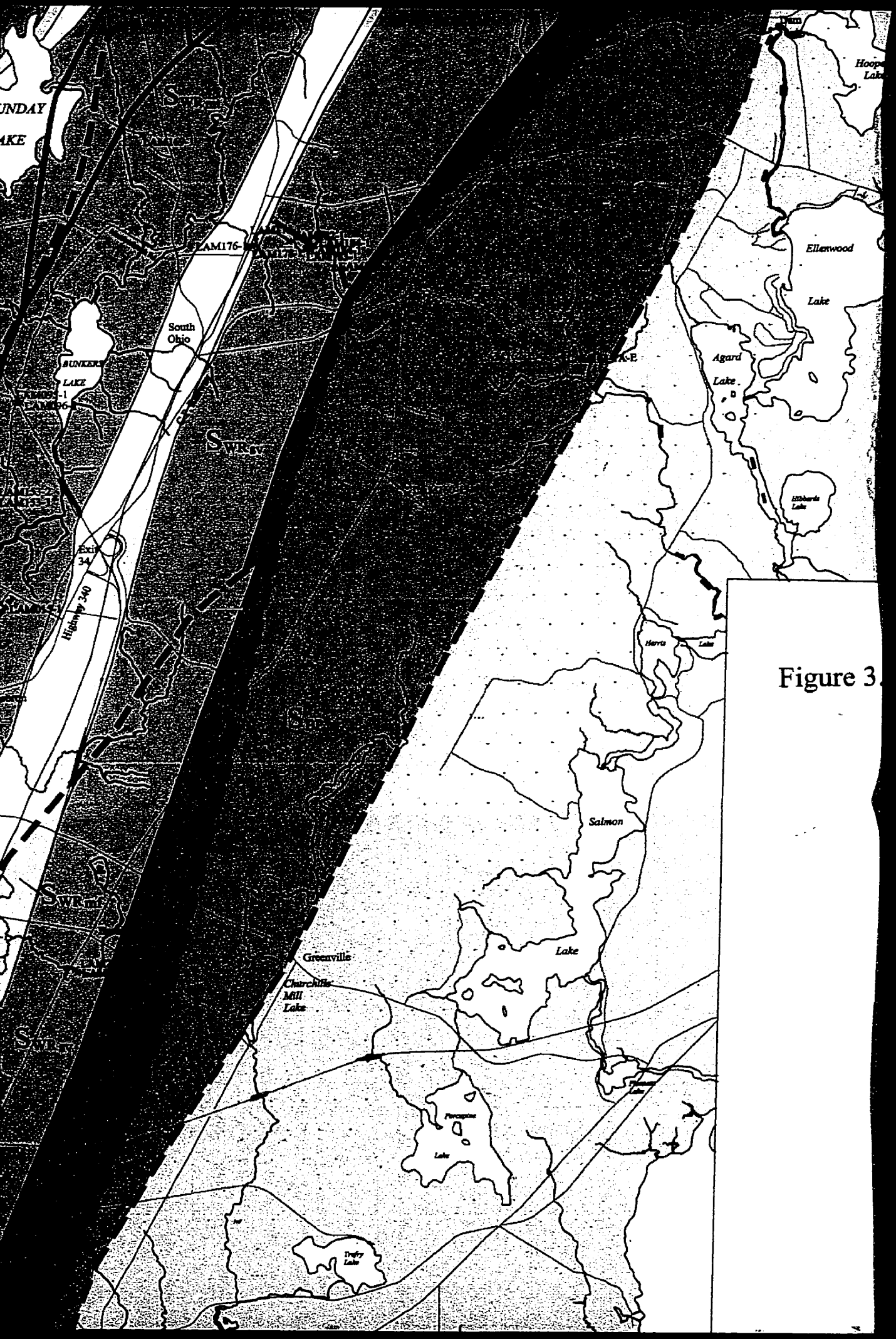
Ellenwood
Lake
Agard
Lake
Salmon
Lake
Greenville
Churchills
Mill
Lake
South
Ohio
Exit
34
Highway 340

Figure 3.

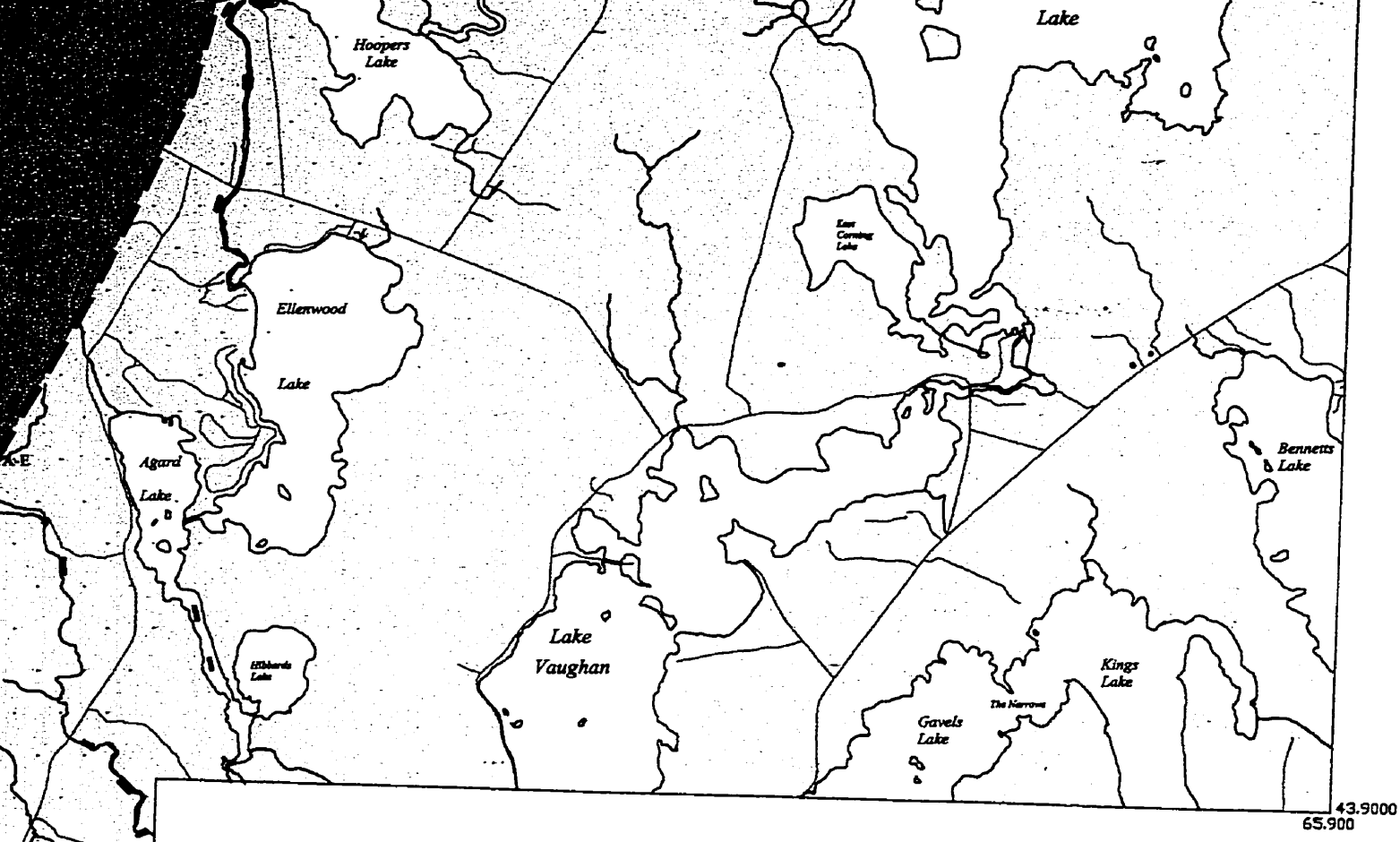

Figure 3.1. Location map for thin sections and geochemical samples.

SYMBOLS

LAM205-1 × Thin section sample location

LAM205-1 × Geochemical sample location

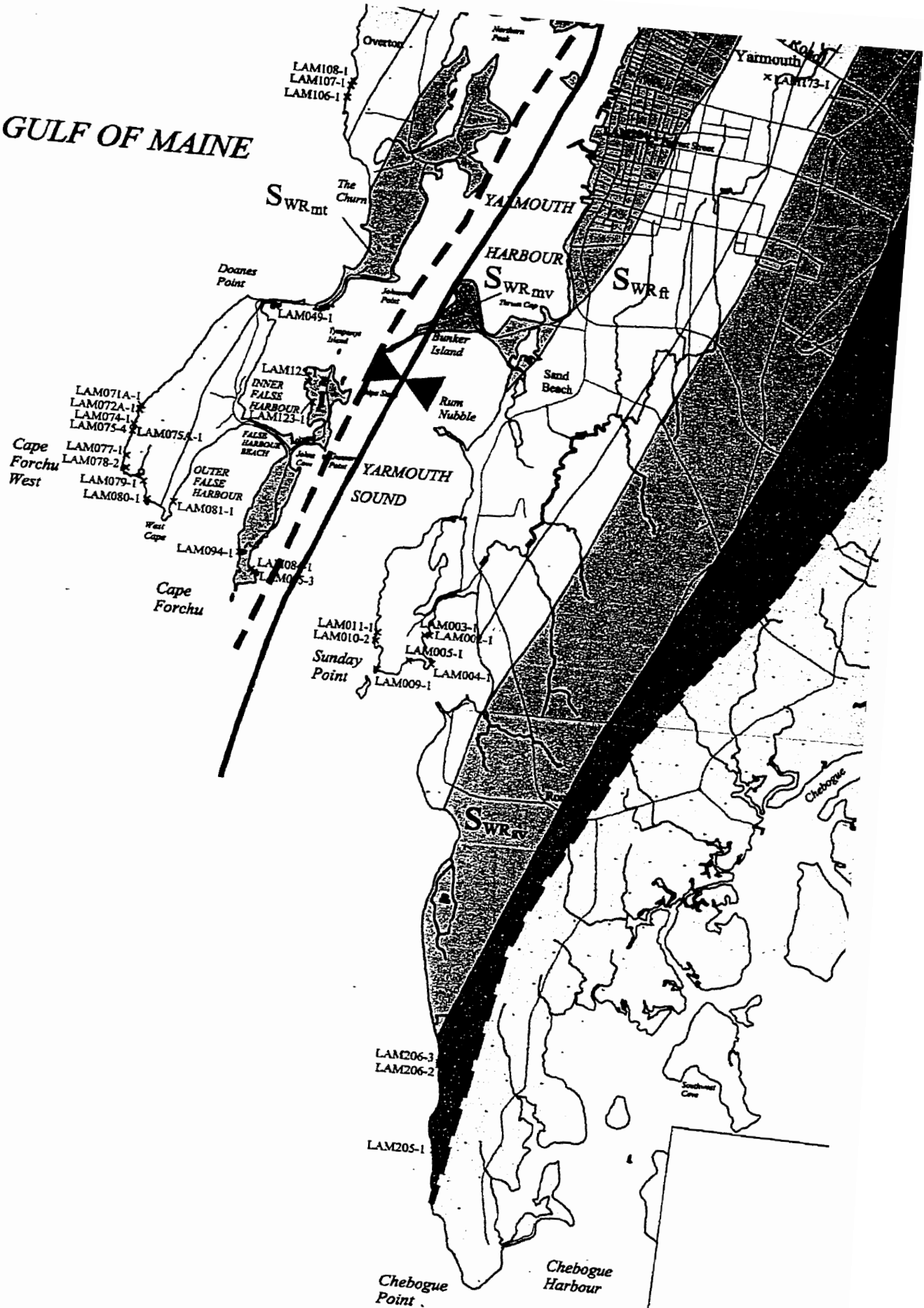
GULF OF MAINE
Overton
LAM108-1
LAM107-1
LAM106-1
Yarmouth
LAM173-1
SWR mt
The Churn
YARMOUTH HARBOUR
SWR mv
SWR ft
Doanes Point
LAM049-1
Bunker Island
Sand Beach
Rum Nubble
LAM125-1
INNER FALSE HARBOUR
LAM123-1
LAM071A-1
LAM072A-1
LAM074-1
LAM075-4
LAM075A-1
FALSE HARBOUR BEACH
Cape Forchu West
LAM077-1
LAM078-2
LAM079-1
LAM080-1
OUTER FALSE HARBOUR
LAM081-1
West Cape
YARMOUTH SOUND
LAM094-1
Cape Forchu
LAM011-1
LAM010-2
LAM003-1
LAM005-1
LAM004-1
Sunday Point
LAM009-1
SWR rv
Chebogue
LAM206-3
LAM206-2
LAM205-1
Chebogue Point
Chebogue Harbour

1: 50 000

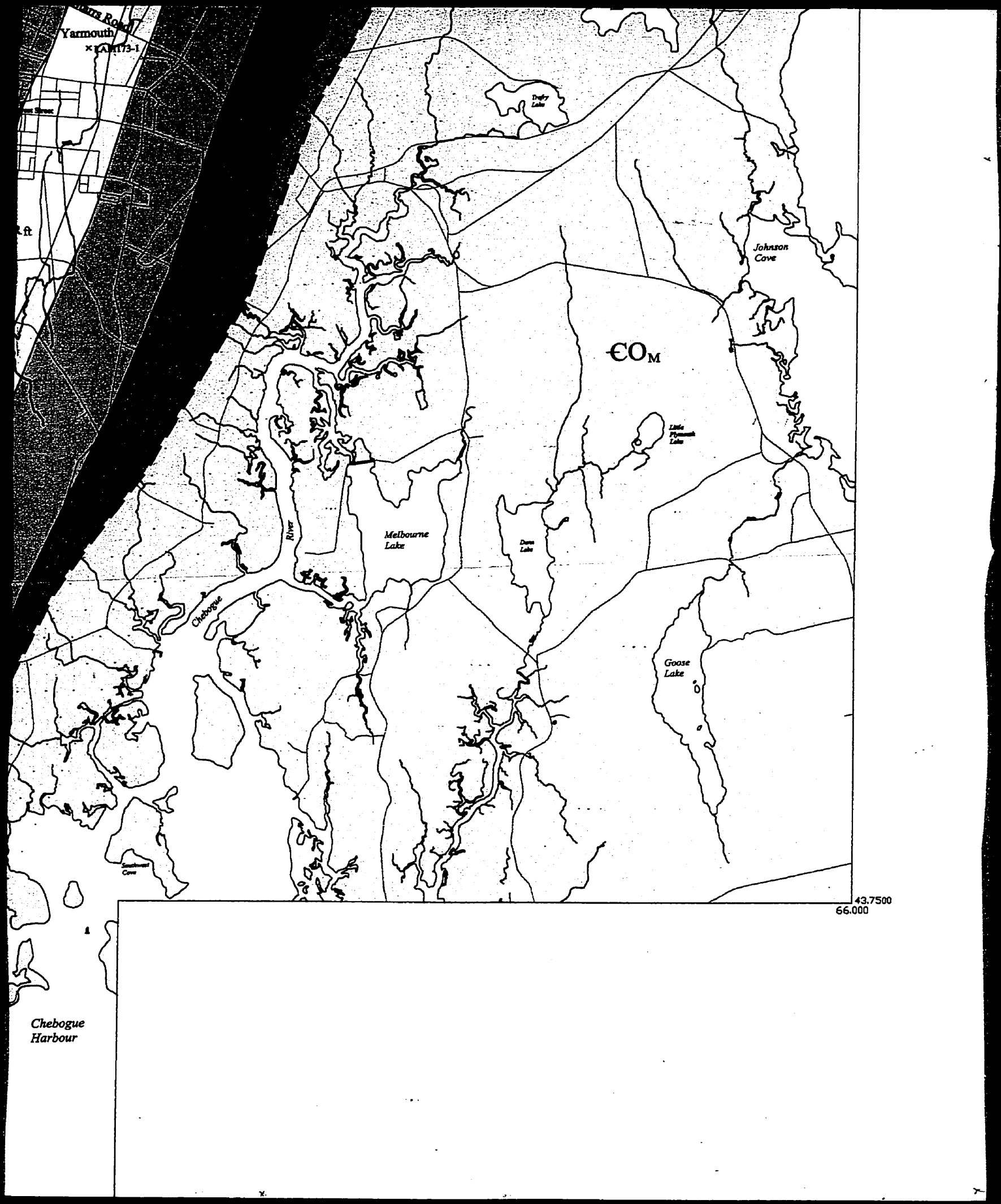
Yarmouth
Johnson Cove
Melbourne Lake
River
Chebogue
Goose Lake
Chebogue Harbour
43.7500
66.000

LAM203-1 X Geochemical sample location

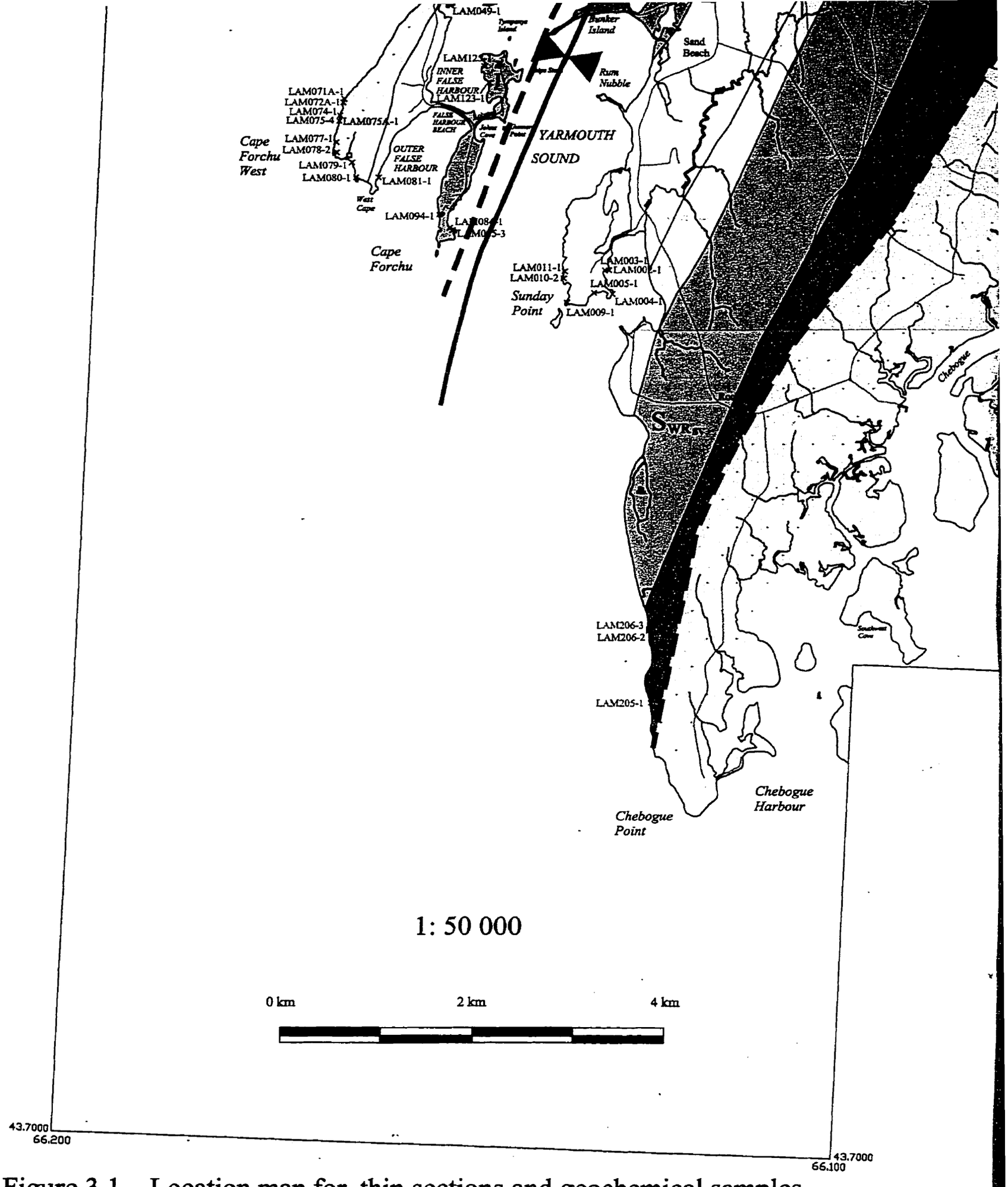

Figure 3.1. Location map for thin sections and geochemical samples.

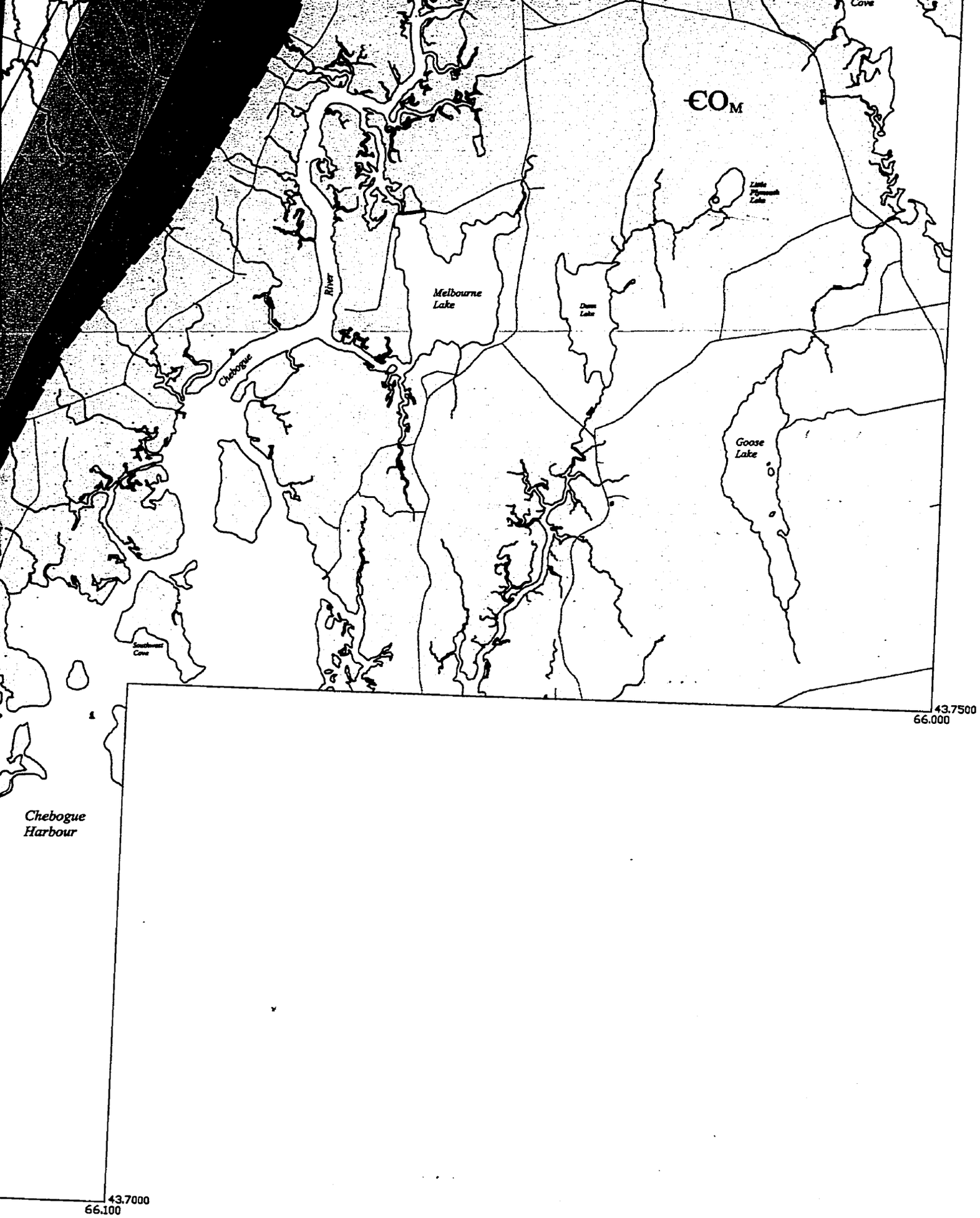
River
Melbourne Lake
Chebogue
Goose Lake
Southwest Cove
Chebogue Harbour
43.7500
66.000
43.7000
66.100

amples.

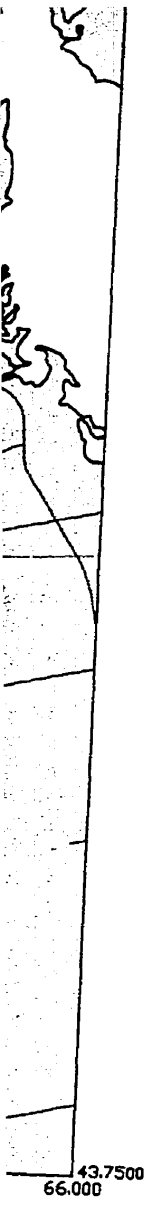
43.7500
66.000

Slate

Three samples of slate were examined in thin section, from units S_{WRmt} and S_{WRss}. They consist predominantly of fine-grained quartz, muscovite, chlorite and opaque minerals. Sample 144-1 from unit S_{WRmt} on Highway 1 contains tabular porphyroblasts of chloritoid <1 mm in length (Plate 3.1). Variation in abundance of chlorite in this sample causes slight compositional banding and elongate grains of chloritoid, chlorite and opaque minerals define the foliation. Sample 175-1 from Pleasant Valley contains idioblastic garnet approximately 1 mm in diameter, and 1 cm long subidioblastic, poikiloblastic staurolite. The composition of the garnet is close to almandine (Fig. 3.2). Elongate clusters of quartz, chlorite and muscovite occur in sample 175-1, as well as sample 14-1 from Crosby Court, and are coarser grained than the matrix. In sample 14-1, the clusters have a core of medium-grained, subidioblastic, poikiloblastic biotite.

Schist

Four samples of schist were examined in thin section, including garnet mica schist and garnet staurolite mica schist from units S_{WRmf} and S_{WRsv} respectively. In sample 179-1 from Government Brook (unit S_{WRmf}), garnet porphyroblasts are poikiloblastic and inclusions are aligned but not parallel to the foliation in the matrix (Plate 3.2). In samples 183-1 and 183-4 from unit S_{WRsv} in Government Brook, garnet is less poikiloblastic and has augen texture. Garnet in sample 184-1 from unit S_{WRmf} in Government Brook is not poikiloblastic and augen texture is not apparent. Biotite porphyroblasts range from fine grained to 3 mm in size, and are xenoblastic to subidioblastic and poikiloblastic with

Plate 3.1. Photomicrograph of chloritoid porphyroblasts in slate. Sample 144-1, unit Swr_{mt}, Highway 1. Field of view is 4mm. XPL.

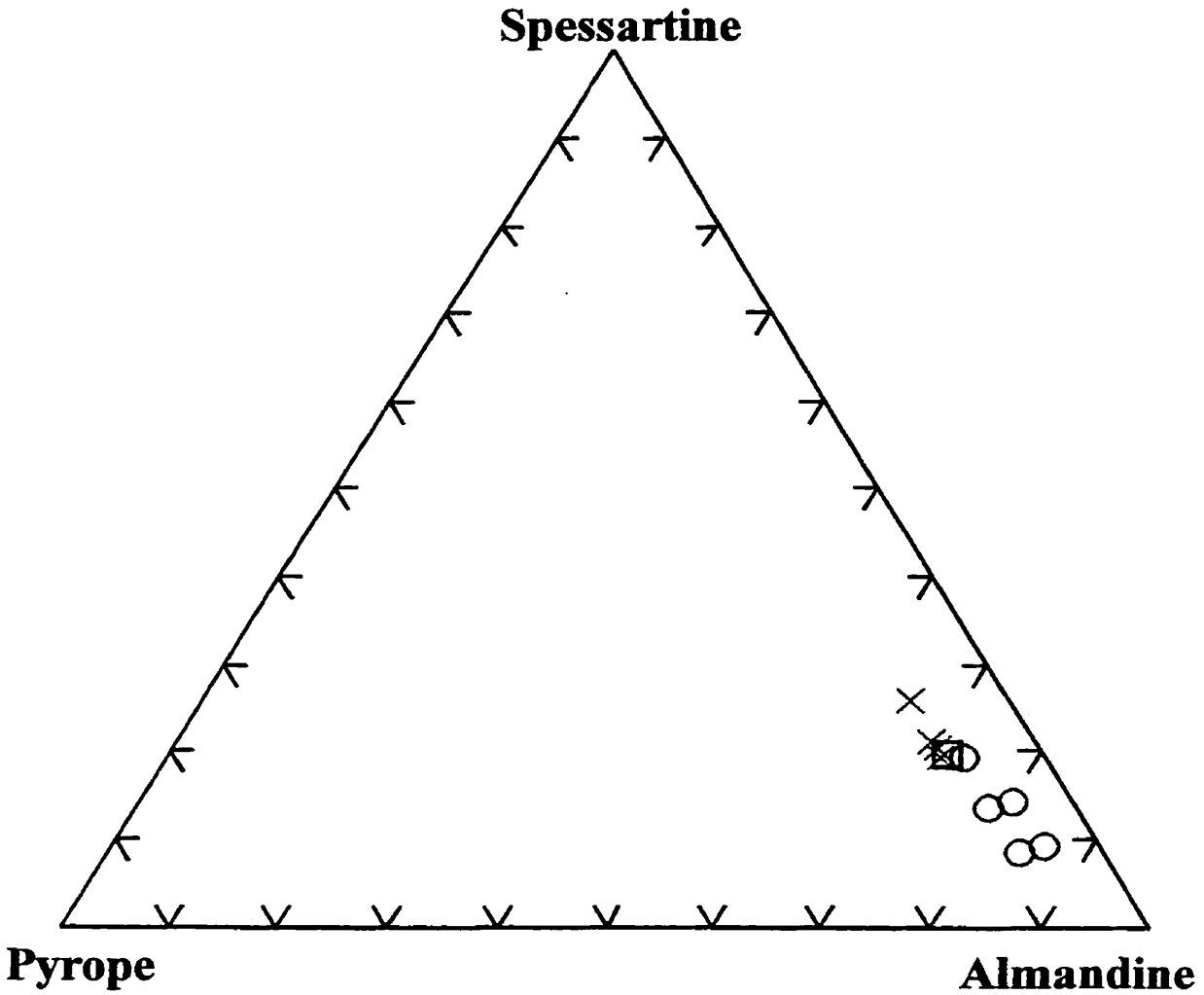

Figure 3.2. Composition of garnet in slate and mafic dykes in the White Rock Formation.

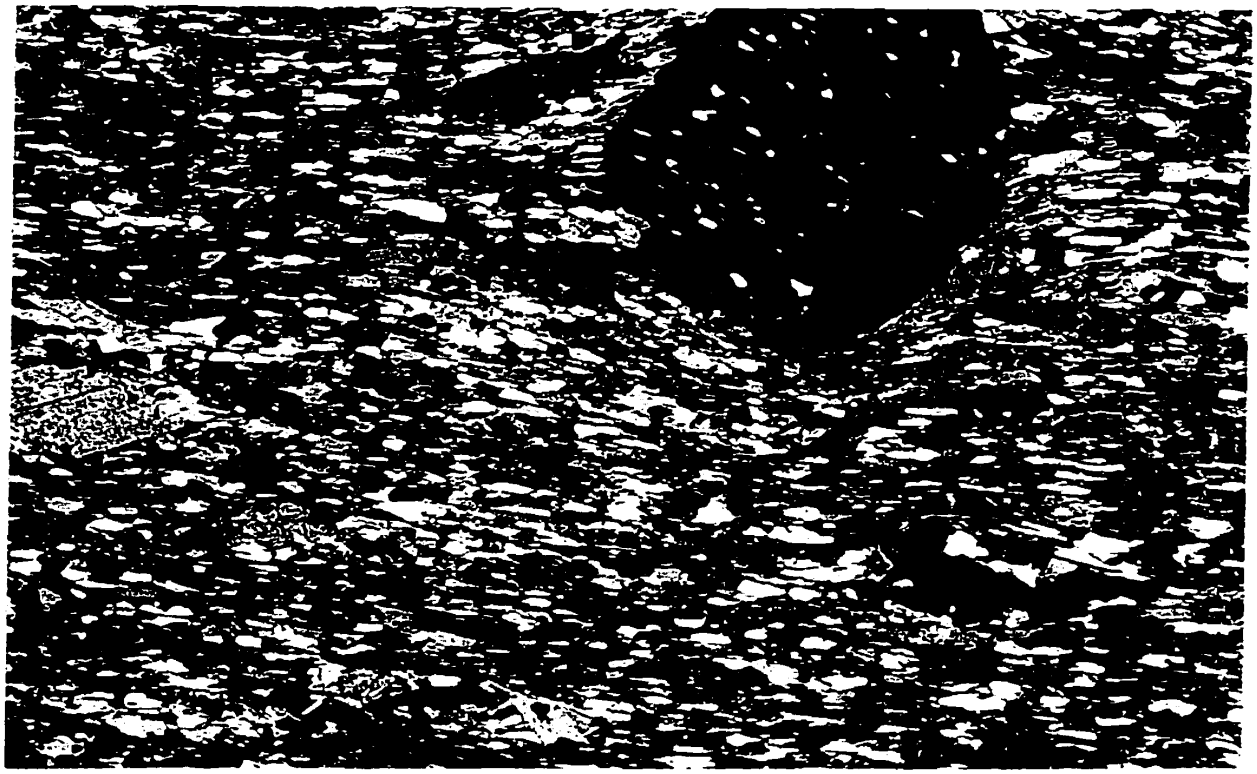

Plate 3.2. Photomicrograph of syn-tectonic, poikiloblastic garnet with aligned inclusions in schist. Sample 179-1, unit Swr_{sv}, Government Brook. Field of view is 4 mm. XPL.

augen texture. Samples 183-4 and 184-1 contain coarse-grained (up to 5 mm) xenoblastic to subidioblastic staurolite porphyroblasts. Staurolite grains have pressure shadows and sieve texture and inclusions are aligned but not with the matrix foliation, indicating rotation of the porphyroblast and/or changes in the matrix foliation (Plate 3.3). Sample 184-1 also contains plagioclase porphyroblasts which are up to 3 mm wide. They are xenoblastic with embayed grain boundaries, poikiloblastic with inclusions of quartz and have pressure shadows. Faint albite twinning is apparent.

Tuffaceous Sandstone

One sample of tuffaceous sandstone was examined from unit S_{WRsv} in Government Brook. It differs in texture and mineralogy from the other metasedimentary rocks. Compositional banding is apparent in hand specimen, although less obvious in thin section, and appears to be a result of variation in mineralogy. Some bands contain medium-grained quartz, plagioclase and microcline porphyroclasts with coarse-grained patches of fibrous epidote, whereas other bands consist of abundant, medium-grained, subidioblastic biotite and epidote or medium- to coarse-grained, subidioblastic clinozoisite, quartz and biotite (Plate 3.4). The matrix of the rock is generally fine-grained, recrystallized quartz and plagioclase with granular texture and lesser amounts of fine-grained, xenoblastic epidote, biotite and muscovite. The sample is inferred to have a volcanic component from the similarity between epidote/clinozoisite-rich areas and volcanic samples from other units.

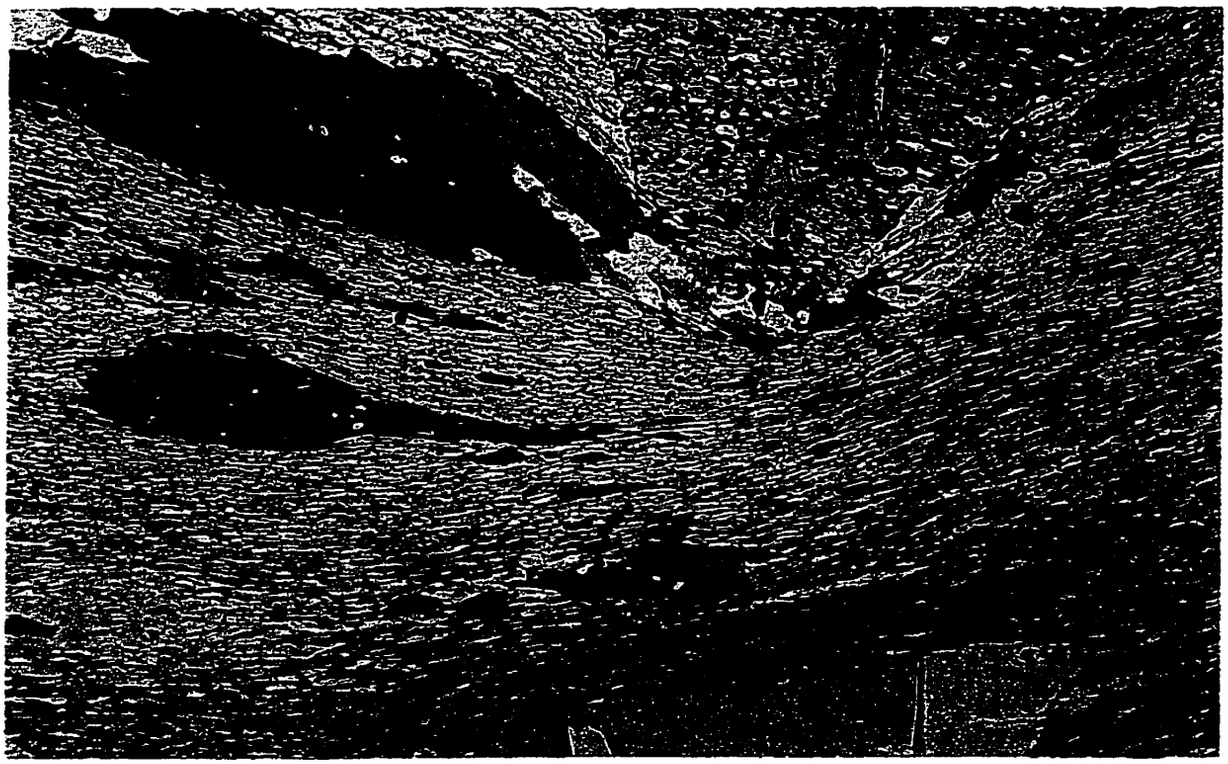

Plate 3.3. Photomicrograph of staurolite porphyroblast with aligned inclusions. Sample 183-4, unit S_{WRsv}, Government Brook. Field of view is 4 mm. XPL.

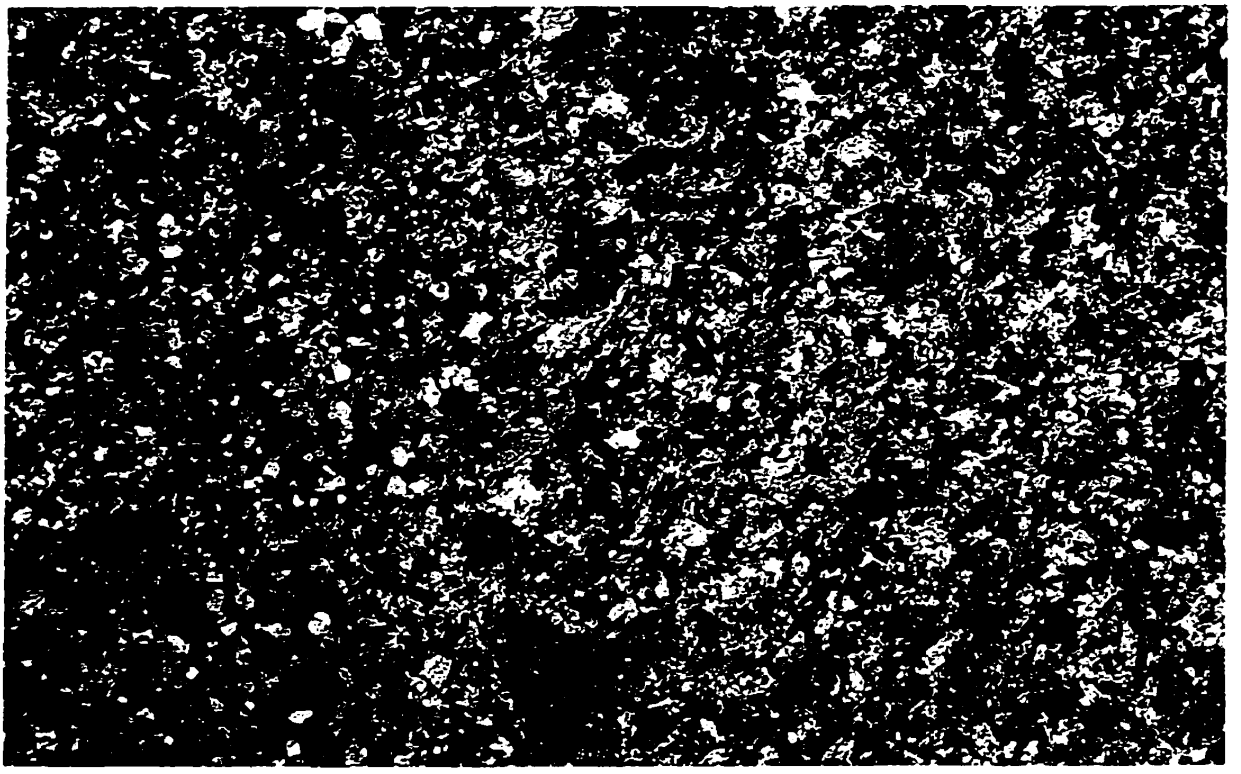

Plate 3.4. Photomicrograph of biotite-epidote rich layer between quartz-feldspar-epidote layers in tuffaceous sandstone. Sample 191-2, unit Swr_{sv}. Field of view is 4 mm. XPL.

3.2.2. Mafic flows

Samples interpreted to represent mafic flows consist mainly of amphibole, quartz, plagioclase and epidote, with less abundant biotite, opaque minerals, carbonate, chlorite and apatite. As a result of metamorphic recrystallization, they retain few relict igneous features and their interpretation as flows is based on field relations as well as their relatively homogeneous appearance, presence of relict porphyritic texture, and rare vesicles or amygdule-like patches. The original igneous groundmass no longer contains plagioclase laths or microlites and glass is absent. Basaltic phenocrysts such as olivine or pyroxene are replaced by amphibole and epidote, and plagioclase composition is likely to have been re-equilibrated under metamorphic conditions.

Quartz is abundant in the matrix, in amygdules, and in pressure shadows around relict crystals of plagioclase. It is typically less than 0.5 mm in size and xenoblastic.

Plagioclase occurs in the recrystallized matrix, as relict crystals and in amygdule-like patches. Plagioclase in the recrystallized matrix is fine to medium grained and ranges from xenoblastic to subidioblastic. Relict plagioclase crystals range up to 1 cm in size and are locally fractured and broken. They are subidioblastic and poikiloblastic with abundant inclusions of epidote, biotite and opaque minerals. The inclusions are not oriented parallel to the foliation in the matrix, which generally wraps around the grains. Plagioclase, quartz, biotite and apatite occur in pressure shadows adjacent to the relict crystals. Plagioclase in the relict amygdules is fine to medium grained and subidioblastic. Three analyses from sample 75A-1 show that plagioclase composition ranges from An_0 to An_{10}, with no difference between core and rim (Appendix B) (Fig. 3.3).

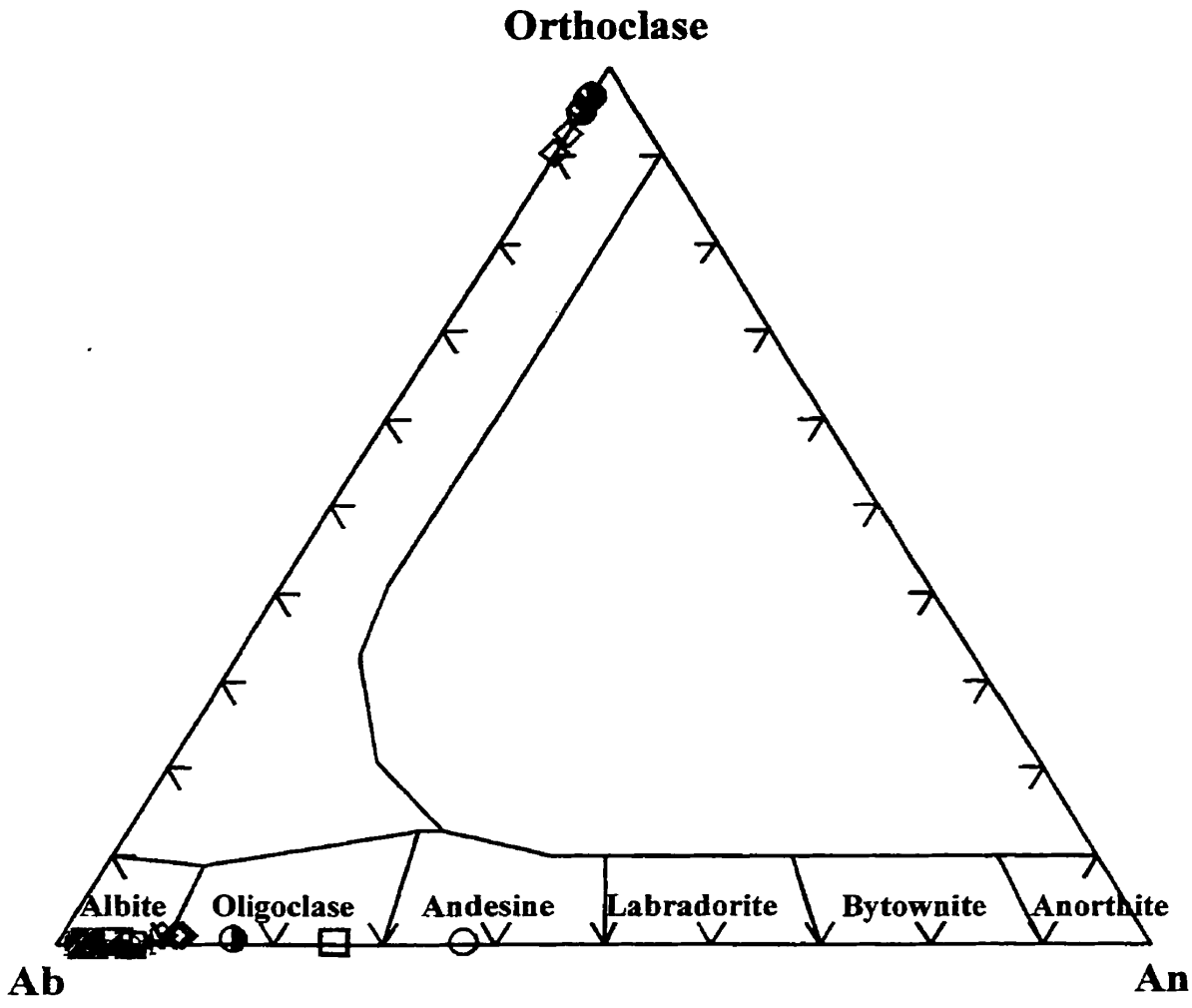

White Rock Formation

- Mafic flow (sample 75A-1) (n = 3)
- × Mafic crystal tuff (sample 78-2) (n = 3)
- Mafic tuff (sample 173-1) (n = 3)
- △ Intermediate crystal tuff (sample 11-1) (n = 5)
- ◑ Felsic crystal tuff (sample 4-1) (n = 9)
- ○ Mafic dyke (sample 199-1) (n = 1)
- \+ Mafic dyke (sample 205-1) (n = 6)

Brenton Pluton

- ◇ Granite (sample 161D-1) (n = 6)

Figure 3.3. Composition of feldspar in metavolcanic samples from the White Rock Formation and granite samples from the Brenton Pluton. Fields from Deer et al. (1992).

Amphibole occurs in the matrix and in porphyroblasts up to 2.5 mm in length. The matrix amphibole is fine to medium grained and varies in different samples from acicular to xenoblastic. It defines the foliation in cleaved and schistose samples. The texture and size of amphibole porphyroblasts also vary among samples. Typical porphyroblasts include medium- to coarse-grained subidioblastic blades or feathery sheafs. The bladed amphibole is typically poikiloblastic, with inclusions of epidote, quartz, biotite and opaque minerals. Most amphibole porphyroblasts parallel the foliation in the rock, but others (especially those with sheaf textures) cross-cut the foliation. Both matrix and porphyroblastic amphibole is pleochroic from yellow to green and blue-green. Amphibole composition was determined in 2 samples (133-1 and 75A-1), representing a range of textural types including bladed and sheaf. Within each sample, bladed amphibole compositions range from magnesiohornblende to tschermakitic hornblende (Fig. 3.4). Sheaf amphibole composition includes actinolite, magnesiohornblende, tschermakitic hornblende and Fe-tschermakite (Fig. 3.4). The cores and rims of two sheaf amphibole grains are alternately actinolite and magnesiohornblende but it is uncertain whether tschermakitic hornblende and Fe-tschermakitic hornblende composition is specific to either a core or rim.

Epidote is abundant is all samples except 123-3 from unit S_{WRmt}. It occurs in the matrix, in amygdules and as porphyroblasts. In the matrix, epidote forms fine-grained, xenoblastic, yellow-green grains. In amygdules it is xenoblastic to subidioblastic and fine to medium grained, with obvious twinning. Epidote porphyroblasts are medium-grained with obvious twinning and xenoblastic. Epidote forms inclusions in plagioclase porphyroclasts and is fine grained and xenoblastic.

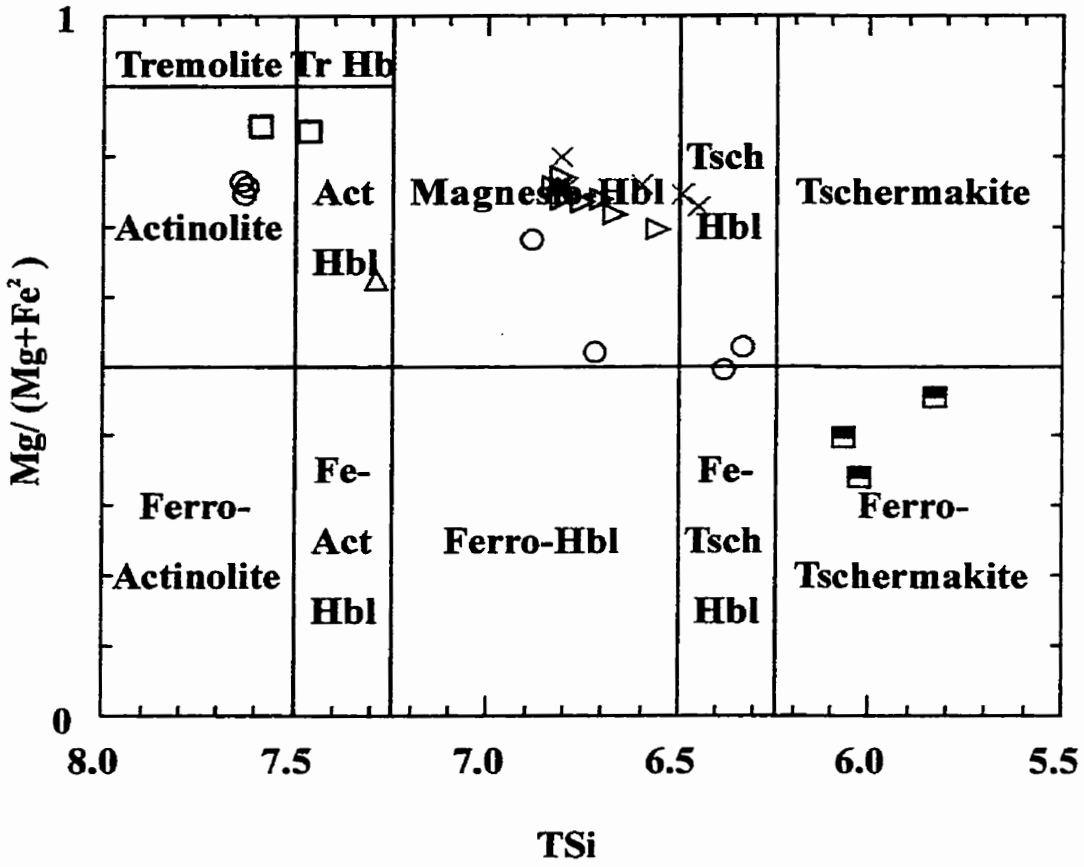

White Rock Formation

- × Mafic flow (sample 133-1) (n = 7)
- ○ Mafic flow (sample 75A-1) (n = 9)
- □ Mafic tuff (sample 173-1) (n = 4)
- ▷ Mafic crystal tuff (sample 78-2) (n = 7)
- ▬ Mafic dyke (sample 196-1) (n = 3)
- △ Mafic dyke (sample 205-1) (n = 1)

Figure 3.4. Composition of amphibole in mafic volcanic rocks and dykes in the White Rock Formation. Classification diagram after Leake (1978).

Biotite occurs in varying amounts in the matrix, in amygdules and as rare porphyroblasts. It is green to brown, fine grained and xenoblastic to subidioblastic. The composition of biotite in sample 133-1 from unit S_{WRmt} is intermediate between phlogopite and annite (Fig. 3.5). In samples with strong foliation the biotite is parallel to the foliation. In amygdules, biotite is medium grained and subidioblastic.

Carbonate occurs in amygdules (or filling vesicles?), in veinlets and in the matrix, where it is medium to coarse grained and xenoblastic. Chlorite is also relatively rare in mafic flows. It occurs in amygdules (or filling vesicles?) or associated with amphibole blades, and is fine to medium grained and xenoblastic to subidioblastic. Opaque minerals are abundant in all samples of mafic flows. In the matrix, they are fine grained, xenoblastic and aligned (when the matrix is foliated). Some grains are medium grained and subidioblastic. Opaque minerals also occur in amygdules and are similar to those in the matrix. Sample 84-1 from the upper part of unit S_{WRmt} contains a coarse-grained, xenoblastic porphyroblast as well as matrix opaques. Apatite occurs in some samples and is fine-grained and subidioblastic.

Mafic flow samples are divided into four general types on the basis of amphibole texture and other metamorphic mineral differences. The distribution and significance of the variation is not known due to the relatively small number of samples examined in thin section. One type is represented by five samples which have characteristics such as a similar strongly foliated nematoblastics texture and fine-grained, acicular amphibole-dominated matrices with lesser amounts of plagioclase, epidote and biotite. Rare relict plagioclase grains which reach a maximum length of 1 cm are also present, along with xenoblastic epidote porphyroblasts, amygdules and vesicles (Plate 3.5). Samples with this

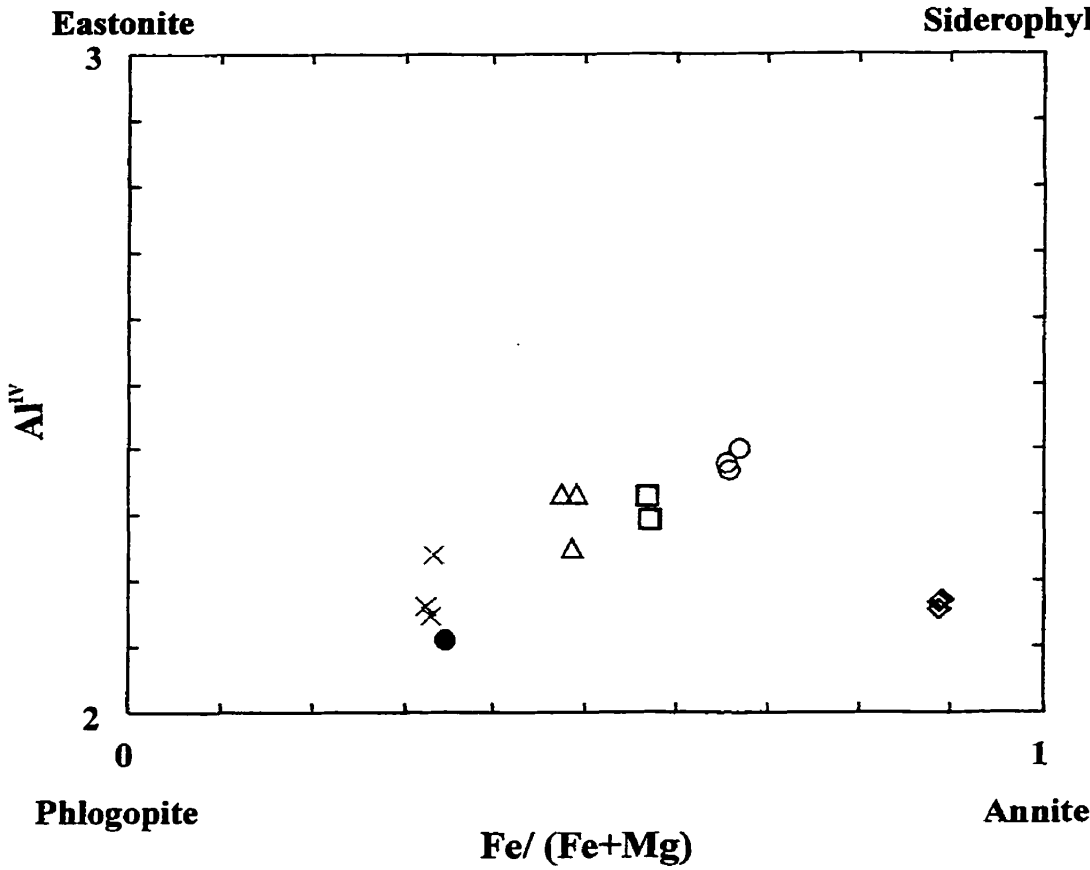

White Rock Formation

- × Mafic flow (sample 133-1) (n = 3)
- ● Mafic crystal tuff (sample 78-2) (n = 1)
- △ Intermediate crystal tuff (sample 11-1) (n = 3)
- □ Mafic dyke (sample 196-1) (n = 2)
- ○ Mafic dyke (sample 199-1) (n = 3)

Brenton Pluton

- ◇ Granite (sample 161D-1) (n = 3)

Figure 3.5. Composition of biotite in mafic samples from the White Rock Formation and granite from the Brenton Pluton. Classification diagram from Deer et al. (1992).

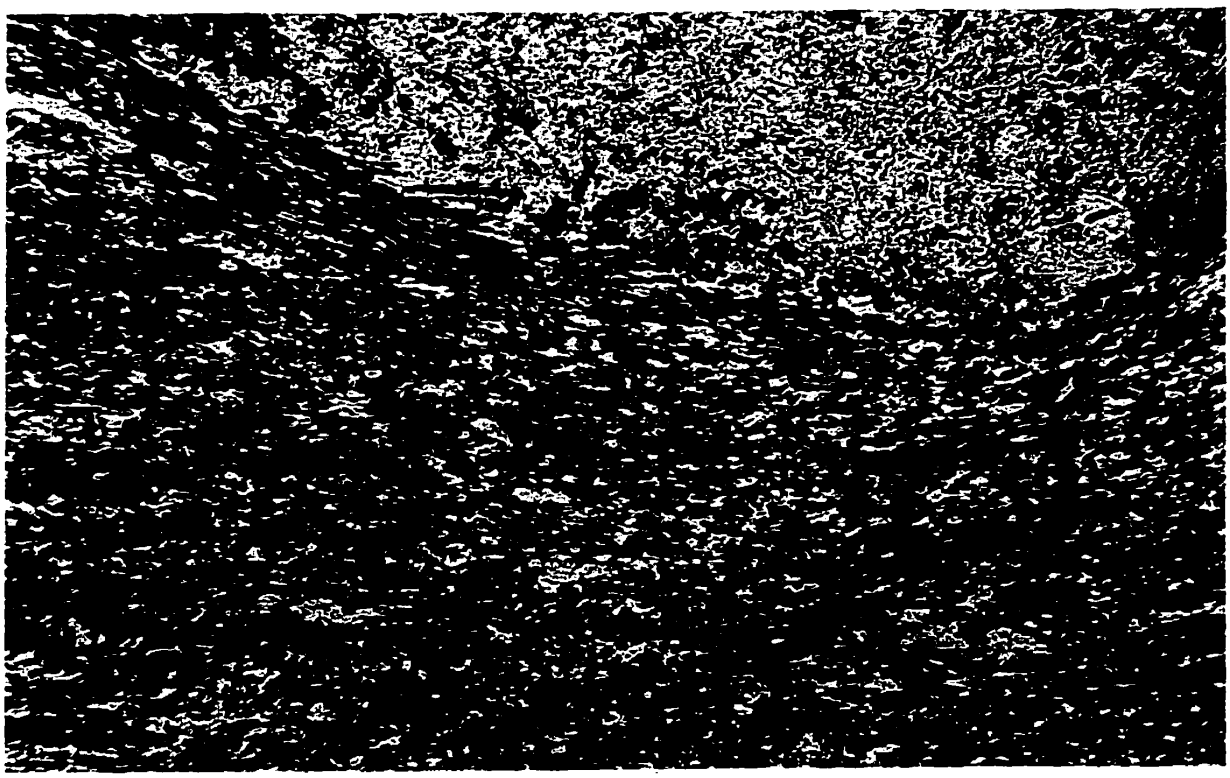

Plate 3.5. Photomicrograph of acicular amphibole texture and relict plagioclase grain in sample 2-1, unit Swr_{ft}, Sunday Point. Field of view is 4 mm. PPL.

texture are from the upper part of unit S_{WRmf} to the middle part of unit S_{WRft}, with one sample from the lower part of unit S_{WRsv}.

The second type includes two samples from the middle and upper parts of unit S_{WRmt}. They display decussate texture and lack pronounced schistosity. They consist of poikiloblastic, bladed amphibole porphyroblasts up to 1 cm in length, xenoblastic epidote porphyroblasts, subidioblastic plagioclase porphyroclasts and a quartz-dominated matrix with lesser amounts of biotite and epidote and no amphibole. Possible quartz amygdules are also present (Plate 3.6).

A third type of texture is represented by two samples from the shear zone at Cape Forchu West in the lower middle part of unit S_{WRmf}, below samples of type 1 described above. They contain sheaf or feather amphibole up to 1 cm long, subidioblastic plagioclase porphyroblasts and a matrix predominantly of fine-grained amphibole and epidote (Plate 3.7). Fine-grained biotite is rare. The samples are not foliated and contain possible amygdules.

A fourth type of texture is represented by four samples from the middle to upper part of unit S_{WRmt}. They consist of very fine-grained, quartz-dominated, recrystallized matrix with abundant fine-to medium-grained xenoblastic epidote, biotite and carbonate. Coarse-grained, xenoblastic relict plagioclase grains occur but are almost completely recrystallized – only faint outlines of the grain boundaries and albite twinning are apparent. The plagioclase is poikiloblastic with abundant inclusions of chlorite, epidote, biotite and carbonate. Fine-to medium-grained, xenoblastic, poikiloblastic biotite porphyroblasts are very abundant, and samples typically contain medium- to coarse-grained, xenoblastic, poikiloblastic amphibole porphyroblasts as well. Some of the

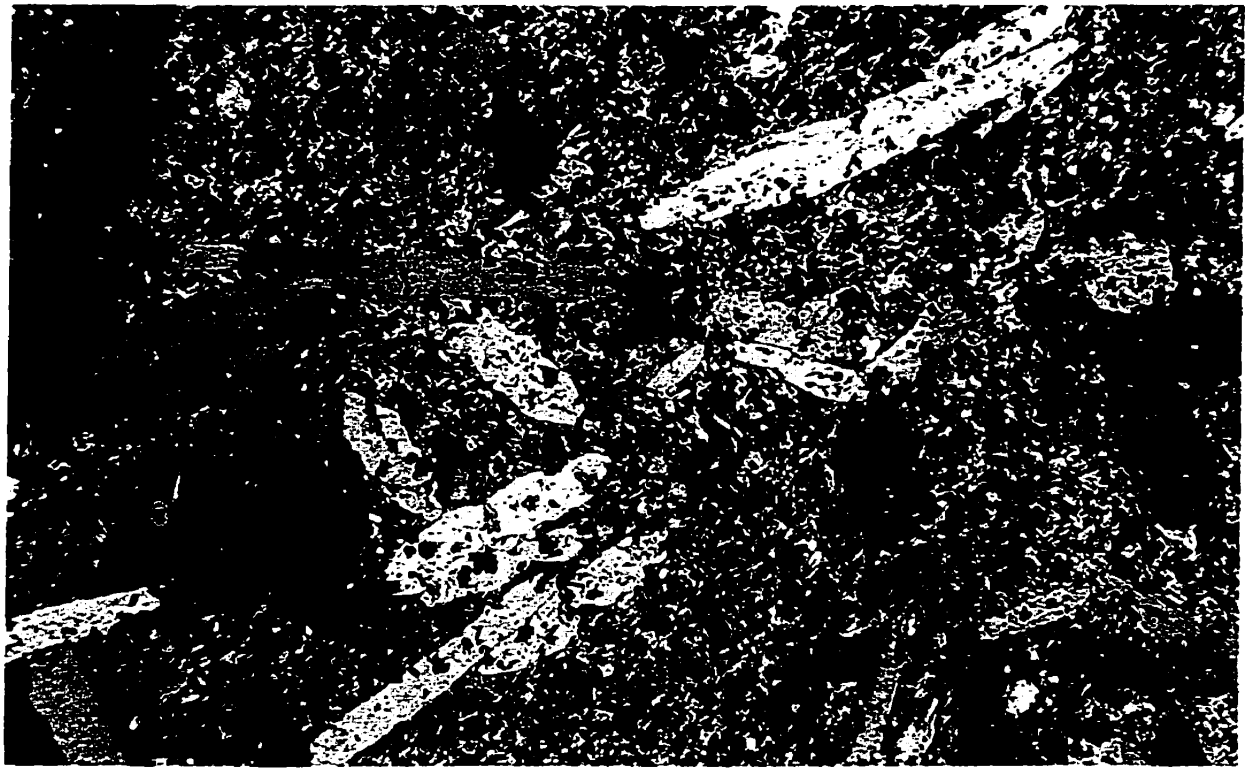

Plate 3.6. Photomicrograph of bladed amphibole texture in flow sample 84-1, unit Swr_{mt}, Cape Forchu. Field of view is 4 mm. XPL.

Plate 3.7. Photomicrograph of sheaf amphibole texture in mafic flow sample 75-4, unit Swr_{mf}, Cape Forchu West. Field of view is 4 mm. XPL.

samples have schistosity which is defined by alignment of biotite and amphibole grains and by carbonate in elongate spaces in the matrix.

3.2.3. Mafic tuff

The mineralogy of mafic tuff samples is generally similar to that in mafic flow samples. Amphibole, quartz, epidote, plagioclase and biotite are the major minerals, with opaque minerals, titanite, chlorite, carbonate, zircon and rutile as minor components. Many of the minerals have the same form and texture as in flows, generally differing only in abundance. As is the case of mafic flows, few original igneous textures are preserved (i.e. lapilli, glass and welded textures are not preserved) and interpretation as tuff is largely based on field relations and appearance in hand specimen.

As in mafic flow samples, quartz occurs in the matrix, in pressure shadows and in elongate clusters where it is fine grained, recrystallized and xenoblastic. Plagioclase is generally less abundant in mafic tuff samples than in mafic flow samples, but similarly occurs in the matrix, as relict crystals and in elongate clusters with quartz. In the recrystallized matrix it is generally fine grained, xenoblastic, sericitized and altered to red-brown clay. Relict plagioclase grains are medium to coarse grained (up to 2 mm in length), and xenoblastic to subidioblastic. The matrix is deflected around the grains and pressure shadows of quartz, carbonate and amphibole have developed. The relict crystals appear more sericitized and altered than in mafic flows and are not poikiloblastic. Plagioclase in elongate clusters is fine-grained, xenoblastic to subidioblastic and altered. Relict plagioclase was analyzed in mafic tuff sample 173-1 from the middle part of unit S_{WRft} and the composition is oligoclase (Fig. 3.3).

Amphibole defines the foliation in cleaved and schistose mafic tuff samples. It occurs in the matrix and as porphyroblasts and has the same colour, shape, and range in texture as amphibole in mafic flows. Amphibole porphyroblasts are typically larger in tuffaceous samples than in flows and may have pressure shadows. Amphibole in one sample (173-1) from the middle part of unit S_{WRft} was analyzed, and the composition ranges between actinolite and actinolitic hornblende with no differences apparent between the cores and rims of grains (Fig. 3.4). Amphibole in mafic tuff samples display the same textural variations that occur in mafic flows. Some samples have nematoblastic texture with porphyroblasts of epidote and an acicular amphibole-dominated matrix with lesser amounts of quartz, opaque minerals and epidote. No relict plagioclase crystals or biotite porphyroblasts are present in tuff samples with nematoblastic texture. Some samples of mafic tuff have poikiloblastic, bladed amphibole porphyroblasts, plagioclase porphyroblasts and a quartz-dominated recrystallized matrix, similar to the second type of mafic flow described in section 3.2.2 but with some differences. Mafic tuff samples with bladed amphibole contain titanite, calcite-filled voids, and quartz-rich clusters, and may be compositionally banded. Compositional banding is seen in sample 204-1 and consists of fine-grained quartz layers separated by layers with quartz, chlorite and epidote. Other samples of mafic tuff contain sheaf or feather amphibole which may be acicular or stubby. They differ from mafic flows with amphibole of this texture as they do not contain relict plagioclase grains, epidote or amygdules. The amphibole with sheaf or feather texture in samples of mafic tuff are typically coarser grained than in samples of mafic flows.

Epidote occurs in the matrix and in elongate clusters but is generally less abundant than in mafic flows. In the matrix and elongate clusters it is fine-grained, yellow and xenoblastic. Epidote porphyroblasts range from fine to medium grained, are generally xenoblastic and may be rimmed by smaller epidote grains. In foliated samples, the matrix wraps around the epidote porphyroblasts, which have pressure shadows of quartz, amphibole and chlorite.

Biotite is also more abundant in tuff than in flow samples. It occurs in the matrix and locally in elongate clusters with quartz and plagioclase where it is typically fine grained, xenoblastic and pleochroic yellow to brown.

Mafic tuff samples contain a variety of minor minerals. Fine-grained, xenoblastic opaque grains occur in the matrix and as fine-to medium-grained, tabular or acicular porphyroblasts. Titanite is abundant in sample 165-1 from unit S_{WRmf} in the Brenton Lake area, and is fine to medium grained and xenoblastic. Rare rutile in the matrix is very fine grained and xenoblastic. Minor zircon (?) is present as very small grains with halos in amphibole. Chlorite is abundant in tuff with sheaf amphibole and occurs in the matrix as fine acicular grains and as fine to-medium xenoblastic grains in clusters. Another minor component of mafic tuff is carbonate which is found in samples with poikiloblastic blades of amphibole. It is fine to medium grained, xenoblastic and occurs in the matrix, in spaces and elongate clusters, in veins and in pressure shadows.

3.2.4. Mafic Lithic Tuff

Four samples of mafic lithic tuff from unit S_{WRmt} were examined in thin section. They contain block and lapilli size fragments. The matrix surrounding the clasts is similar

in the four samples and comprised of fine-grained polygonal quartz, xenoblastic biotite (some of which is altered to chlorite), acicular amphibole and lesser amounts of subidioblastic plagioclase and xenoblastic opaque minerals. Medium-grained, acicular amphibole porphyroblasts are also present. The lithic fragments consist predominantly of fine-grained, matted, acicular amphibole with only minor quantities of quartz, epidote and medium-grained, xenoblastic opaque minerals less than 1 mm long (Plate 3.8). The lithic fragments also contain plagioclase porphyroblasts which are up to 1 mm long. The plagioclase porphyroblasts are subidioblastic, almost completely recrystallized, and commonly associated with fine-grained, polygonal quartz. Both clasts and matrix have strong foliation evident by parallel alignment of amphibole needles.

3.2.5. Amphibolite

Three samples from units S_{WRsv} (from Lake George and Brazil Lake Road) and S_{WRft} (Cape Forchu West) are of unknown protolith and are referred to as amphibolite. They are generally coarse grained with a fine-grained, recrystallized matrix of plagioclase and quartz with mosaic texture. Amphibole porphyroblasts are abundant in all three samples and compose approximately 50 % to 70 % (by volume) of the rock. They have bladed texture in samples 81-1 and 170-1 and a poikiloblastic sheaf texture in sample 172-1. In all three samples, amphibole porphyroblasts are coarse grained (approximately 3 mm long) and subidioblastic. The samples contain fine grained, subidioblastic-to xenoblastic opaque minerals. Samples 172-1 and 81-1 have minor chlorite which is fine- to medium grained in both samples. In sample 81-1, chlorite has partially replaced

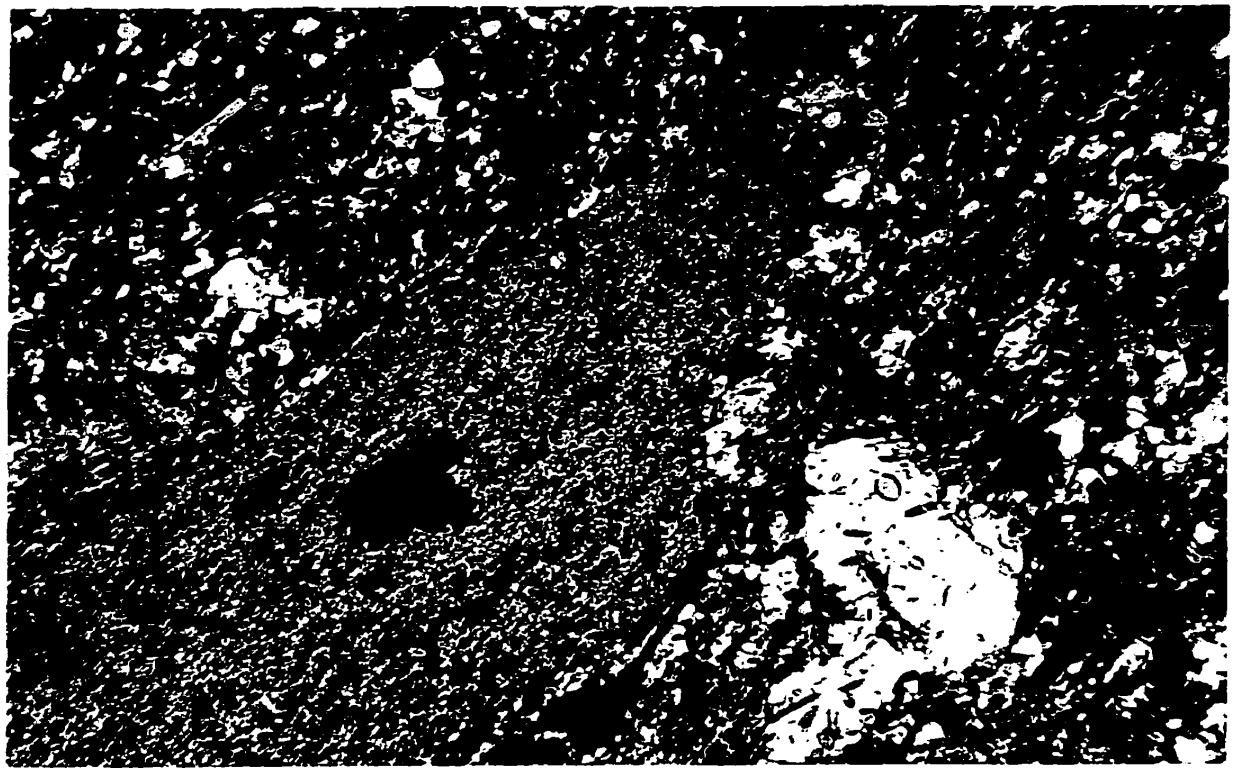

Plate 3.8. Photomicrograph of amphibole-rich lithic fragments. Sample 15-1, unit S_{WRmt}, Cemetery Road. Field of view is 4 mm. XPL.

amphibole, whereas in sample 172-1 it appears porphyroblastic. Sample 81-1 contains abundant fine-to medium grained xenoblastic epidote, carbonate and leucoxene. Samples 170-1 and 172-1 contain fine grained, xenoblastic zircon within amphibole porphyroblasts and minor rutile.

3.2.6. Intermediate Flows

Intermediate flows vary in composition, mineralogy and texture. Andesitic samples contain more amphibole whereas more dacitic samples have a greater abundance of quartz. Samples of andesitic composition are petrographically similar to mafic flows but with less amphibole (matrix and porphyroblastic), and fewer relict plagioclase grains which are also finer grained than those in mafic flows, and epidote occurs in the matrix but not as porphyroblasts as it does in mafic flows.

Intermediate flows typically have a fine-grained, quartz-dominated, recrystallized matrix with abundant fine-to medium-grained xenoblastic epidote, biotite and carbonate (Plate 3. 9). Coarse-grained plagioclase porphyroclasts occur but are almost completely recrystallized, with only faint outlines of albite twinning apparent. The plagioclase has abundant inclusions of chlorite, epidote, biotite and carbonate. Fine-to medium-grained, xenoblastic, poikiloblastic biotite porphyroblasts are very abundant. Samples also generally contain medium-to coarse-grained, xenoblastic, poikiloblastic amphibole porphyroblasts. Some flows have schistosity which is defined by alignment of biotite and amphibole grains and by elongate carbonate in the matrix.

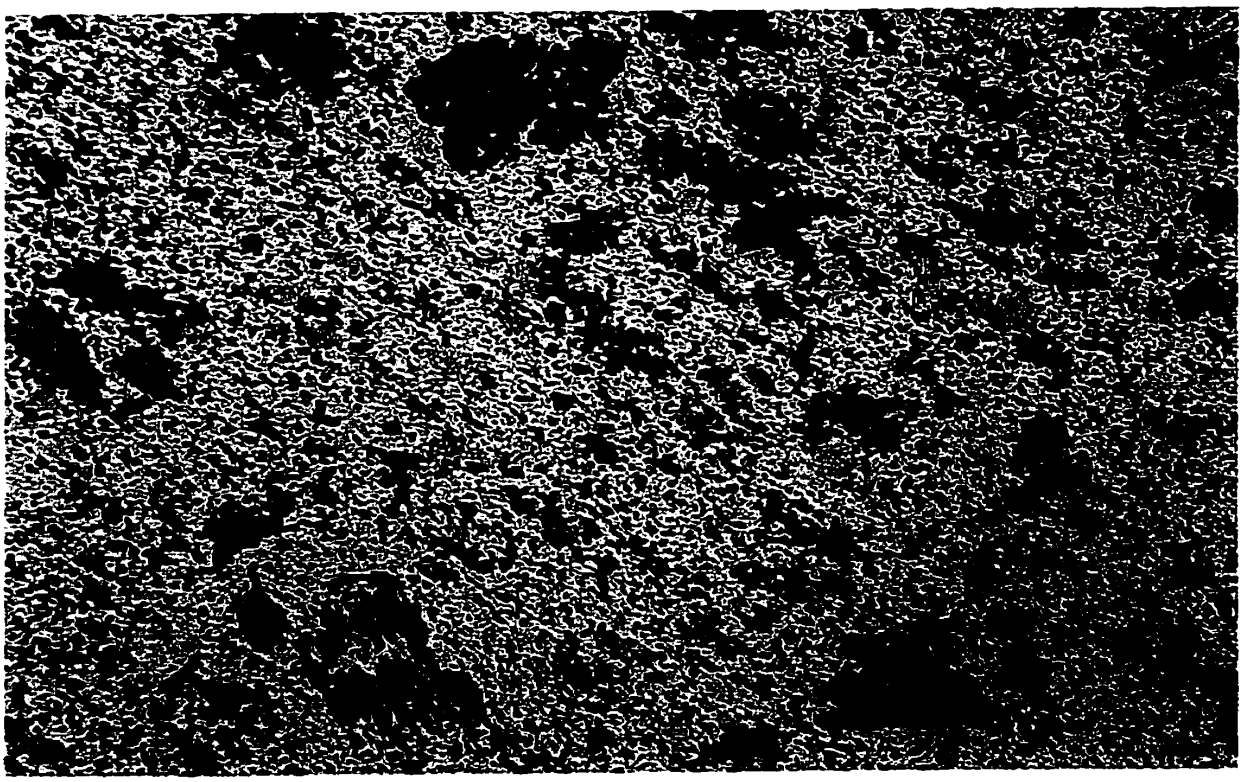

Plate 3.9. Photomicrograph of intermediate flow sample 125-1. Unit S_{WRmf}, Ships Stern. Field of view is 4 mm. PPL.

3.2.7. Mafic and Intermediate Crystal Tuff

Crystal tuff samples with intermediate composition typically contain less amphibole and more biotite than those of mafic composition. In samples with mafic composition, the matrix is preominantly fine-grained biotite, recrystallized plagioclase, opaque minerals, epidote, chlorite and quartz. The matrix of samples with intermediate composition is predominantly fine-grained crystallized plagioclase, biotite, opaque minerals, quartz , chlorite and epidote. Foliation is well developed in the matrix of both mafic and intermediate samples and is deflected by porphyroblasts and relict crystals (Plate 3.10).

Crystal tuff samples are characterized by relict plagioclase crystals which typically appear broken or show signs of ductile deformation such as deformation bands and irregular extinction. Relict plagioclase grains are up to 5 mm long and subidioblastic with inclusions of epidote, quartz, carbonate and biotite. The composition of relict plagioclase in samples 11-1 and 78-2 from units S_{WRft} and S_{WRmf}, respectively, is albite with no difference between core and rim (Fig. 3.3). Some grains of plagioclase have embayed grain boundaries (or possible relict igneous features) (Plate 3.10) and some grains may be rimmed by fine-grained biotite and epidote. Alteration to sericite is evident in most samples.

Other major minerals present include amphibole, epidote, biotite and rare muscovite. Amphibole porphyroblasts are typically medium-to coarse-grained, subidioblastic blades or xenoblastic sheafs (Plate 3.11), except in intermediate sample 9-1. In sample 78-2, amphibole is of magnesiohornblende composition (Fig. 3.4). Epidote porphyroblasts are abundant and generally form medium-sized, xenoblastic grains, except

Plate 3.10. Photomicrograph of a fine grained matrix deflected around a relict plagioclase grain in intermediate crystal tuff sample 11-1, unit S_{WRft}, Sunday Point. Field of view is 4 mm. XPL.

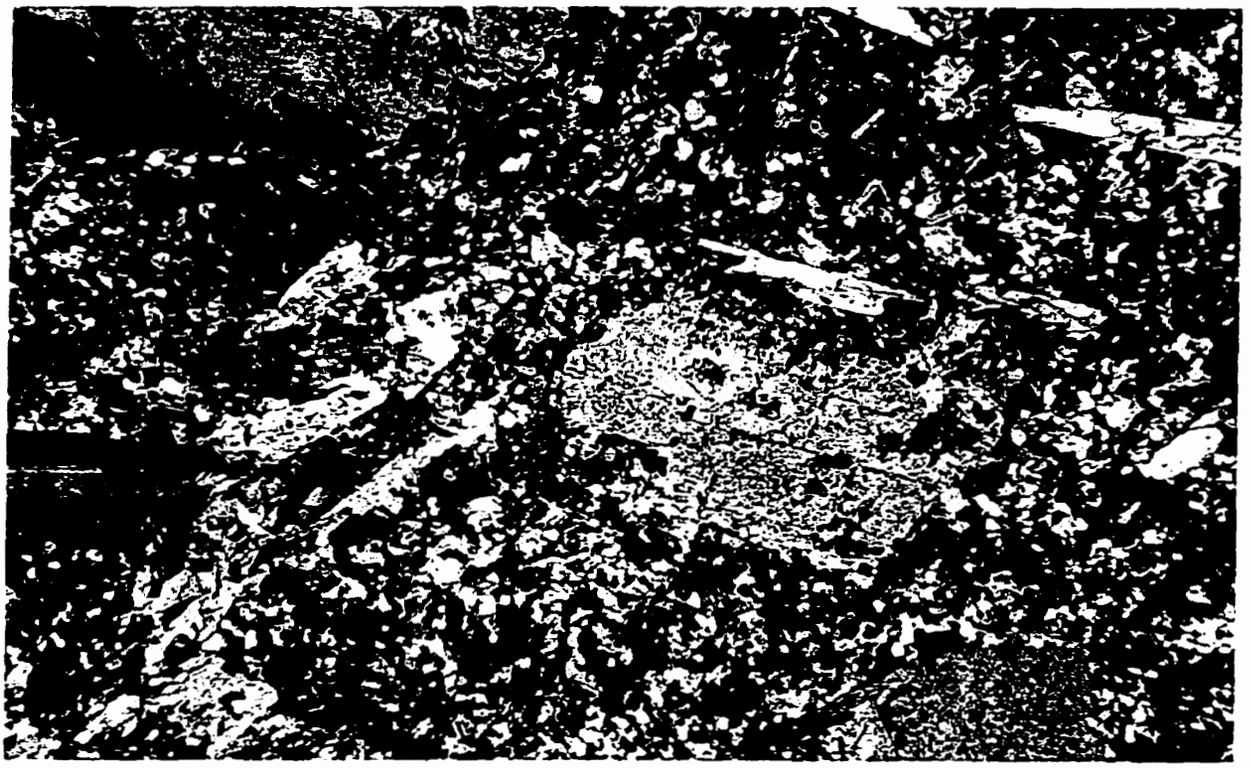

Plate 3.11. Photomicrograph of a relict plagioclase grain with embayed grain boundaries and subidioblastic bladed amphibole. Sample 78-2, unit S_{WRmf}, Cape Forchu West. Field of view is 4 mm. XPL.

in sample 11-1 where epidote porphyroblasts are coarse-grained (up to 1 mm) and idioblastic with rims of very fine-grained epidote. Biotite and muscovite porphyroblasts are rare, medium grained and subidioblastic, and typically associated with plagioclase pressure shadows. Biotite compositions in sample 78-2 and 11-1 are intermediate between phlogopite and annite (Fig. 3.5). Minor minerals in mafic to intermediate crystal tuff include opaque minerals and apatite. Opaque minerals are porphyroblastic in sample 11-1 and are typically xenoblastic with rims of leucoxene. Fine-to medium-grained, idioblastic apatite grains are abundant in sample 11-1 and have pressure shadows.

3.2.8. Felsic Crystal Tuff

Samples interpreted to have felsic crystal tuff protoliths are composed predominantly of quartz, plagioclase and K-feldspar (Plate 3.12). Sample 4-1 (unit S_{WRfl}) is slightly less felsic than samples 208-1 and 209-1 (unit S_{WRsv}) and contains epidote, biotite and muscovite. Felsic crystal tuff samples show deformation features such as mortar texture matrix, quartz ribbons, and deformation bands and fracturing of feldspar grains. The matrix consists of fine-grained, polygonal quartz and plagioclase with abundant saussurite and opaque minerals (samples 208-1 and 209-1) but tends to be granoblastic, fine-grained, xenoblastic recrystallized quartz and plagioclase with biotite and epidote in the less felsic sample (Plate 3.13).

Relict crystals of quartz, plagioclase and K-feldspar are less than 5 mm in size and subidioblastic, and have pressure shadows and signs of strain. Some relict quartz grains have embayed boundaries, possibly relict igneous resorption features. They display undulatory extinction and some have undergone grain size reduction either completely or

Plate 3.12. Photomicrograph of felsic crystal tuff sample 209-1. Unit S_{WRsv}, south of Brooklyn. Field of view is 4 mm. XPL.

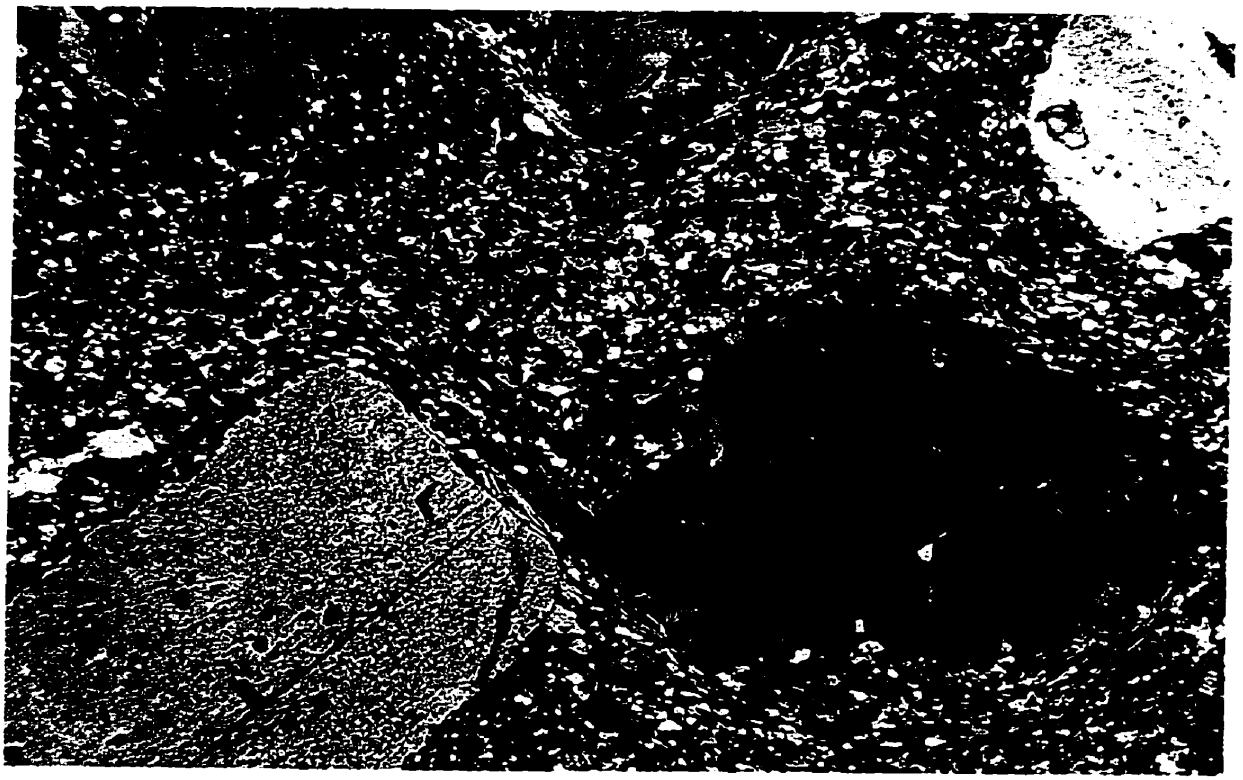

Plate 3.13. Photomicrograph of felsic crystal tuff sample 4-1, unit S_{WRft}, Sunday Point. Field of view is 4 mm. XPL.

around rims. In felsic sample 209-1, some clasts have granophyric texture (Plate 3.14). Plagioclase and K-feldspar relict crystals are typically fractured and have slight undulatory extinction and deformation bands. Some plagioclase grains have embayed boundaries and are partially replaced by epidote. Twinning is faint in some grains, and some grains are vermicular. Plagioclase composition in sample 4-1 is albite to oligoclase and K-feldspar composition approaches orthoclase (Fig. 3.3). Sample 4-1 has medium-grained porphyroblasts of epidote, biotite and muscovite. In this sample epidote occurs in a variety of forms including xenoblastic aggregates, columnar grains or as fibrous rosettes. Biotite and muscovite are associated and typically xenoblastic to subidioblastic. Biotite is pleochroic from pale green to dark green.

Minor components in the samples include opaque minerals, apatite, chlorite, zircon and xenotime.

3.3. Mafic Dykes and Sills

In general, the mafic dykes and sills are coarse grained with abundant amphibole porphyroblasts which comprise up to 85% of the rock. The porphyroblasts are up to 1 cm in length and display a variety of textures. Most common is bladed texture (Plate 3.15), followed by sheaf or feather texture (Plate 3.16), tabular or prismatic texture (Plate 3.17), and acicular texture (Plate 3.18). Samples with bladed amphibole are from Chegoggin Point, Overton, near Pleasant Valley, Cape Forchu West and Chebogue Point. Samples with sheaf texture are from Chegoggin Point and Overton, tabular samples are from Chebogue Point and Cranberry Head and acicular amphibole samples are from Cape Forchu. Hence, no correlation of texture with location or host rock (Halifax or White

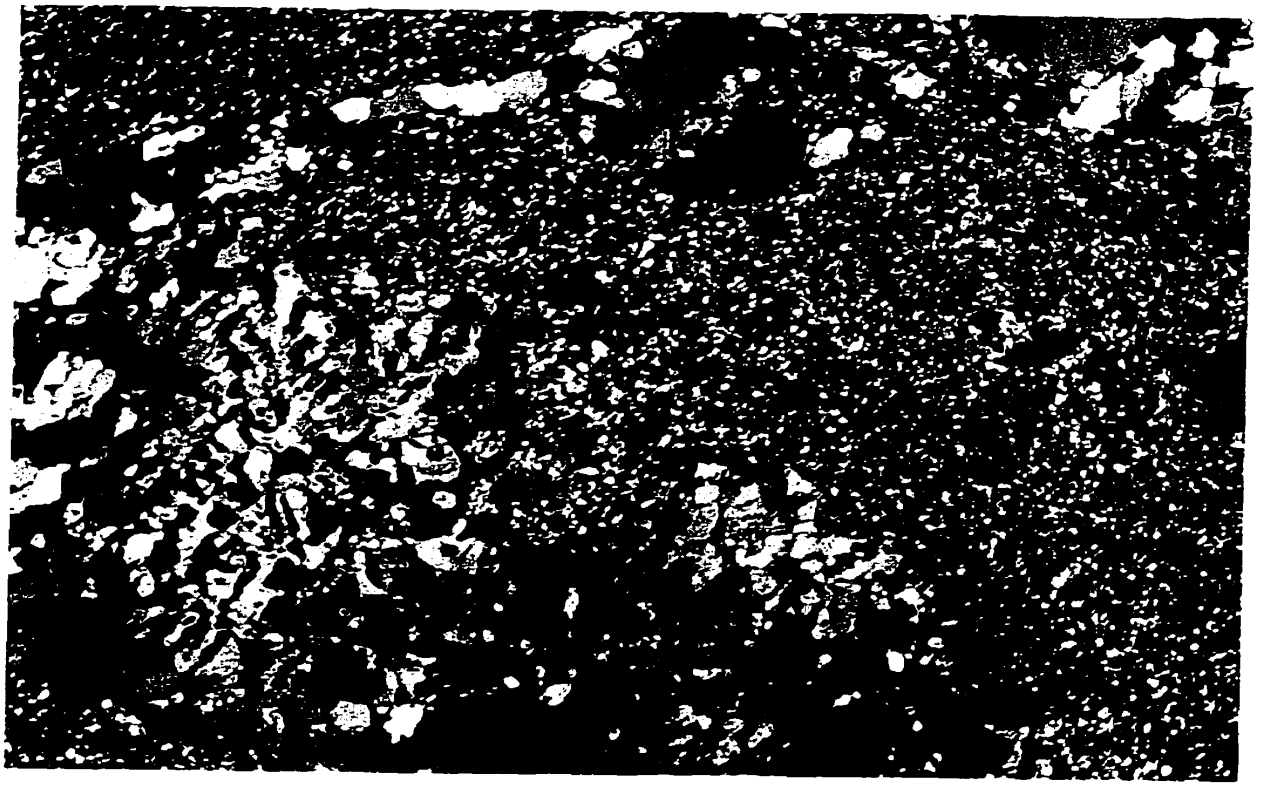

Plate 3.14. Photomicrograph of granophyre texture in sample 209-1, unit S_{WRsv}, south of Brooklyn. Field of view is 4 mm. XPL.

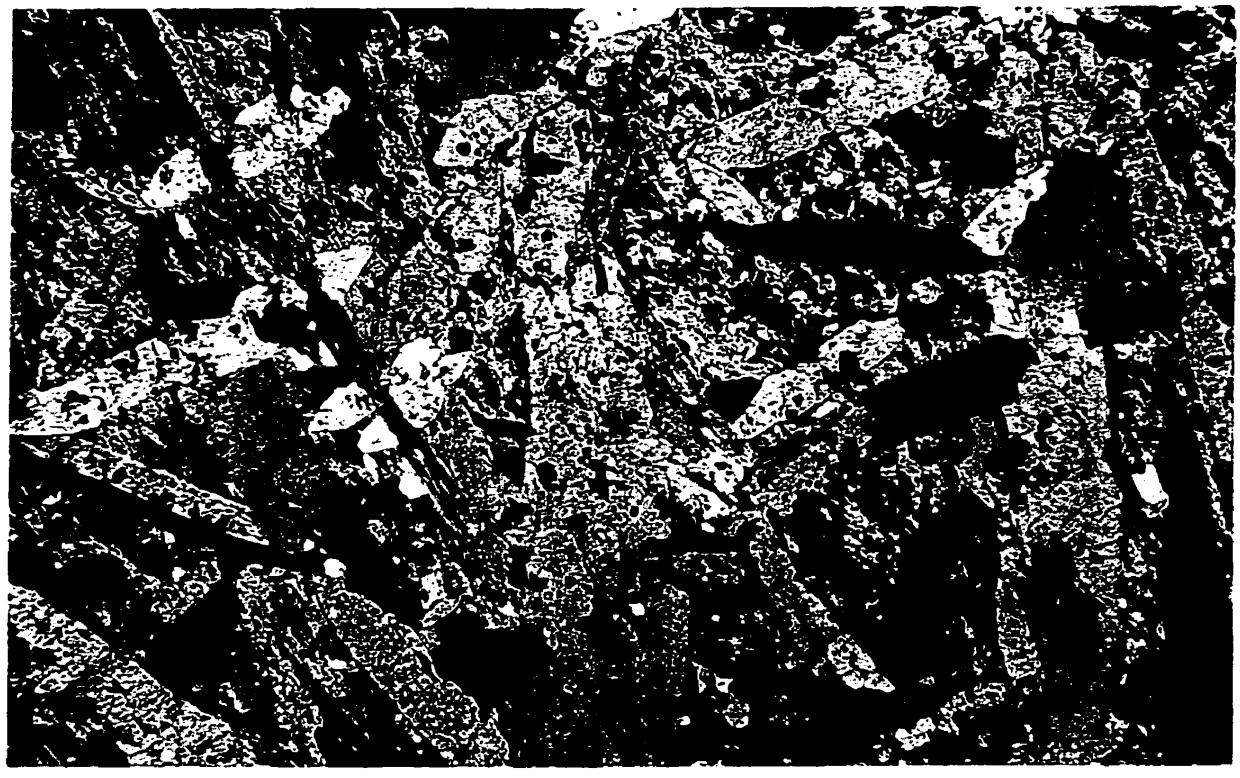

Plate 3.15. Photomicrograph of bladed amphibole in dyke sample 198-1, north of Chegoggin Point. Field of view is 4 mm. XPL.

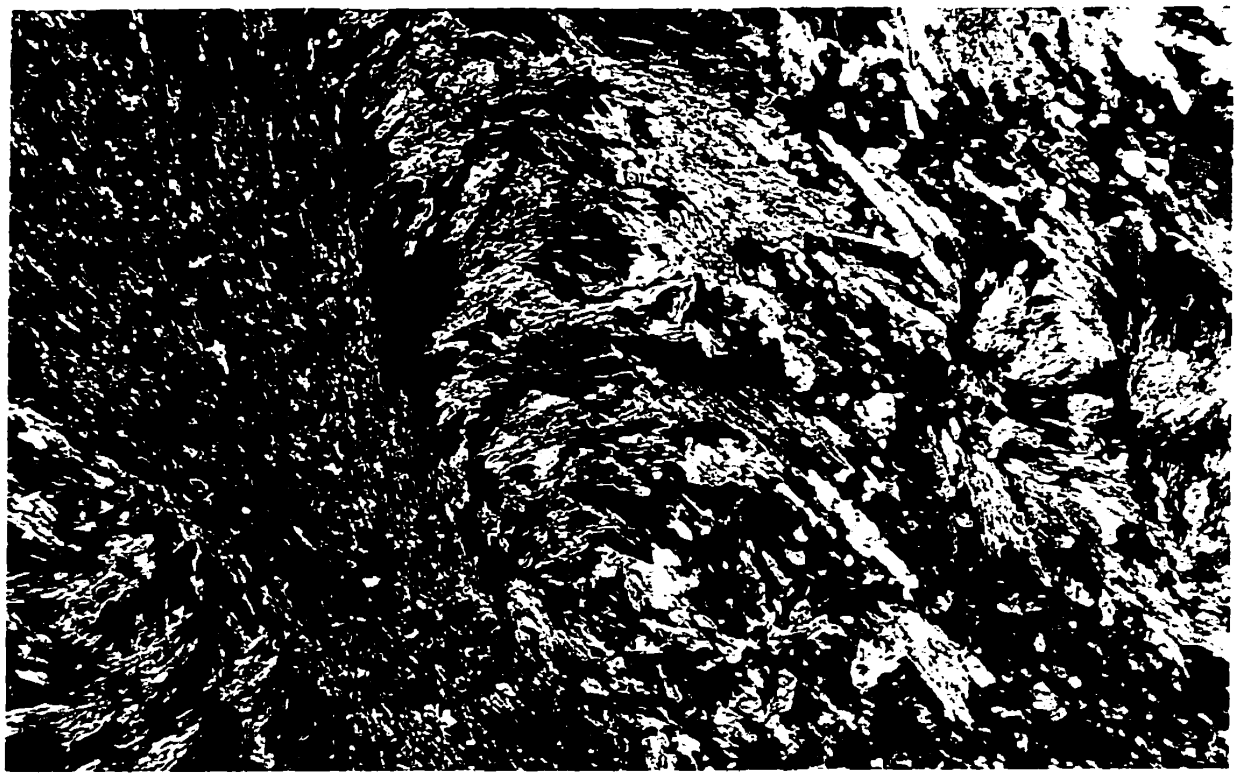

Plate 3.16. Photomicrograph of sheaf texture of amphibole in dyke sample 200-1, north of Chegoggin Point. Field of view is 4 mm. XPL.

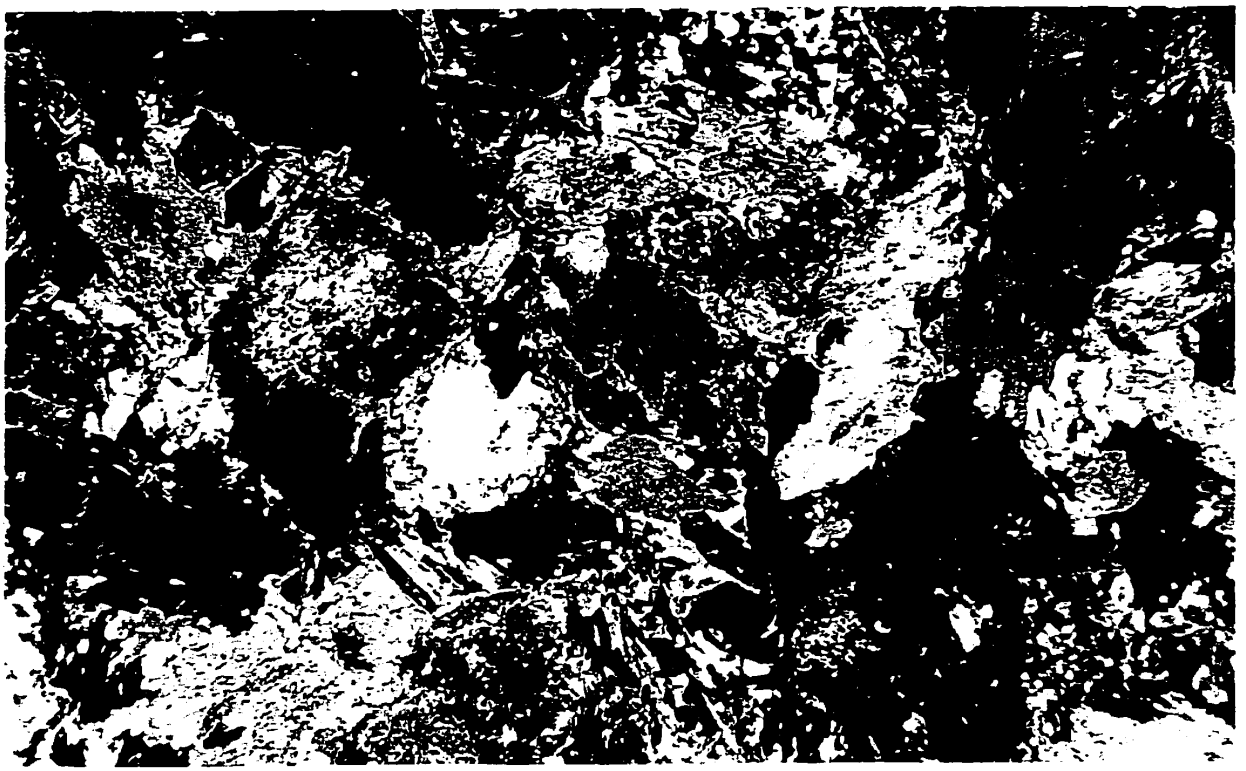

Plate 3.17. Photomicrograph of tabular texture of amphibole in dyke sample 202-1, Cranberry Head. Field of view is 4 mm. XPL.

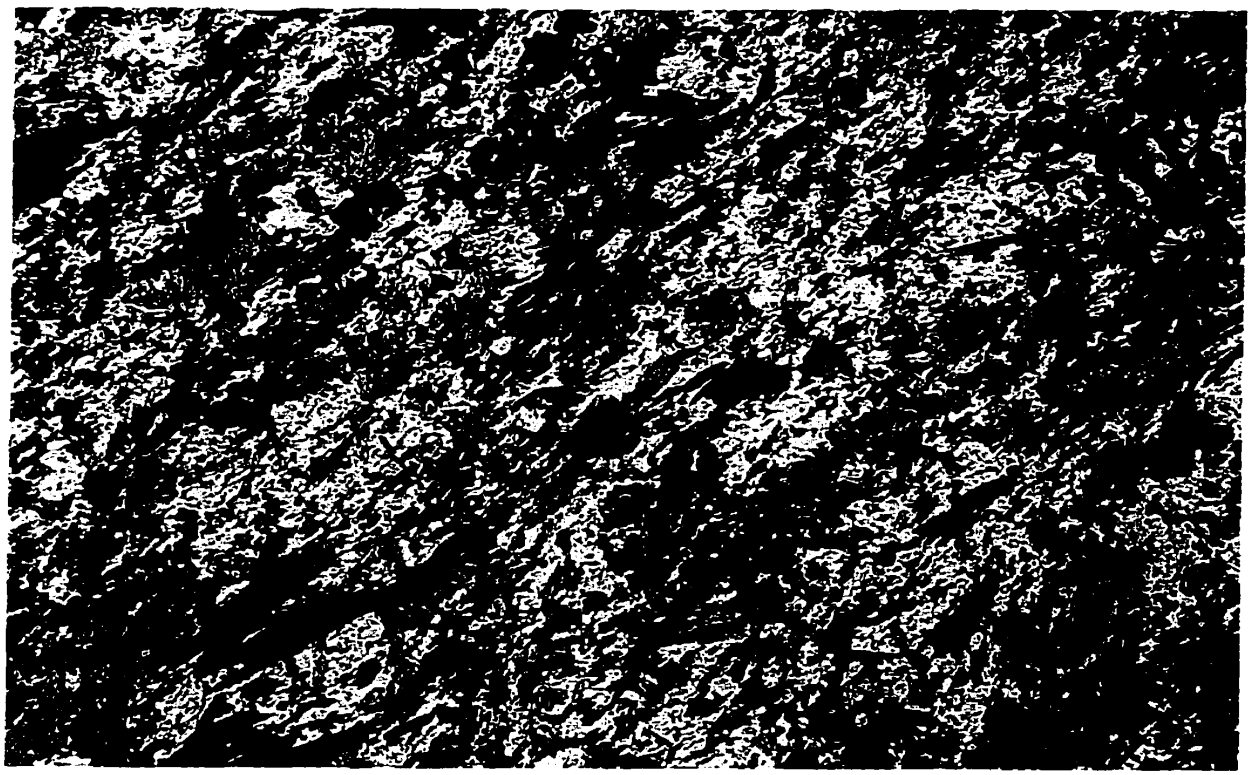

Plate 3.18. Photomicrograph of acicular amphibole texture in dyke sample 94-1, Cape Forchu. Field of view is 4 mm. PPL.

Rock formations) is apparent. Samples from different dykes near the same location (e.g. samples 206-2 and 206-3 from Chebogue Point) display different amphibole textures (bladed and tabular). Multiple samples from a single dyke or sill were not examined, so it is not known whether the texture varies within a single unit.

Bladed and sheaf/feather textured amphibole porphyroblasts may be poikiloblastic and contain quartz and opaque minerals. Amphibole porphyroblasts are generally largest when the texture is sheaf or feather. Samples with bladed amphibole grains also contain plagioclase porphyroblasts. The plagioclase grains are typically medium grained and appear recrystallized and have embayed grain boundaries. Some grains also have vermicular texture. The composition of the bladed amphibole in sample 196-1 is ferro-tschermakite and the composition of tabular amphibole in sample 205-1 is magnesiohornblende (Fig. 3.4). Samples with bladed amphibole porphyroblasts generally have a granoblastic matrix with fine-grained quartz, xenoblastic biotite, titanite, epidote and plagioclase. Saussurite, apatite, zircon and chlorite are minor components. Samples with amphibole of sheaf or feather texture also have a granoblastic matrix with fine-grained quartz, plagioclase, opaque minerals, apatite, zircon and rare epidote and biotite. Samples with tabular amphibole porphyroblasts also contain abundant plagioclase porphyroblasts. These appear subidioblastic to xenoblastic and prismatic with medium to coarse grain size. Albite twinning is sharp. The plagioclase grains are commonly altered to epidote which forms fine-grained granular clusters in the cores. The composition of the plagioclase from a sample with tabular amphibole (sample 205-1) is albite (Fig. 3.3). Samples with tabular-textured amphibole have only a minor amount of matrix, comprised of quartz, epidote, chlorite and opaque minerals.

Other types of porphyroblasts in mafic dykes and sills are not common. Opaque minerals in four samples (207-1, 94-1, 107-1 and 205-1) are up to 0.5 mm long and are subidioblastic to xenoblastic. Sample 196-1 contains medium-grained, xenoblastic biotite which is intermediate in composition between phlogopite and annite (Fig. 3.5) and rare grains of medium-grained, subidioblastic, poikiloblastic garnet of almandine composition (Fig. 3.2).

Samples with acicular amphibole porphyroblasts have a granoblastic matrix with fine-grained quartz, fine to medium-grained plagioclase, abundant xenoblastic biotite, acicular amphibole, epidote and opaque minerals.

Sample 199-1 from S_{WRss} north of Chegoggin Point is from the margin of the unusual dyke described in section 2.6. It contains pale pink garnet porphyroblasts which are up to 1.25 cm in diameter. The porphyroblasts are idioblastic and of almandine composition (Fig. 3.2). The garnet grains appear to have more than one stage of growth, as parts of the grains are poikiloblastic with abundant inclusions of opaque minerals and quartz, whereas other parts contain only a few grains of biotite, quartz or opaque minerals. The matrix of the sample is predominantly coarse-grained, subidioblastic biotite which is slightly poikiloblastic. The composition of the biotite is intermediate between phlogopite and annite but is slightly closer to annite (more Fe-rich) than biotite in samples from the White Rock Formation (Fig. 3.5). Medium-grained quartz and slightly vermicular plagioclase of andesine composition are minor components (Fig. 3.3). Medium-grained subidioblastic chlorite flakes and rare partially chloritized grains of amphibole are also present. Fine-grained opaque minerals are abundant and zircon grains

are common in biotite. Areas of biotite adjacent to parts of garnet grains with few inclusions also lack inclusions, and are slightly coarser grained than in other areas.

Foliation is evident in samples 94-1, 107-1, 207-1 and 206-2 and marked by alignment of amphibole grains. Sample 198-1 shows foliation in the matrix marked by parallel biotite grains, which are overgrown by amphibole.

3.4. Brenton Pluton

The Brenton Pluton consists of syenogranite to monzogranite with approximately equal amounts of quartz and K-feldspar and less abundant plagioclase (Plate 3.19). Other minerals present in minor quantities include biotite, muscovite, apatite, garnet and zircon. The samples typically have a strong overall foliation with parallel elongate grains of K-feldspar, plagioclase, biotite and muscovite. Elongate clusters of medium-to coarse-grained quartz, K-feldspar and plagioclase grains are also aligned.

Quartz is fine to medium grained and anhedral with a sutured appearance. It occurs locally in myrmekitic texture with plagioclase. Plagioclase is fine to coarse grained, anhedral to subhedral, and also has sutured boundaries. Plagioclase compositions obtained from sample 161D-1 are approximately An_{10} (Fig. 3.3). It displays polysynthetic twinning and inclusions of white mica, biotite, quartz and apatite. The K-feldspar is fine to coarse grained and anhedral to subhedral, with sutured grain boundaries. It is perthitic, displays cross-hatched twinning characteristic of microcline and contains inclusions of quartz, plagioclase, apatite, white mica, biotite and garnet. The composition of the K-feldspar in sample 161D-1 is close to orthoclase (Fig. 3.3). Biotite occurs as fine-to medium-grained, anhedral blades which are pleochroic yellow to green to dark green. It

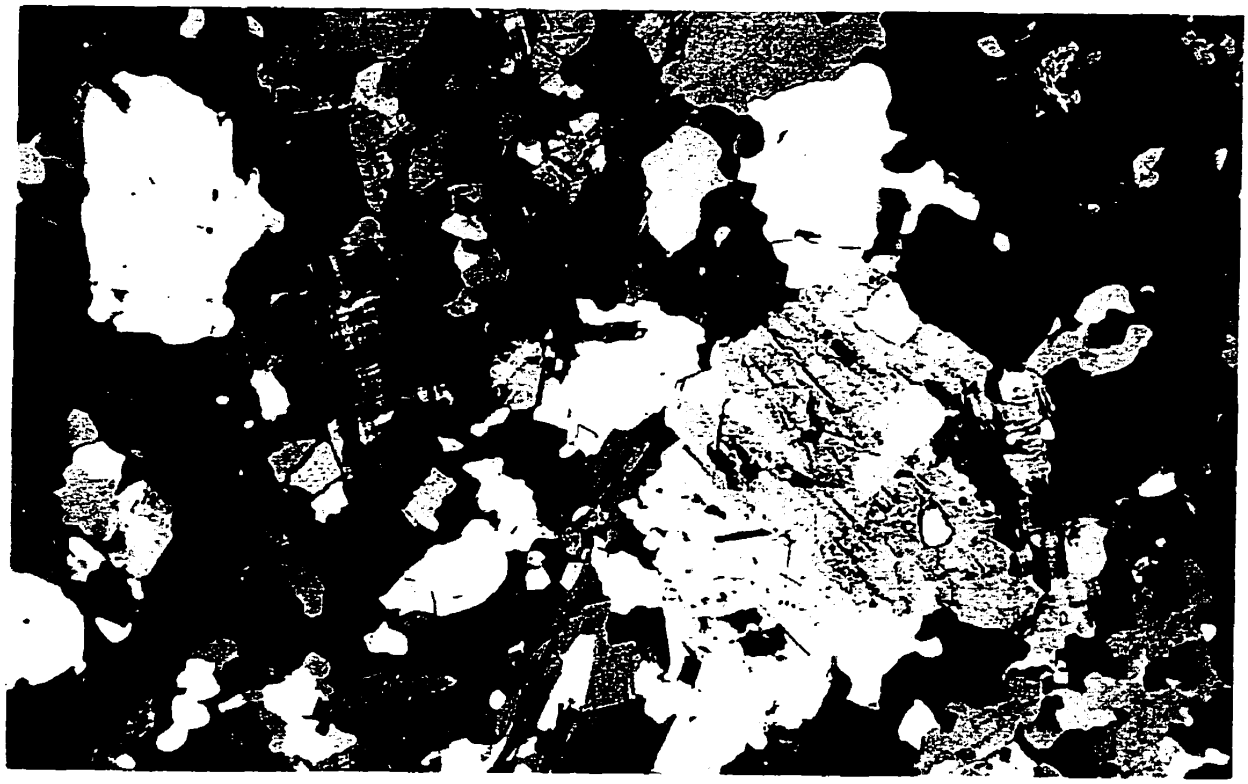

Plate 3.19. Photomicrograph showing sutured texture in granite sample 161D-1, Brenton Pluton. Field of view is 4 mm. XPL.

is commonly intergrown with muscovite and has inclusions of apatite and zircon. The composition of two biotite grains in sample 161D-1 is close to annite (Fig. 3.5). Muscovite forms fine-to medium-grained, anhedral flakes. Apatite is abundant and occurs as fine-grained, rounded, subhedral to euhedral grains. Minor pale pink, fine-to medium grained anhedral garnet was observed in nine of eleven samples. The composition of the garnet is $Alm_{59}Sp_{36}Gr_0$ (O'Reilly, 1976). Zircon is common and mainly (but not exclusively) associated with biotite. It is fine grained, subhedral to anhedral, very pale yellow-green, and rimmed by high relief, cryptocrystalline material.

Samples 157-1, 158-1, 159-1, 160-1, 161-1 and 162-1 appear more altered than samples 161A-1 through 161E-1. Feldspar grains in the altered samples are associated with reddish-brown clay, and biotite and muscovite are altered to yellow/brown clay along fractures and cleavage. Biotite is partially altered to chlorite and opaque minerals in samples 160-1 and 162-1.

3.5. Metamorphism and Deformation

Evidence for metamorphic recrystallization in metavolcanic rocks in the study area includes replacement of mafic igneous minerals (probably olivine and pyroxene) by amphibole and epidote, conversion of plagioclase to albitic compositions, and textures such as mortar, mosaic, granoblastic, polygonal and nematoblastic. Metamorphic minerals such as garnet, staurolite and chloritoid are present in metasedimentary rocks. Equilibrium conditions are indicated by polygonal textures in some matrices, large grain sizes for amphibole, garnet, staurolite and some biotite, and idioblastic grain shapes of garnet and staurolite.

Previous work by O'Reilly (1976), Hwang (1985) and Culshaw and Liesa (1997) reported chlorite zone assemblages in the Halifax and Goldenville formations and biotite and garnet zone assemblages in the White Rock Formation in theYarmouth Syncline. The present study indicates the presence of amphibolite-facies assemblages and possibly greenschist-facies assemblages in the study area. A staurolite-garnet-biotite-quartz-plagioclase assemblage occurs in metasedimentary rocks in the outer limbs of the syncline in unit S_{WRss} at Chegoggin Point, near Pleasant Valley and in the eastern part of Government Brook, indicating staurolite zone (amphibolite facies) conditions (Yardley, 1989). Toward the core of the syncline, the grade appears to decrease to upper greenschist and greenschist facies. The apparent decrease in grade may be an effect of the change in rock type from predominantly metasedimentary to metavolcanic. Because changes in metabasite under greenschist- and amphibolite-facies conditions are the result of continuous reactions, the boundary between these two facies is not clearly defined (Yardley, 1989) and therefore metamorphic conditions are better defined by the pelitic assemblage.

Most mafic metavolcanic rocks in units S_{WRmf}, S_{WRft} and S_{WRmt} contain actinolite, actinolitic hornblende (possibly retrograde?), magnesiohornblende and tschermakitic hornblende with albitic plagioclase and epidote. One tuff sample (196-1) from unit S_{WRft} contains oligoclase and both actinolite and actinolitic hornblende, suggesting amphibolite-facies conditions. Felsic metavolcanic rocks contain epidote and biotite. Metasedimentary rocks near the core in unit S_{WRmt} have chloritoid, indicating garnet zone metamorphism (Yardley, 1989). Mafic dykes and sills show greenschist facies to amphibolite-facies assemblages, such as albitic plagioclase and amphibole compositions

ranging from actinolitic hornblende to Fe-tschermakite, similar to their host rocks (Yardley, 1989).

O'Reilly (1976) and Hwang (1985) reported evidence for a contact metamorphic aureole associated with the Brenton Pluton, in the form of amphibolite-facies rocks located near the western and northern contacts of the pluton. O'Reilly (1976) reported a change in metamorphic grade in the country rock (Halifax Formation) east of the pluton from amphibolite facies to chlorite grade, and interpreted the change to indicate a contact aureole. Hwang (1985) did not find evidence of a contact aureole east of the pluton but attributed the absence to a faulted contact between the Brenton Pluton and the Halifax Formation. No compelling evidence for contact metamorphism was found in this study. The high metamorphic grade on the western and northern margins of the pluton is consistent with the regional metamorphic grade observed locally in the White Rock Formation away from the Brenton Pluton.

Culshaw and Liesa (1997) interpreted two episodes of deformation and metamorphism in the Yarmouth area. The first episode, D1, was a single-phase episode during the Acadian orogeny (ca. 415 – 370 Ma) to which they attributed the formation of major folds, initiation of the shear zone at Cape Forchu, and the formation axial planar cleavage. A U-Pb age of 380 +/- 3 Ma for monazite in the Brenton Pluton has been interpreted to be the age of low-pressure, high-temperature metamorphism (J.D. Keppie, written comm., NSDNR, 1999), which indicates peak metamorphism at ca. 380 Ma in the Yarmouth area. Metamorphic grade achieved during this episode was variable but locally reached garnet zone.

The second episode of deformation (D2) was described by Culshaw and Liesa (1997) as polyphase, with effects such as the overturning of D1 folds, reactivation of older shear zones and initiation of shear zones on the outer limbs of the D1 fold at Cranberry Head and Chebogue Point. Greenschist-facies metamorphism which accompanied the deformation included temperatures sufficient to reset micas and variably overprint earlier grade. $^{40}Ar/^{39}Ar$ dating of muscovite grains in D2 shear zones by Culshaw and Reynolds (1997) indicated a Mid-Carboniferous (Alleghanian-Variscan) age of ca. 320 Ma for the D2 event.

The foliation in the White Rock Formation and Brenton Pluton (Fig. 2.1) developed during D1. In thin section, the foliation is defined by alignment of minerals such as amphibole and mica. Foliation in the White Rock Formation is best developed in metasedimentary rocks, particularly slate and schist. Slate sample 144-1 from unit S_{WRmt} near the core of the syncline shows evidence for one episode of deformation with pre- or syndeformational growth of chloritoid porphyroblasts. Schist samples from Government Brook reveal a more complex history. Biotite porphyroblasts contain randomly oriented inclusions, indicating growth prior to foliation of the matrix. Plagioclase porphyroblasts contain aligned inclusions but the orientation is not parallel with the matrix, indicating that plagioclase growth occurred after initial foliation of the matrix and that deformation continued after plagioclase growth. Garnet porphyroblasts also have aligned inclusions which are not parallel with the matrix, indicating syndeformational growth of garnet. Staurolite grains also contain aligned inclusions but the trend of the inclusions is close to the trend of the matrix foliation. This relationship may indicate that staurolite growth was later than garnet or plagioclase formation.

Slate and phyllite with well developed crenulation at Cranberry Head and Chebogue Point are within D2 shear zones proposed by Culshaw and Liesa (1997). Minor faults also occur at Chegoggin Point, Overton, Cape Forchu West and Sunday Point which may be the result of either D1 or D2. A possible metamorphic feature of D2 is the growth of amphibole which cuts across previous foliation, seen in some samples of mafic tuff and flows. Another effect of D2 greenschist metamorphism is possible retrogression of hornblende (characteristic of upper greenschist and amphibolite facies) to more actinolitic compositions (characteristic of greenschist-facies conditions).

Local metasomatism of dykes may be indicated by unusual mineralogy and texture exhibited by samples such as 199-1 and samples with very coarse-grained sheaf texture amphibole (131-1 and 132-1). These samples are not foliated, suggesting metasomatism post-dated D1 deformation.

Chapter 4 Geochemistry and Age

4.1. Introduction

The purpose of this chapter is to describe and interpret the chemical characteristics of the igneous rocks in the study area. The chemical data are also used to assess the relationship between the volcanic rocks of the White Rock Formation and the Brenton Pluton, and to interpret the tectonic setting in which they were formed. A U-Pb date and Sm-Nd data are presented for a felsic volcanic sample from the White Rock Formation to assist in the interpretation of petrogenesis of the felsic rocks and establish the age.

Geochemical data obtained during the present study include major and trace elements from 40 samples. Results and methods of analysis are presented in Appendix C. Twenty-one of the samples are from the White Rock Formation: 7 samples from inferred mafic flows in units S_{WRft}, S_{WRmf}, and S_{WRmt}, 5 samples from mafic tuff in units S_{WRmf} and S_{WRmt}, 3 mafic lithic tuff samples from unit S_{WRmt}, 1 sample of mafic crystal tuff from unit S_{WRmf}, 3 amphibolite samples from units S_{WRsv} and S_{WRft}, an intermediate crystal tuff sample from unit S_{WRft}, and a felsic crystal tuff sample from unit S_{WRft} (Fig. 3.1). Eight samples are from mafic dykes and sills, six hosted by the White Rock Formation and two by the Halifax Formation. The remaining 11 analyzed samples are from the Brenton Pluton (Fig. 3.1).

In addition, rare earth element data (Appendix D) were obtained for 7 of these samples (3 mafic flow samples, 1 felsic crystal tuff sample, 2 samples from mafic sills, and 1 sample from the Brenton Pluton). The felsic crystal tuff sample was also analyzed

for Sm and Nd isotopes (Appendix E), and zircon from the sample was dated using the U-Pb method by J. Ketchum at Memorial University , St. John's, Newfoundland.

4.2. Effects of Alteration and Metamorphism

Field and petrographic evidence described in chapters 2 and 3 shows that metamorphism and alteration have affected the rocks in the study area. Original igneous minerals, which probably included olivine, pyroxene and plagioclase, have been metamorphosed to phases such as amphibole, biotite, and albite. Quartz veining is extensive and calcite veins and infilling of voids are also common. Samples contain abundant chlorite, epidote, sericite, saussurite and carbonate minerals. Rocks which have undergone these mineralogical and textural changes are likely to also have undergone element mobility (e.g. Rollinson, 1993). Generally, incompatible elements of low field-strength (e.g. Cs, Rb, K, Ba, Sr) are likely to be most mobile (Brewer and Atkin, 1989; Rollinson, 1993; Brewer and Menuge, 1998). Under greenschist- and amphibolite-facies metamorphic conditions, elements such as Fe, Mg, Na, K, Si, Ca, and Na are known to be mobile in basalts (Rollinson, 1993). In contrast, high field-strength elements such as REE, Sc, Y, Th, Zr, Hf, Ti, Nb, Ta, P are typically immobile (Floyd and Winchester, 1978; Rollinson, 1993). Mobility of transition metals varies; Mn, Zn and Cu tend to be mobile (particularly under high-temperature conditions) whereas Co, Ni, V, and Cr tend to be immobile (Rollinson, 1993).

Loss on ignition (LOI) values also provide an indication of the degree of alteration in mafic rocks. Mafic samples from the study area have LOI values ranging from 0.1 % to 4.01 % (Appendix C). Mafic tuff samples have the highest values of LOI

of the volcanic samples, and mafic flows and dykes and sills have the lowest values. Samples from the Brenton Pluton have the lowest average LOI values.

In order to assess mobility of elements analyzed in samples from this study, diagrams were constructed which plot typically immobile elements against both mobile and other potentially immobile elements (Fig. 4.1, 4.2). Plots of "mobile" elements and oxides such as SiO_2, CaO, Na_2O, K_2O, Rb, and Sr versus relatively "immobile" Nb show little correlation, indicating these elements are probably unreliable (Fig. 4.1, 4.2), whereas plots of TiO_2 against Nb, Zr versus Nb, V versus TiO_2 and Y versus Zr (Fig. 4.2) show linear correlation among the mafic samples, particularly mafic flows, indicating immobility or at least "coherent mobility" during alteration or metamorphism. Therefore, elements such as Zr, Nb, V, Ti and Y are likely to be more reliable indicators of original chemical characteristics than Si, Ca, Na, K, Rb, or Sr. The plot of Y versus Nb, although linear, does not have an origin at 0,0, indicating some mobility (enrichment) on the part of Y (Rollinson, 1993). The more felsic volcanic samples and samples from the Brenton Pluton generally plot separately from the mafic samples. Samples from the Brenton Pluton show internal consistency and generally plot together, whereas the two intermediate and felsic crystal tuff samples typically plot in different places.

Another method of gauging alteration is to plot data on an "igneous spectrum" diagram (Fig. 4.3), which uses the typically mobile components K_2O and Na_2O to illustrate degree of alteration. Most samples from mafic flows plot in or near the igneous spectrum, whereas tuffaceous samples scatter into both the spilite and keratophyre fields (Fig. 4.3). Mafic dyke and sill samples also show scatter. Samples from the Brenton Pluton and felsic crystal tuff sample 4-1 also plot in or near the igneous spectrum, but

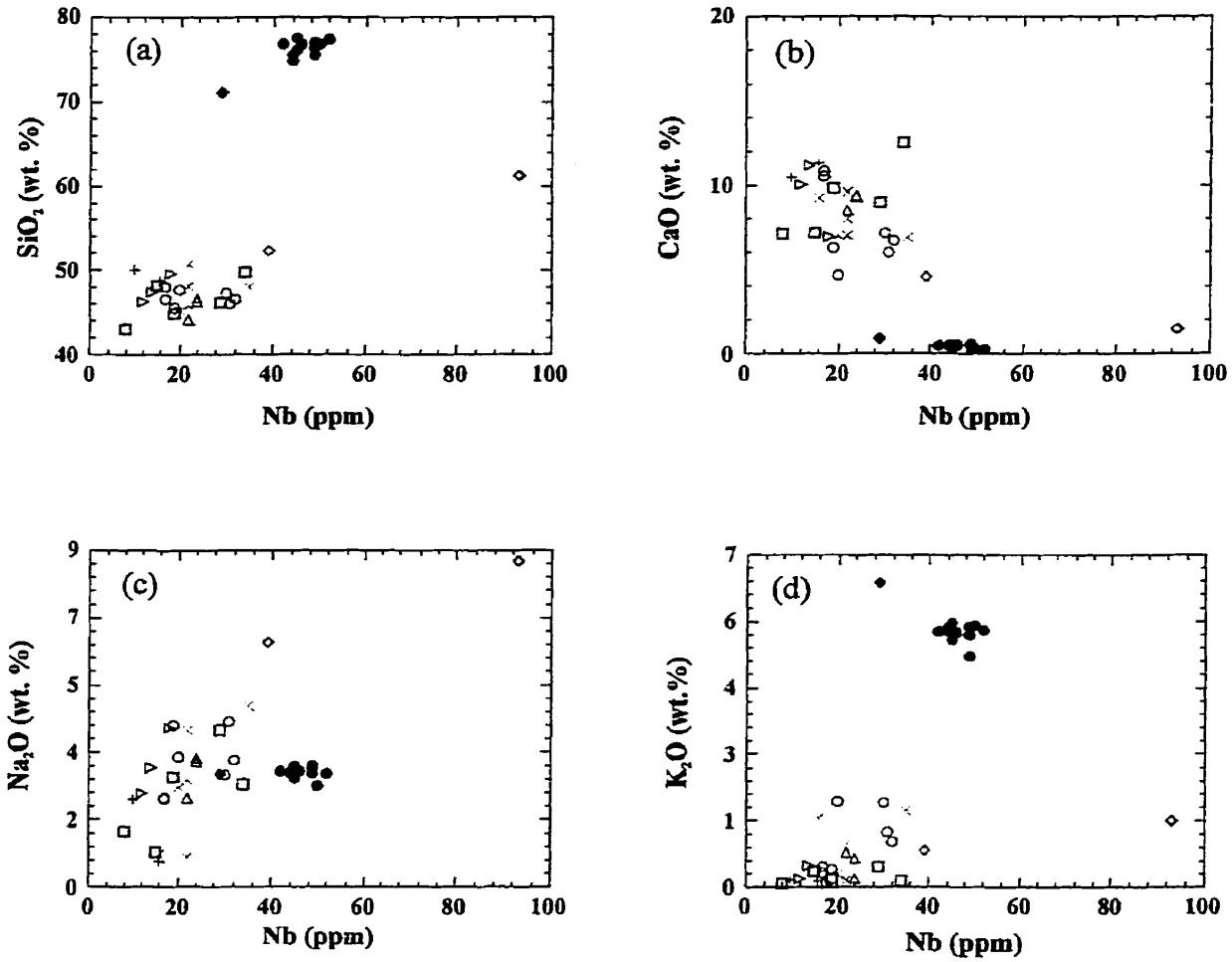

Figure 4.1. Plots of (a) SiO_2, (b) CaO, (c) Na_2O, and (d) K_2O against Nb to evaluate degree of chemical alteration in analyzed samples.

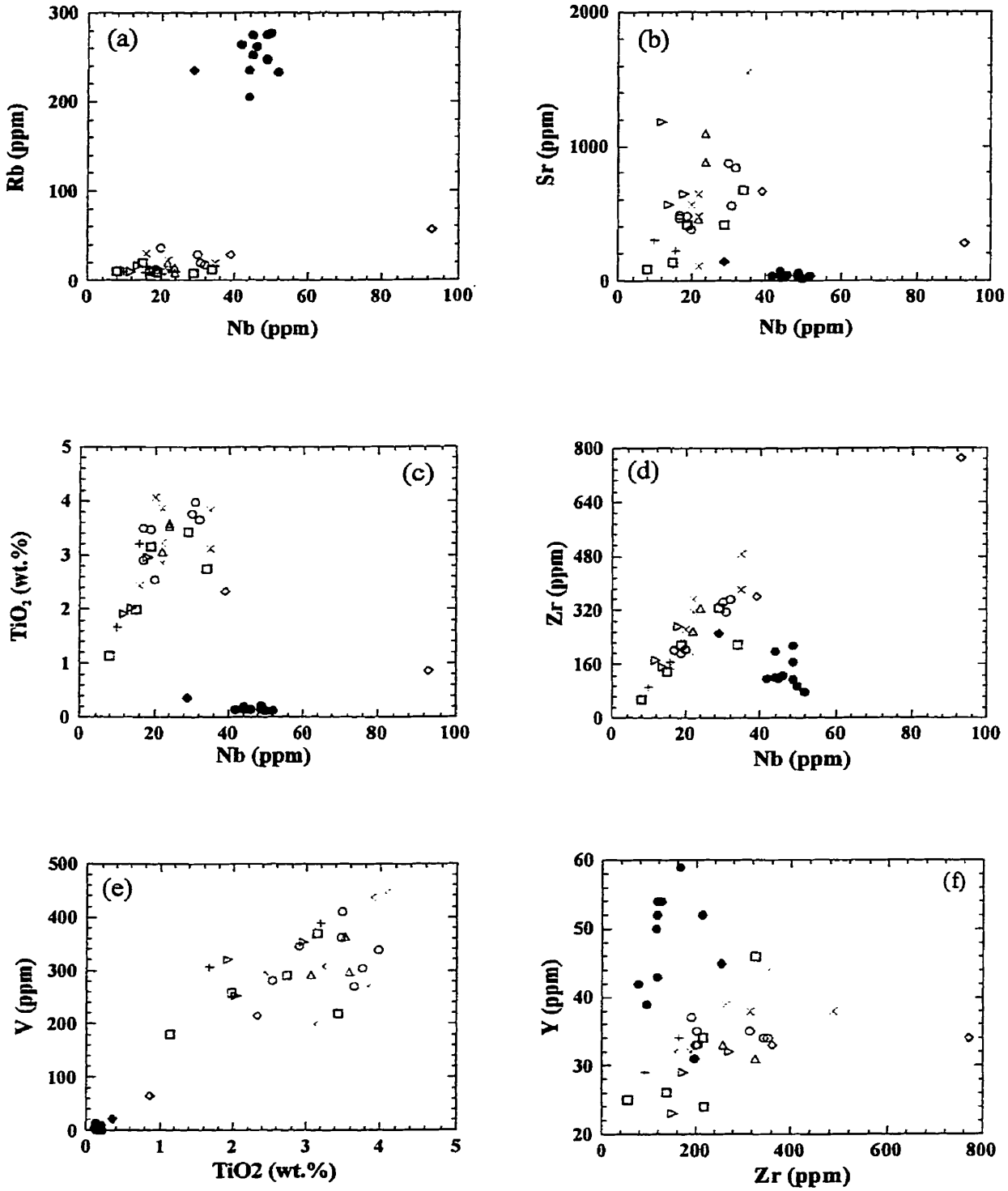

Figure 4.2. Plots of (a) Rb, (b) Sr, (c)TiO_2 and (d) Zr against Nb, (e) V against TiO_2, and (f) Y against Zr to assess degree of chemical alteration in analyzed samples. Symbols as in Figure 4.1.

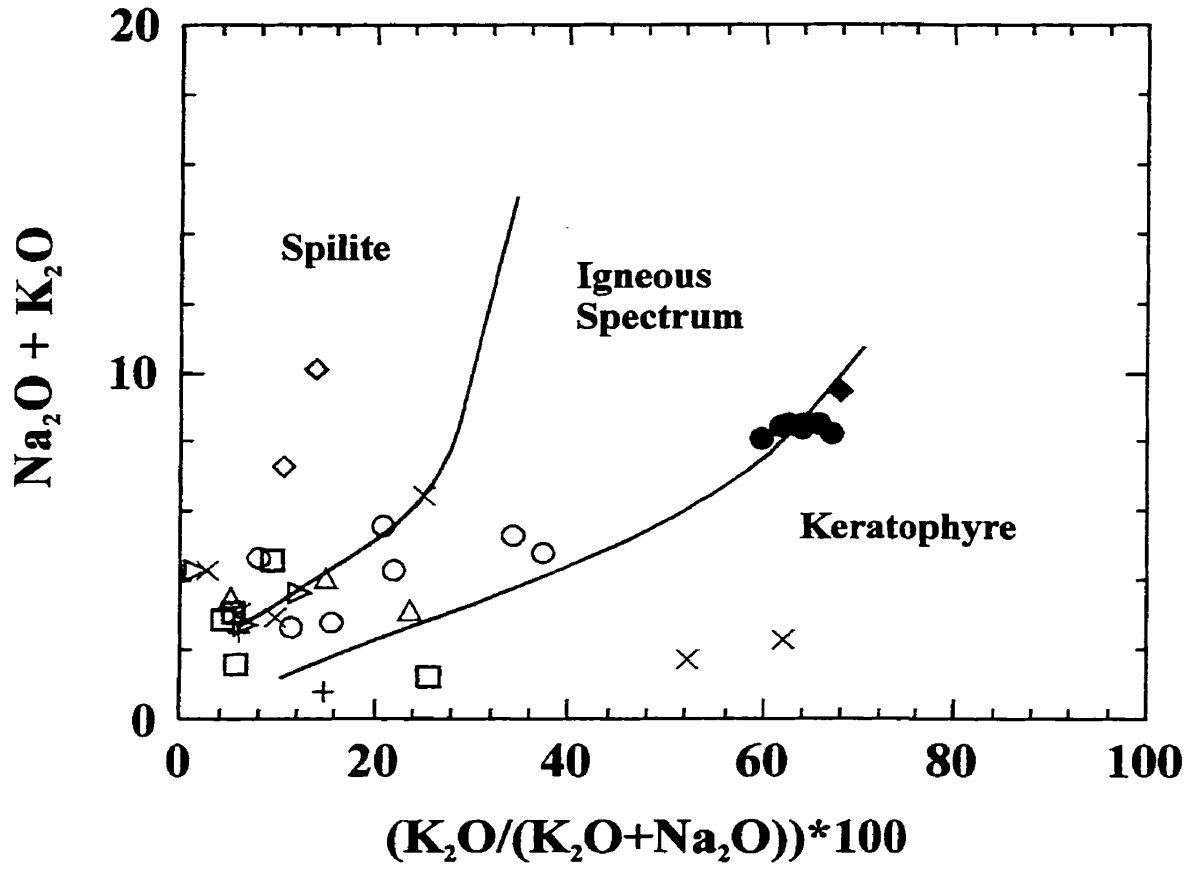

Figure 4.3. Samples from the study area plotted on the igneous spectrum of Hughes (1973). Symbols as in Figure 4.1.

the intermediate crystal tuff sample 9-1 plots in the spilite field. The anomalous composition of sample 9-1 is also apparent in figures 4.1 and 4.2 (i.e., high Na_2O, Nb, and Zr and low K_2O and Rb).

4.3. Major Element Geochemistry

4.3.1. Mafic Volcanic Rocks

Silica contents in mafic volcanic samples range from 43.01 % to 52.40 % (Fig. 4.4). Mafic tuff samples generally have a wide spread in major element contents, probably reflecting, at least in part, the primary inhomogeneity of tuffaceous samples. The mafic flows show less variation than the tuffaceous samples, with a range of SiO_2 between 45.55 % and 48.03 % (Fig. 4.4). A plot of TiO_2 versus SiO_2 (Fig. 4.4a) shows a weak negative correlation with SiO_2. Higher values of TiO_2 in mafic rocks are consistent with higher abundance of Ti-bearing minerals such as magnetite and titanite. Plots of $Fe_2O_3^t$, MnO and MgO also show a weak negative correlation with SiO_2 (Fig. 4.4c, d, e). Higher abundance of these elements in low-SiO_2 volcanic samples is consistent with higher abundance of ferromagnesian minerals such as amphibole, biotite and epidote compared to samples with higher SiO_2.

CaO shows no apparent correlation with SiO_2 values (Fig. 4.4g). Samples from mafic flows show a range in CaO content from 4.64 % to 10.81 % and mafic tuff samples (including lithic tuff) range from 7.13 % to 12.51 %. CaO values in the three samples of amphibolite range from 6.95 % to 11.18 % (Fig. 4.4g). Al_2O_3 show no correlation with SiO_2 (Fig. 4.4b). Most mafic volcanic samples have between 13% and 17% Al_2O_3, except for a sample of mafic crystal tuff which contains 19.04 %. Values of CaO and Al_2O_3 are

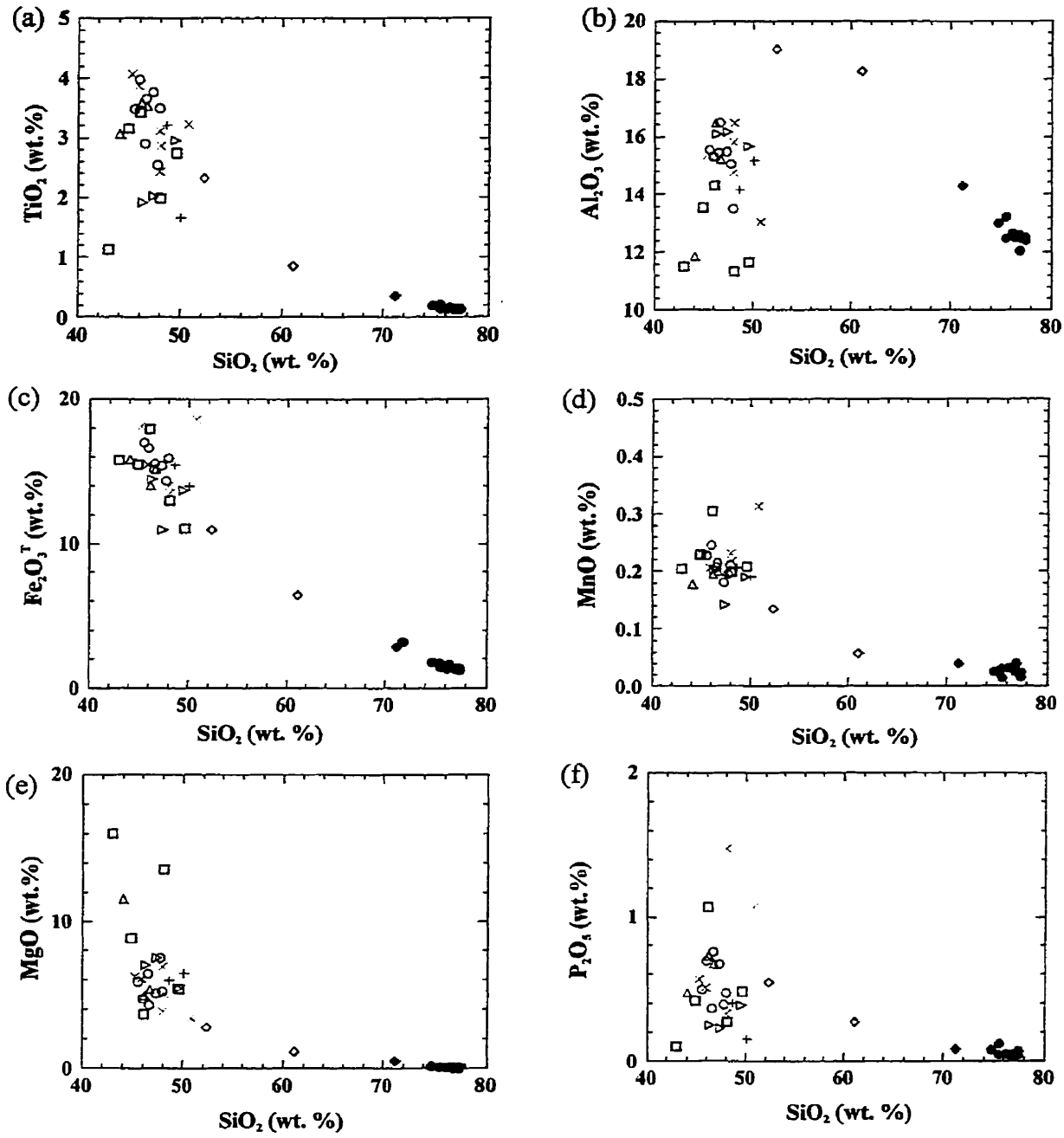

Figure 4.4. Major element variation diagrams for samples from the study area.

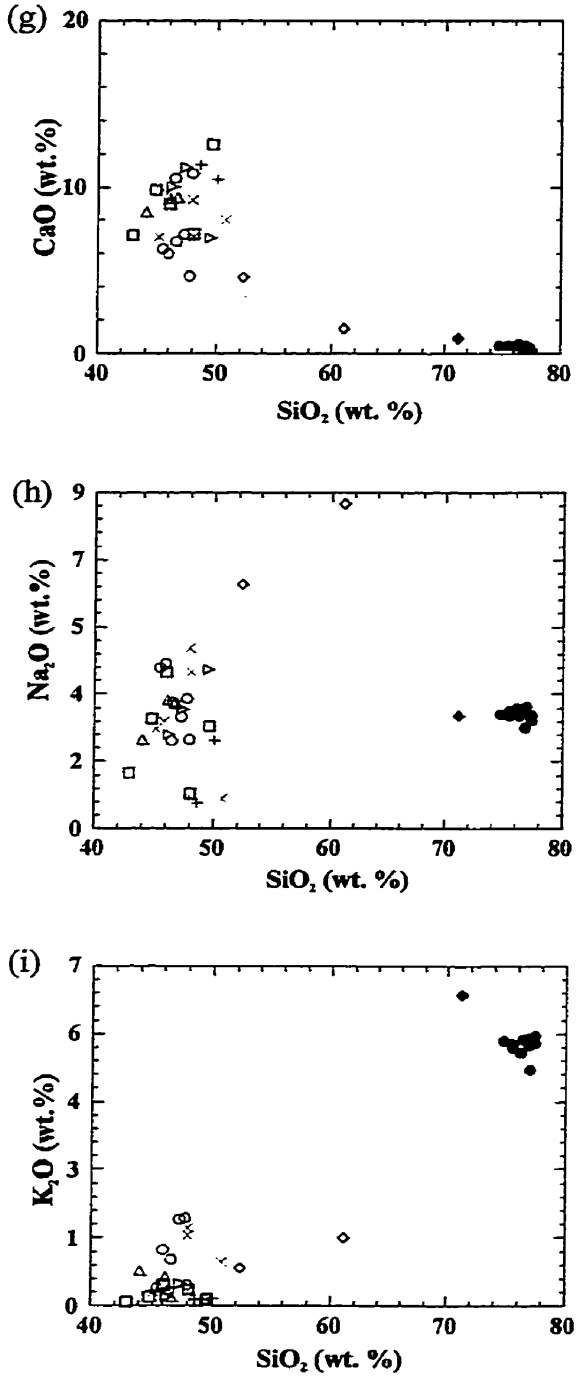

Figure 4.4. continued.

consistent with very high plagioclase content in the mafic samples (relict crystals and matrix grains). Samples with lower values are a lithic tuff sample and mafic tuff samples with very low plagioclase content, abundant alteration and abundant amphibole and epidote.

Plots of Na_2O and K_2O also show no correlation with SiO_2 (Fig. 4.4h, i), reflecting high mobility demonstrated in Figure 4.2c and d. The variation diagram of Na_2O shows wide range in mafic volcanic samples, especially among tuffaceous samples, with values from approximately 1 % to 6.5 %. Na_2O values in flow samples cluster between 2.5 % and 4.5 %, correlating with less alteration, as suggested in Figure 4.3, and greater homogeneity compared to tuffaceous samples. The range in K_2O values among mafic samples is much less than Na_2O, and values are within a 2 % range. Samples with higher values have higher biotite abundances.

Mafic volcanic samples generally contain similar levels of P_2O_5 (Fig. 4.4f) but mafic tuff samples display a wider range of values than mafic flow or amphibolite samples.

4.3.2. Intermediate and Felsic Volcanic Rocks

The intermediate crystal tuff (sample 9-1) has a SiO_2 content of 61.16 %, whereas the felsic crystal tuff (sample 4-1) contains 71.17 % SiO_2 (Fig. 4.4). TiO_2, $Fe_2O_3^t$, MnO, MgO, CaO and P_2O_5 values are low compared to those in mafic samples, consistent with low abundances of opaque minerals, ferromagnesian minerals, titanite and apatite relative to mafic rocks. Sample 9-1 has high Na_2O content, (8.71 %), consistent with its high

abundance of (sodic) plagioclase. In contrast, sample 4-1 has high K_2O content (6.43 %), consistent with its high content of modal K-feldspar.

4.3.3. Mafic Dykes and Sills

Most of the samples from mafic dykes and sills are chemically similar to the mafic volcanic samples (Fig. 4.4). The samples plot within the range of mafic volcanic samples in Al_2O_3, $Fe_2O_3^t$, MgO, K_2O and CaO contents, but some samples are outside the mafic volcanic field on other plots. In the case of MnO and P_2O_5, mafic dyke samples 199-2 and 94-1 have higher abundances relative to other dykes and sills and to mafic volcanic samples. Sample 199-2 has elevated MnO content which is consistent with the abundance of almandine-spessartine garnet porphyroblasts, and both sample 199-2 and 94-1 have higher P_2O_5 contents, consistent with high abundances of apatite observed in thin section. Samples 207-1 and 199-2 have lower Na_2O content relative to other dykes and sills, as well as to mafic volcanic samples. These samples have less plagioclase and abundant sericite alteration. Sample 202-1 from a dyke in the Halifax Formation has an anomalously low TiO_2 value with respect to other dykes and sills and contains a lower abundance of opaque minerals.

4.3.4. Brenton Pluton

The 11 analyzed samples from the Brenton Pluton consistently cluster together on the SiO_2 variation diagrams (Fig. 4.4). They have higher SiO_2 contents (74.78 % -77.48 %) than felsic crystal tuff sample 4-1 (71.17 %) and correspondingly lower TiO_2, $Fe_2O_3^t$,

MnO, MgO, CaO and P_2O_5 contents. They also have lower Al_2O_3 and K_2O contents, but similar Na_2O contents (Fig. 4.4).

4.4. Trace Element Geochemistry

4.4.1. Mafic Volcanic Rocks

Concentrations of Ba in mafic samples from the Yarmouth area range from less than 1 ppm to 659 ppm, but most values are less than 400 ppm (Fig. 4.5a). Mafic flows have a slightly higher average Ba concentration than mafic tuff samples, consistent with overall higher biotite abundance. Rb concentrations are less than 40 ppm and form a coherent cluster with little variation (Fig. 4.5b).

A plot of Sr versus SiO_2 shows little correlation with SiO_2 (Fig. 4.5c). Sr has a wide spread of values in mafic rocks, consistent with variable abundance of plagioclase and amphibole. Mafic flow samples show less variation than tuff samples. Amphibolite samples and samples of mafic lithic tuff have similar Sr concentrations and similar plagioclase and amphibole contents. Mafic tuff contains the least Sr on average compared to other mafic rocks, reflecting lower plagioclase contents and lack of relict plagioclase crystals.

No correlation is apparent between Y and SiO_2 (Fig. 4.5d). Y values range from 23 ppm to 46 ppm, and samples of mafic tuff have the widest spread of concentrations, consistent with inhomogeneity of the samples. Less variation is seen in amphibolite and mafic flow samples.

Values of Zr are between 55 ppm and 480 ppm in the mafic samples and no correlation with SiO_2 is apparent (Fig. 4.5e). Mafic flows have slightly higher average

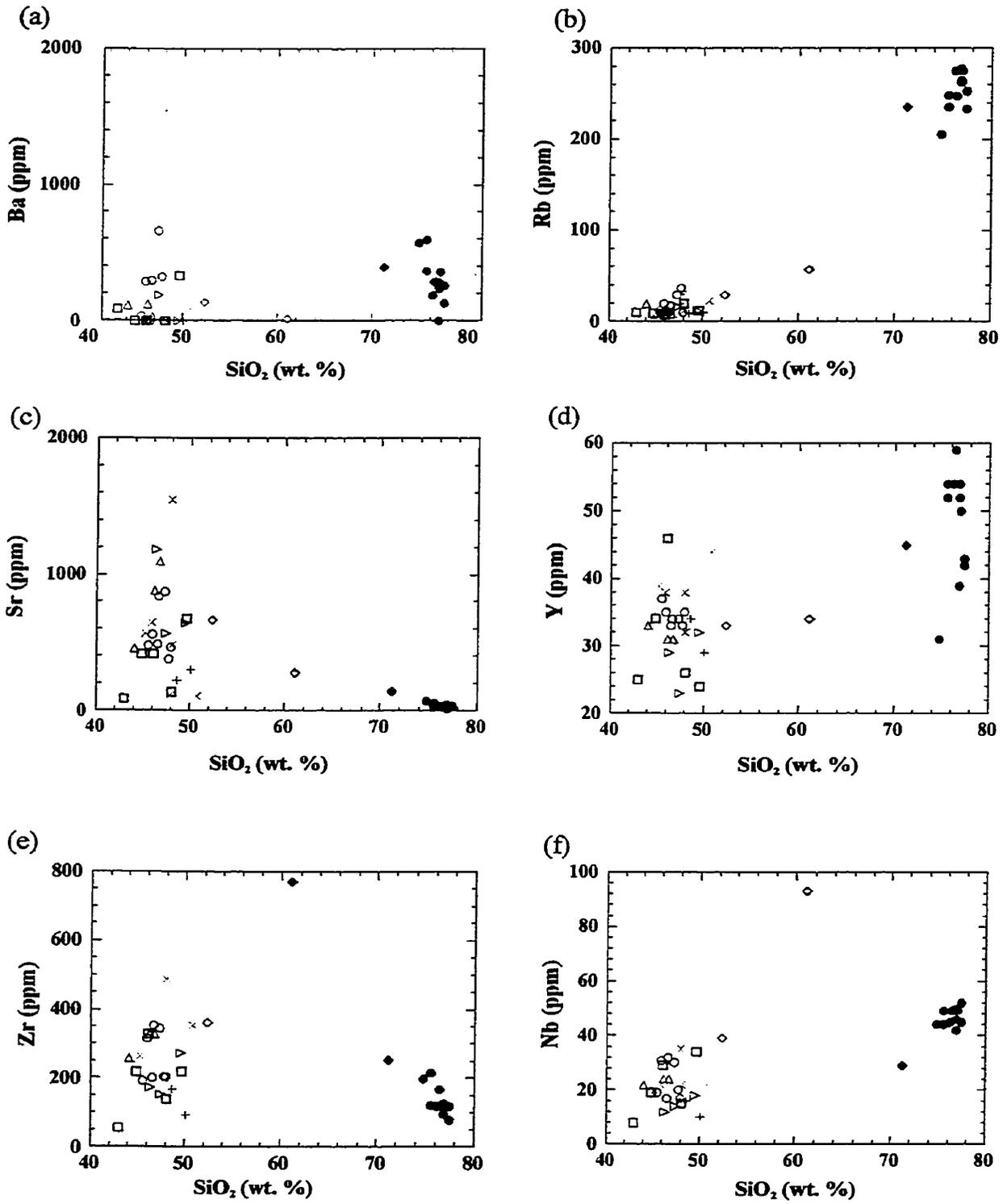

Figure 4.5. Trace element variation diagrams for samples from the study area. Symbols as in Figure 4.4.

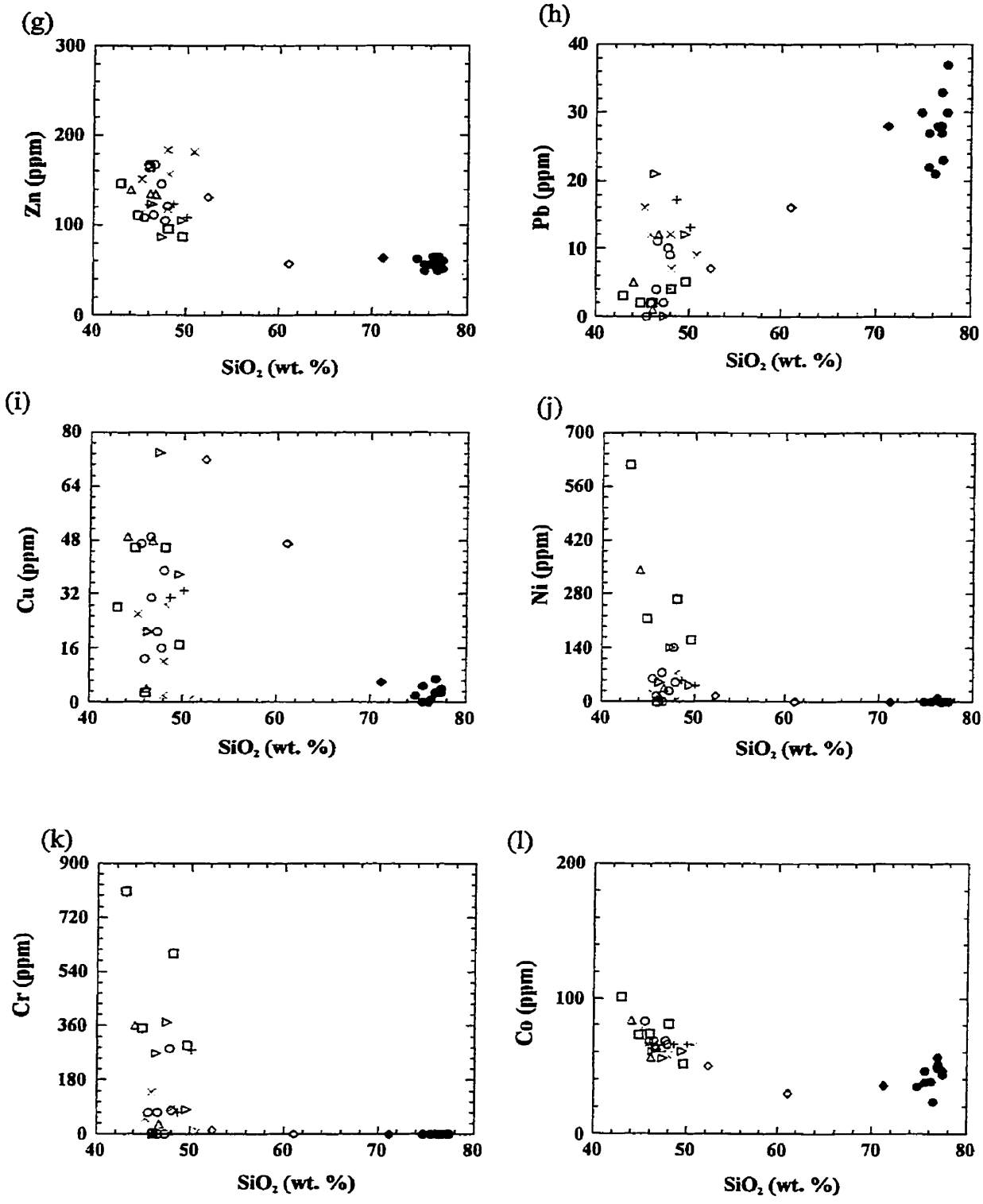

Figure 4.5. continued.

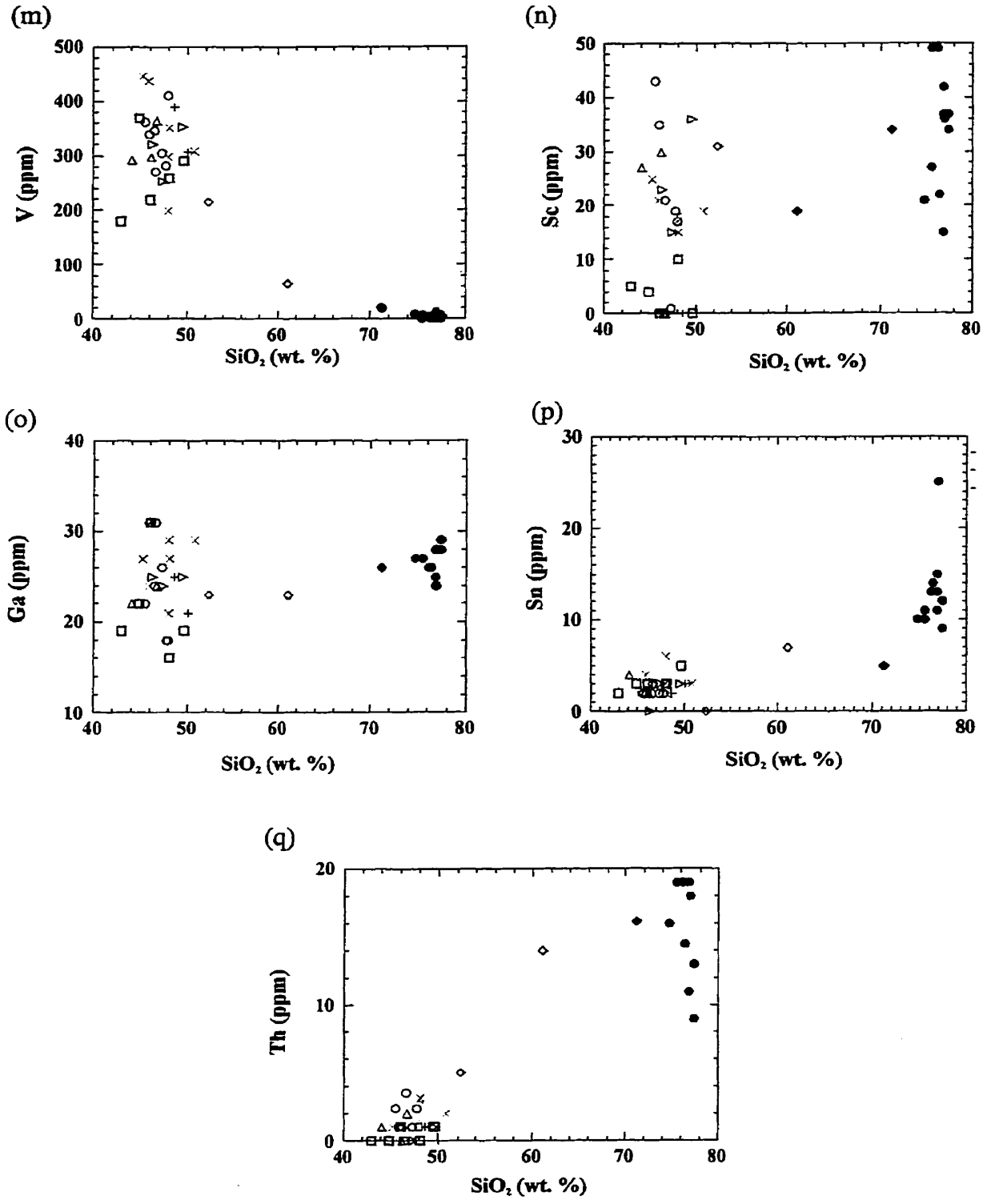

Figure 4.5. continued.

concentrations than mafic tuff or amphibolite. Values of Nb in mafic volcanic rocks are between 8 ppm and 39 ppm with no correlation with SiO_2 (Fig. 4.5f). Mafic tuff samples contain the widest range of Nb and lithic tuff and amphibolite show the least variation. Samples with elevated Zr concentrations also have elevated Nb values.

The abundance of Zn in mafic volcanic samples ranges from 80 ppm to 175 ppm and shows weak negative correlation with SiO_2 (Fig. 4.5g). The concentration of Pb ranges from <1 ppm and 21 ppm (Fig.4.5h). The amount of Cu in mafic volcanic samples ranges from < 1 ppm to 72 ppm (Fig. 4.5i). The samples with highest Cu concentration have the lowest Zn levels and vice versa.

The abundance of Ni in samples from the study area varies between <1 ppm to 618 ppm but most values are less than 100 ppm (Fig. 4.5j). Mafic tuff samples have the largest spread of values and highest Ni contents whereas mafic flow samples plot together with between <1 ppm and 120 ppm Ni. Chromium contents range from less than 1 to 805 ppm (Fig. 4.5k). As with Ni, mafic tuff samples have the highest values of Cr and the widest concentration range and samples of flows have more consistent in Ni contents. Samples high in Ni and Cr also have high MgO and may orginally have contained more olivine and pyroxene.

Cobalt values range from 50 ppm to 101 ppm and show negative correlation with SiO_2 (Fig. 4.5l), reflecting higher amounts of ferromagnesian minerals present in the mafic rocks.

Abundance of V in mafic volcanic samples varies from 180 ppm to 410 ppm (Fig. 4.5m). Mafic tuff and mafic flow samples show a similar range of values. Samples with abundant V also have high amounts of TiO_2 and the highest concentrations occur in

samples with the highest titanite and opaque mineral content. Sc levels range from <1 ppm to 44 ppm and show no correlation with SiO_2 content (Fig. 4.5n). Tuffaceous samples tend to have lower Sc contents than samples of mafic flows. Concentrations of Ga vary between 16 ppm and 43 ppm (Fig. 4.5o). Concentrations of Sn and Th are low in mafic samples, ranging from <1 ppm to 5 ppm and <1 ppm to 3 ppm, respectively (Fig. 4.5p, q).

4.4.2. Intermediate and Felsic Volcanic Rocks

Felsic crystal tuff sample 4-1 contains higher Ba and Rb contents than the intermediate sample 9-1 (Fig. 4.5). Higher concentrations of Ba and Rb are consistent with a higher abundance of K_2O in sample 4-1 and related to the higher K-feldspar content. The intermediate sample 9-1 has a higher Sr content than the felsic sample, consistent with higher plagioclase content. Rb and Sr (and Ba as well) are mobile in these rocks as illustrated in Figure 4.3, and sample 9-1 is more altered than sample 4-1 (Fig. 4.3). Therefore comparison of these elements between the 2 samples is not likely to reflect the original relationship. Sample 9-1 also displays higher Zr, Nb and Cu concentrations than the felsic sample (Fig. 4.5e, f, i). Abundances of Zn, Pb, Ni, Cr, Co, V, Sc, Ga, and Th and are generally similar between the two samples (Fig.4.6g, h, j, k, l, m, n, o, q).

4.4.3. Mafic Dykes and Sills

Mafic dyke sample 94-1 from the White Rock Formation has the highest concentrations of Ba, Sr, Zr, and Zn of all the mafic samples (Fig. 4.5a, c, e, g) and has higher concentrations of Nb, Cu, Ni, Ga, and Sn than other dykes or sills (Fig. 4.5f, i, j, o, p). No correlation is apparent between trace element concentrations and amphibole textures described in section 3.3. Trace element values in mafic dykes and sills are similar to those in mafic volcanic samples, except for slightly higher abundances of Zn and V (Fig. 4.5).

4.4.4. Brenton Pluton

Most trace elements show only slight variation in samples from the Brenton Pluton. The exceptions are Y (31 ppm – 59 ppm; Fig. 4.6d) and Zr (78 ppm – 215 ppm; Fig. 4.5e). Compared to the felsic crystal tuff sample 4-1, most trace element concentrations are similar, except for lower Zr (Fig. 4.5e), higher Nb (Fig. 4.5f), and higher Sn (Fig. 4.5p) in the granite samples.

4.5. Rare Earth Element Geochemistry

4.5.1. Mafic Volcanic Rocks

Three samples from mafic flows in units S_{WRmf}, S_{WRft}, and S_{WRmt} show enrichment in light REE (LREE) relative to chondrite abundance and less enrichment in heavy REE (HREE) relative to chondrite composition (Fig. 4.6). Samples 2-1 and 75A-1 have similar REE patterns overall and are lower in LREE than sample 85-3, but all three samples show similar depletion in HREE. The REE patterns of the mafic samples are

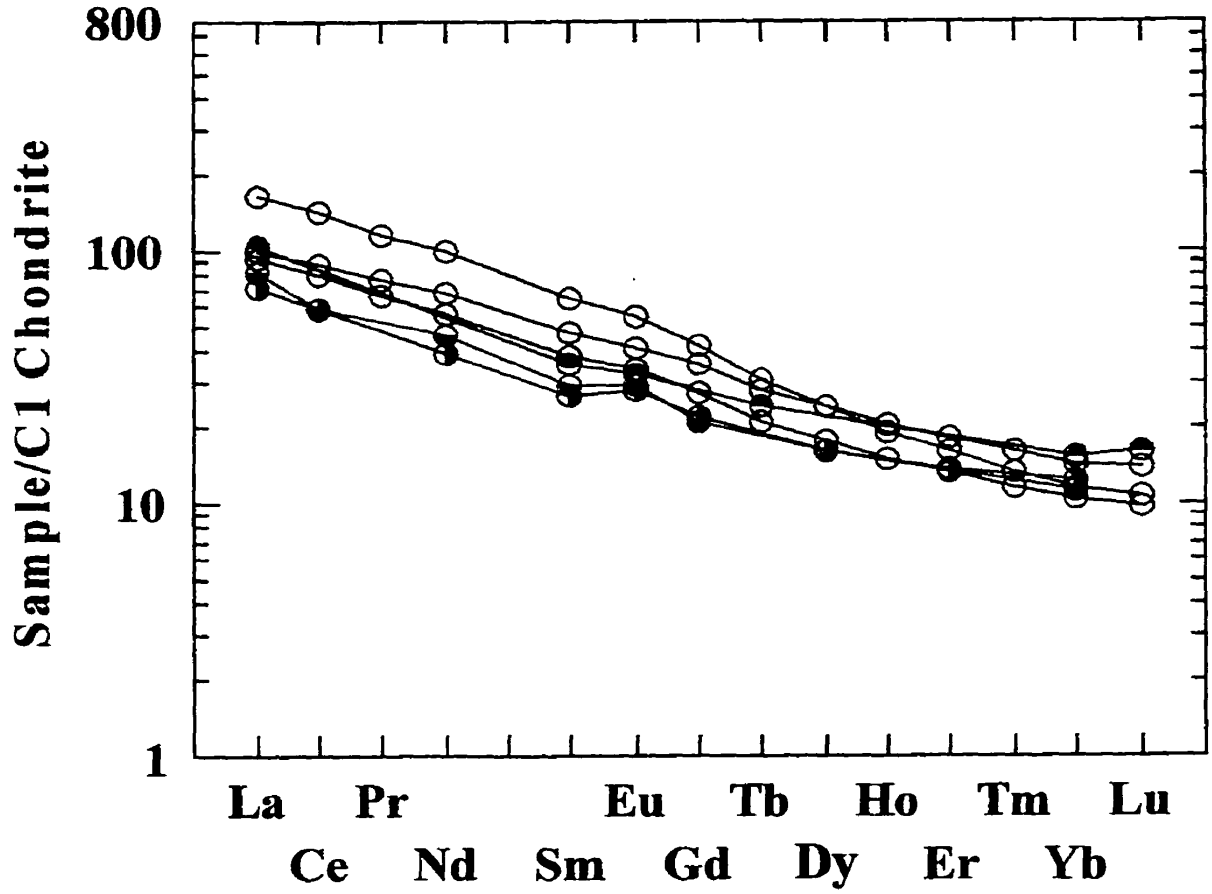

Figure 4.6. Chondrite-normalized REE diagram for mafic flow samples from the White Rock Formation and the East African Rift. Chondrite normalizing values are from Sun and McDonough (1989).

similar to patterns of basalt samples from the East African (continental) Rift zone (Fig. 4.6), but show higher values of middle REE (Sm, Eu, Gd). They show no Eu anomalies, suggesting that feldspar fractionation was not a significant process in their evolution. La/Sm values for mafic volcanic samples range from 3.23 to 3.95 and Gd/Lu values are between 20.36 and 31.68.

4.5.2. Felsic Crystal Tuff

Felsic crystal tuff sample 4-1 shows enrichment in LREE, a negative Eu anomaly, and depletion in HREE concentrations (Fig. 4.7). The sample has a REE pattern similar to that of trachyte and rhyolite samples from the East African Rift (Fig. 4.7), except the overall REE abundance is much lower. The La/Sm value for sample 4-1 is 6.40, higher than found in the mafic volcanic samples. The value of Gd/Lu is 11.73, lower than the Gd/Lu values found in the mafic volcanic samples.

4.5.3. Mafic Sills

Two samples from mafic sills in the White Rock Formation were analyzed for REE and, like mafic flow samples, are enriched in LREE relative to chondrite abundances (Fig. 4.8). The REE patterns are generally similar to those of mafic flow samples, especially samples 2-1 and 75A-1. The similarity supports a comagmatic relationship between the sills and dykes and the mafic volcanic rocks of the White Rock Formation. They resemble trends shown by basalt from the East African Rift (Fig. 4.8). The La/Sm values for the sill samples are 3.93 and 3.47 and the values of Gd/Lu are 23.81 and 19.34, similar to values found in mafic volcanic samples.

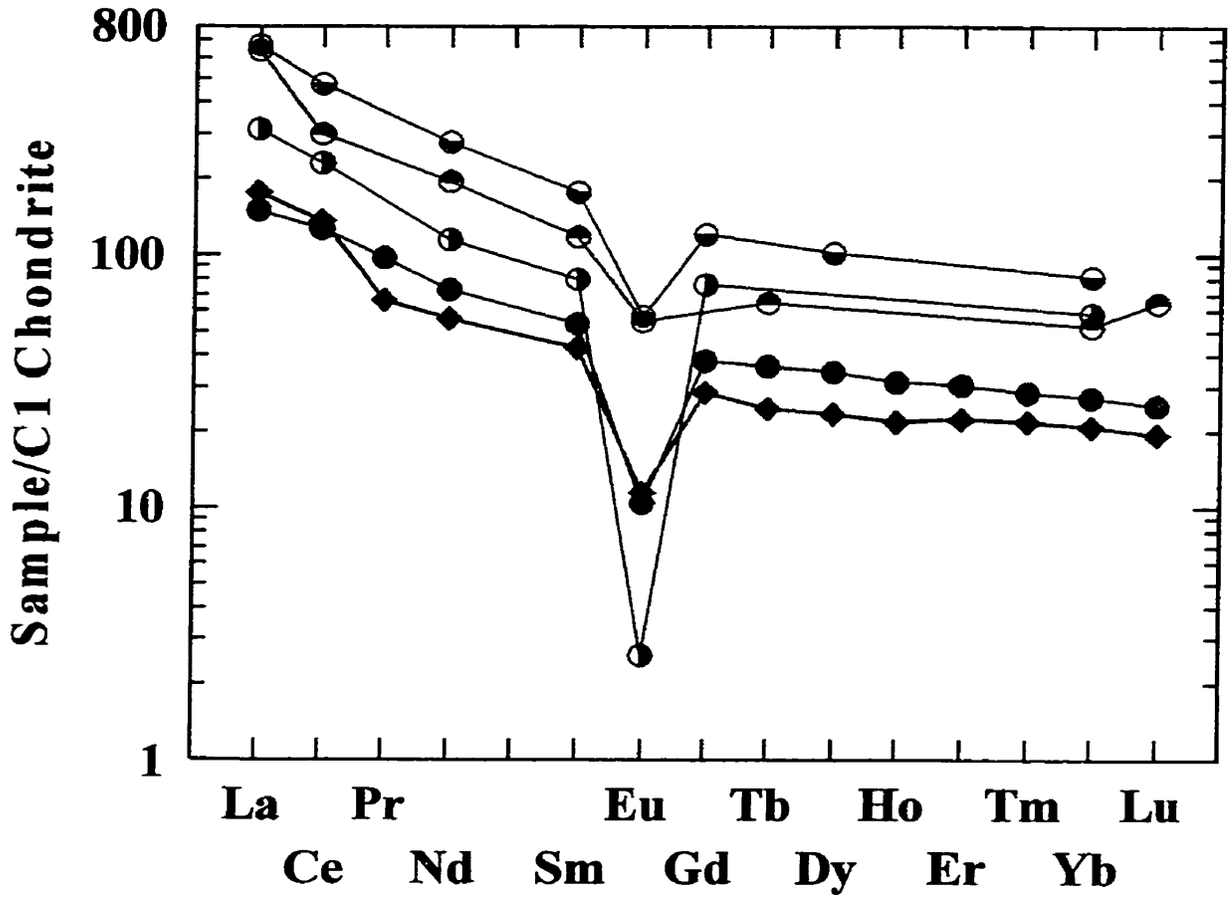

Figure 4.7. Chondrite-normalized REE diagram for a felsic crystal tuff from the White Rock Formation, a granite sample from the Brenton Pluton and felsic samples from the East African Rift. Chondrite normalizing values are from Sun and McDonough (1989).

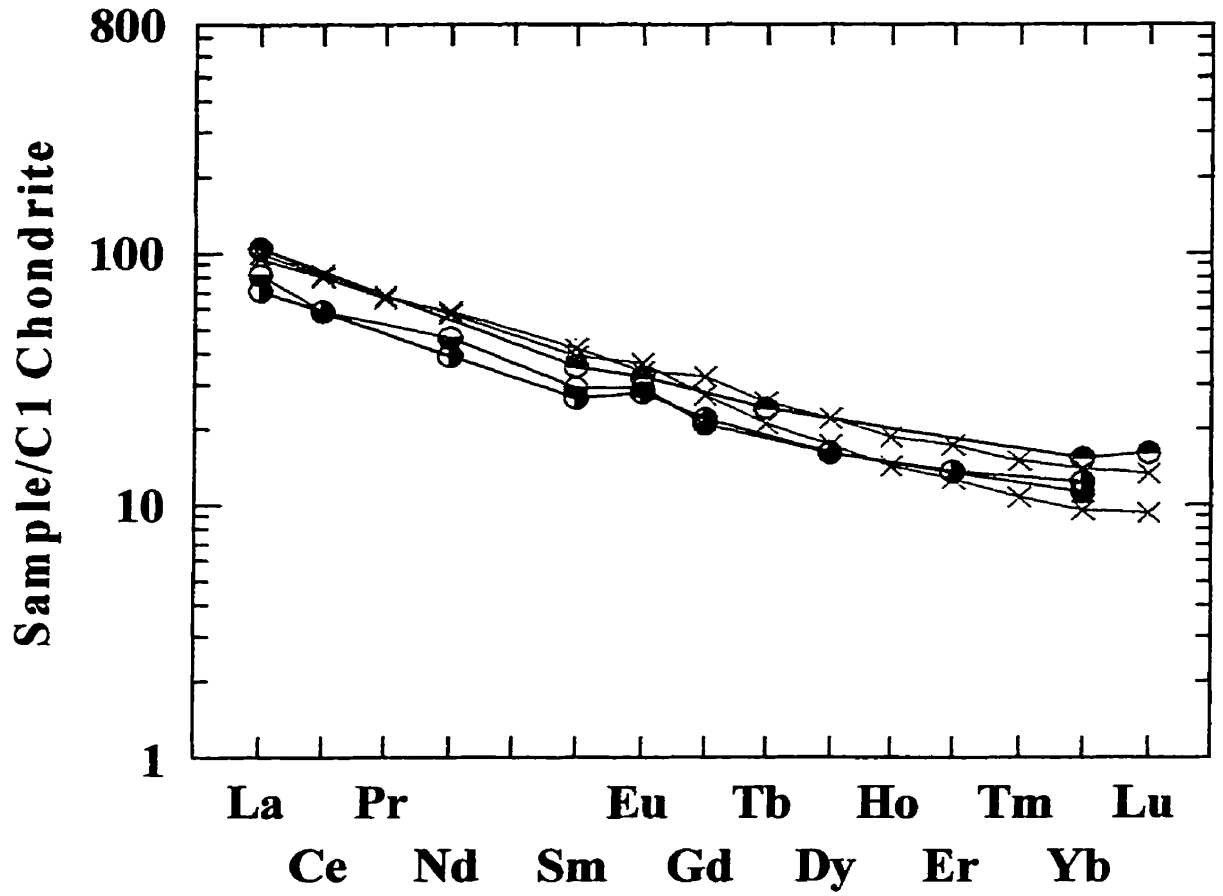

Figure 4.8. Chondrite-normalized REE diagram for mafic dyke samples from the White Rock Formation and mafic samples from the East African Rift. Chondrite normalizing values are from Sun and McDonough (1989).

4.5.4. Brenton Pluton

The chondrite-normalized REE pattern of sample 161D-1 from the Brenton Pluton is slightly different from that of the felsic crystal tuff (Fig. 4.7). The sample is slightly less enriched in La and Ce, but overall, it is slightly more enriched in LREE and middle REE than the felsic volcanic sample. The granite sample also has a stronger Eu anomaly and is less depleted in HREE. The patterns for both samples are generally parallel, indicating a possible comagmatic relationship between the two units or similar sources. The La/Sm value for the sample from the Brenton Pluton is 4.93, slightly higher than found in the felsic volcanic sample. The value of Gd/Lu is 12.24, similar to the value found in sample of felsic volcanic rock.

4.6. Chemical Affinity and Tectonic Setting

4.6.1. Mafic Volcanic Rocks

Interpretation of chemical affinity and tectonic setting of altered and/or metamorphosed rocks is possible by using elements which are relatively immobile during these processes (Winchester and Floyd, 1977; Floyd and Winchester, 1978; Rollinson, 1993). As was shown in section 4.2, the elements Ti, Zr, Nb and V appear to be relatively immobile, or at least coherently mobile, in the mafic samples from the study area. These elements are used to assess the original igneous character and tectonic setting.

A plot of Zr/TiO_2 against Nb/Y confirms that the rocks have basaltic compositions (Fig. 4.9). Ratios of Nb/Y are between 0.3 and 1.5, suggesting that the rocks range from subalkalic to alkalic, but as shown in Figure 4.2f, Y contents may not

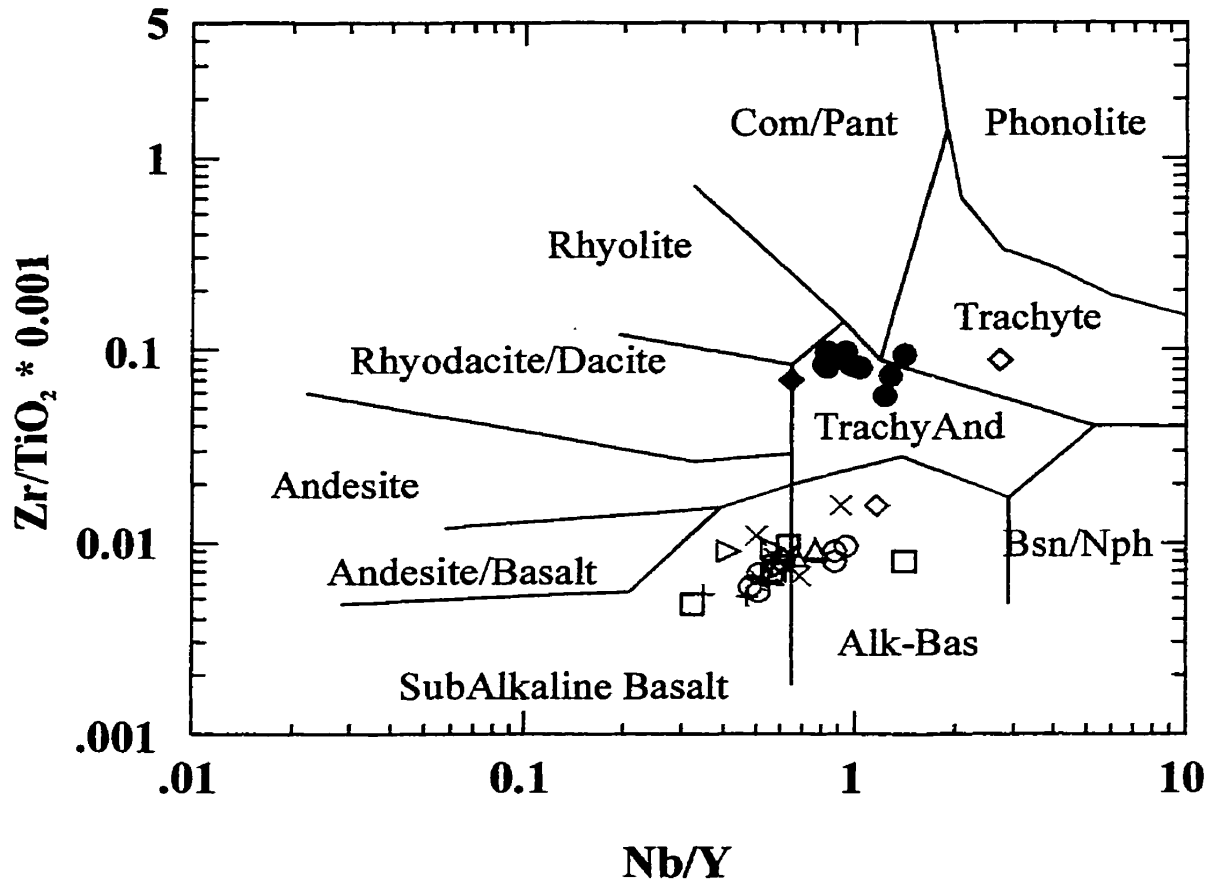

White Rock Formation
- ○ Mafic flow
- □ Mafic tuff
- ◇ Mafic crystal tuff
- △ Mafic lithic tuff
- ▷ Amphibolite
- ◇ Intermediate crystal tuff (sample 9-1)
- ◆ Felsic crystal tuff (sample 4-1)

- • **Brenton Pluton**

Mafic Dykes and Sills
- + Halifax Formation
- × White Rock Formation

Figure 4.9. Zr/TiO_2 vs. Nb/Y diagram showing the chemical affinity of samples from the study area. Fields after Winchester and Floyd (1977).

reflect the original rock compositions, and may be elevated relative to Nb. Therefore the samples may have been more alkalic than suggested by this diagram.

A ternary plot of Zr-Ti-Y (Fig. 4.10) distinguishes within-plate basalt (WPB) from mid-ocean ridge basalt (MORB) and calc-alkaline basalt (CAB). Samples of mafic flows, amphibolite and mafic lithic tuff plot together in the WPB field. One mafic tuff sample (148-1) plots anomalously in the low potassium tholeiite and ocean-floor basalt fields due to its low TiO_2 and Zr contents relative to Y. A within-plate affinity is also shown on a plot of Th-Hf-Ta (Fig. 4.11) where three mafic volcanic rocks (flows) analyzed for Hf (as part of the REE analytical suite; Appendix D) plot in the E-MORB/within-plate tholeiitic field. A within-plate affinity is supported by a Zr-Nb-Y diagram (Fig. 4.12), on which the mafic samples plot mainly in the within-plate field, except for mafic tuff sample 148-1 (discussed above). A V-Ti discrimination diagram (Fig. 4.13) suggests that the majority of the samples are alkalic because they do not show the increase in V with Ti that is characteristic of tholeiitic suites (Shervais, 1982). Sample 148-1 also plots in an anomalous position on the V vs Ti diagram due to to a high V content relative to Ti.

Multi-element (spider) diagrams using relatively immobile elements have been used to fingerprint various mafic suites (Pearce, 1996). The mafic flow samples are most similar to the average within-plate alkalic basalt, as suggested by higher Th, Nb, Ce, Zr, and TiO_2 contents compared to the average within-plate tholeiitic basalt (Fig. 4.14a). Patterns of mafic sills from the White Rock Formation appear similar to patterns of average within-plate alkalic and average within-plate tholeiitic samples (Fig. 4.14a) but the patterns of sill samples have slightly steeper slope and they are more enriched in

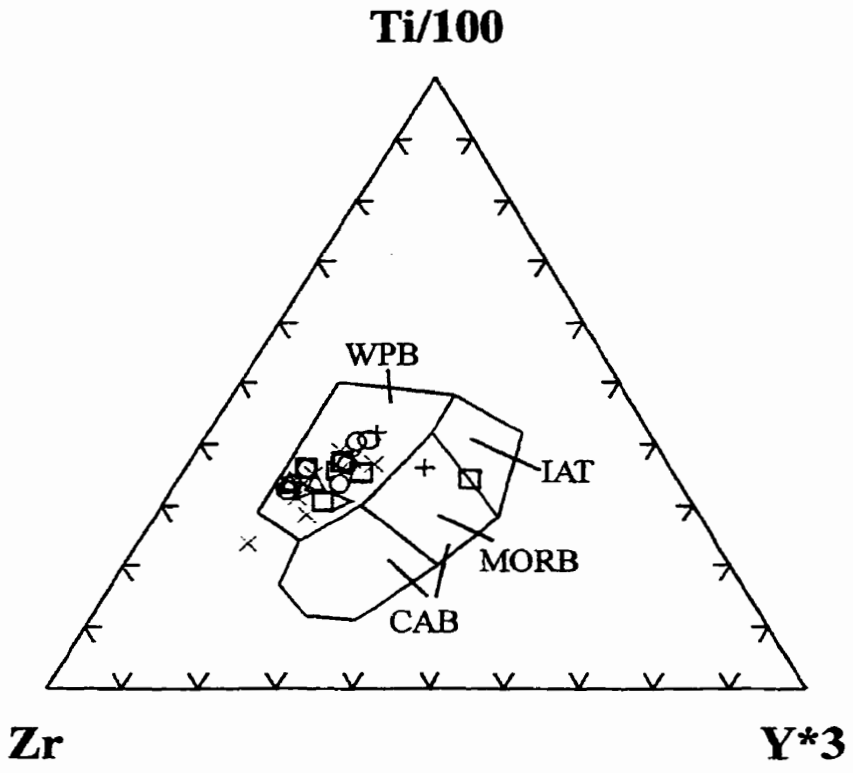

WPB	within-plate basalt
CAB	calc-alkaline basalt
MORB	mid-ocean ridge basalt
IAT	island-arc tholeiitic basalt

Figure 4.10. Zr-Ti-Y ternary discrimination diagram for mafic samples from the study area with fields from Pearce and Cann (1973). Samples plot mainly in the within-plate basalt (WPB) field. Symbols as in Figure 4.9.

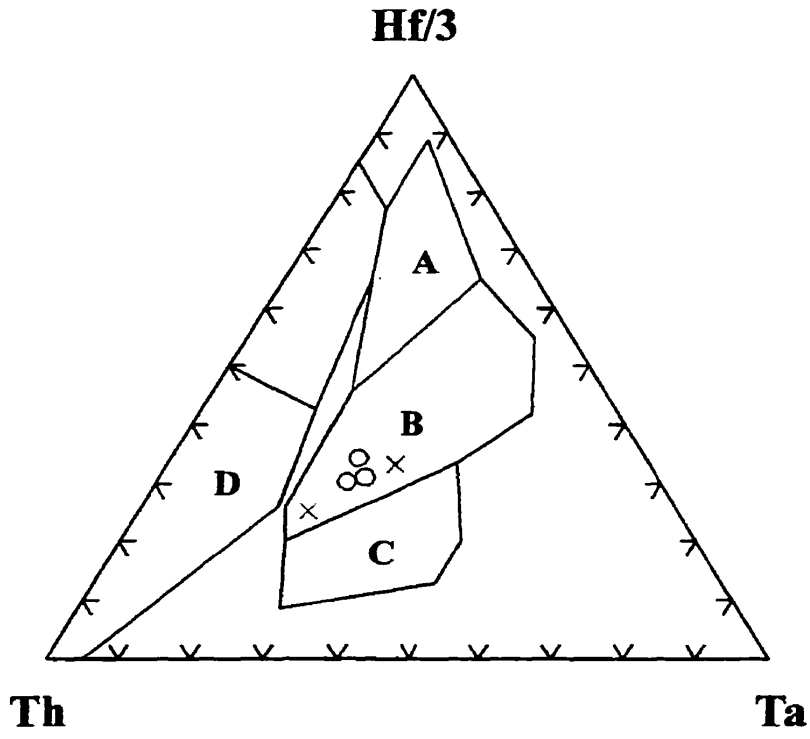

A N-MORB
B E-MORB and WPB
C WPB (within-plate basalt)
D VAB (volcanic arc basalt)

Figure 4.11. Th-Hf-Ta ternary discrimination diagram for mafic flow and dyke samples from the White Rock Formation. Samples plot mainly in the E-MORB and within-plate field. Fields from Wood (1980). Symbols as in Figure 4.9.

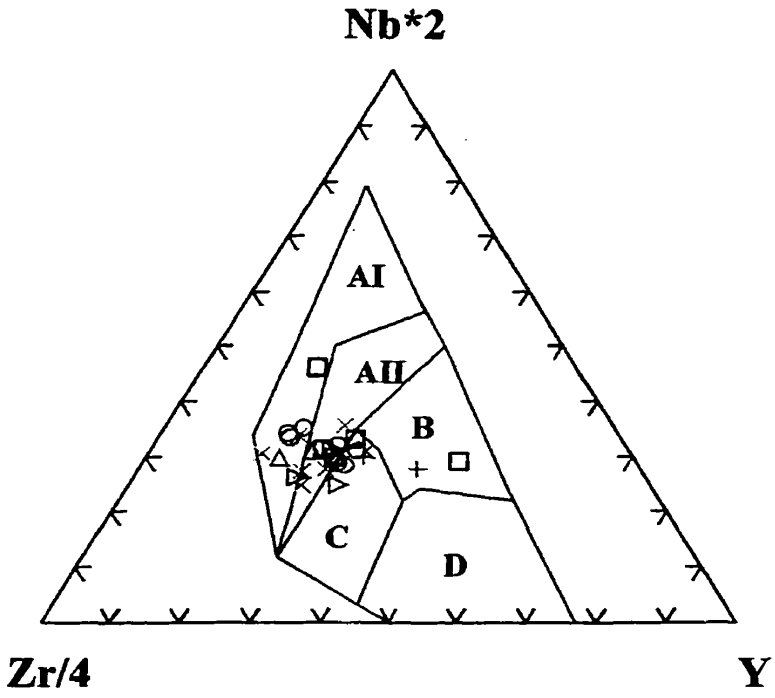

AI, AII	within-plate alkali basalt
AII, C	within-plate tholeiitic basalt
B	P-MORB
D	N-MORB
C,D	volcanic arc basalt

Figure 4.12. Zr-Nb-Y ternary discrimination diagram for mafic samples from the study area. Fields after Meschede (1986). Samples plot mainly in the within-plate fields. Symbols as in Figure 4.9.

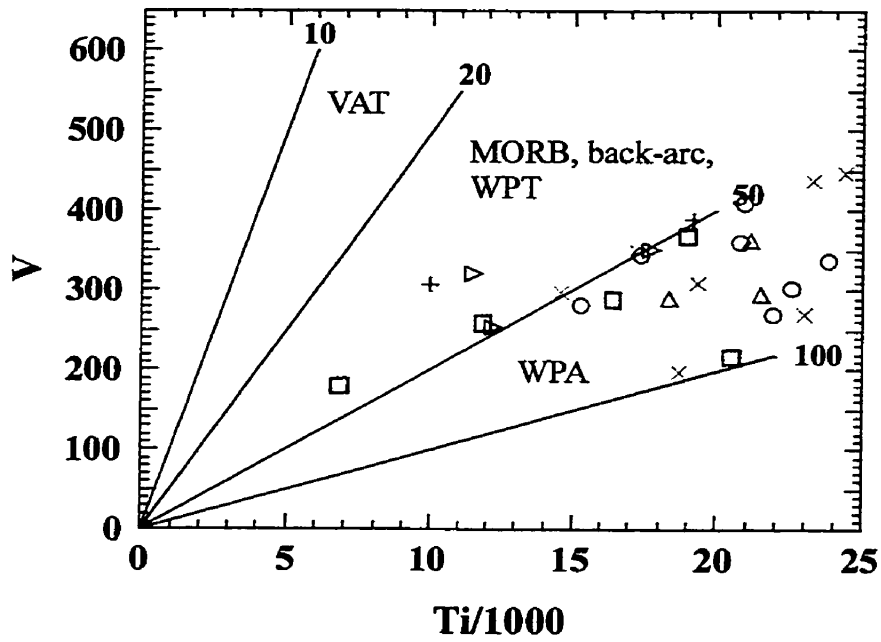

Figure 4.13. V vs. Ti discrimination diagram for mafic samples from the study area. Samples plot mainly in the within-plate alkalic field. Fields from Shervais (1982). Symbols as in Figure 4.9.

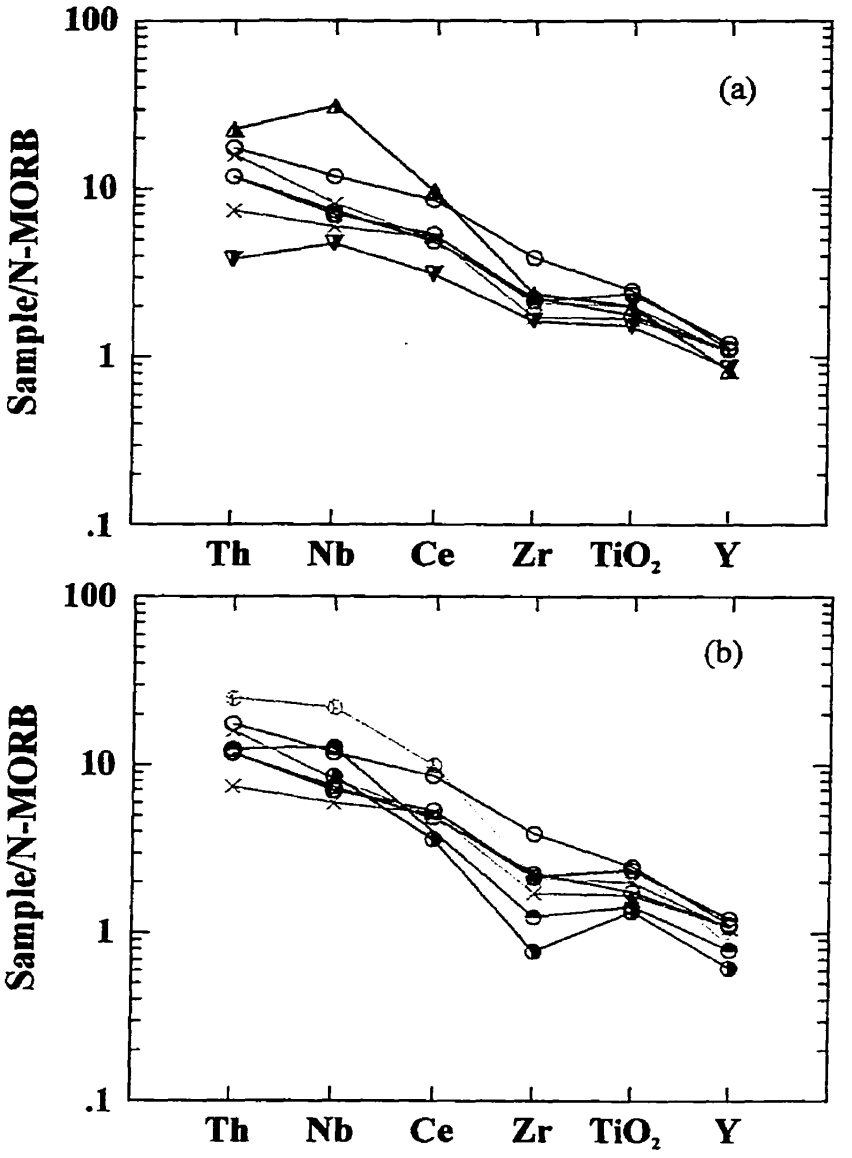

Figure 4.14. N-MORB-normalized spider diagrams for mafic flow and sill samples compared (a) to average within-plate alkalic and thloleiitic samples from Pearce (1982) and (b) mafic samples from the East African Rift from Wilson (1989). Normalizing values from Pearce (1996).

incompatible elements than the pattern of the average within-plate tholeiite sample. The samples from the White Rock Formation appear to resemble the pattern from the alkalic basalt from the Gregory (Kenya) Rift more closely than the other samples from the East African Rift on the diagram (Fig. 4.14b).

4.6.2. Intermediate and Felsic Volcanic Rocks

On a plot of Zr/TiO_2 versus Nb/Y (Fig. 4. 9), sample 9-1 plots in the trachyte field, whereas sample 4-1 plots near the "triple junction" between the rhyodacite, trachyandesite, and rhyolite fields. Because of the anomalous composition of sample 9-1 (e.g. Figure 4.2), the apparent trachytic composition is not likely a primary igneous feature. On the Rb-Y+Nb and Nb-Y tectonic setting discrimination diagrams, the samples have within-plate chracteristics (Fig. 4.15). Sample 4-1 has a high Ga/Al ratio, indicative of A-type affinity in felsic rocks (Whalen et al. 1987) (Fig. 4.16). A-type granites generally are characterisitc of continental within-plate tectonic settings (Whalen et al. 1987; Eby 1990). A plot of Y-Nb-Ga suggests a mainly mantle source for intermediate sample 9-1 but possible derivation from crustal sources for sample 4-1 (Fig. 4.17) (Eby, 1992).

4.6.3. Mafic Dykes and Sills

As shown in sections 4.3, 4.4, and 4.6, samples from mafic dykes and sills in both the White Rock and Halifax formations have chemical compositions similar to the mafic volcanic rocks of the White Rock Formation. Hence, they also have a similar chemical affinity and tectonic setting (Fig. 4.9 – 4.14). Two samples (202-1 from the Halifax

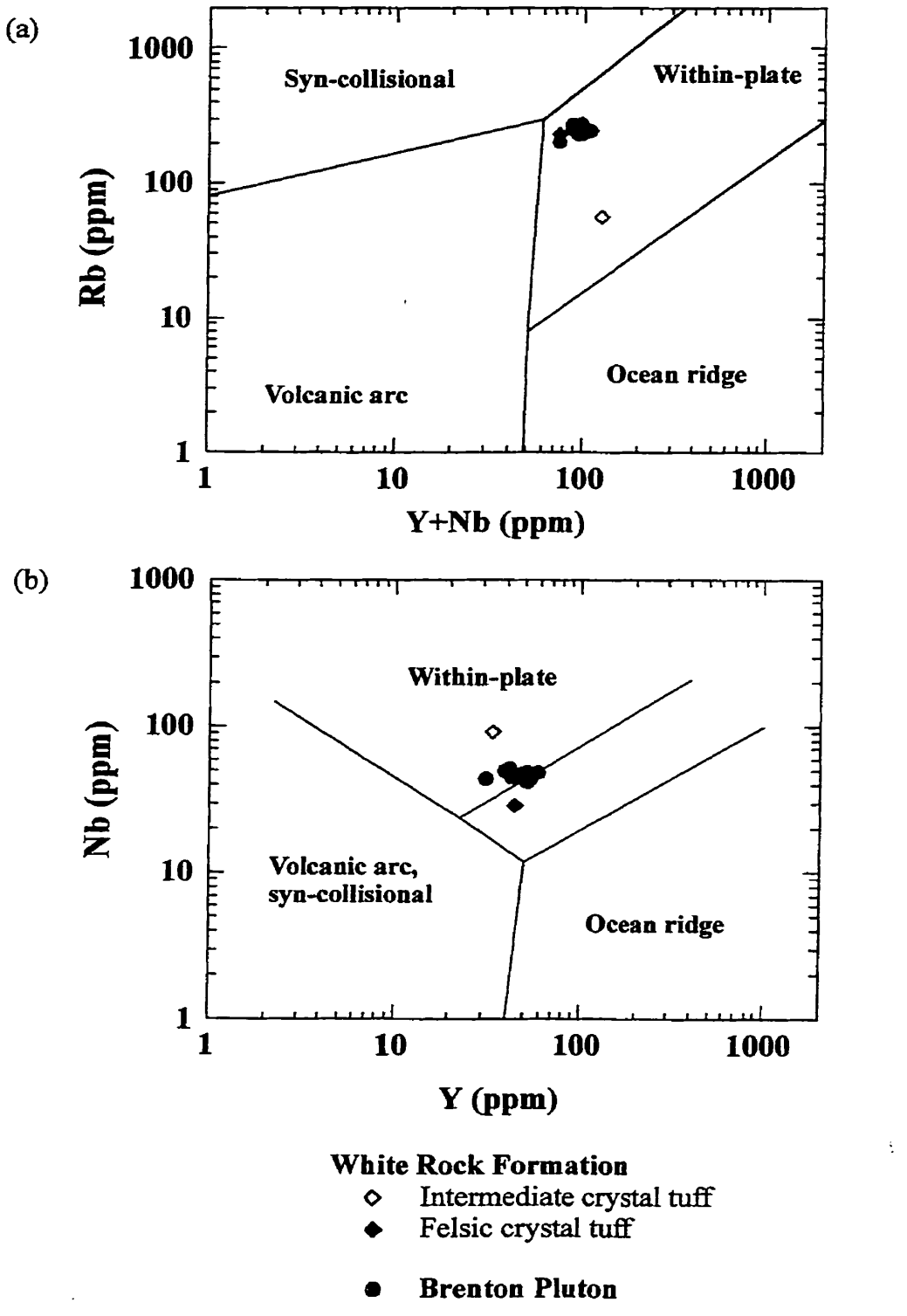

Figure 4.15. (a) Rb versus Y+Nb and (b) Nb versus Y discrimination diagrams for felsic rocks from Pearce et al. (1984). Samples plot in the within-plate fields.

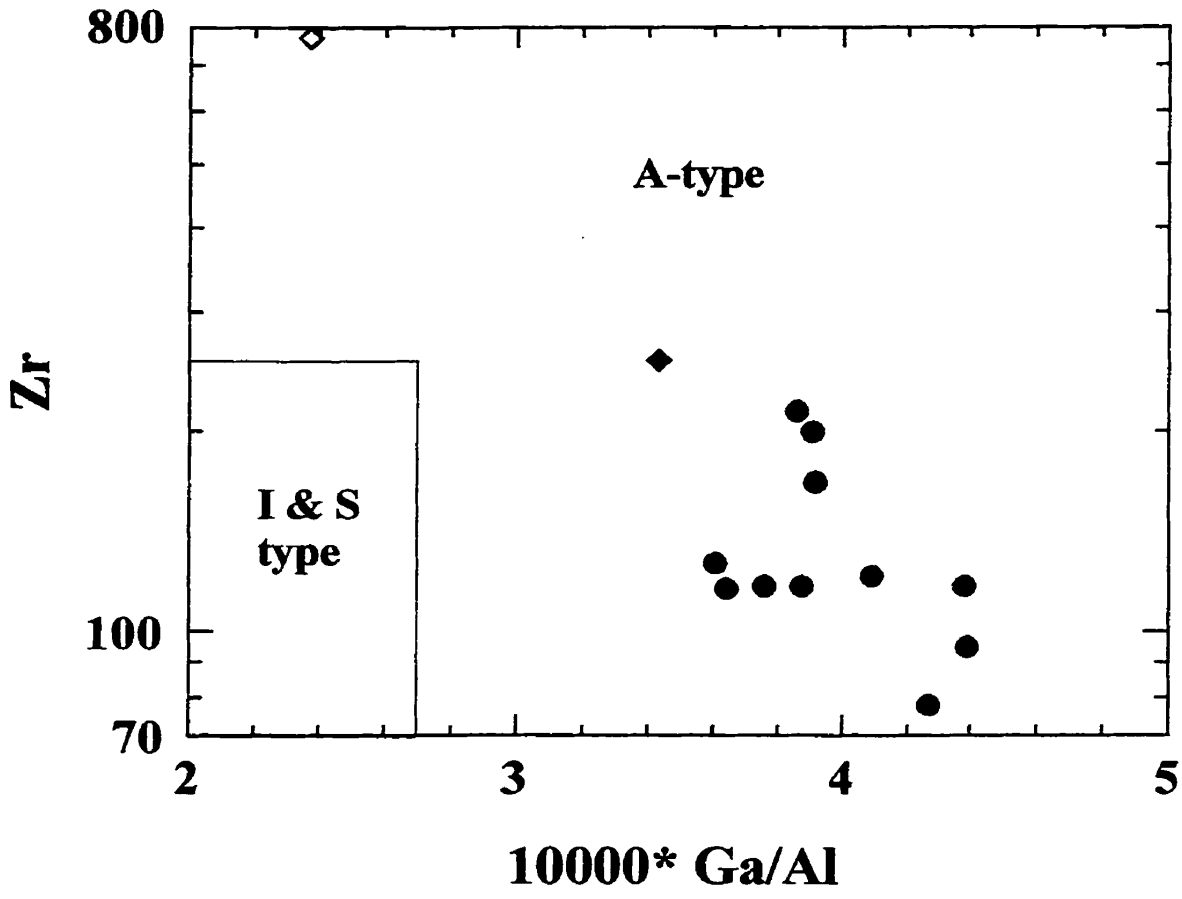

Figure 4.16. Zr versus Ga/Al discrimination diagram for felsic rocks from Whalen et al. (1987). Samples from the study area plot in the A-type granite field. Symbols as in Figure 4.15.

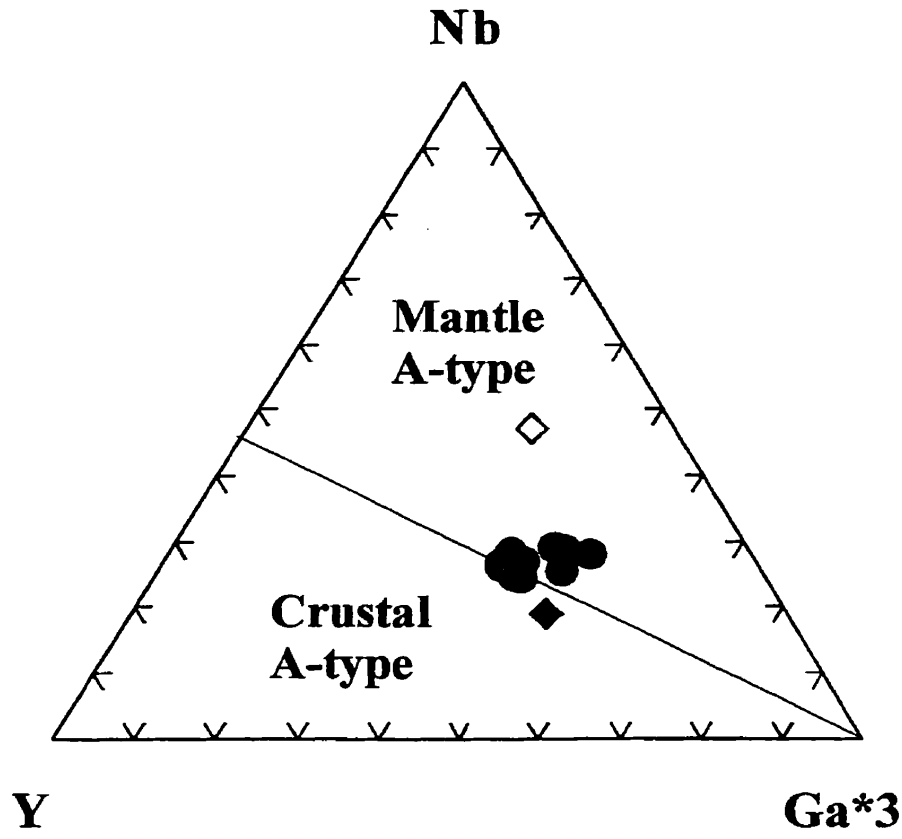

White Rock Formation

Felsic crystal tuff sample 4-1

◇ Intermediate crystal tuff sample 9-1

Brenton Pluton

Figure 4.17. Y-Nb-Ga*3 ternary diagram for distinguishing between mantle and crustal A-type granitoids from Eby (1992).

Formation and sample 94-1 from the White Rock Formation) tend to plot anomalously in other fields on the diagrams, due to low TiO_2 and Zr contents and anomalously high Zr contents, respectively.

4.6.4. Brenton Pluton

On the Zr/TiO_2 versus Nb/Y diagram (Fig. 4.9), samples from the Brenton Pluton plot mainly in the trachyandesite field, indicating a slightly alkalic character. On a plot of $Al_2O_3+Na_2O+K_2O$ versus $Al_2O_3+CaO+Na_2O+K_2O$ (ANK vs ACNK), they are predominantly in the peraluminous field (Fig. 4.18). Classification as peraluminous is consistent with the presence of aluminum-rich minerals such as garnet (Chapter 3). However, the samples have high Ga/Al ratios, indicative of A-type granites (Fig. 4.16). They also plot in the within-plate granite field on tectonic setting discrimination plots (Fig. 4.15). An anorogenic, within-plate character is suggested for the Brenton Pluton. On the Y-Nb-Ga*3 diagram, samples plot mainly in the mantle-source field (Fig. 4.17).

4.7. U-Pb Age of Felsic Crystal Tuff in the White Rock Formation

In order to better constrain the age of the White Rock Formation in theYarmouth area, felsic crystal tuff sample 4-1 from unit S_{WRft} at Sunday Point was collected for U-Pb dating. Analyses were done and interpreted by J. Ketchum at Memorial University. Six fractions were analyzed; four fractions were prismatic and strongly discordant with an upper intercept age of 2061 +/- 24 Ma and a lower intercept age (crystallization age) of 438 +/- 10 Ma (Fig. 4.19). The two remaining fractions were small colourless, euhedral needles which plot at or near the lower intercept of the prismatic fractions at ca. 438 +3/-

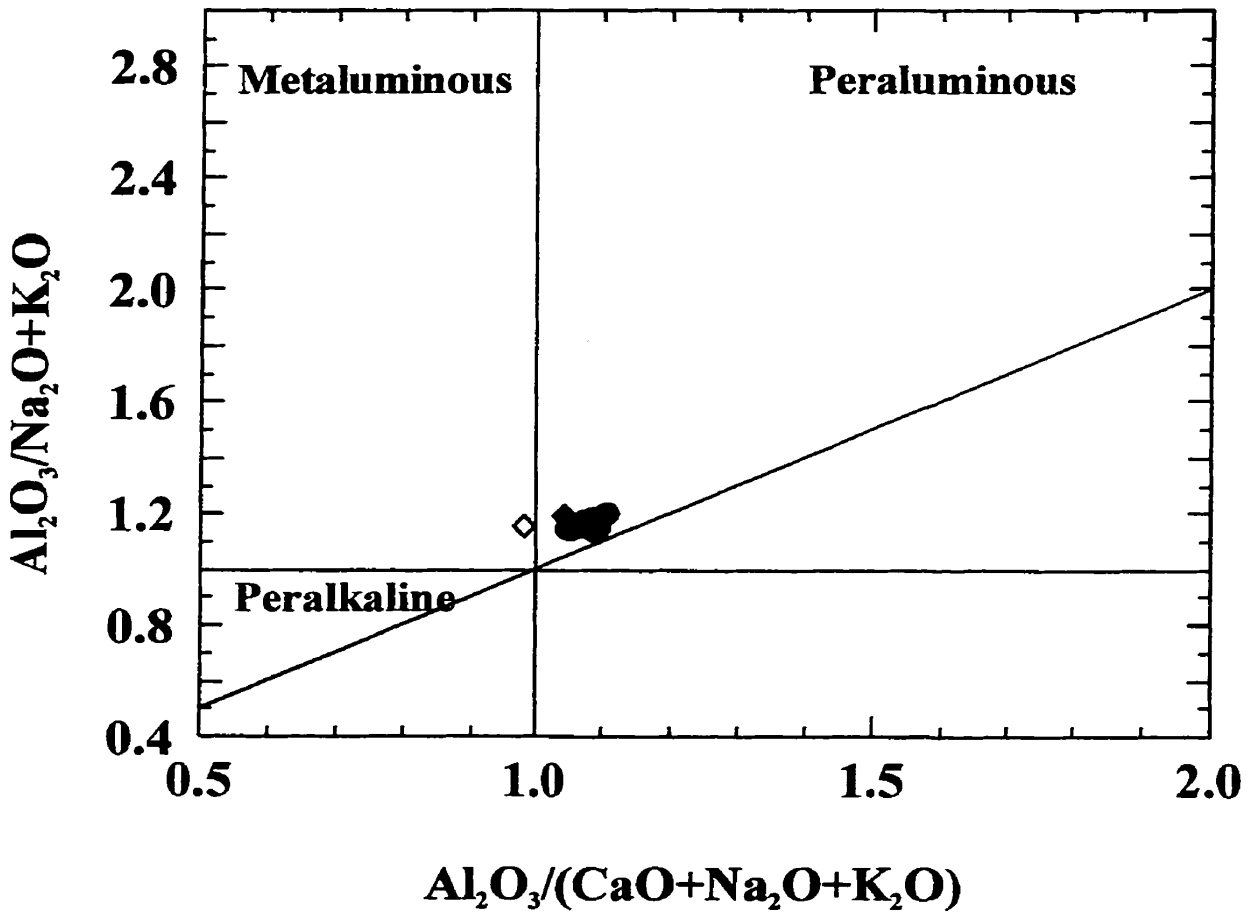

Figure 4.18. ANK versus ACNK discrimination diagram for felsic rocks from Maniar and Piccoli (1989). Felsic rocks from the study area plot in the peraluminous field. Symbols as in Figure 4.17.

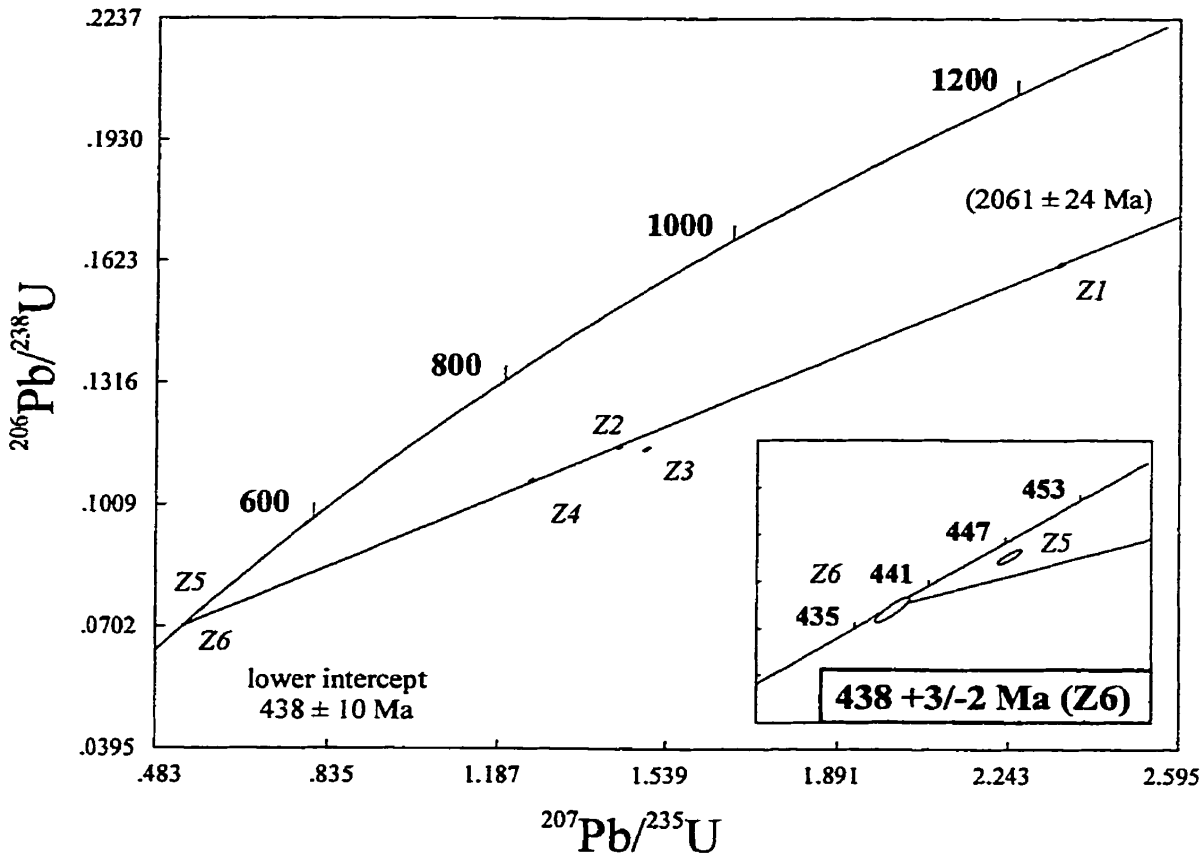

Figure 4.19. Concordia diagram for felsic crystal tuff sample 4-1, unit S_{WRR}. Age of crystallization is 438 +3/-2 Ma.

2 Ma. The upper intercept age is from zircons inherited from the crust, either during melting or by contamination (Rollinson, 1993). The age given by the prismatic fractions (438 +3/-2 Ma) is considered to be the time of crystallization of the tuff and its significance is discussed in Chapter 5.

4.8. Sm-Nd Isotopic Data

Sample 4-1 was also analyzed at Memorial University for Sm and Nd isotopes (Appendix E) (Fig. 4.20). The calculated εNd value is +1.37 at 440 Ma and the depleted mantle age (T_{DM}) is 1209 Ma. The εNd value is higher than expected for a direct crustal melt (εNd near –6 at ca. 2000 Ma), but too low to be an uncontaminated mantle melt (εNd near +9 at ca. 440 Ma) (Fig. 4.20) (Rollinson, 1993; Raymond, 1995), suggesting that the mantle-derived magma interacted with crustal material. Crustal contamination is also supported by the zircon inheritance described in section 4.7.

4.9. Petrogenesis

4.9.1. Mafic Volcanic Rocks

The chemical characteristics of the mafic rocks are most compatible with an alkalic affinity and origin in a within-plate, continental tectonic setting. The similarities in major and trace element compositions are consistent with a comagmatic relationship among the samples. The range of SiO_2 values in mafic samples is small and the number of samples with intermediate composition is limited, making trends on variation diagrams

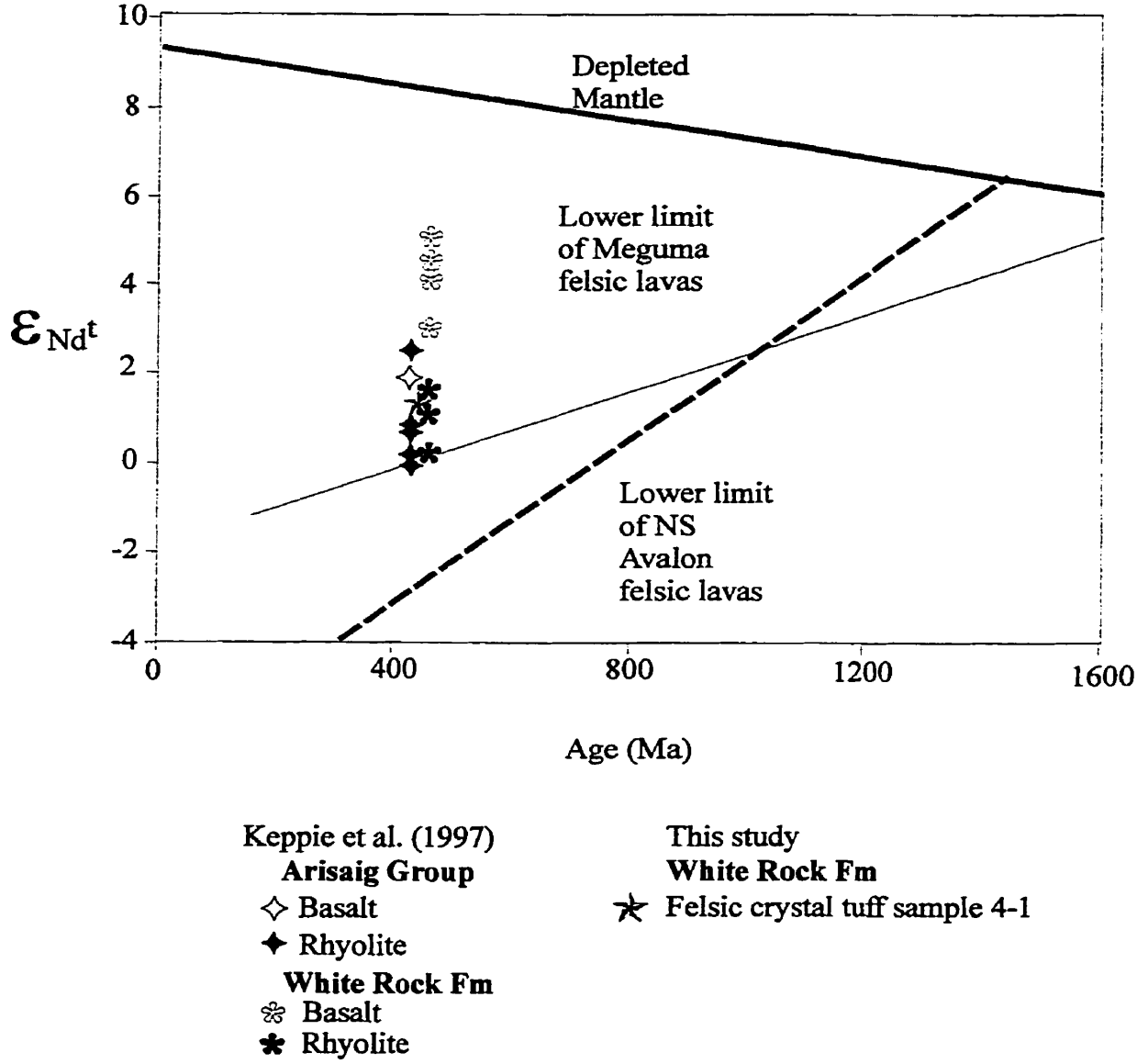

Figure 4.20. εNd diagram from Keppie et al. (1997) for basalt and rhyolite from the White Rock Formation and Arisaig Group with a sample of felsic crystal tuff (sample 4-1) from this study.

difficult to identify with confidence. Scatter in variation diagrams of CaO, K_2O, Na_2O, Ba, Rb, and Sr is probably due to metamorphism and/or alteration, making original trends indicative of feldspar fractionation difficult to identify. The negative correlation of MgO and $Fe_2O_3^t$ with SiO_2 suggests olivine and/or pyroxene fractionation, although neither of these minerals is present now. To better identify trends possibly associated with fractional crystallization, mafic samples are plotted on axes other than SiO_2 in order to increase spread of the samples. On plots of Ni vs FeO^t/MgO, Cr vs FeO^t/MgO, and TiO_2 vs FeO^t/MgO, linear trends are observed, particularly in samples from mafic flows (Fig. 4.21). Decreasing Ni and Cr values with increasing FeO^t/MgO suggests fractionation of both olivine and pyroxene. Increasing TiO_2 with FeO/MgO (Fig. 4.21c) is characteristic of tholeiitic suites in which no Ti-bearing minerals crystallize in the early stages, thus concentrating Ti in the melt. However, such patterns also occur in alkali suites.

Three mafic flow samples have approximately parallel REE patterns, but the third sample is slightly less depleted in heavy REE, possibly the result of less fractionation of accessory phases, the presence of residual garnet in the source, or variable degrees of partial melting (Wilson, 1989). Sample 2-1 and 75A-1 are both enriched in LREE, suggesting sources which may have been enriched in LREE relative to chondrite abundance (Wilson, 1989). Sample 2-1 has low concentrations of HREE relative to both LREE and chondrite values, suggesting a source which may have had garnet and or pyroxene (Wilson, 1989; Rollinson, 1993). Sample 75A-1 has concentrations of HREE greater than 10 times chondrite values, indicating that the source may have been garnet-free (Wilson, 1989). Sample 85-3 is very enriched in LREE compared to both chondrite and HREE abundances and has relatively low HREE abundance compared to chondrite

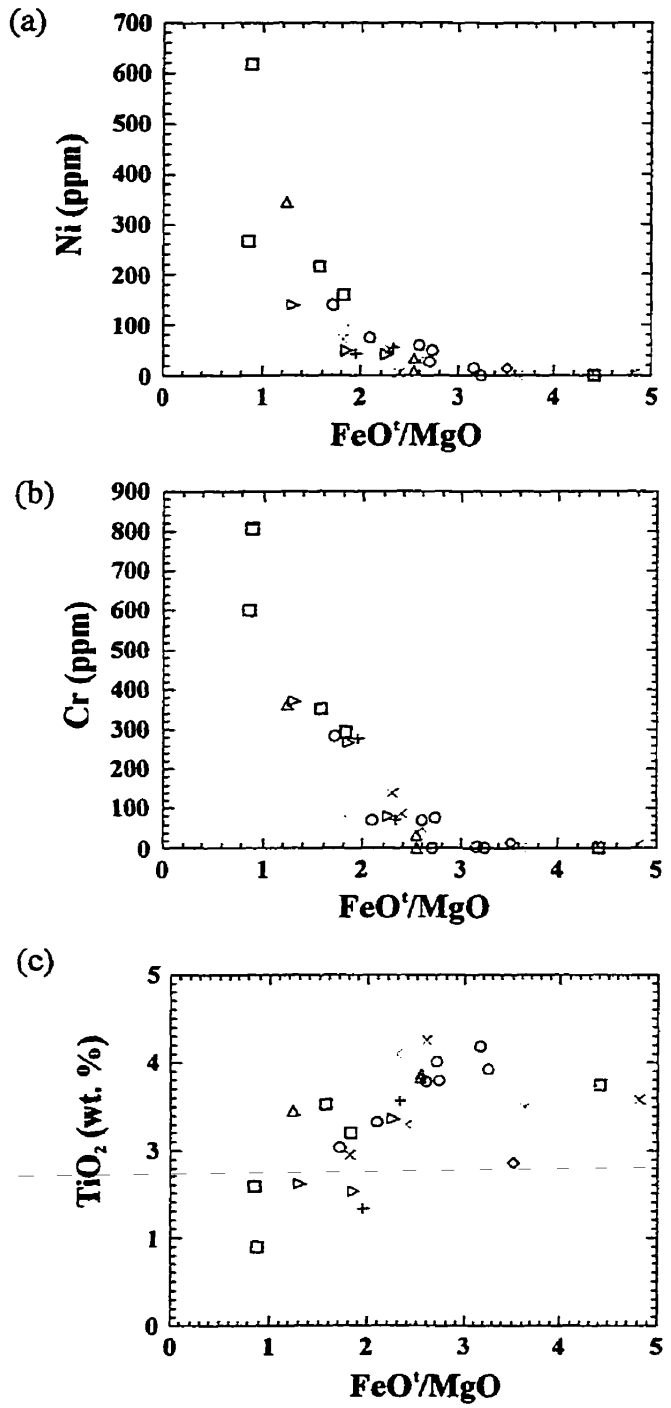

Figure 4.21. Plots of (a) Ni, (b) Cr, and (c) TiO_2 against FeO^t/MgO for mafic samples in the study area. Symbols as in Figure 4.9.

values. This pattern is suggestive of small degrees of partial melting or a source enriched in LREE (Wilson, 1989).

Plots of incompatible elements such as Zr, Nb, Hf, La, and Ce show positive trends when magmas are evolved by fractional crystallization due to the retention of element ratios (Wilson, 1989). Ratios of incompatible elements for mafic volcanic samples (Fig. 4.22) show trends within each rock type. Mafic flow samples show the best correlation. The linearity of mafic tuff and mafic lithic tuff samples is not as developed in as mafic flows, probably because they do not represent a single magma composition.

4.9.2. Felsic Volcanic Rocks

Fractionation of feldspar or the presence of residual feldspar in the source after partial melting is suggested by the negative Eu anomaly in crystal tuff sample 4-1, and depletion of HREE may indicate the presence of accessory phases such as zircon (Rollinson, 1993; Hanson, 1980). Major and trace element data are inconclusive about whether the intermediate and felsic samples are comagmatic with the mafic volcanic rocks (felsic samples show typical trends even if rocks are unrelated). REE patterns indicate that both mafic and felsic volcanic rocks came from sources enriched in LREE (or garnet was in source?). Ratios of incompatible elements (Nb/Zr, La/Zr, Nb/La) show consistency of ratios between mafic and felsic volcanic samples, suggesting a possible comagmatic relationship and evolution through fractional crystallization (Fig.4.22). A comagmatic relationship with the Brenton Pluton does not seem likely (see section 4.9.4). Sm-Nd data from a sample of felsic crystal tuff supports a comagmatic relationship with the mafic rocks but shows evidence for crustal contamination. The $^{143}Nd/^{144}Nd$ ratio for

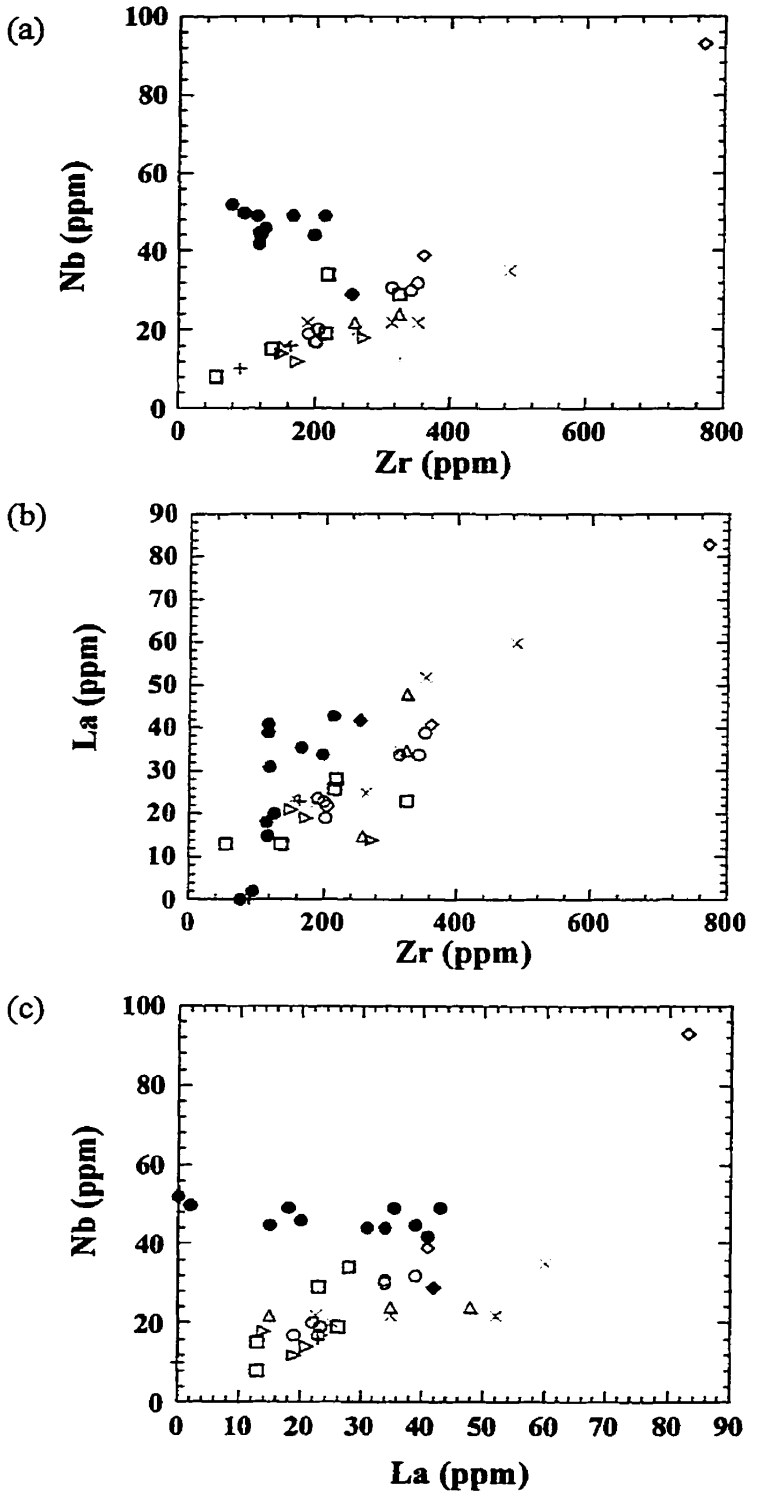

Figure 4.22. Incompatible element plots for samples from the study area. Symbols as in Figure 4.9.

the sample is 0.512601, less than bulk Earth value of 0.51264, reflecting crustal contamination or crustal source (Raymond, 1995). Crustal contamination is supported by the εNd value of +1.37. A crustal source is not likely given the consistency of the incompatible element ratios of Figure 4.22 and the relatively high εNd value. A crustal source is suggested by Y-Nb-Ga ratios (Fig. 4.17).

4.9.3. Mafic Dykes and Sills

The eight samples of mafic dykes and sills have major, trace and rare earth element compositions similar to those of mafic volcanic rocks. The similarity suggests a possible comagmatic relationship or at least the same source. The source of sample 131-1 may have had residual garnet or pyroxene present, as HREE concentrations are only slightly above chondrite values. The REE pattern of sample 131-1 corresponds closely with the pattern of mafic volcanic sample 2-1, suggesting a comagmatic relationship. Sample 205-1 has a slightly negative Eu anomaly which is suggestive of fractional crystallization of plagioclase or equilibrium with a plagioclase-bearing mantle source (Wilson, 1989; Rollinson, 1993).

Incompatible element ratios in the sills and dykes appear consistent with those in the mafic volcanic rocks (Fig. 4.22). Therefore dykes may be from the same source (given the REE and major/trace element similarities) and may be related by fractional crystallization (from same primary/parental magma).

4.9.4. Brenton Pluton

Most major and trace element data are similar for the felsic volcanic rock and samples from the Brenton Pluton but the REE pattern of a sample from the Brenton Pluton is slightly different than that of the felsic crystal tuff sample (section 4.5.4). The mineralogy of the Brenton Pluton and the sample of felsic tuff are also different. Differences in REE patterns and mineralogy may indicate different sources, also supported by the ratios of incompatible elements, which in these samples, are different (Fig. 4.22). The source for the Brenton Pluton appears to have had fractional crystallization of feldspar or contained residual feldspar after partial melting, suggested by the negative Eu anomaly. Zircon may have been present as well in order to produce the observed depletion in HREE (Rollinson, 1993; Hanson, 1980). The REE patterns indicate that the source of the Brenton Pluton may be similar to the source of the felsic volcanic sample but the differences in La, Ce and incompatible element ratios which make a comagmatic relationship (related by fractional crystallization from a similar or the same parent magma) unlikely.

Chapter 5 Discussion

5.1. Introduction

The purpose of this chapter is to compare the results of this study with previous work on the White Rock Formation in the Yarmouth area, and in the Cape St. Mary and Torbrook areas (Fig. 1.1). The White Rock Formation is also compared to the Arisaig Group of northern mainland Nova Scotia. The regional setting of the White Rock Formation is discussed in relation to volcano-sedimentary sequences of similar age elsewhere in Nova Scotia, New Brunswick and Newfoundland.

5.2. Comparison with Previous Work in the Yarmouth Area

5.2.1. Age of the White Rock Formation and Brenton Pluton

Lane (1979) identified the trace fossil chondrites, gastropods and brachiopods in metasedimentary beds in lower parts of the White Rock Formation at Overton (in unit S_{WRmf} of this study). However, the assemblage is not very age-restricted and the range estimated for the brachiopod is Caradoc-Pennsylvanian. The age obtained as part of the present study places the age of the volcanic rocks in upper units (S_{WRft}) at 438 +3/-2 Ma (section 4.7).

An identical (within-error) crystallization age of 439 +4/-3 Ma (U-Pb, zircon) has been obtained for the Brenton Pluton (J.D. Keppie written comm., NSDNR, 1999).

5.2.2. Stratigraphic and Structural Interpretations

As described in Chapter 1, previous mapping of the White Rock Formation in the Yarmouth area was done by Taylor (1967), Lane (1979) and Hwang (1985). Each map contains interpretations significantly different from previous work, as well as from results of this study.

The location of the northern contact between the White Rock and Halifax formations south of Cranberry Head is placed in the same position in this study as in previous studies (Taylor, 1967; Lane 1979; Hwang, 1985), between the lowest exposed metasiltstone and slate of the White Rock Formation north of Chegoggin and the first outcrop of phyllite characteristic of the Halifax Formation. However, the interpretation of the location of the southern contact between the White Rock and Halifax formations near Chebogue Point is not the same. Previous studies placed the contact farther north than shown on Figure 2.1 by a few hundred meters (Taylor, 1967) and as much as one kilometer (Lane, 1979). In this study, the contact at Chebogue Point is placed at a fault which separates green-grey slate from black slate. This location is also marked by an abrupt change in aeromagnetic signature, similar to the change observed between the Halifax and White Rock formations at Cranberry Head (Fig.2.2). Taylor (1967) placed the contact arbitrarily beneath the lowest volcanic horizon of the White Rock Formation, whereas Lane (1979) placed the base at the bottom of felsite and arenite beds at Sand Beach and Brooklyn, which he considered to be the first distinctive lithologies of the White Rock Formation. According to this study, the felsite and arenite beds at these locations are not equivalent. Figure 2.1 shows that the beds near Brooklyn are stratigraphically lower (in unit S_{WRsv}) than beds at Sand Beach (in unit S_{WRft}). If the

contact is placed beneath the felsite and arenite beds at Brooklyn, then the location is within a few hundred meters of the placement in this study. Hwang (1985) placed the contact in this area between metagreywacke that he assigned to the White Rock Formation and black slate that he designated as the Halifax Formation. Placement at this location does not correspond with the abrupt change in aeromagnetic signature as closely as the location shown on Figure 2.1. Also, according to Hwang (1985), the White Rock and Halifax formations are in faulted contact in inland areas, yet he placed the fault at Chebogue Point farther north between units of the White Rock Formation, implying a geological contact between the formations in this area.

Keppie and Dallmeyer (1995) reported a shear zone (named the Deerfield Shear Zone) between the White Rock and Halifax formations on the east limb of the Yarmouth Syncline but did not describe it in detail. Culshaw and Liesa (1997) described evidence for shear zones centred at the contacts on both the limbs of the synclines at Cape St. Mary and Yarmouth (Cape St. Mary Shear Zone, Cranberry Point Shear Zone and Chebogue Point Shear Zone - the Chebogue Point Shear Zone corresponds with the Deerfield Shear Zone of Keppie and Dallmeyer, 1995) and near the core of the Yarmouth Syncline (Cape Forchu Shear Zone). Evidence for the shear zones includes features such as development of a second foliation (S2), re-orientation of lineations, retrogression of D1 porphyroblasts, development of a second lineation (L2), transposition of layering parallel to S2, cleavage that locally overprints D1 porphyroblasts, and a second generation of folds (F2). Taylor (1967) and Lane (1979) inferred a gradational contact between the Halifax and White Rock Formation. Hwang (1985) interpreted the western contact as a fault (although this is not clear on his map) and the eastern contact as gradational near the

coast and faulted inland, but the locations of the faults are not the same as shown on Figure 2.1. Hwang (1985) placed the fault at the contact on the western limb slightly south of the location shown on Figure 2.1 and the fault on the eastern limb is north of the location shown on Figure 2.1 but coincides inland near the Brenton Pluton. Hwang (1985) stated that there is no clear evidence of faults, such as breccia zones, and that the faults are not exposed. Therefore the presence of faults was inferred from local variations in stratigraphy, trends of lineations, kink fold axes, foliations and bedding planes as well as interpretation from aeromagnetic maps. However, there is evidence for the fault at Chebogue Point, previously described in Chapter 2.

Both Taylor (1967) and Hwang (1985) inferred an intrusive contact between the Brenton Pluton and the Halifax and White Rock formations, based on inferred relative ages. Because the White Rock Formation and the Brenton Pluton are now known to be of identical age but not necessarily comagmatic (Chapter 4), an intrusive relationship is less likely. The Chebogue Point Shear Zone of Culshaw and Liesa (1997) (Deerfield Shear Zone of Keppie and Dallmeyer, 1995) coincides with the contacts between the Halifax Formation and Brenton Pluton, supporting the interpretation of a faulted contact. O'Reilly (1976) also reported shearing along this contact. The Chebogue Point Shear Zone of Culshaw and Liesa (1997) extends to the contact between the White Rock Formation and the Brenton Pluton, and the White Rock Formation near the western contact with the pluton appears brecciated and schistose, indicating the presence of a fault on the western side of the pluton. The strong foliation in the pluton is parallel to these faulted margins.

The occurrence and location of minor folds and major faults in the Yarmouth Syncline are interpreted differently in the present study compared to previous studies. Taylor (1967) showed the White Rock Formation in a simple, southwest-plunging, synclinal structure. Lane (1979) indicated the presence of two vertical faults within the syncline, both of which subparallel the axial trace of the syncline. They are located near the core of the syncline (similar to that shown on Fig. 2.1) and south of Chegoggin Point. The location of the central fault coincides with location on Figure 2.1 but no field evidence was observed during this study for a fault south of Chegoggin Point. According to Lane (1979), vertical faults in these locations caused repetition of stratigraphy on the western limb but no evidence for repetition was found in this study.

Culshaw and Liesa (1997) suggested from trends of lineations that the faults on the limbs of the Yarmouth Syncline (Cranberry Point and the Chebogue Point shear zones) have dip-slip displacement with a local strike-slip component and that the central shear zone (Cape Forchu Shear Zone) displays strike-slip movement. Displacement shown on Figure 2.1 along the axis of the syncline is consistent with strike-slip movement. Hwang (1985) showed a series of high-angle, major NNE-trending faults at Cranberry Head, south of Chegoggin Point and north of Chebogue Point, which he suggested were formed during the opening of the Atlantic Ocean in the Early Jurassic.

Hwang (1985) also indicated two minor synclines separated by an anticline within the major Yarmouth Syncline. Aeromagnetic data in combination with field observations during this study and data from Culshaw and Liesa (1997) confirmed the presence of a fault subparallel to the trace of the syncline. Furthermore, aeromagnetic data and inferred stratigraphy suggest that minor synclines separated by a anticline occur within the

Yarmouth Syncline only in the northeastern part of the map area (Fig. 2.1). However, paucity of outcrop in this area makes confirmation from field observation difficult. Culshaw and Reynolds (1997) presented $^{40}Ar/^{39}Ar$ ages of ca. 320 Ma for muscovite from the Cape St. Mary and Cranberry Point shear zones, and cited similar published data from the Chebogue Point Shear Zone as evidence for an Alleghanian-Variscan (Carboniferous) age for the shear zones. However, the shear zone at Cape Forchu was interpreted to be Acadian by Culshaw and Liesa (1997) as it lacks D2 features described previously.

The differences in structural interpretations between this study and previous studies leads to differences in inferred stratigraphy. It is generally agreed that the outer limbs of the syncline contain mainly metasedimentary rocks and that the core is dominated by metavolcanic rocks. Both Taylor (1967) and Lane (1979) based their maps on lithology rather than stratigraphy, resulting in a more generalized map with fewer units. In the case of Taylor (1967), subdivision of the White Rock Formation on a lithological basis does not indicate stratigraphy within the formation. For example, slate in the core of the syncline, and therefore near the top of the sequence, is shown as the same slate which occurs on the outer limbs, the structurally lowest levels. In the case of Lane (1979), lithological subdivision resulted in a map that is overly generalized and does not recognize minor lithologies that are present within the general groupings. For example, Lane (1979) described the core of the syncline as volcanic rocks, whereas in reality it includes both sedimentary rocks and a wide variety of volcanic rocks (Fig. 2.1). Another difference between the map of this study and that of Lane (1979) is the postulated repetition of the sequence of lithologies on the western limb of the syncline suggested by Lane (1979) which was attributed to displacement along vertical faults.

Hwang (1985) also made a stratigraphic interpretation, but it differs from the stratigraphy of this study. His interpretation of two synclines separated by an anticline within the major syncline produced a stratigraphic sequence that is reversed in comparison with the stratigraphy presented in this thesis. According to Hwang (1985), the general succession within the White Rock Formation in Yarmouth is a lower sequence of volcanic rocks overlain by a package of metasedimentary rocks (Table 5.1). Approximate correlation of stratigraphic units between Hwang (1985) and this study (Table 5.1) shows inversion of the stratigraphic sequence as presented in this thesis.

5.2.3. Geochemistry of the White Rock Formation

Geochemical results for the White Rock Formation from this study are compared to those of Sarkar (1978). Complete comparison is not possible as the same suites of trace and rare-earth element data are not available. Most samples from Sarkar (1978) were collected from coastal sections, with only 5 samples from inland areas, and 3 of those are from the same location. Sarkar (1978) grouped the samples as metabasite, "metamafelsite" and metafelsite and each group contains a variety of rock types. Metabasite includes the assumed metamorphic equivalents of basalt, pyroclastic rocks, diabase and gabbro. The "metamafelsite" are transitional between metabasite and metafelsite and consist of metamorphosed equivalents of intermediate rocks such as trachyandesite, mugearite and their intrusive counterparts, and metafelsite includes assumed equivalents of benmoreite, trachyte, rhyolite and their intrusive counterparts or

Table 5.1. Correlation of units of Hwang (1985) with units of this study.

RELATIVE AGE	HWANG, 1985	RELATIVE AGE	THIS STUDY
Youngest ↓	Sw10 (metabasite and metapyroclastic rocks)	Oldest ↑	S_{WRsv}
	Sw9 (quartzite and arenite)		S_{WRqt}
	Sw8 (siltstone, phyllite, schist, metarhyolite)	youngest ↓	S_{WRss}, S_{WRmf}, S_{WRmv}, S_{WRmt}
	Sw7 (metabasite, metarhyolite, conglomerate)		S_{WRft}
	Sw6 (metaclastic rocks)		S_{WRmf}, S_{WRft}, S_{WRmt}
	Sw5 (metarhyolite, metabasite)		S_{WRft}
	Sw4 (slate)		S_{WRft}
	Sw3 (metabasite, slate, pyroclastic rocks)		S_{WRsv}, S_{WRmf}
↓	Sw2 (slate- interpreted from aeromagnetic maps)	↓	S_{WRqt}, S_{WRsv}
oldest	Sw1 (unknown lithology- interpreted from aeromagnetic maps)	oldest	S_{WRss}

arkose. The protolith for each sample is not clear in Sarkar (1978), making it difficult to compare rocks within each group (i.e. it is not possible to compare tuff and flow samples) and with the more detailed classification (mafic flow, mafic tuff, mafic crystal tuff, mafic lithic tuff, felsic crystal tuff) in this thesis. Sarkar (1978) did not separate dykes and sills from other mafic rocks, and host rocks were not identified, making it impossible to compare chemistry of dykes and other mafic rocks, and of dykes/sills from the White Rock Formation to those from the Halifax Formation. Eight samples from Sarkar (1978) have trace element data, but no major element data and no petrographic descriptions, making it difficult to know whether to compare them to mafic, intermediate or felsic rocks. These samples are not included in the present comparison.

The data set from Sarkar (1978) consists of 80 homogeneous metaigneous rocks analyzed by atomic absorption spectrometry for major elements and 59 samples analyzed by XRF for a partial trace element data set. Because of the uncertainties described above, the overall data sets are compared without distinction among composition or rock type (Fig. 5.1, 5.2, 5.3, 5.4). Overall, the two data sets are very similar. The only consistent differences are in Nb, which tends to be higher in the analyses of Sarkar (1978), and Co which tends to be lower. Because of the difference in Nb, the samples from Sarkar (1978) generally have more alkalic signatures compared to those of the present study (Fig. 5.3 a, b, c, f, g), but plot in similar fields on diagrams not using Nb (e.g. Fig. 5.3d and e).

Partial REE data are available for 22 samples, analyzed using neutron activation methods (Sarkar, 1978). Patterns exhibited by mafic samples show the same trends as found in the present study, with enriched LREE values relative to chondrite (Fig. 5.5). Data from mafic samples of this study plot within the range of patterns shown by mafic

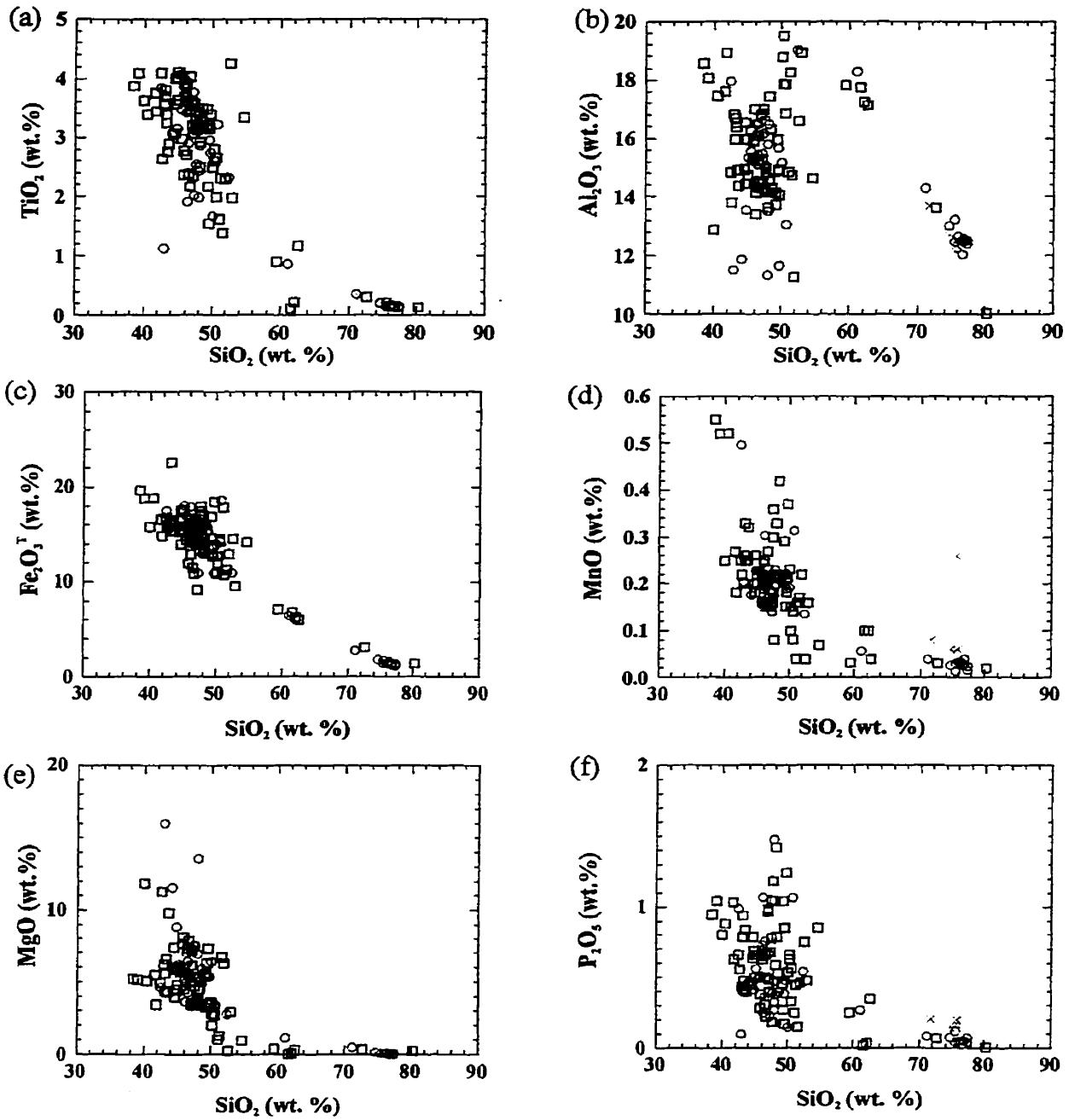

Figure 5.1. Major element variation diagrams for the White Rock Formation in the Yarmouth area and the Brenton Pluton, comparing data from the present study to those of Sarkar (1978) and O'Reilly (1976).

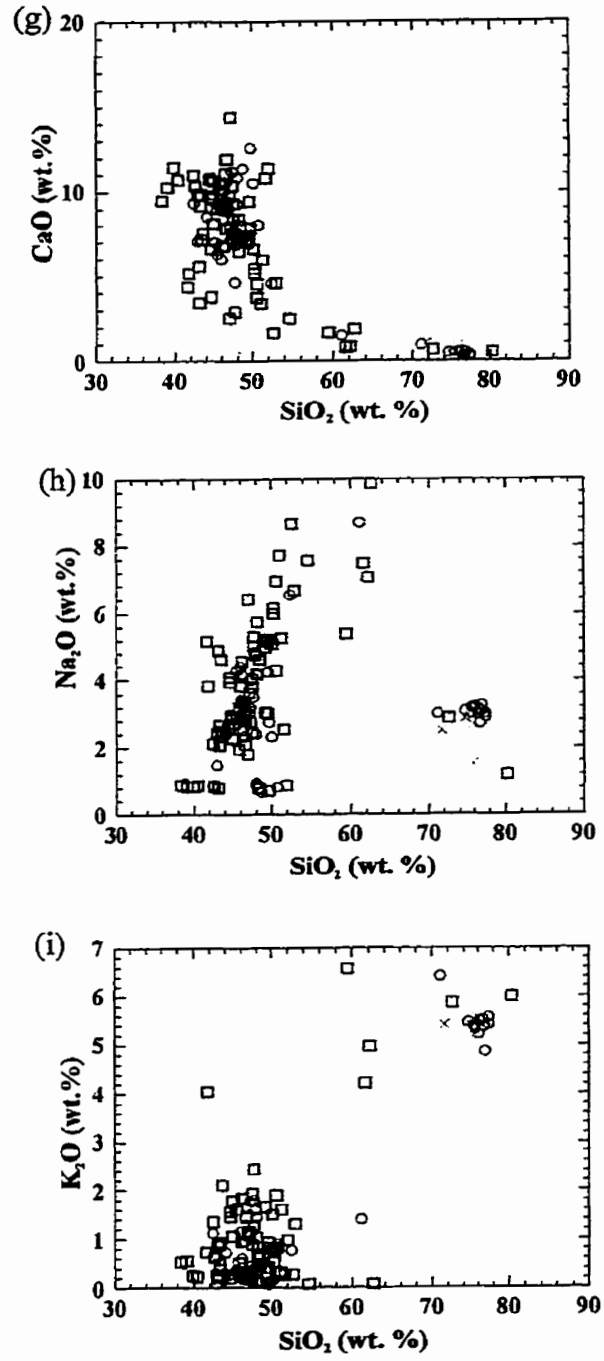

Figure 5.1. continued.

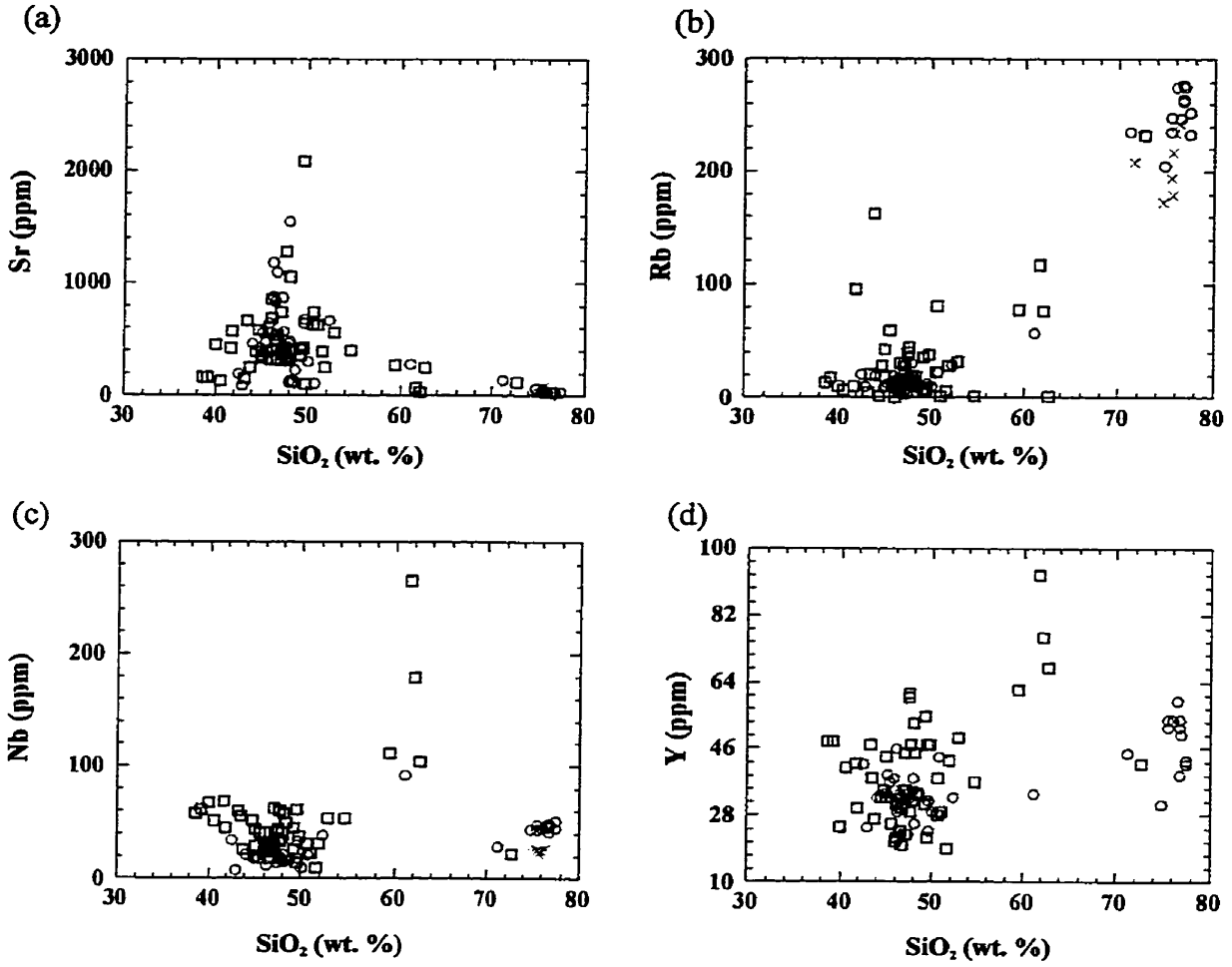

White Rock Formation
- ○ This study
- □ Sarkar (1978)

Brenton Pluton
- ○ This study
- · O'Reilly (1976)

Figure 5.2. Trace element variation diagrams for samples from the White Rock Formation and Brenton Pluton, comparing data from the present study to those from Sarkar (1978) and O'Reilly (1976).

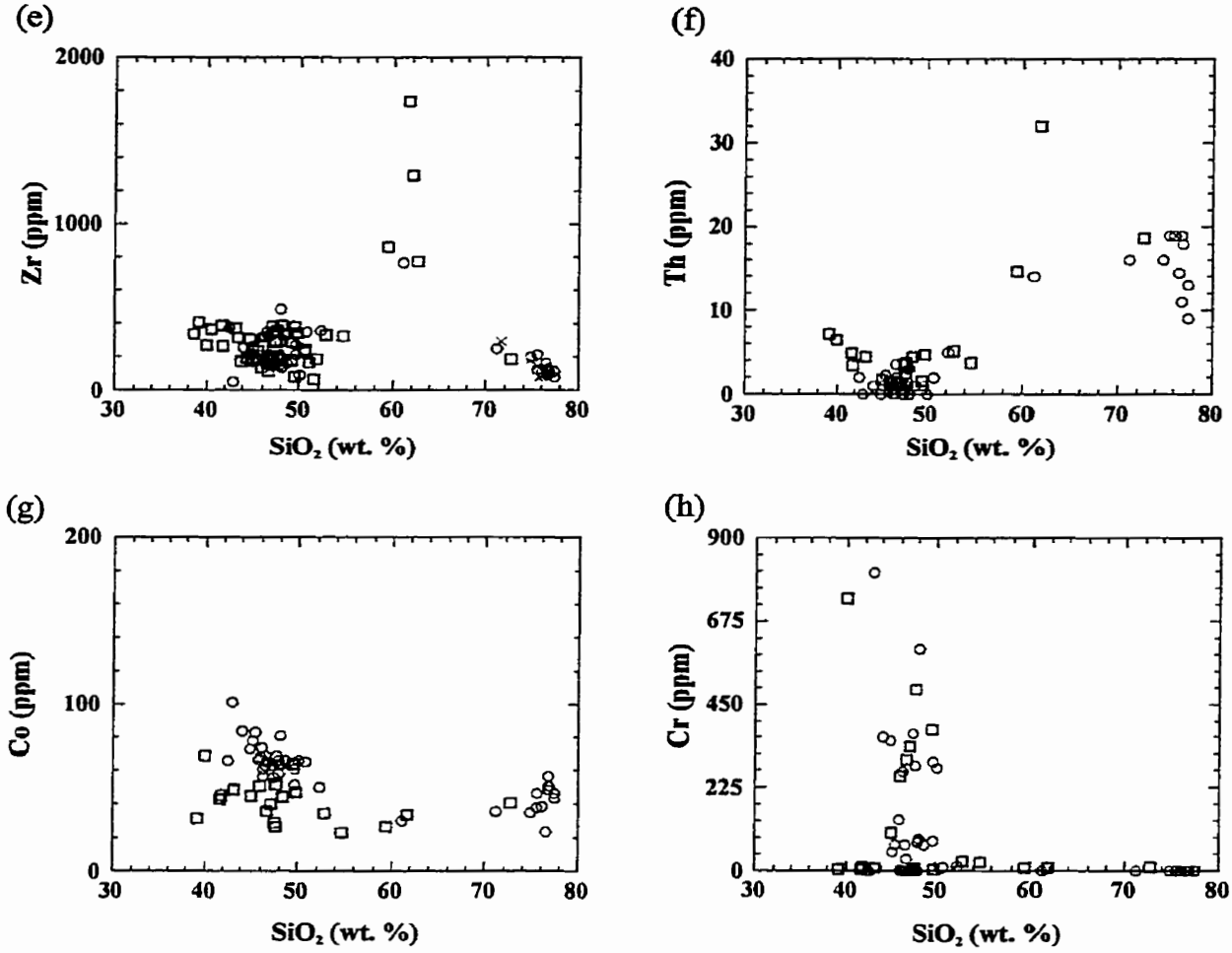

Figure 5.2. continued.

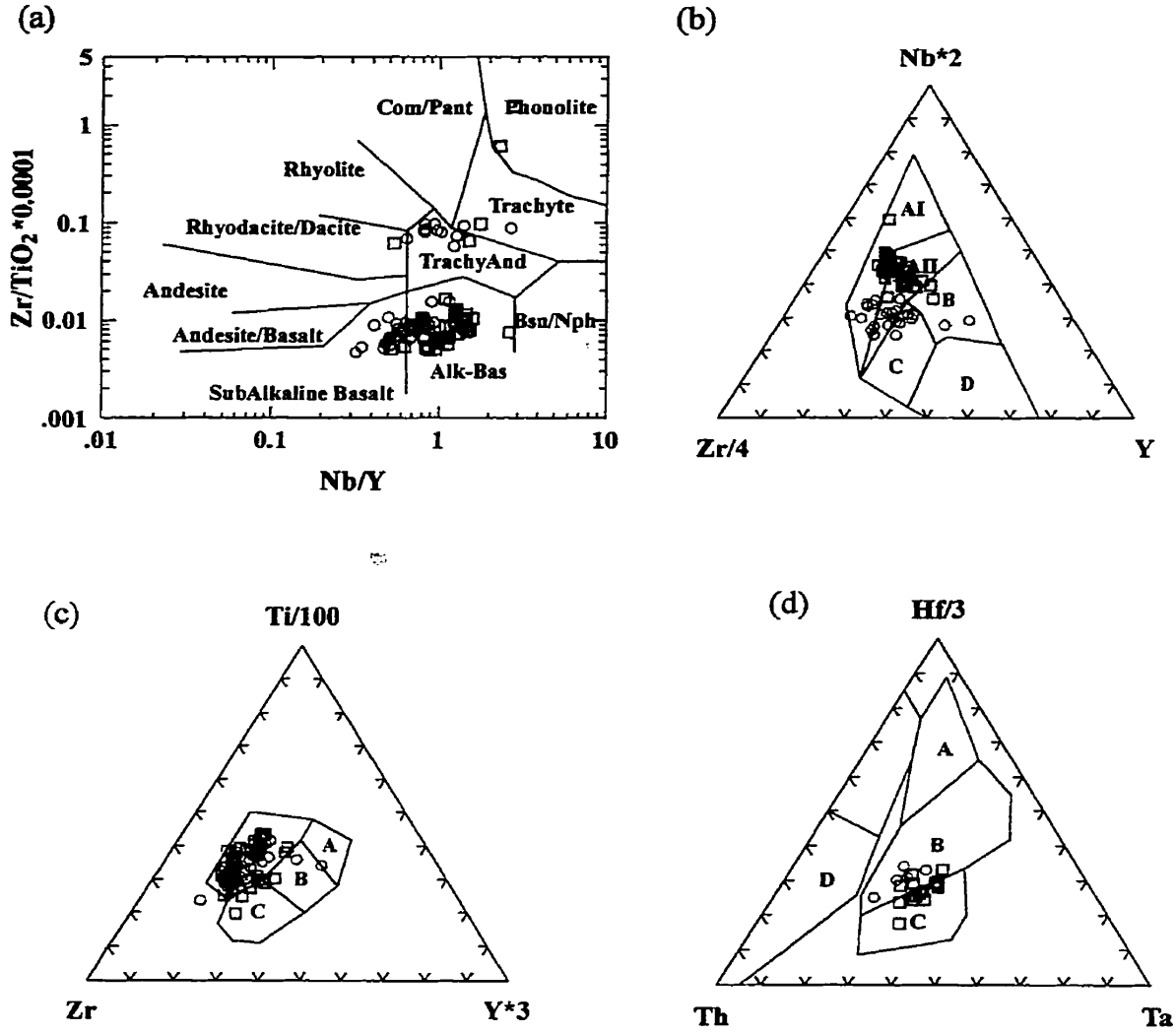

White Rock Formation
○ This study
Sarkar (1978)

Figure 5.3. Discrimination diagrams for mafic samples from the White Rock Formation, Yamourth area, comparing data from the present study to those of Sarkar (1978). Fields and sources as in figures 4.9, 4.10, 4.11, 4.12.

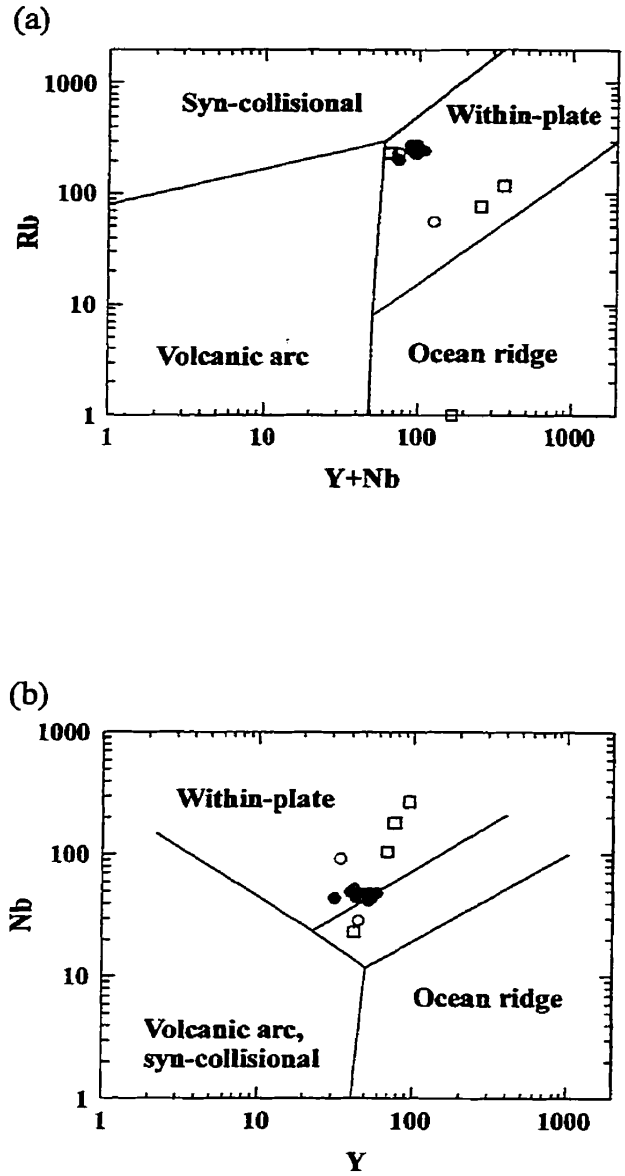

Figure 5.4. Discrimination diagrams for felsic samples from the White Rock Formation and Brenton Pluton, comparing data from the present study to data of Sarkar (1978). Fields are from Pearce et al. (1984).

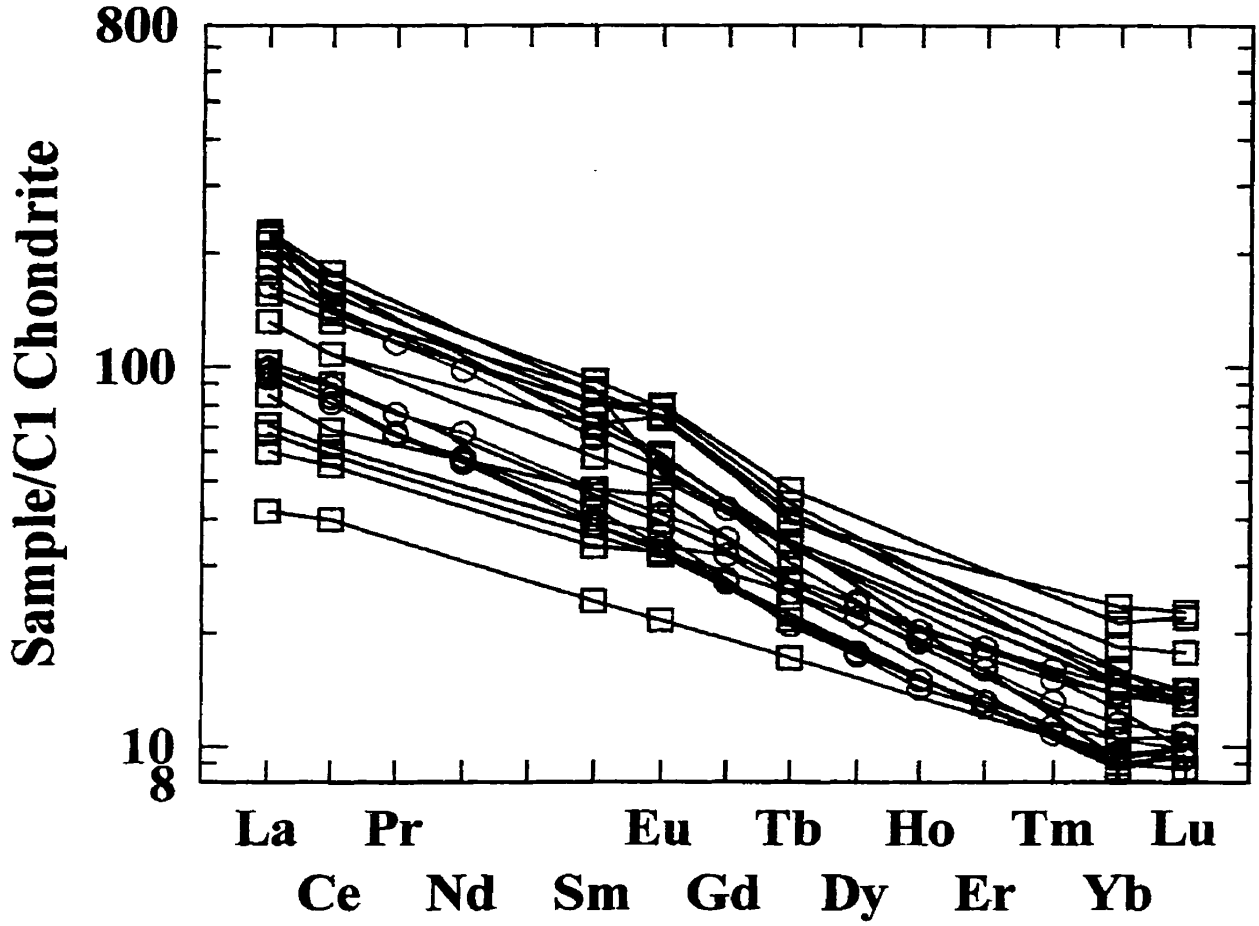

Figure 5.5. Chondrite-normalized REE plot for mafic samples from the White Rock Formation in the Yarmouth area, comparing data from the present study to those of Sarkar (1978). Chondrite normalizing values are from Sun and McDonough (1989).

rocks from Sarkar (1978) and samples from both studies show only a slight positive Eu anomaly or no Eu anomaly (Fig. 5.5). A REE plot of felsic samples from Sarkar (1978) shows enrichment in LREE compared to chondrite values and HREE, similar to the felsic patterns of this study (Fig. 5.6). One sample from Sarkar (1978) has a REE pattern almost identical to the pattern of a sample from the Brenton Pluton, whereas the other appears more evolved as it is more enriched in all REE except Lu.

The suggestion by Sarkar (1978) that two magmatic series are represented (a strongly differentiated, mildly alkaline basalt trachyte series and an olivine tholeiite-rhyolite series) is not substantiated by this study. Sarkar (1978) suggested the presence of two series based on trends observed on a plot of MgO against Fe_2O_3 +FeO, an AFM diagram and the D.I. (normative Q+Or+Ab+Ne+Lc) versus SiO_2 diagram. These plots use elements that are known to be mobile (Fig. 4.2-4) and therefore may not accurately represent the original composition of the samples. Figures 5.1 and 5.2 indicate similarity between the samples from this study and those from Sarkar (1978) and figures 5.3 and 5.4 show predominantly alkalic, within-plate signatures for samples from both studies.

5.2.4. Geochemistry of the Brenton Pluton

Seven samples of the Brenton Pluton were analyzed by O'Reilly (1976) for major elements and a partial set of trace element (Rb, Sr, Zr, and Nb). Samples were collected from various locations, including north, south and western areas from 3 outcrops considered poor quality, 2 outcrops considered fair quality and 2 outcrops considered good quality by O'Reilly (1976). Five of the seven samples were collected near the

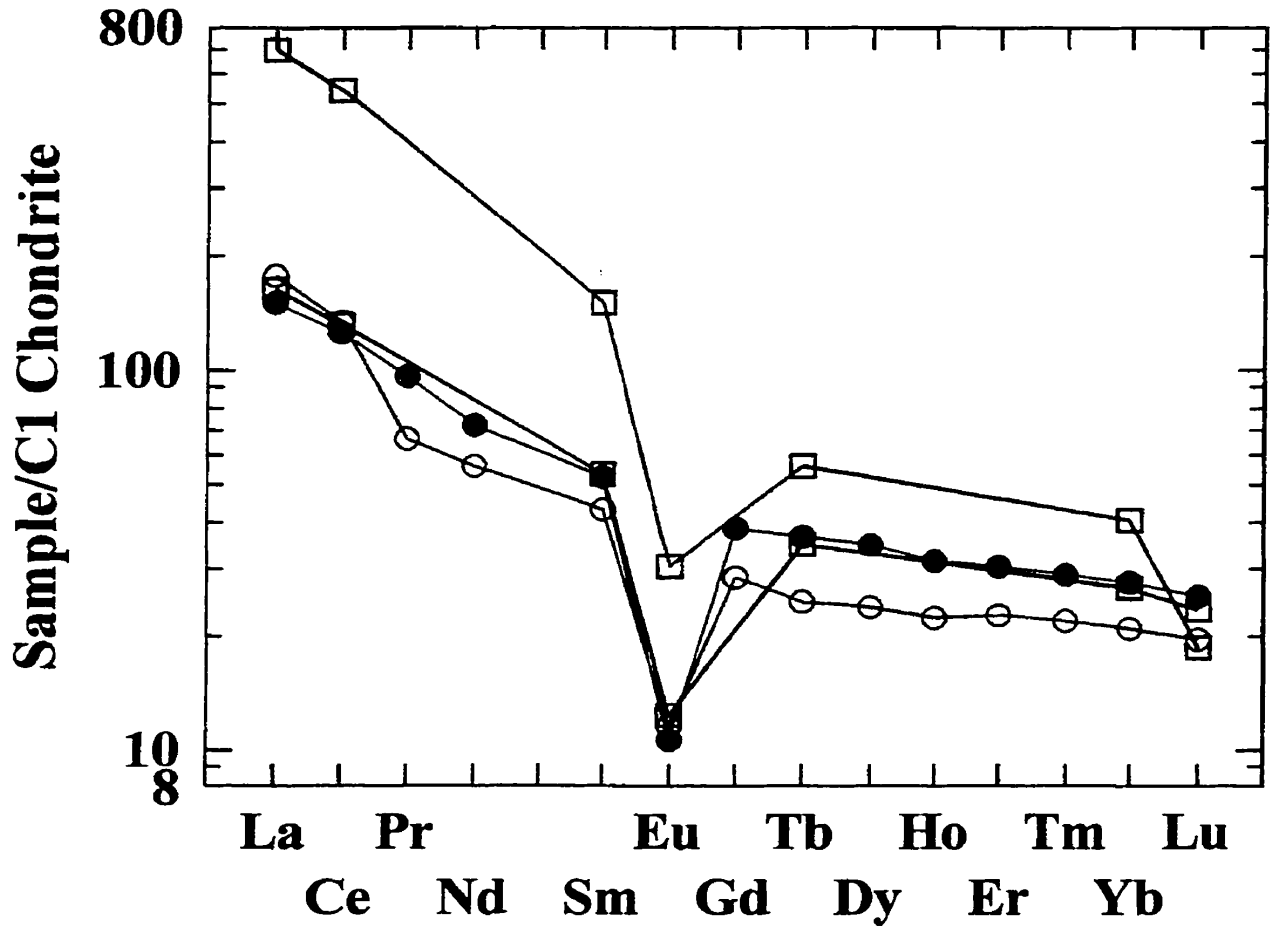

Figure 5.6. Chondrite-normalized REE plot for felsic samples from the White Rock Formation in the Yarmouth area and the Brenton Pluton, comparing data from the present study and Sarkar (1978). Chondrite normalizing values are from Sun and McDonough (1989).

approximated contact with the White Rock Formation. The eleven samples from this thesis were taken from more central locations in the middle and northern regions of the pluton. Outcrop quality in the central portion is excellent and samples were extremely fresh as they were newly excavated from a quarry.

Major element data in the two data sets are similar, with the exception of MnO which is slightly higher in the samples of O'Reilly (1976) (Fig. 5.1). Plots of trace element data (Fig. 5.2.) show that samples from O'Reilly (1976) contain similar concentrations of Sr and Zr and slightly lower levels of Nb and Rb.

5.3. Comparison of the Yarmouth Area with Other Areas of the White Rock Formation

5.3.1. Stratigraphy

Volcanic rocks represent a major component of the White Rock Formation in both the Yarmouth and Cape St. Mary areas. In contrast, no volcanic rocks are present the Bear River area (White et al. 1998), or in the Black River area (Lane, 1979) (Fig. 1.1). However, in the Torbrook area (Fig. 1.1), the formation contains felsic and mafic rocks near the base (Cullen et al, 1996; Trapasso, 1979; Lane, 1979). The formation is thickest in the Yarmouth area, reaching up to approximately 4 km (Fig. 2.1). In the Bear River and Torbrook areas, thicknesses are approximately 1200 m (White et al., 1998) and 500 m (Lane, 1979), respectively. At Cape St. Mary and in the Black River area, thickness is approximately 100 m or less (Kendall, 1981; Crosby, 1962). The variation in lithology

and thickness may indicate lateral facies changes which are typically complex in volcanic successions (Cas and Wright, 1988).

The western limb of the Yarmouth syncline from Cranberry Head to Overton Beach contains excellent coastal exposure of the formation and was commonly used as the basis for stratigraphic sections in previous work (Taylor, 1965; Lane 1979; Hwang, 1985). Although the exposure is good, gaps occur in the sequence, and portions of units S_{WRss} and S_{WRsv} are not exposed. In order to build a more complete stratigraphic section than is represented on the western limb, in this study the stratigraphy of the western and eastern limbs was integrated. The integrated section is compared to units in the formation in the Cape St. Mary, Bear River, Torbrook and Black River areas (Fig. 5.7). Only the lower portions of the stratigraphy in these areas (except for Cape St. Mary) may be correlated with units in Yarmouth. Correlation between the Yarmouth area and other areas is made primarily on the basis of age of units and the presence of similar lithologies in similar stratigraphic order.

Correlation is in part constrained by the age of overlying and underlying formations. The New Canaan Formation in the Black River area is Pridolian (419 +/- 3 to 418 +/- 2) (Crosby, 1962; Okulitch, 1999). The age of the Torbrook Formation is known from fossils in the Torbrook and Bear River areas to be early Devonian (418 +/- 2 Ma to 394 +/- 2 Ma) (Bouyx et al, 1997; Okulitch, 1999). The Kentville Formation (which may be the lateral equivalent of the upper part of the White Rock Formation in the Bear River and Torbrook areas) ranges from Wenlock to Pridolian (430 +/- 3 Ma to 418 +/- 2 Ma) (Bouyx et al, 1997; Okulitch, 1999). Absolute age constraints within the White Rock Formation are provided by felsic volcanic rocks near the base in the Torbrook area which

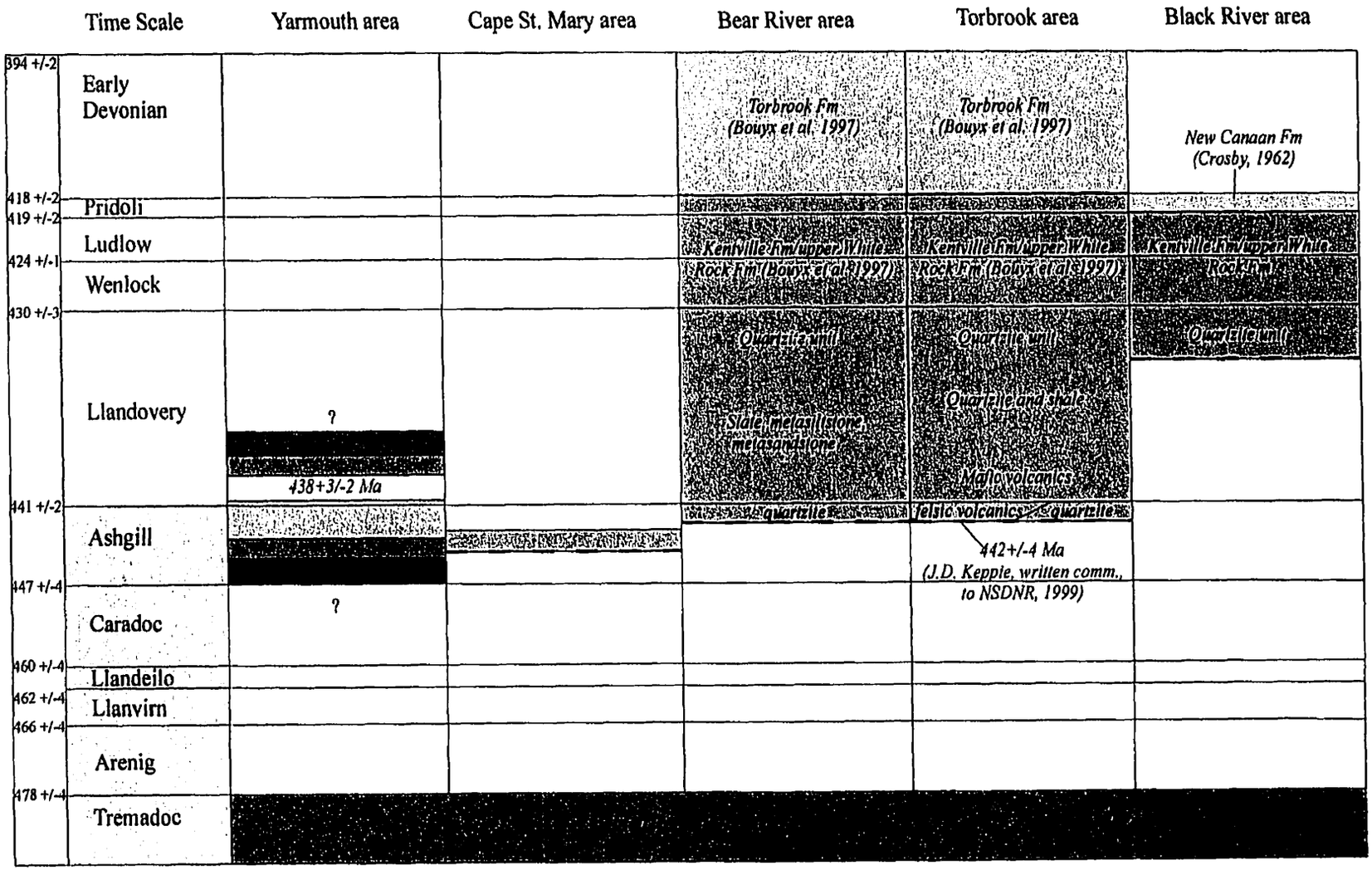

Figure 5.7. Correlation of White Rock Formation stratigraphy from the Yarmouth area to the Black River area.

gave a U-Pb (zircon) date of 442 +/- 4 Ma (J.D. Keppie written comm. to NSDNR, 1999) and felsic volcanic rocks in the upper volcanic sequences in Yarmouth area which gave an age of 438 +3/-2 Ma (section 4.7).

Correlation with Cape St. Mary is based on the stratigraphy presented by Kendall (1981). Felsic volcanic rocks near the base at Cape St. Mary appear to correlate with felsic volcanic rocks in the middle part of unit S_{WRsv}. Stratigraphically higher mafic volcanic and quartzite beds are correlated with mafic volcanic rocks and tuffaceous sandstone in the lower and middle portions of S_{WRmf}. The upper quartzite bed in the Cape St. Mary section is correlated with the quartzite at Overton (unit S_{WRmf}) and psammitic/pelitic and metabasite beds near the top of the Cape St. Mary sequence may correspond to tuffaceous sandstone and mafic volcanic beds in unit S_{WRmf} at Overton Beach (Fig. 5.7).

Correlation between the formation in the Yarmouth area and the section in the Bear River area is more difficult. The mainly psammitic and pelitic lithologies in the Bear River section (White et al. 1998) do not directly correspond to the units observed in the Yarmouth area. Quartzite near the base of the White Rock Formation in Wade Brook (White et al. 1998) may correlate with the quartzite bed in unit S_{WRmf} at Overton Beach but stratigraphically higher slate and arenaceous beds in the Bear River area may be lateral equivalents of the metavolcanic and metasedimentary rocks in units S_{WRft}, S_{WRmt} and S_{WRmv}. The upper quartzite and slate beds observed by White et al. (1998) are probably stratigraphically higher than the sequence in the Yarmouth area (Fig. 5.7).

No volcanic layers were observed by White et al. (1998), although Lane (1979) noted a felsic volcanic bed above the lower quartzite layer in Bear River which could correlate with the felsic volcanic bed in unit S_{WRmf} at Cape Forchu West.

The units of Cullen et al. (1996) in the Torbrook area also appear to be stratigraphically higher than those exposed in the Yarmouth area. The lower subunits OSwd, OSwe and OSwf of Cullen et al. (1996) (laterally equivalent felsic volcanic rocks, conglomerate and arenite) near the base of the formation may correlate with felsic volcanic rocks, quartzite and conglomerate in unit S_{WRmf} at Overton. The overlying subunit OSwc (mafic volcanic rocks) may correlate with mafic volcanic rocks in unit S_{WRft} (with thinning and pinching out of felsic volcanic rocks). Subunit OSwb (arenite, siltstone and shale) may represent the lateral equivalent of S_{WRmt} or S_{WRmv} with thinning and pinching of layers, or may be stratigraphically higher than the beds exposed in Yarmouth. Subunit OSwa (quartz arenite) probably represents stratigraphically higher rocks than contained in the sequence in the Yarmouth area (Fig. 5.7).

Quartzite units described by Taylor (1965) and Lane (1979) in the Black River area probably represent stratigraphically higher units in the formation which are not present in the Yarmouth area (Fig. 5.7).

5.3.2. Comparison with Other Stratigraphic Interpretations

The correlations made in this study between the White Rock Formation in the Yarmouth area and the other areas are different from those presented by Schenk (1995). He interpreted the Yarmouth and Cape St. Mary sections to include the Halifax, White Rock, Kentville and New Canaan formations. According to Schenk (1995) the White

Rock Formation is defined by sections in the Bear River and Torbrook areas and includes basal volcanic rocks overlain by quartz arenite interbedded with shale and siltstone, overlain by a sandstone and black slate sequence (the slate contains a felsic volcanic layer in the Torbrook area). Using this definition, Schenk (1995) assigned metasedimentary and metavolcanic rocks closer to the core of the synclines in the Yarmouth and Cape St. Mary area to the Kentville and New Canaan formations. In this study, the upper units in the Yarmouth area are the lateral equivalents of the quartz arenite, shale and siltstone beds in the White Rock Formation described by Schenk (1995). The upper sandstone and black slate sequence designated as the top of the White Rock Formation by Schenk (1995) are stratigraphically higher than the rocks occuring in the Yarmouth area, according to this study.

Schenk (1995) described the contact between the Halifax and White Rock formations as paraconformable, except at Cape St. Mary and in the Torbrook area where it is an angular unconformity and a disconformity, respectively. Culshaw and Liesa (1997) indicated that the contacts between the formations are within shear zones in the Yarmouth and Cape St. Mary areas and observations during the present study indicate faulted contacts (which may have been originally unconformable) between the Halifax and White Rock formations in the Yarmouth area and at Cape St. Mary and unconformable contacts elsewhere.

Schenk (1995) assumed that the felsic volcanic rocks constitute the lowest part of the White Rock Formation except in the Black River area. Observations from the present study suggest that the basal units of the White Rock Formation in the Yarmouth area are metasedimentary (section 5.2.1) and stratigraphically below the base designated by

Schenk (1995). In contrast to the interpretation of Schenk (1995), White et al. (1998) reported no volcanic rocks anywhere in the sequence in the Bear River area.

The correlations made by Schenk (1995) were based on the assumption that the complete stratigraphy of the White Rock Formation is represented by rocks exposed in the Bear River and Torbrook areas. Schenk (1995) used the package of rocks from these areas to define the White Rock Formation, and placed rocks above and below the package in other formations. In contrast, the present study is constrained by ages of units within, above and below the White Rock Formation. In this study, the layers above and below the package described by Schenk (1995), such as the volcanic rocks in the cores of the synclines at Cape St. Mary and in the Yarmouth area, and the metasedimentary layers on the outer limb of the Yarmouth Syncline, are accommodated within the White Rock Formation. This accommodation is justified by U-Pb ages from volcanic rocks in the White Rock Formation in the Torbrook and Yarmouth areas. The U-Pb age of 442 +/- 4 Ma (J.D. Keppie written comm. to NSDNR, 1999) from the basal rhyolitic tuff in the Torbrook area, which, according to the correlation of Schenk (1995) would be equivalent to the base of the White Rock Formation in Yarmouth, is identical (within error) to the age of 438 +3/-2 Ma obtained during the present study for volcanic rocks in the upper part of the Yarmouth sequence (unit S_{WRB}). Schenk (1995) placed the latter volcanic rocks in the New Canaan Formation but they are significantly older than the late Silurian (Pridolian) age (419 Ma – 418 Ma; Okulitch, 1999) assigned to this formation (Crosby, 1962). An age of 438 +3/-2 Ma for the upper volcanic rocks in the Yarmouth area also correlates with faunal (graptolite) ages for the White Rock Formation in the Torbrook area which are Llandovery and Wenlock (441+/- 2 Ma – 424 Ma) (Bouyx et al., 1997;

Okulitch, 1999), confirming that placement within the White Rock Formation is more likely than in the New Canaan Formation.

Chemical comparison of samples from the New Canaan Formation from James (1998) and the White Rock Formation indicate that samples from both formations are alkalic and from a within-plate tectonic setting (Fig. 5.8). However, in detail, incompatible elements ratios show differences between the White Rock and New Canaan formations (Fig. 5.9) which support the stratigraphic evidence presented above that shows that they are not comagmatic.

5.3.3. Geochemical Comparisons

Kendall (1981) presented chemical analyses for 4 samples of metabasite (unspecified as to whether the samples were from tuff, flow or dyke) and one sample of metafelsite of volcaniclastic origin from the Cape St. Mary section. The samples were analyzed for major elements using the electron microprobe and atomic absorption spectrometry, and trace elements (Ba, Co, Cr, Cs, Hf, Sc, Ta, Th, U), and rare earth elements (La, Ce, Nd, Sm, Eu, Yb, Tb, Lu) using instrumental neutron activation analysis. Keppie et al. (1997) reported chemical data from two basalt and two rhyolite samples from the Cape St. Mary and Torbrook areas but did not specify which samples are from which area. The suite of analyses includes major and trace elements (by XRF) and REE (by ICP-MS). The protoliths of the samples also were not specified.

Samples from the Cape St. Mary and Torbrook areas have compositions similar to those of the suite of samples from the Yarmouth area analyzed during the present study (Fig. 5.10, 5.11). K_2O abundances are slightly lower in felsic samples from Cape St.

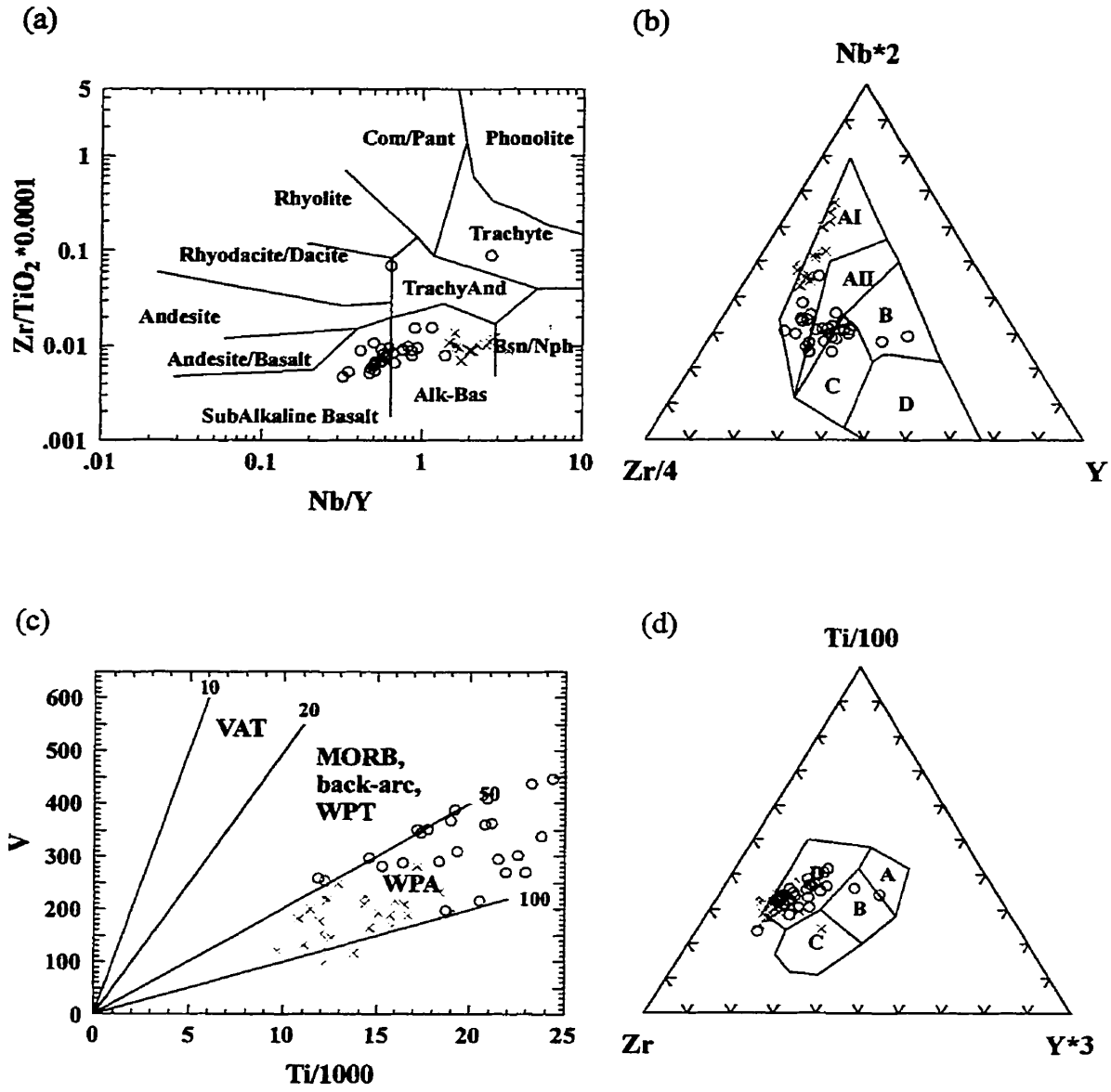

White Rock Formation
o This study

New Canaan Formation
× James, 1998

Figure 5.8. Geochemical comparison of volcanic rocks in the White Rock and New Canaan formations. Fields and sources of diagrams as in figures 4.9, 4.10, 4.12, and 4.13.

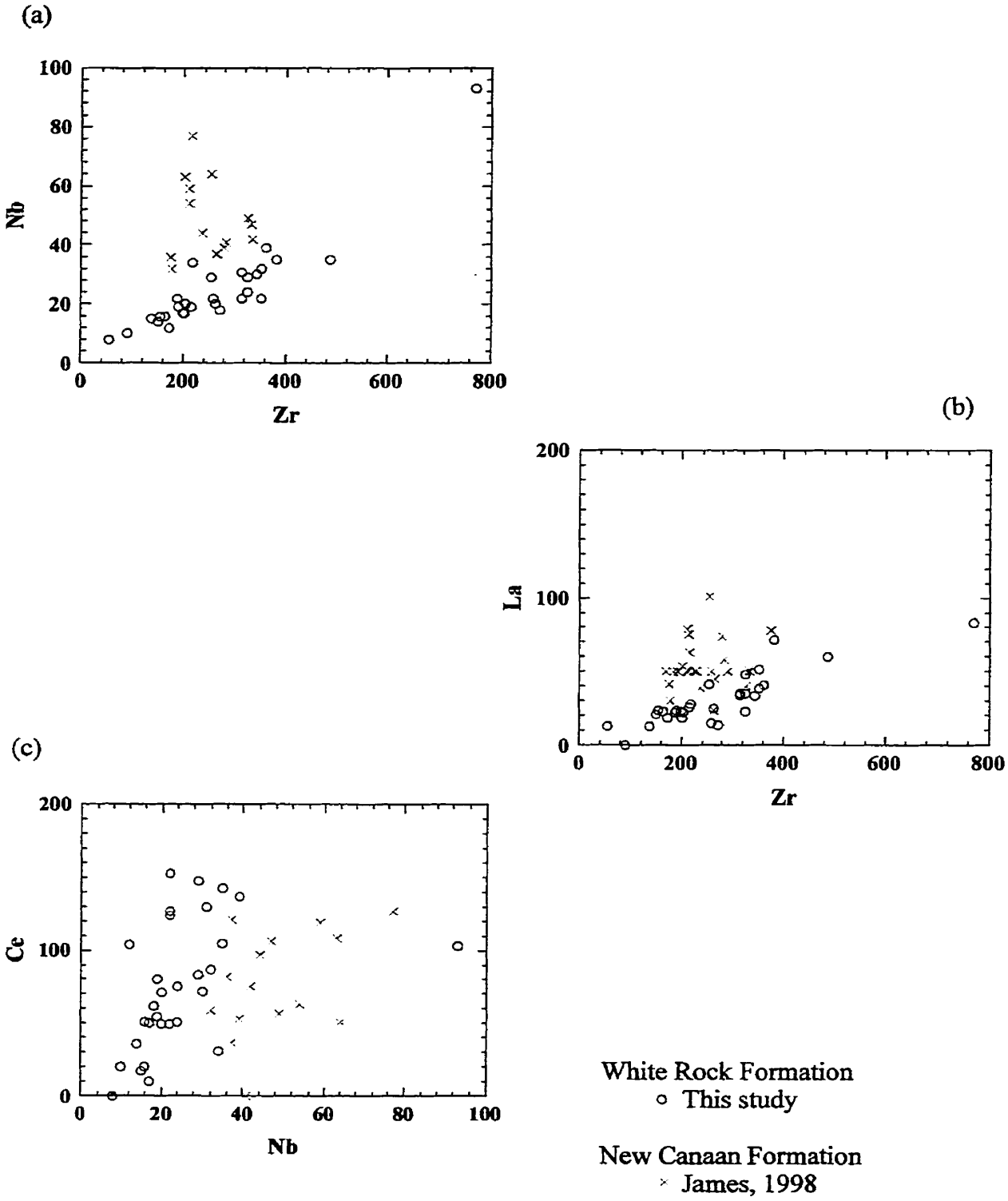

Figure 5.9. Plots of incompatible elements in samples from the White Rock and New Canaan formations.

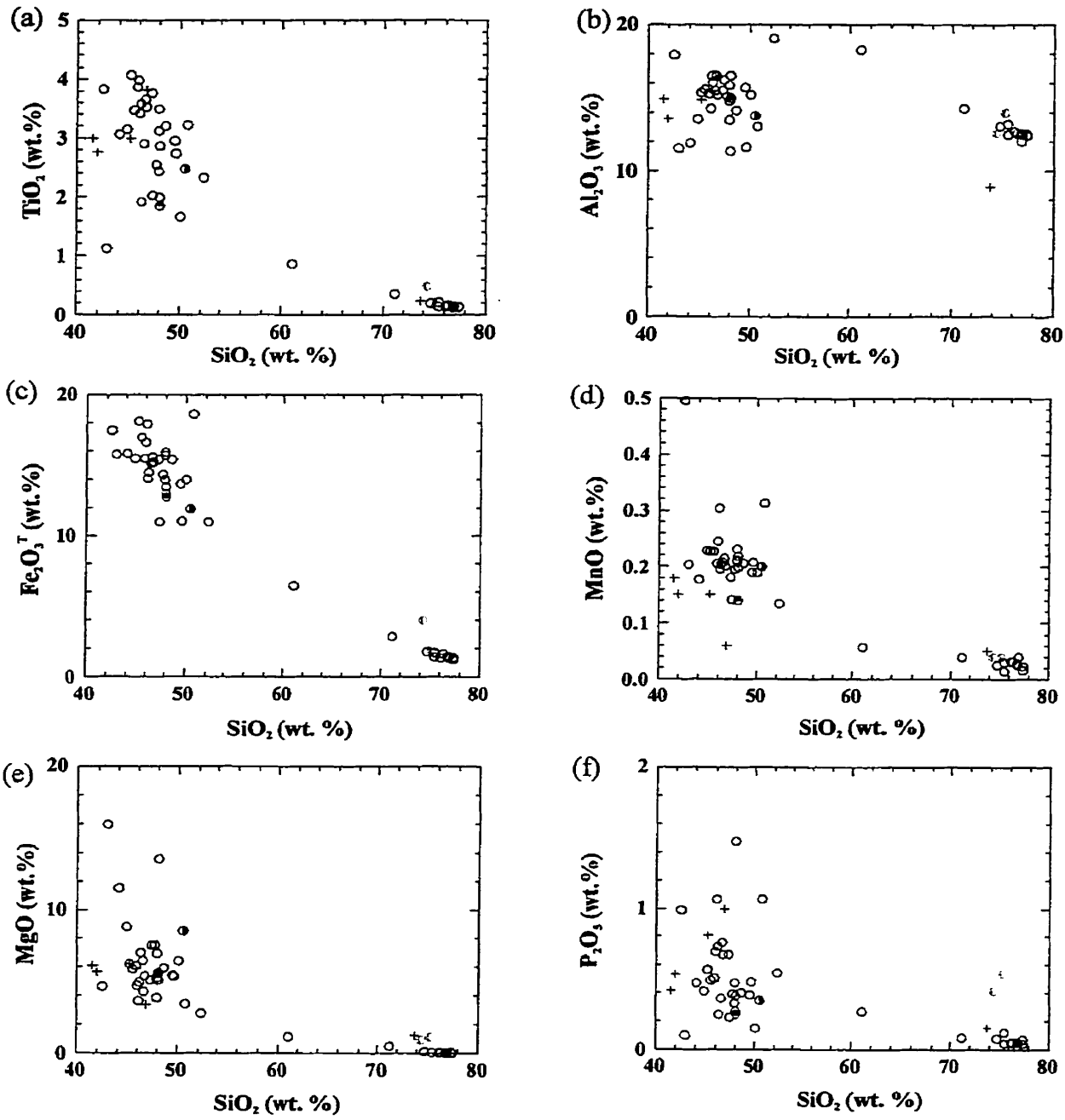

White Rock Formation
- Yarmouth (This study)
- Cape St. Mary (Kendall, 1981)
- Cape St. Mary (Keppie et al. 1997)
- Torbrook area: mafic, felsic (Keppie et al. 1997)

Fig. 5.10. Major element variation diagrams for samples from the White Rock Formation in the Yarmouth, Cape St. Mary and Torbrook areas.

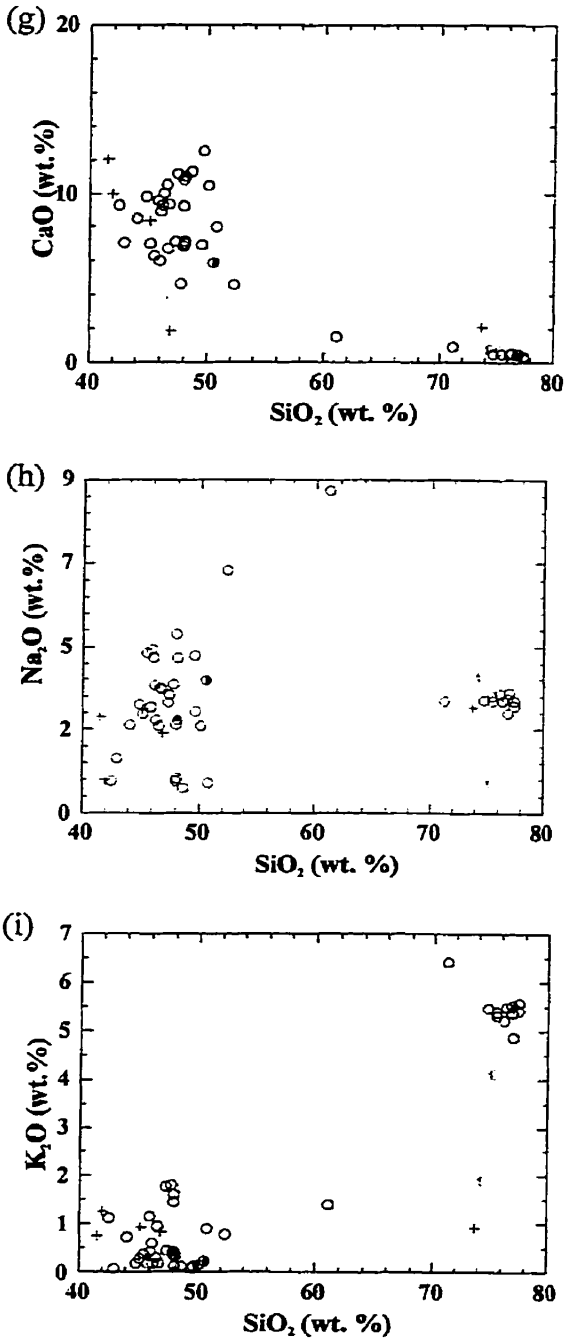

Fig. 5.10. continued.

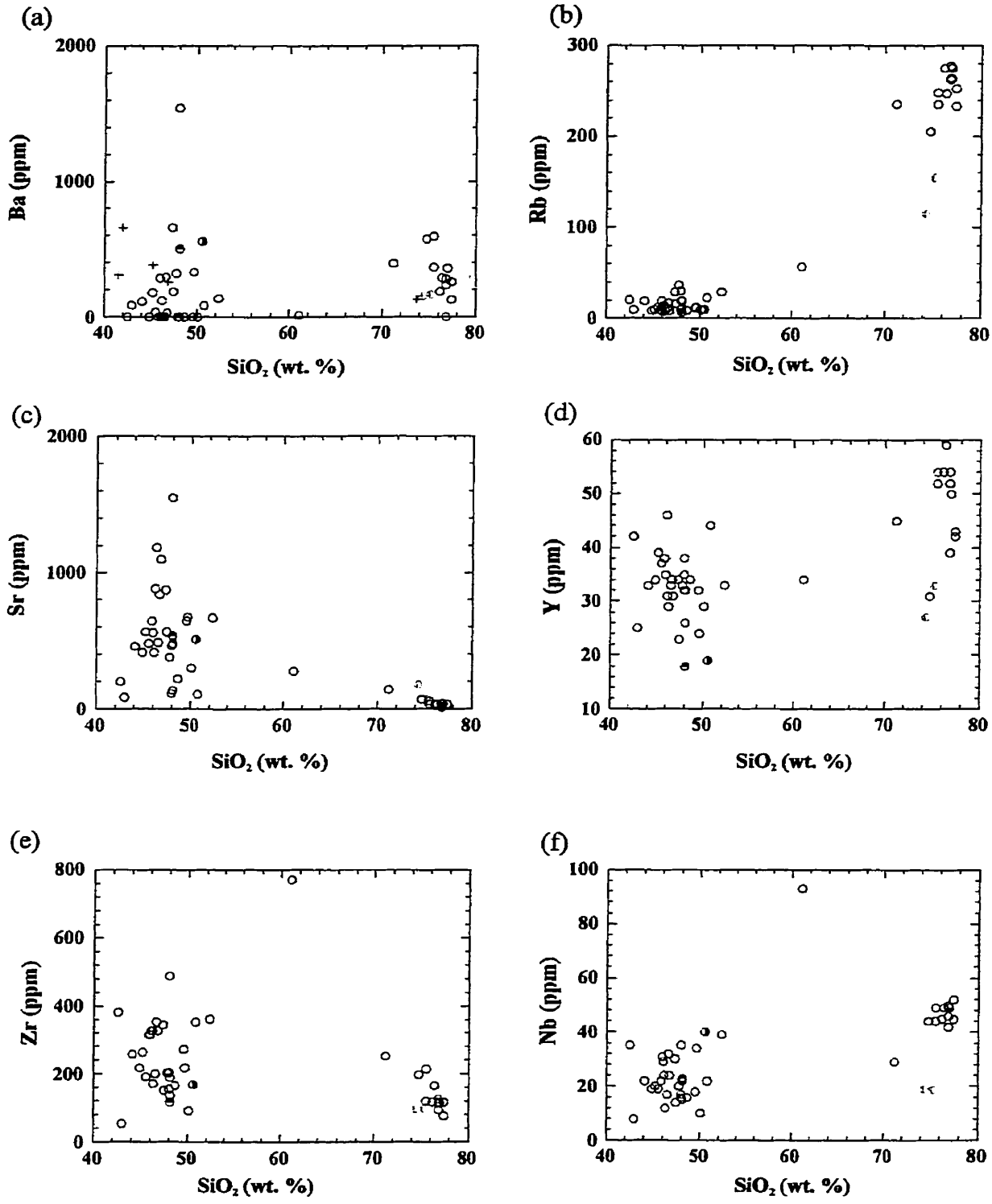

Fig. 5.11. Trace element variation diagrams for samples from the White Rock Formation in the Yarmouth, Cape St. Mary and Torbrook areas. Symbols as in Figure 5.10.

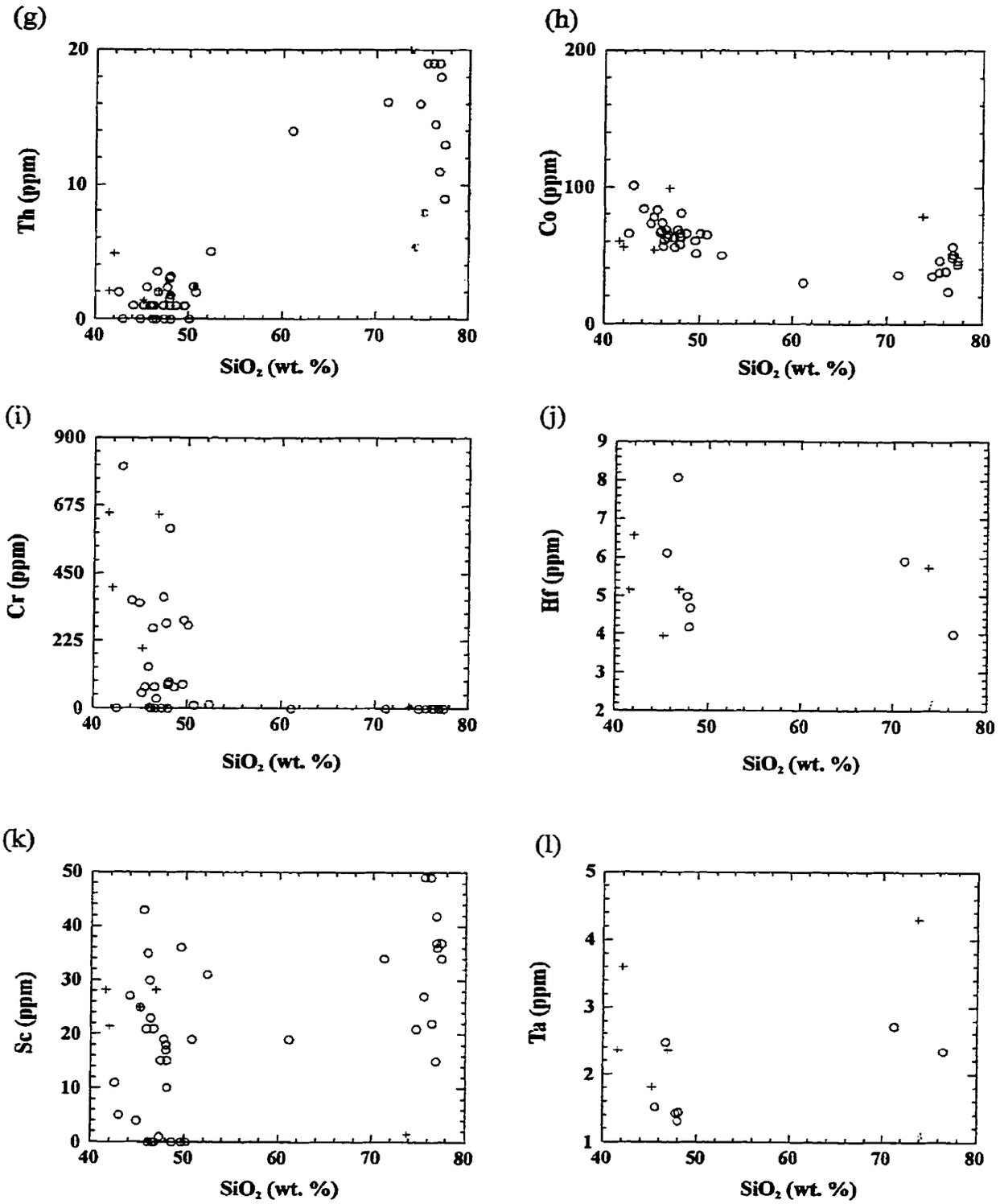

Fig. 5.11. continued.

Mary and Torbrook. P_2O_5 levels are slightly higher in felsic samples from Keppie et al. (1997) than in felsic samples from the Yarmouth area.

Trace element contents in samples from the Cape St. Mary and Torbrook areas are generally similar to those from the Yarmouth area (Fig. 5.11). Some variation exists between felsic samples from different locations but data is insufficient for meaningful comparison.

REE patterns for both mafic and felsic samples from Cape St. Mary from Kendall (1981) are similar to those from the Yarmouth area (Fig. 5.12). The felsic sample (Fig. 5. 12b) is more depleted in heavy REE. REE patterns in the 2 mafic samples of Keppie et al. (1997) (Fig. 5.13) show slight divergence from each other. The pattern for the sample from Cape St. Mary is almost parallel to that of mafic flow sample 85-3 from this study, whereas the pattern for the sample from the Torbrook area is subparallel to that of mafic flow samples 75A-1 and 2-1. REE patterns for felsic rocks from all locations also have consistent enrichment trends but samples of Keppie et al. (1997) display slightly positive Dy anomalies (Fig. 5.13b). The REE patterns of felsic samples from Keppie et al. (1997) appear to parallel that of the sample from the Brenton Pluton more closely than that of the sample of crystal tuff, but results are ambiguous on plots of incompatible elements (Fig. 5.14). The felsic sample of Kendall (1981) and all samples of Keppie et al. (1997) appear less evolved than samples from the Yarmouth area. This observation would be reasonable according to stratigraphic correlations made in section 5.3.2 which place the units exposed at Cape St. Mary and the Torbrook area at lower stratigraphic levels than layers containing the mafic flows and felsic tuff analyzed for REE in this study.

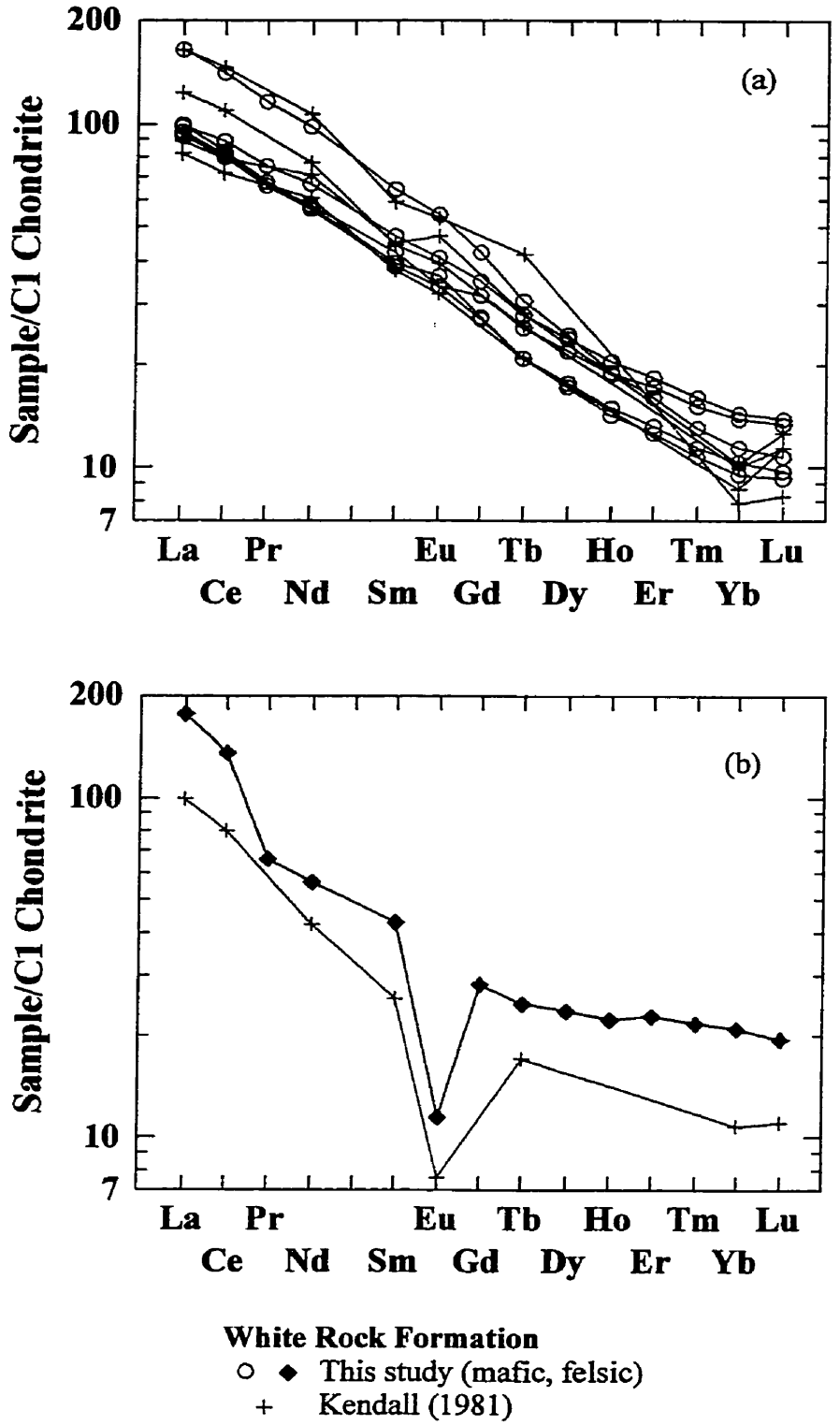

Figure 5.12. Chondrite-normalized REE diagrams for (a) mafic and (b) felsic rocks from the Yarmouth area (present study) and Cape St. Mary area (Kendall, 1981). Chondrite normalizing values are from Sun and McDonough (1989).

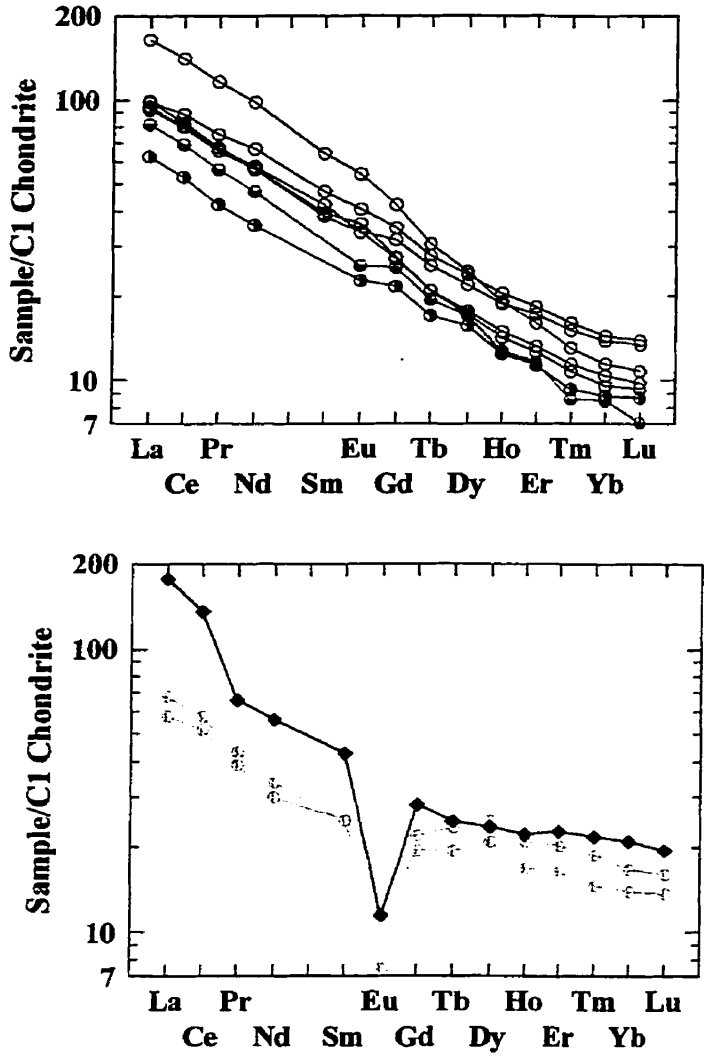

Figure 5.13. Chondrite-normalized REE diagrams for (a) mafic and (b) felsic rocks from the Yarmouth area (present study), Cape St. Mary and Torbrook areas (Keppie et al., 1997). Chondrite normalizing values as from Sun and McDonough (1989).

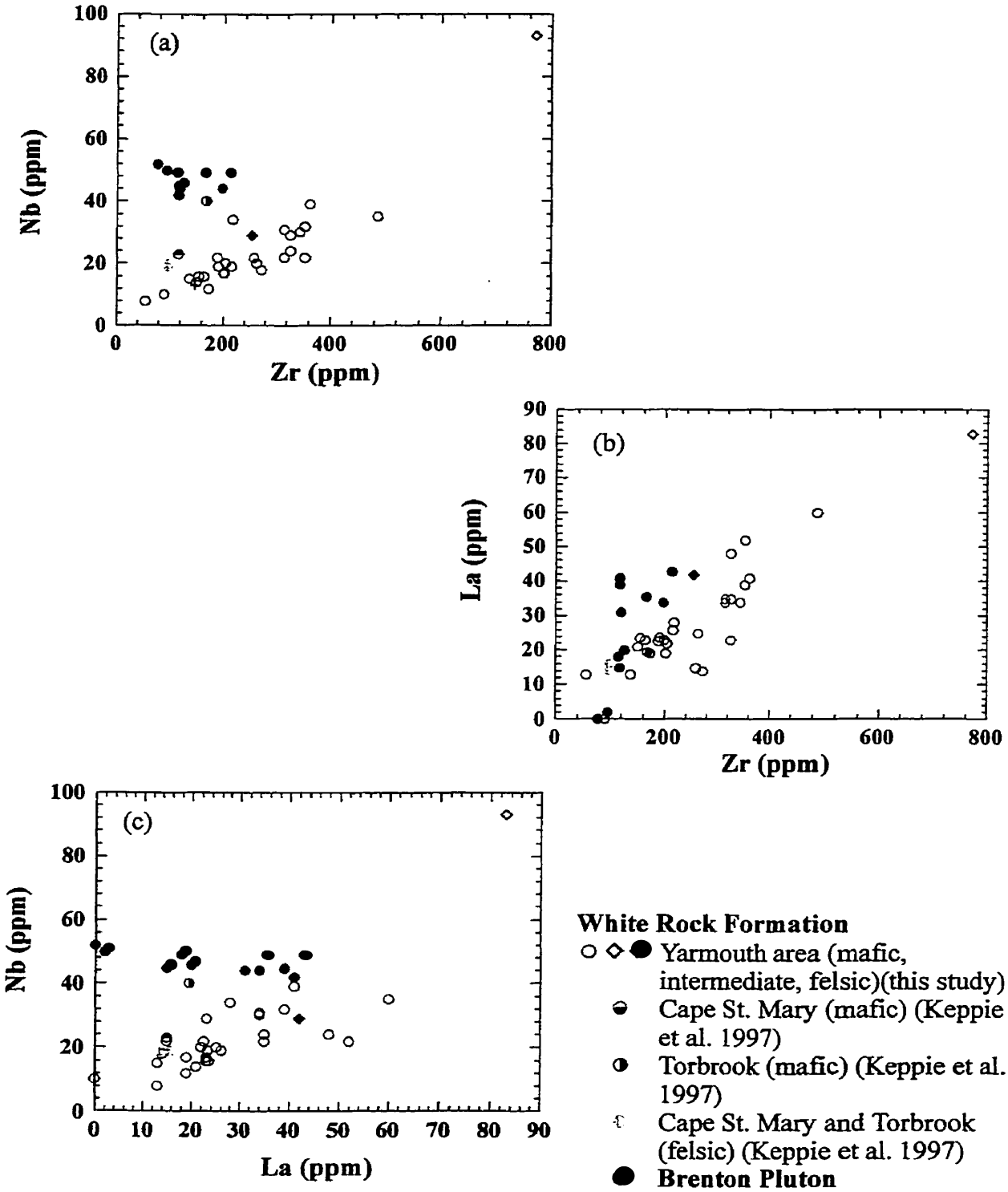

Figure 5.14. Incompatible element plots for samples from the Yarmouth area (this study), Cape St. Mary and Torbrook areas (Keppie et al. 1997).

Data from Keppie et al. (1997) from the Cape St. Mary and Torbrook areas expands the petrogenetic interpretations made in section 4. 9. εNd values were obtained for basalts in the Cape St. Mary and Torbrook areas that range from + 3 to + 6.8, lower than depleted mantle values (c. 8-8.5) (Keppie et al. 1997). These values indicate derivation from a different source than depleted mantle, or that the primary magmas were contaminated by a crustal component (Keppie et al. 1997). On the basis of Nb and Ti depletion in basalts and lack of Th enrichment, Keppie et al. (1997) discounted crustal contamination. They attributed differences in the slope of REE patterns and incompatible element ratios to derivation from compositionally distinct sources or different degrees of melting of a garnet-bearing source. A possible source suggested by Keppie et al. (1997) is a heterogenous upper asthenosphere composed mainly of a depleted mantle matrix (εNd approximately +8) with incompatible element enriched enclaves or veins.

Keppie et al. (1997) obtained εNd values of +1.6 and +0.2 for samples of rhyolite, close to the εNd value of +1.37 obtained in this study (section 4.8). They also noted negative Nb, Sr, Eu and Ti anomalies but highly enriched Th values. From these observations, Keppie et al. (1997) interpreted that the rhyolites were derived by increased fractionation from coeval basaltic magmas, probably accompanied by crustal contamination. The evidence for zircon inheritance in the dated felsic crystal tuff sample from the Yarmouth area supports this interpretation.

5.4. Regional Comparisons

5.4.1. Arisaig Group

The Arisaig Group is an Upper Ordovician to Lower Silurian sequence of metavolcanic and metasedimentary rocks located in the Avalon Terrane in northeastern Nova Scotia (Murphy et al., 1991). The lower formations in the group include both metasedimentary and metavolcanic rocks whereas the upper formations are mainly metasedimentary (Murphy et al., 1991). The two formations in the lower part of the Arisaig Group which contain metavolcanic layers are the Bears Brook and Beechill Cove formations (Murphy et al., 1991). The Bears Brook Formation consists of conglomerate, arkose and shale interbedded with mafic and felsic volcanic rocks (flows, ignimbrite and tuff) and is conformably to disconformably overlain by the Beechill Cove Formation. The Beechill Cove Formation includes arkose, siltstone and felsic volcanic rocks (Murphy et al., 1991).

Volcanic rocks in the Arisaig Group have been interpreted to be transitional between tholeiitic and alkalic and formed in a continental, within-plate, extensional setting, based on high concentrations of TiO_2, Zr and high field strength elements in mafic samples, moderate enrichment in light ion lithophile elements and slight depletion in high field strength elements (Murphy et al., 1991).

Data from 13 mafic and 8 felsic samples from the Bears Brook Formation, 2 felsic samples from the Beechill Cove Formation (Murphy et al., 1991) and 2 mafic samples from unknown locations in the Arisaig Group (Keppie et al., 1997) are plotted with samples from the Yarmouth area (Fig. 5.15). Differences in major and trace element chemistry (particularly TiO_2, Al_2O_3, $Fe_2O_3^t$, CaO and Zr) are shown on Figure

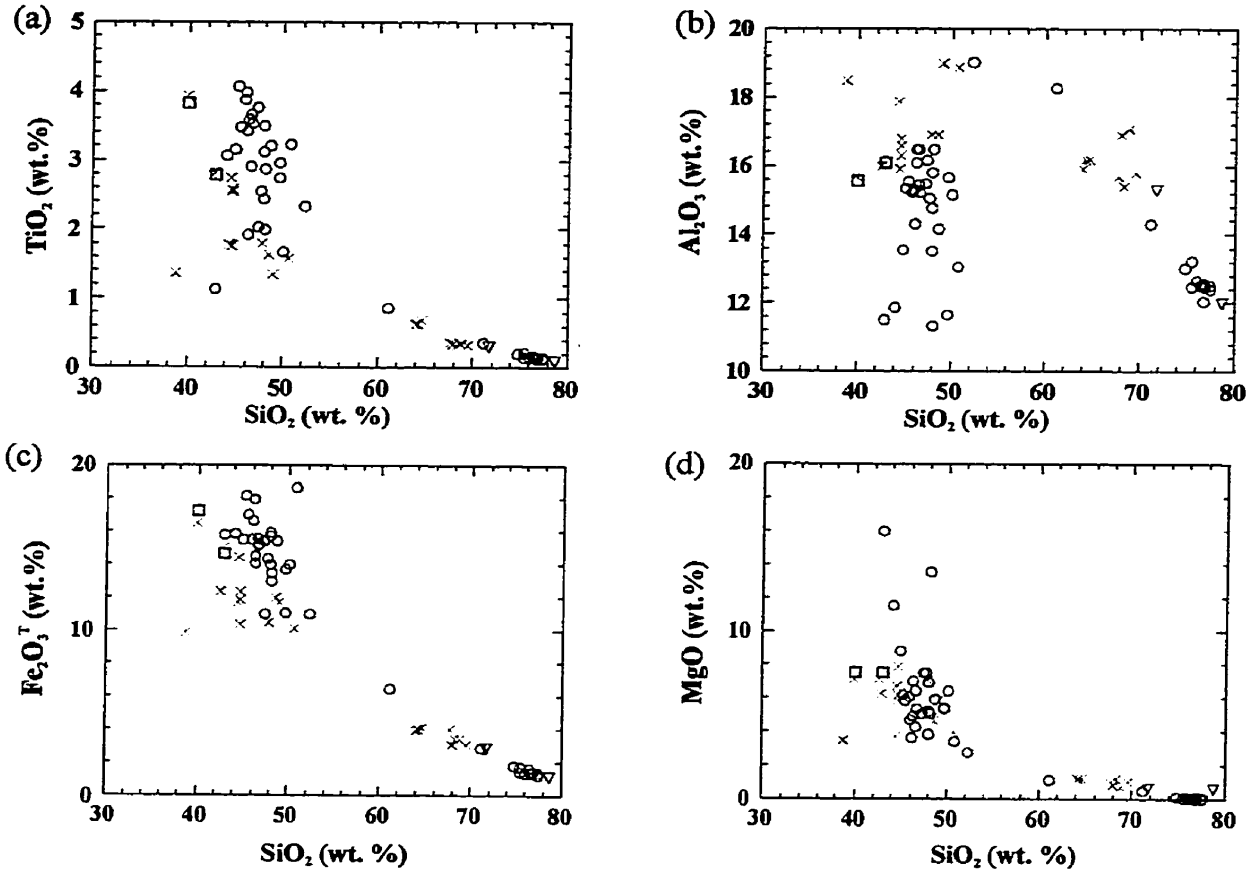

White Rock Formation
- ○ This study

Bears Brook Formation
- × Murphy et al. (1991); Murphy et al. (1996)

Beechill Cove Formation
- ▽ Murphy et al. (1991)

Arisaig Group
- □ Keppie et al. (1997)

Figure 5.15. Major element variation diagrams for samples from the White Rock Formation and samples from the Arisaig Group from Murphy et al.(1991), Murphy et al. (1996), and Keppie et al. (1997).

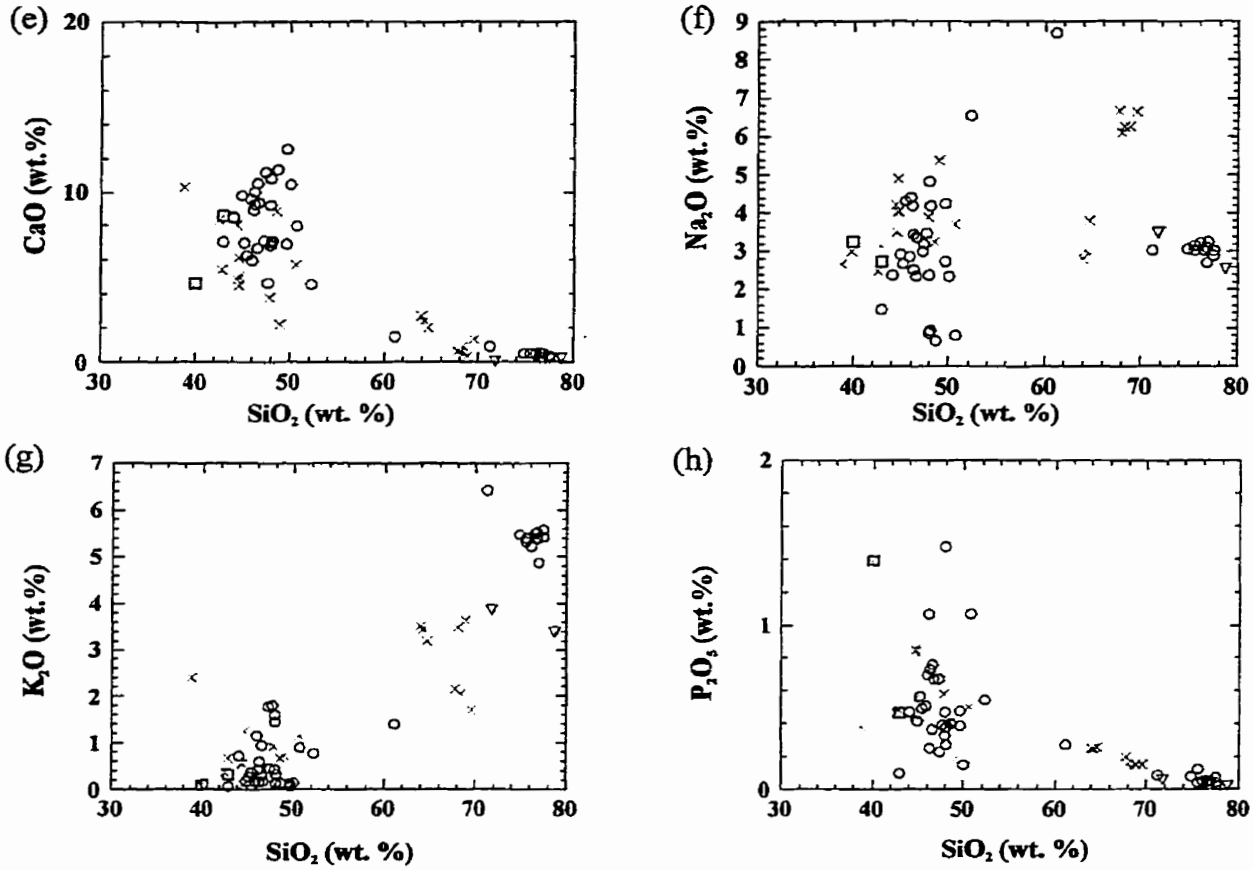

Figure 5.15. continued

5.15 and 5.16. REE patterns of the Arisaig Group show overall trends similar to those of samples from the White Rock Formation (Fig. 5.17), including enriched LREE compared to chondrite and HREE values, but have distinctly different individual patterns. Only a partial data set is available for samples from the Bears Brook Formation, but nonetheless most mafic samples show distinct negative Nd anomalies and slight positive Lu and Eu anomalies. Mafic samples from the Arisaig Group also show slight positive Eu anomalies. The similar overall trend between the Arisaig Group and the White Rock Formation demonstrates similar within-plate continental tectonic setting with a possible garnet lherzolite source, but differences in REE patterns indicate separate sources. REE patterns for samples within the Arisaig Group are generally subparallel, indicating the same source or very similar sources.

Felsic volcanic rocks from the Arisaig Group also show similar overall REE trends as samples from the White Rock Formation and Brenton Pluton, but distinctly different individual REE patterns (Fig. 5.17). Felsic samples form both the Bears Brook and Beechill Cove formations have slight positive Lu anomalies but samples from the Bears Brook Formation also display positive Eu anomalies. Felsic samples from the Arisaig Group do not appear to subparallel samples from the White Rock Formation or the Brenton Pluton, suggesting different sources. Samples from within the Arisaig Group may be subparallel but incompleteness of the data set prevents clear interpretation.

A significant difference between the White Rock Formation and the Arisaig Group is that the felsic volcanic rocks of the Arisaig Group are probably not comagmatic with the mafic volcanic rocks (Murphy et al.,1991). Fractional crystallization of mafic magmas to form a felsic derived magma is not considered likely in the case of the Arisaig

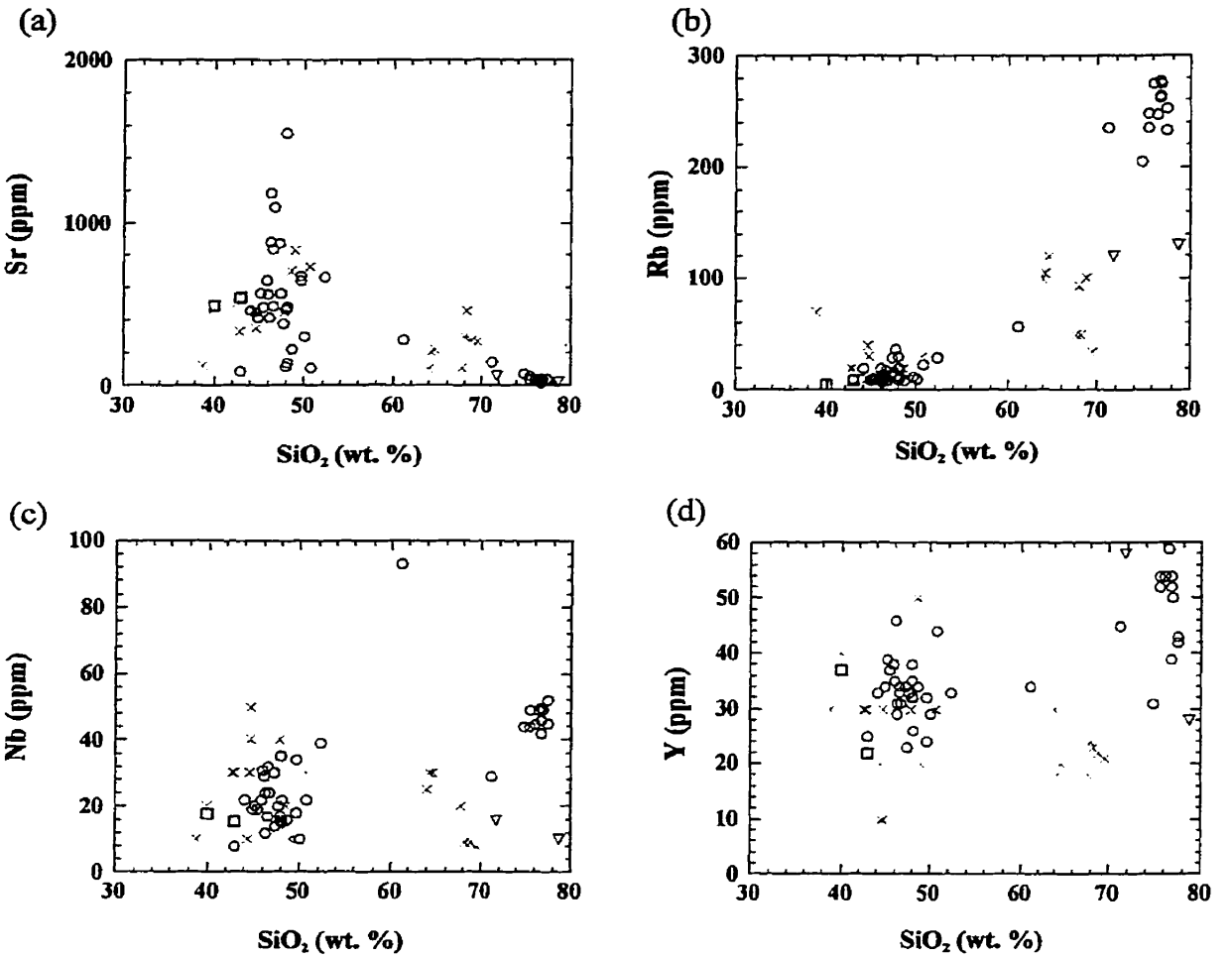

Figure 5.16. Trace element variation diagrams for samples from the White Rock Formation and samples from the Arisaig Group from Murphy et al.(1991), Murphy et al.(1996), and Keppie et al. (1997). Symbols as in Figure 5.15.

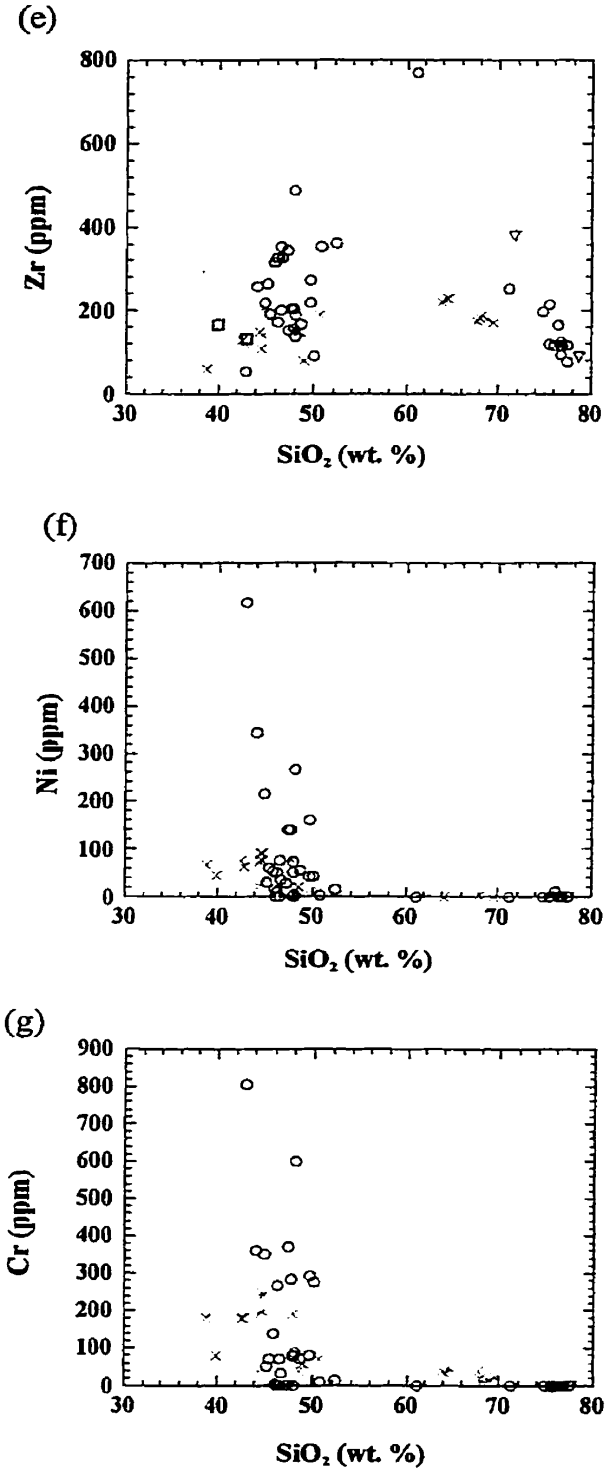

Figure 5.16. continued.

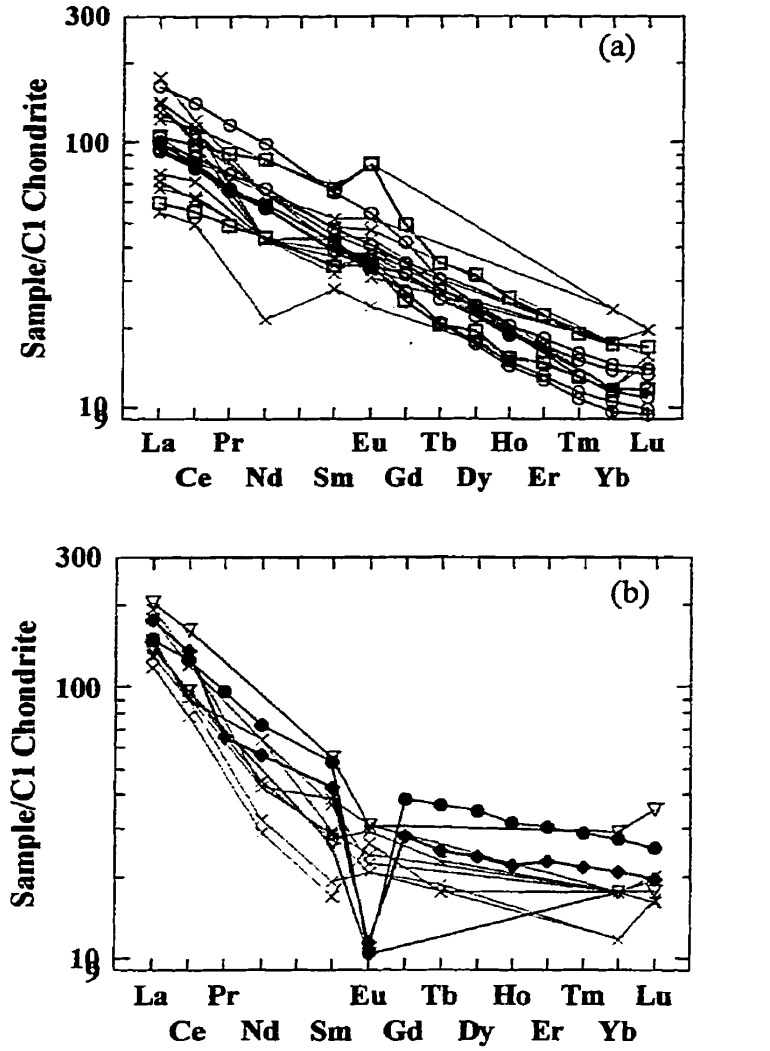

Figure 5.17. Chondrite-normalized REE diagrams for (a) mafic and (b) felsic samples from the study area, Bears Brook Formation (Murphy et al., 1991, Murphy et al., 1996), Beechill Cove Formation (Murphy et al., 1991) and the Arisaig Group (Keppie et al., 1997). Chondrite normalizing values as from Sun and McDonough (1989).

suite. The felsic rocks contain lower MgO, $Fe_2O_3^t$, CaO and P_2O_5 values than the mafic rocks, requiring fractionation of pyroxene, magnetite and apatite, and resulting in enrichment in incompatible elements such as Zr, Nb and Rb, relative to mafic rocks (Murphy et al., 1991). Incompatible element ratios in samples of the White Rock Formation show linear trends between mafic and felsic volcanic samples but no linearity is observed between samples from the Arisaig Group (Fig. 5.18). Also, in contrast to the White Rock Formation, felsic volcanic rocks are more voluminous than mafic rocks in the Arisaig Group, difficult to account for if felsic magmas were derived from mafic by fractional crystallization (Murphy et al., 1991). Therefore, felsic rocks of the Arisaig Group are interpreted to have been derived from crustal anatexis (Murphy et al., 1991). Isotopic data from felsic rocks in the Arisaig Group support a strong crustal influence. Table 5.2. shows a range of εNd values for mafic rocks from +4.3 to +5.1, higher than values of the felsic volcanic samples which range from – 0.1 to +2.5. The $^{143}Nd/^{144}Nd$ ratios for mafic samples are also significantly higher than those for felsic samples, and the latter are lower than bulk earth values. Differences in isotopic values suggest different sources or crustal contamination but with combined with other data, crustal anatexis seems more likely (Murphy et al., 1991). Although εNd values are similar for the White Rock Formation and the Arisaig Group, the linearity of incompatible element ratios in samples from the White Rock Formation suggests a comagmatic relationship with the mafic components. The depleted mantle age obtained from the White Rock Formation is older than those obtained from samples of the Arisaig Group, suggesting a larger crustal component.

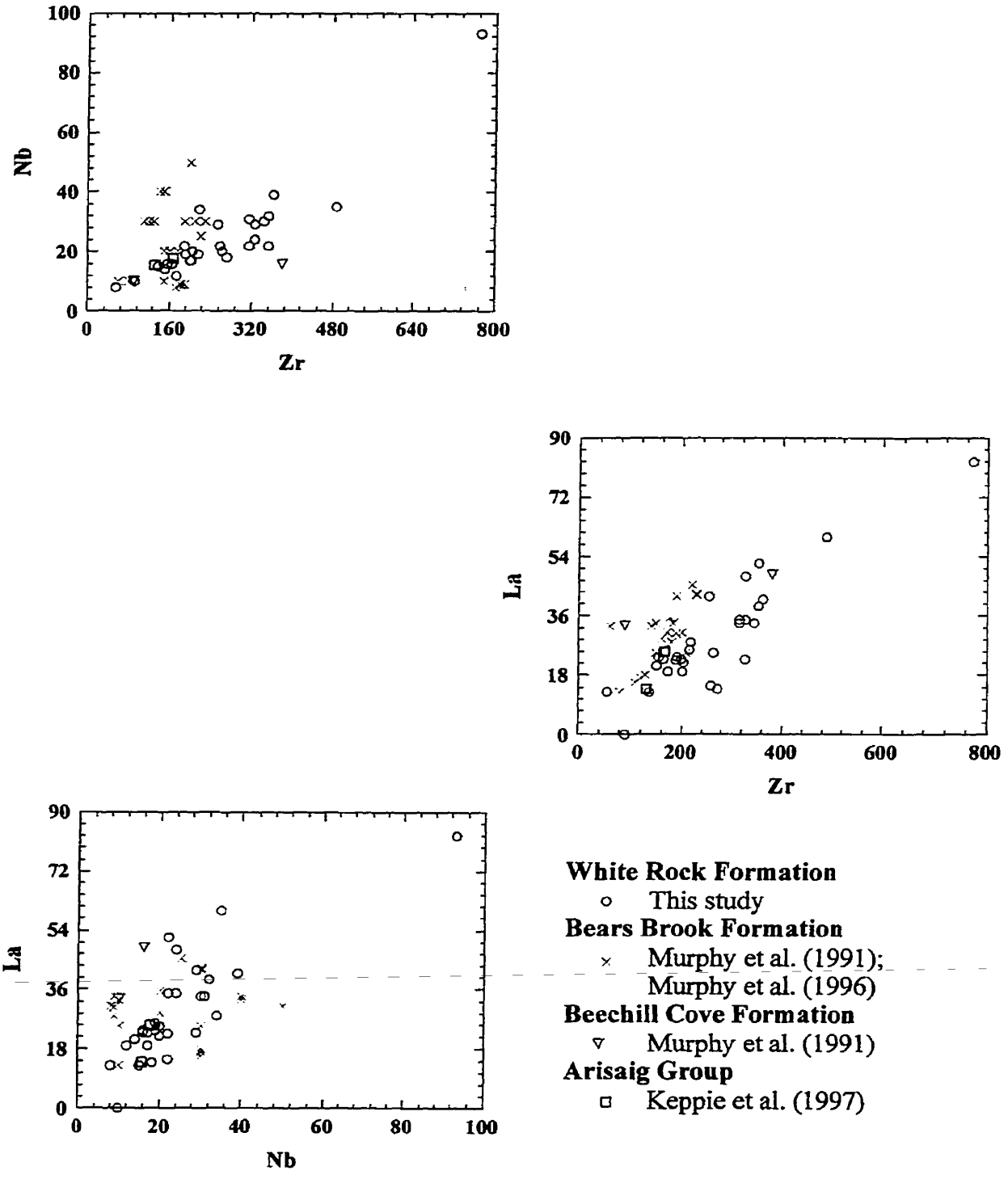

Figure 5.18. Incompatible elements ratios in samples from the White Rock Formation and Arisaig Group.

Table 5.2. Sm/Nd isotope data for the Arisaig Group and White Rock Formation. Data from the Arisaig Group compiled from Murphy et al.(1996) and data from the Cape St. Mary and Torbrook areas compiled from Keppie et al. (1997).

SAMPLE	ROCK TYPE	AGE	εND	T_{DM}
Arisaig Group				
G02	Basalt	430	+4.27	960
G02-12	Basalt	430	+5.08	878
84-1	Rhyolite	430	+2.49	946
84-4	Rhyolite	430	-0.11	1041
84-10	Rhyolite	430	+0.17	1046
84-12	Rhyolite	430	+0.66	1016
White Rock Formation				
Yarmouth area (present study)	Rhyolite	440	+1.37	1209
Cape St. Mary and Torbrook areas				
680	Basalt	460	+4.5	797
681	Basalt	460	+3.0	953
685	Basalt	460	+4.1	835
686	Basalt	460	+6.8	569
694	Basalt	460	+5.0	716
675	Rhyolite	460	+1.6	1150
676	Rhyolite	460	+1.1	1320
677	Rhyolite	460	+0.2	1837

5.5. Regional Implications

The timing and sequence of major tectonic events in the northern Appalachian orogen continues to be the subject of much discussion, and distinction between tectonic setting of terranes is still being unraveled (Keppie, 1993; van Staal et al., 1998; Barr et al., 1998; Murphy et al., 1999). The tectonic environment of the White Rock Formation has implications for the location and type of tectonic event in the Meguma terrane during the Early Silurian.

Chandler et al. (1987) reported that sequences in the Humber and Dunnage terranes of Newfoundland, including the Botwood Group, Cape St. John Group, Micmac Lake Group, Sops Arm Group, King George IV Lake, Topsails igneous complex and the Stony Lake volcanics, are of similar age (ca. 430 Ma) and similar lithology. They interpreted these similarities to imply origin under similar supracratonic conditions. Based on subaerial to shallow marine rock types with an abundant bimodal volcanic component, Chandler et al. (1987) interpreted the environment to be extensional within a continental terrane.

Chandler et al. (1987) also noted temporally and lithologically similar sequences in Cape Breton Island (Jumping Brook Complex), mainland Nova Scotia (Arisaig Group and White Rock Formation), and New Brunswick (Passamaquoddy Bay). They correlated these sequences across Newfoundland, Nova Scotia and New Brunswick, and inferred that the zones represented by these regions (Humber, Dunnage, Avalon and Meguma) were adjacent by ca. 430 Ma in order to have experienced the same conditions in which these sequences formed.

The interpretation by Chandler et al. (1987) is not consistent with recent work in the northern Appalachian orogen which indicates that the Silurian was a time of orogenic activity in which different tectonic environments existed in various separate terranes (Dunning et al. 1990; Barr and Jamieson, 1991; Barr et al. 1999; Fyffe et al., 1999). In order to correlate the sequences, Chandler et al. (1987) assumed that similarity of age and lithology indicated similar and related conditions of formation (i.e. tectonic environment). Although the Springdale Group, Arisaig Group and White Rock Formation all apparently formed in within-plate, continental extensional environments (Chandler et al. 1987; Murphy et al., 1991; this study), other volcanic sequences of comparable age in these zones did not. Geochemistry of Ordovician-Silurian metasedimentary and metavolcanic sequences in southwestern Newfoundland, such as the La Poile Group and Port aux Basques gneiss, indicate formation in a volcanic arc setting under subduction-related compressional conditions (Barr and Jamieson, 1991). In Cape Breton Island, Silurian sequences in the Aspy terrane (Money Point Group, Jumping Brook Complex, Sarach Brook metamorphic suite and Clyburn Brook Formation) appear to be arc- related (Barr and Jamieson, 1991; Lister, 1998; Barr and Raeside, 1998). Silurian (ca. 435 Ma) sequences such as the Bayswater Group in the Kingston terrane of New Brunswick appear to be related to a continental-margin volcanic arc setting (Barr et al., 1999).

In addition to variation in tectonic environment across terranes, there are also differences in tectonothermal histories. Sequences such as the Port aux Basque gneiss and the Jumping Brook complex contain high-grade metamorphic rocks (Barr and Jamieson, 1991) whereas other sequences of similar age such as the White Rock Formation and Arisaig Group are less metamorphosed (this study; Murphy et al., 1991). Variations in

metamorphic grade among sequences are not consistent with the suggestion of a single (continental) tectonic regime in the Silurian, as proposed by Chandler et al. (1987).

These variations in tectonic setting and metamorphic grade show that, although of similar age and lithology, sequences in the Humber, Dunnage, Avalon and Meguma zones cannot be correlated during the Early Silurian. It appears that both subduction-related and continental rift-related environments existed during this time. The shelf-margin, transgressive metasedimentary and metavolcanic rocks of the White Rock Formation (Schenk, 1997) are chemically and lithologically consistent with formation in an extensional environment, of which the volcanic component is analogous to the East African Rift. The location and relationship between this extensional environment and the compressional regimes indicated by the other sequences is not known.

Chapter 6 Conclusions

1) As a result of mapping and petrological studies, the White Rock Formation in the Yarmouth area is divided into seven stratigraphic units (S_{WRss}, S_{WRqt}, S_{WRsv}, S_{WRmf}, S_{WRft}, S_{WRmt}, and S_{WRmv}).Units near the base of the formation are predominantly metasedimentary but grade upward into predominantly metavolcanic lithologies. The lithologies present were identified by field and petrographic examination and include slate, metasandstone, metasiltstone, phyllite, quartzite, schist, metaconglomerate, tuffaceous metasandstone, metamorphosed mafic flows, mafic tuff, mafic crystal tuff, mafic lithic tuff, intermediate flows, intermediate crystal tuff, felsic crystal tuff , and amphibolite.

2) Petrographic examination indicates upper greenschist to amphibolite facies metamorphism in the White Rock Formation and associated sills and dykes, based on the presence of staurolite in metasedimentary rocks and tschermakitic hornblende in metavolcanic rocks.

3) Re-mapping of the Yarmouth area in combination with published second derivative aeromagnetic maps, prompted re-interpretation of the structure of the White Rock Formation and the nature of the contacts with the Halifax Formation and Brenton Pluton. The White Rock Formation forms a syncline that becomes smaller anticlines separated by a syncline in the northeastern part of the map area. The contacts with the Halifax Formation were originally unconformable and are now within shear zones.

The contact in the southeastern part of the map area is also coincident with a fault. The contact with the Brenton Pluton also lies within a shear zone and is coincident with a fault. The nature of the original contact between the White Rock Formation and the Brenton Pluton is not known. Because no contact aureole was observed and a comagmatic relationship is not likely, an intrusive contact is not favoured.

4) Chemical analyses of the volcanic rocks in White Rock Formation and associated sills and dykes indicate alkalic affinity and a within-plate, continental tectonic setting, perhaps analogous to the present-day East African Rift. Similarities in major, trace and rare earth element abundance, and consistency of incompatible element ratios among mafic volcanic samples and between mafic volcanic and mafic sill and dyke samples, indicate a comagmatic relationship.

5) Similarity of incompatible element ratios between mafic volcanic samples and intermediate and felsic volcanic samples also suggests a comagmatic relationship.

6) εNd values and zircon inheritance indicate that the felsic volcanic rocks experienced some crustal contamination.

7) Although major, trace and rare earth element chemistry is similar between the felsic volcanic samples and those from the Brenton Pluton, distinct mineralogies and differences in incompatible element ratios do not favour a comagmatic relationship.

8) A U-Pb crystallization age of 438 +3/- 2 Ma for zircon in a felsic crystal tuff sample establishes the age of the upper volcanic sequence of the White Rock Formation in the Yarmouth area. This date, in combination with published dates from other units within, above and below the White Rock Formation, provides constraints for the stratigraphic correlation of the White Rock Formation in other areas in southwest Nova Scotia.

9) The stratigraphy of the White Rock Formation in the Yarmouth area can be correlated with sections in the Cape St. Mary, Bear River, Torbrook and Black River areas. The stratigraphy in the Yarmouth area correlates mainly with lower parts of the White Rock Formation in the other areas, except the Cape St. Mary section which appears to correlate with units S_{WRsv} and S_{WRmf}. The correlations made during this study differ significantly from previous work.

10) Comparison of geochemical data from the Yarmouth area with the Cape St. Mary and Torbrook areas from previous work indicates similarities in chemical affinity and tectonic setting and a probable comagmatic relationship.

11) Geochemical comparison with lithologically similar rocks of similar age and tectonic setting in the Antigonish Highlands shows differences in rare earth element and incompatible element ratios, indicating different sources.

12) The tectonic setting of the White Rock Formation differs from tectonic settings of other volcanic-sedimentary units of similar age elsewhere in the northern Appalachian orogen, indicating that the Meguma terrane was not yet joined to the rest of the Appalachian orogen in the Silurian.

References

Barr, S.M. and Jamieson, R.A. 1991. Tectonic setting and regional correlation of Ordovician-Silurian rocks of the Aspy Terrane, Cape Breton Island, Nova Scotia. Canadian Journal of Earth Sciences, **28**: 1769-1779.

Barr, S.M., and Raeside, R.P. 1998. Petrology and tectonic implications of Silurian (?) metavolcanic rocks in the Clyburn Brook area on Ingonish Island, northeastern Cape Breton Island, Nova Scotia. Atlantic Geology, **34**: 27-37.

Barr, S.M., White, C.E., and McLeod, M.J. 1999. Geology of the Silurian Kingston Terrane, southern New Brunswick. *In* Current Research 1998. *Edited by* B.M.W. Carroll. New Brunswick, Department of Natural Resources and Energy, Minerals and Energy Division, Mineral Resources Report 99-4, pp. 1-17.

Bevier, M.L. and Whalen, J.B. 1990. Tectonic significance of Silurian magmatism in the Canadian Appalachians. Geology, **18**: 411-414.

Blaise, J., Bouyx, E., Goujet, D., Le Menn, J., and Paris, F. 1991. Le Silurien Superieur de Bear River (Zone de Meguma, Nouvelle Ecosse): faune, biostratigraphie et implications paleographiques. Geobios, **24**: 167-182.

Bouyx, E., Blaise, J., Brice, D., Degardin, J.M., Goujet, D., Gourvennec, R., Le Menn, J., Lardeux, H., Morzadec, P., and Paris, F. 1997. Biostratigraphie et paleobiogeographie du Siluro-Devonien de la zone de Meguma (Nouvelle-Ecosse, Canada). Canadian Journal of Earth Sciences, **34**: 1295-1309.

Brewer, T.S., and Atkin, B.P. 1989. Elemental mobilities produced by low-grade metamorphic events. A case study from the Proterozoic supracrustals of southern Norway. Precambrian Research, **45**: 143-158.

Brewer, T.S., and Menuge, J.F. 1998. Metamorphic overprinting of Sm-Nd isotopic systems in volcanic rocks: the Telemark Supergroup, southern Norway. Chemical Geology, **145**: 1-16.

Cas, R.A.F., and Wright, J.V. 1988. Volcanic successions: modern and ancient. Unwin Hyman, London.

Chandler, F.W., Sullivan, R.W., and Currie, K.L. 1987. The age of the Springdale Group, western Newfoundland, and correlative rocks-evidence for a Llandovery overlap assemblage in the Canadian Appalachians. Transactions of the Royal Society of Edinburgh: Earth Sciences, **78**: 41-49.

Crosby, D.G. 1962. Wolfville map-area, Nova Scotia. Geological Survey of Canada, Memoir 325.

Culshaw, N. and Liesa, M. 1997. Alleghenian reactivation of the Acadian fold belt, Meguma Zone, southwest Nova Scotia. Canadian Journal of Earth Sciences, **34**: 833-847.

Culshaw, N. and Reynolds, P. 1997. $^{40}Ar/^{39}Ar$ age of shear zones in the southwest Meguma Zone between Yarmouth and Meteghan, Nova Scotia. Canadian Journal of Earth Sciences, **34**: 848-853.

Cullen, M., Webster, P., and Hudgins, B. 1996. Silurian metallogeny project Lawrencetown to Morristown area Annapolis and Kings County, Nova Scotia. Nova Scotia Department of Natural Resources, Minerals and Energy Branch, Open File Report 96-010.

Deer, W.A., Howie, R.A., and Zussman, J. 1992. An introduction to the rock forming minerals, 2nd edition. Longman Group Limited, London.

Dunning, G.R., O'Brien, S.J., Colman-Sadd, S.P., Blackwood, R.F., Dickson, W.L., O'Neill, P.P., and Krogh, T.E. 1990. Silurian orogeny in the Newfoundland Appalachains. Journal of Geology, **98**: 895-913.

Eby, G.N. 1990. The A-type granitoids: a review of their occurrence and chemical characteristics and speculations on their petrogenesis. Lithos, **26**: 115-134.

Eby, G.N. 1992. Chemical subdivision of the A-type granitoids: petrogenetic and tectonic implications. Geology, **20**: 641-644.

Floyd, P.A. and Winchester, J.A. 1978. Identification and discrimination of altered and metamorphosed volcanic rocks using immobile elements. Chemical Geology, **21**: 291-306.

Fyffe, L.R., Pickerill, R.K. and Stringer, P. 1999. Stratigraphy, sedimentology and structure of the Oak Bay and Waweig formation, Mascarene Basin: implications for the paleotectonic evolution of southwestern New Brunswick. Atlantic Geology, **35**: 59-84.

Hanson, G., 1980. Rare earth elements in petrogenetic studies of igneous systems. Annual Review Earth and Planetary Science, **8**: 371-406.

Hughes, C.J. 1973. Spilites, keratophyres and the igneous spectrum. Geological Magazine, **6**: 513-527.

Hwang, S. 1985. Geology and structure of the Yarmouth area, southwestern Nova Scotia. M.Sc. thesis, Acadia University, Wolfville, Nova Scotia.

James, J.A. 1998. Stratigraphy, petrochemisrty and economic potential of the Silurian

New Canaan Formation, Meguma Terrane, Nova Scotia. B.Sc. thesis, Acadia University, Wolfville, Nova Scotia.

Kendall, A.J.D. 1981. The White Rock Formation metavolcanics at Cape St. Mary, Nova Scotia: petrography, geochemistry and geologic affinities. B.Sc. thesis, Dalhousie University, Halifax, Nova Scotia.

Keppie, J.D. 1993. Synthesis of Palaeozoic deformational events and terrane accretion in the Canadian Appalachians. Geologische Rundschau, **82**: 381-431.

Keppie, J.D., and Dallmeyer, R.D. 1995. Late Paleozoic collision, delamination, short-lived magmatism, and rapid denudation in the Meguma Terrane (Nova Scotia, Canada): constraints from $^{40}Ar/^{39}Ar$ isotopic data. Canadian Journal of Earth Sciences, **32**: 644-659.

Keppie, J.D., Dostal, J., Murphy, J.B., and Cousens, B.L. 1997. Paleozoic within-plate volcanic rocks in Nova Scotia (Canada) reinterpreted: isotopic constraints on magmatic source and paleocontinental reconstructions. Geological Magazine, **134**: 425-447.

King, M.S. 1997. Meguma Terrane Enhanced (Second Vertical Derivative) Aeromagnetic Digital Data, NTS Map Sheet 21A/04, Wentworth Lake, Yarmouth and Digby Counties, Nova Scotia. Nova Scotia Department of Natural Resources, Minerals and Energy Branch, Open File Map 97-025, scale 1:50 000.

Lane, T.E. 1979. The stratigraphy and sedimentology of the White Rock Formation (Silurian), Nova Scotia, Canada. M.Sc. thesis, Dalhousie University, Halifax, Nova Scotia.

Leake, B.E. 1978. Nomenclature of amphiboles. Canadian Mineralogist, **16**: 501-520.

Lister, K.J. 1998. Petrology and tectonic implications of the Silurian Sarach Brook metamorphic suite, southern Cape Breton Highlands, Nova Scotia. B.Sc. thesis, Acadia University, Wolfville, Nova Scotia.

Longerich, H., Jenner, G.A., Fryer, B.J., and Jackson, S.E. 1990. Inductively coupled plasma- mass spectrometric analysis of geochemical samples. A critical evaluation based on case studies. Chemical Geology, **83**: 105-118.

Maniar, P.D., and Piccoli, P.M. 1989. Tectonic discrimination of granitoids. Geological Society of America Bulletin, **101**: 635-643.

Meschede, M. 1986. A method of discriminating between different types of mid-ocean ridge basalts and continental tholeiites with the Nb-Zr-Y diagram. Chemical Geology, **56**: 207-218.

Murphy, J.B., Keppie, J.D., Dostal, J., and Cousens, B.L. 1996. Repeated late Neoproterozoic-Silurian lower crustal melting beneath the Antigonish Highlands, Nova Scotia: Nd isotopic evidence and tectonic interpretations. *In* Avalonian and related peri-Gondwanan terranes of the circum-North Atlantic: Boulder, Colorado. *Edited by* Nance, R.D., and Thompson, M.D. Geological Society of America, Special Paper 304, pp.109-120.

Murphy, J.B., Keppie, J.D, and Hynes, A.J. 1991. The geology of the Antigonish Highlands, Nova Scotia. Geological Survey of Canada, Paper 89-10.

Murphy, J.B., Van Staal, C.R., and Keppie, J.D. 1999. Middle to late Paleozoic Acadian orogeny in the northern Appalachians: a Laramide-style plume-modified orogeny? Geology, **27**: 653-656.

Okulitch, A.V. 1999. Geological time scale, 1999. Geological Survey of Canada, Open File 3040 (National Earth Science Series, Geological Atlas) – Revision.

O'Reilly, G.A. 1976. The petrology of the Brenton Pluton, Yarmouth County, Nova Scotia. B.Sc. thesis, Dalhousie University, Halifax, Nova Scotia.

Pearce, J.A. 1982. Trace element characteristics of lavas from destructive plate boundaries. *In* Andesites. *Edited by* Thorpe, R.S. John Wiley and Sons, Chichester, p. 525-547.

Pearce, J.A., 1996. A user's guide to basalt discrimination diagrams. *In* Trace element geochemistry of volcanic rocks: applications for massive sulphide exploration. *Edited by* Wyman, D.A. Geological Association of Canada, Short Course Notes, **12**: 79-113.

Pearce, J.A. and Cann, J.R. 1973. Tectonic setting of basic volcanic rocks determined using trace element analysis. Earth and Planetary Science Letters, **19**: 290-300.

Pearce, J.A., Harris, N.W.B., and Tindle, A.G. 1984. Trace element determination diagrams for the tectonic interpretation of granitic rocks. Journal of Petrology, **25**: 956-983.

Raymond, L.A. 1995. Igneous petrology. W.C. Brown Communications, Inc., Boston.

Rollinson, H. 1993. Using geochemical data: evaluation, presentation, interpretation. Longman Scientific and Technical, Harlow.

Sarkar, P.K. 1978. Petrology and geochemistry of the White Rock metavolcanic suite, Yarmouth, Nova Scotia. Ph.D. thesis, Dalhousie University, Halifax, Nova Scotia.

Schenk, P.E. 1995. Annapolis belt. *In* Geology of the Appalachian-Caledonian orogen in

Canada and Greenland. *Edited by* H. Williams. Geological Survey of Canada, Geology of Canada, no. 6, pp. 367-383.

Schenk, P.E. 1997. Sequence stratigraphy and provenance on Gondwana's margin: The Meguma Zone (Cambrian to Devonian) of Nova Scotia, Canada.. Geological Society of America Bulletin, **109**: 395-409.

Shervais, J.W. 1982. Ti-V plots and the petrogenesis of modern and ophiolitic lavas. Earth and Planetary Science Letters, **59**: 101-118.

Smitheringale, W.G. 1960. Geology of the Nictaux-Torbrook map-area, Annapolis and Kings counties, Nova Scotia. Geological Survey of Canada, Paper 60-13, 32 p.

Smitheringale, W.G. 1973. Geology of parts of Digby, Bridgetown, and Gaspereau map-areas, Nova Scotia. Geological Survey of Canada, Memoir 375, 78 p.

Sun, S.-s. and McDonough, W.F. 1989. Chemical and isotopic systematics of oceanic basalts: implications for mantle composition and processes. *In* Magmatism in the ocean basins. *Edited by* A.D. Saunders and M.J. Norry. Geological Society, London, pp. 313-345.

Taylor, F.C. 1965. Silurian stratigraphy and Ordovician-Silurian relationships in southwestern Nova Scotia. Geological Survey of Canada Memoir 375.

Taylor, F.C. 1967. Reconnaissance Geology of Shelburne map-area, Queens, Shelburne, and Yarmouth Counties, Nova Scotia. Geological Survey of Canada Memoir 349.

Taylor, F.C. 1969. Geology of the Annapolis-St. Mary's Bay area, Nova Scotia (west-half). Geological Survey of Canada, Map 1225A, scale 1:126 720.

Trapasso, L.S. 1979. The geology of the Torbrook Syncline, Kings and Annapolis counties, Nova Scotia. M.Sc. thesis, Acadia University, Wolfville, Nova Scotia.

Van Staal, C.R., Dewey, J.F., MacNiocaill, C., and McKerrow, W.S. 1998. The Cambrian-Silurian tectonic evolution of the Appalachians and British Caledonides: History of a complex, west and southwest Pacific-type segment of Iapetus. *In* Lyell: The past is the key to the present. *Edited by* D.J. Blundell, and A.C. Scott. Geological Society, Special Publication 5, pp. 199-242.

White, C.E., Horne, R.J., Muir, C., and Hunter, J. 1998. Preliminary bedrock geology of the Digby map sheet, southwestern Nova Scotia. *In* Minerals and Energy Branch, report of activities 1998. Nova Scotia Department of Natural Resources, Mines and Energy Branch, Report 98-1, pp. 119-134.

Whalen, J.B., Currie, K.L., and Chappell, B.W. 1987. A-type granites: geochemical characteristics, discrimination and petrogenesis. Contributions to Mineralogy and Petrology, **95**: 407-419.

Wilson, M. 1989. Igneous petrogenesis: A global tectonic approach. Unwin Hyman, London.

Winchester, J.A. and Floyd, P.A. 1977. Geochemical discrimination of different magma series and their differentiation products using immobile elements. Chemical Geology, **20**: 325-343.

Wood, D.A. 1980. The application of a Th-Hf-Ta diagram to problems of tectonomagmatic classification and to establishing the nature of crustal contamination of basaltic lavas of the British Tertiary Volcanic Province. Earth and Planetary Science Letters, **50**: 11-30.

Yardley, B.W.D. 1989. An introduction to metamorphic petrology. Longman Scientific and Technical, Harlow.

APPENDIX A PETROGRAPHIC DESCRIPTIONS

Abbreviations used

Amph = amphibole
Plag = plagioclase
Qtz = quartz
Musc = muscovite
Porphs = porphyroblasts
Vfg = very fine grained
Fg = fine grained
Mg = medium grained
Cg = coarse grained
Vcg = very coarse grained
Recryst = recrystallized

Appendix A - Petrographic Description

Sample Number	Rock Type	Mineralogy	Description	Composition
Mafic flows				
LAM002-1	Possible flow	Plag, epidote, biotite, quartz, amphibole, oxides	Matrix is fg qtz, plag, biotite, amph. Strongly foliated (amph grains aligned). Plag grains <1 cm, subhedral. Abundant inclusions of epidote, hornblende, oxides, and cryptocrystalline material. Porphyroblasts. Epidote is fg-mg, subidioblastic. Some grains show twinning. Amphibole is fg-mg, subidioblastic, elongate, green, aligned, very abundant. Biotite very abundant, fg, anhedral,brown, aligned. Oxides are fg, abundant. Igneous texture still preserved.	Basaltic
LAM010-2	Flow?	Plag, qtz, epidote, oxides, amph	Rare cg plag crystals, subhedral. Matrix is fg needles of green amph, fg-mg xenoblastic epidote, fg-mg subhedral plag, mg qtz. Igneous texture preserved. Foliated.	Basaltic
LAM075-4	Possible flow	Amph, epidote. Qtz, oxides, plag	Amph porphs are fg-mg, subidio-xenoblastic, acicular and pale green. Epidote is rare, fg, xenoblastic. Matrix is qtz and plag, only minor recrystal.	Basaltic

Appendix A - Petrographic Description continued

Sample Number	Rock Type	Mineralogy	Description	Composition
Mafic flows				
LAM080-1	Possible flow	Amph, epidote, qtz, plag, oxides, minor biotite?	Fg needles of blue-green amph(hornblende?), fg xenoblastic epidote, recryst qtz, plag and oxides. Cluster of mg, undulose qtz. Strong foliation (alignment of amph).	Basaltic
LAM084-1	Possible flow	Amph, biotite, epidote, qtz, plag, oxides, carbonate	Cg, subidioblastic, blue-green amph porphs, poikiloblastic, filled with epidote and qtz. Fg & mg, epidote porph, xenoblastic. Biotite is fg, brown, subidioblastic (elongate) and very abundant. Plag and qtz are mg-fg, recrystallized, except for very rare plag crystals (vcg~ 0.5 cm) which has many inclusions and appears embayed and corroded. Rare cluster of cg-mg qtz and cg-mg biotite, and cg qtz, carbonate, biotite.	Basaltic
LAM123-3	Flow?	Amph, biotite, qtz, oxides, plag, epidote	Mg-cg, subidioblastic blades of slightly poikiloblastic blue-green amph. Matix contains fg, xenoblastic brown biotite, fg, xenoblastic epidote and fg, recryst qtz, rare fg plag.	Basaltic

Appendix A - Petrographic Description continued

Sample Number	Rock Type	Mineralogy	Description	Composition
Mafic flows				
LAM128-5	Flow	Amph, epidote, biotite, qtz, plag	Matrix is fg needles of green-blue amph, fg epidote, mg oxides. Common mg xenoblastic epidote porphs. Also commonly have clusters of mg, undulose qtz, mg plag, mg epidote, mg brown biotite. Strongly foliated.	Basaltic
LAM211-1	Flow?	Amph, epidote, qtz, plag, oxides	Mg needles of green-blue amph, rare mg subhedral plag with grain size reduction, in a matrix of fg-mg recryst qtz, fg epidote.	Basaltic
Intermediate flow				
LAM049-1	Flow?	Amph, plag, qtz, epidote, oxides, minor biotite	Cg porphs of subidioblastic, blue-green amph blades. Matrix is recyst qtz, plag, fg epidote, brown biotite? Rare, xenoblastic, mg biotite porph	Andesitic-basaltic

Appendix A - Petrographic Description continued

Sample Number	Rock Type	Mineralogy	Description	Composition
Intermediate flow				
LAM085-3	Possible flow	Biotite, epidote, plag, qtz, oxides, carbonate, chlorite	Cg plag grains, embayed, abundant inclusions (epidote) and very corroded. Abundant brown biotite porphs are mg, xenoblastic with embayed edges, poikiloblastic - filled with qtz and epidote. Mg, xenoblastic epidote porphs are abundant. Mg, xenolastic carbonate also abundant. Matrix is fg qtz, epidote, oxides, chlorite, carb. Igneous texture preserved.	Andesitic
LAM125-1	Flow	Amph, biotite, plag, carbonate, qtz, oxides, rare epidote	Cg, subhedral, embayed plag grain partially replaced by chlorite, amph, biotite and carb. Mg-cg, xenoblastic, poikiloblastic blue-green amph. Mg, xenoblastic, brown biotite. Matrix is vfg, recryst qtz, abundant fg xenoblastic carb, fg, xenoblastic biotite, and fg epidote. Igneous texture preserved. Foliated.	Andesitic

Appendix A - Petrographic Description continued

Sample Number	Rock Type	Mineralogy	Description	Composition
Intermediate flow				
LAM133-1	Possible flow	Amph, biotite, carbonate, chlorite, qtz, oxides, epidote,	Amph is cg-mg, xenoblastic, poikiloblastic, green, hrnblde. Biotite is mg, brown, subidio-xenoblastic, poikiloblastic. Carb is fg-mg, xenoblastic, very abundant. Epidote porphs are very rare, fg, xenoblastic. Chlorite porphs mg, elongate, subidio. Matrix is recryst fg qtz and oxides. Strong foliation.	Andesitic
Mafic tuffs				
LAM071A-1	Tuff	Amph (actinolite?), chlorite, qtz, plag, oxides.	Decussate texture. Mostly amph & chlorite with minor and qtz and very rare plag. Amphi is very very pale green (almost colourless), mg, subidioblastic and fibrous (sheaf-like), not pleochroic. Chlorite is fg, very pale yellow/brown. Qtz is mg, xenoblastic with undulatory extinction. Plag appears to be extensively altered-replaced by sauaaurite and sericite. Some areas contain more qtz, less chlorite and amphibole.	Basaltic

Appendix A - Petrographic Description continued

Sample Number	Rock Type	Mineralogy	Description	Composition
Mafic tuffs				
LAM077-1	Tuff?	Amph, epidote, qtz, chlorite, oxides, plag?	Mg, subidioblastic epidote whichhas partially replaced plag. Rare cluster of mg qtz, chlorite, epidote. Igneous texture still faintly preserved. Matrix is fg amph and qtz.	Basaltic
LAM079-1	Tuff	Amph, qtz, plag, oxides, epidote, biotite	TS is fg with fg needles of blue-green amph, fg recryst qtz, fg, xenoblastic plag and fg xeno, epidote. Rare clusters of mg qtz, epidote and plag and biotite. Rare mg of plag. Amph grains strongly aligned.	Basaltic
LAM096-1	Tuff?	Amph, plag, qtz, biotite, oxides	Mg-cg, subidioblastic, colourless-green amph blades (porphs) in a matrix of granoblastic qtz and plag and fg, xeno biotite. Some areas of the thin section are fg, subidioblastic amph and cg oxides with minor fg qtz and biotite. Other areas are mg, xenoblastic plag and qtz with abundant fg, xenoblastic biotite and rare, mg-cg colourless amph. Some igneous texture preserved. Foliated.	Andesitic-basaltic.

Appendix A - Petrographic Description continued

Sample Number	Rock Type	Mineralogy	Description	Composition
Mafic tuffs				
LAM148-1	Mafic tuff	Amph, chlorite, oxides, qtz, minor biotite	Almost 100% pale green-yellow amph. Amph is sheaf-like and also acicular, cg-fg. Qtz, biotite only minor and fg. Abundant fg chlorite replacing amph.	
LAM165-1	Mafic tuff	Amph, carbonate, oxides, sphene, qtz	Thin section appears banded- into qtz layers and amphibole layers. The qtz is fg, recryst, except occasional cg which displays a mosaic texture. Amph is fg-cg, xenoblastic, poikiloblastic, bladed and sheaf-like. Mg-fg.subidioblastic sphene is associated with amph. Carbonate is abundant, xenoblastic, mg-cg, in both layers.	Basaltic
LAM173-1	Mafic tuff	Amph, qtz, epidote, plag, oxides	Fg amph, qtz and epidote matrix with clusters of mg plag and qtz with epidote. Xenoblastic porphs of mg epidote and subidioblastic, fg green/blue amph. Elongate grains and clusters are aligned - strongly foliated.	Basaltic
LAM176-1	Tuff	Amph, qtz, oxides, very rare biotite	Matrix with fg needles of green amph and minor qtz. Qtz-rich clusters (fg-mg). Biotite and minor amph. Strongly foliated.	Basaltic

Appendix A - Petrographic Description continued

Sample Number	Rock Type	Mineralogy	Description	Composition
Mafic tuffs				
LAM182-1	Tuff?	Amph, plag, oxides, qtz	Vcg, green, sheaf-like amph in clusters separated by fg needle amph, fg, granoblastic qtz (not recryst) and rare fg plag. Foliated.	Basaltic
LAM204-1	Mafic tuff	Amph, qtz, carb, chlorite, oxides, epidote, plag	Mg, sheaf and blade, blue-green amph, slightly poikoblastic. Abundant mg carbonates. Matrix is recryst qtz, plag and epidote. Mg epiodte porphs. Slightly foliated.	Basaltic
Mafic crystal tuff				
LAM003-1	Crystal tuff?	Plag, amph, chlorite, qtz, oxides, epidote, biotite?	Crystals of cg, subhedral plag with inclusions of epidote. Some grains appear broken. Matrix is feathers of chlorite and amph, recyst qtz , fg plag and minor biotite, and fg epidote. Also have mg-cg porphs of xeno-subidio, blue-green amph. Igneous texture is well preserved. Foliation is present.	Basaltic
LAM005-1	Crystal tuff	Plag, epidote, qtz, biotite, oxides, chlorite, carbonate	Vcg subhedral plag grains which may contain epidote and carbonate. Occasional xenoblastic, mg qtz grain. Matrix contains abundant, fg-mg epidote, fg green-brown biotite, fg recyst qtz. Igneous texture preserved. Foliated.	Basaltic

Appendix A - Petrographic Description continued

Sample Number	Rock Type	Mineralogy	Description	Composition
Intermediate crystal tuff				
LAM009-1	Crystal tuff	Plag, qtz, biotite, musc, oxides, chlorite, apatite, zircon	Matrix isfg recrystallized plag and qtz. Plag grains <0.75 cm, subhedral. Biotite and musc porphs are fg-mg, sub-xenoblastic, often found around feldspar or in clusters. Musc much more abundant and coarser than in 4-1. Much less epidote. Epidote porphs are fg, xenoblastic and rare. Frequently found in clusters. Igneous textures preserved --matrix not very recryst, porphyritic texture, plag in matrix.	Andesitic
LAM011-1	Crystal tuff	Plag (albite), epidote, biotite, muscovite, apatite, oxides, quartz	Matrix is fg plag, qtz, biotite, epidote, oxides. Plag <1cm euhedral with abundant inclusions of epidote, biotite, apatite, oxides. Epidote is mg, anhedral. Often rimmed by vfg epidote. Biotite is fg-mg, sub-anhedral, green, commonly surrounding plag grains. Musc is fg, anhedral-subhdral, rare, commonly associated with biotite and plag. Apatite is fg, sub-euhedral, rare. Original igneous textures preserved. Strongly foliated.	Andesitic

Appendix A - Petrographic Description continued

Sample Number	Rock Type	Mineralogy	Description	Composition
Intermediate crystal tuff				
LAM078-2	Crystal tuff	Plag, amph, biotite, epidote, chlorite, qtz, oxides	Matrix is fg ~recryst plag, epidote, oxides, chlorite, qtz.Grains of ~1 cm subhedral plag. Porphs or cg (<0.5 cm) subidioblastic blue-green amph needles. Mg, subidio-xenoblastic, brown biotite. Fg, xenoblastic epidote in matrix and in plag grains. Igneous texture preserved.	Andesitic
Felsic crystal tuff				
LAM004-1	Crystal tuff	Plag, qtz, Kspar, epidote, biotite,musc, apatite, oxides, zircon, chlorite.	Matrix is fg recrystallized qtz and plag, biotite, epidote. Crystals of plag are <0.75 cm, subhedral, contain abundant inclusions. Epidote porphs are fg-mg, xeno-subidioblastic, abundant. Often associated with biotite or plag.Epidote replacing plag---plag almost gone and only epidote left. Biotite and musc porphs are fg, sub-xenoblastic, aligned. Some areas of the TS contain slightly coarser grains of qtz with biotite --possible lithic fragments with similar composition. Quartz appears quite undulose. Foliated.	Rhyolitic-dacitic

Appendix A - Petrographic Description continued

Sample Number	Rock Type	Mineralogy	Description	Composition
Felsic crystal tuff				
LAM208-1	Crystal tuff?	Plag, qtz, microcline, biotite, musc, oxides, minor epidote, perthite	MAtrix is fg, recryst, granoblastic qtz, fg green biotite, oxides. Relict crystals are cg qtz, xenoblastic with mosaic texture; subidio-xenoblastic plag with some recryst along grain boundaries; perthite and Kspar mg-cg with grains size reduction, xeno-subidio shape. Fg-mg green biotite in strain shadows. Strongly foliated. Igneous texture preserved.	Rhyolitic
LAM209-1	Crystal tuff	Plag, qtz, Kspar	Matrix is fg recryst, granoblastic qtz, minor fg biotite, rare musc, minor oxides. Cg xenocrysts of subhedral plag with minor grain size reduction. Cg, subhedral kspar xenocrysts. Cg xenocrysts of euhedral-subhedral qtz with some embayed internal boundaries and granophyric texture. No alteration or grain size reduction. Igneous texture well preserved. Strong foliation.	Rhyolitic

Appendix A - Petrographic Description continued

Sample Number	Rock Type	Mineralogy	Description	Composition
Lithic tuff				
LAM015-1	Lithic tuff	Amph, qtz, plag, biotite, oxides, minor epidote	Matrix is fg "matted", green-blue amph. Cg grains of subhedral plag which have amph and biotite within and are commonly surrounded by fg, recryt qtz. Other areas contain mosaic qtz, plag, biotite, epidote and mg needles of amph. Igneous texture partially preserved. Foliated.	Clasts are basaltic. Matrix is basaltic
LAM077-1	Lithic tuff	Amph, epidote, qtz, chlorite, oxides, plag?	Mg, subidioblastic epidote which is replacing plag. Rare cluster of mg qtz, chlorite, epidote-- possible clast of dacitic composition? Igneous texture still faintly preserved? Matrix is fg amph and qtz.	Basaltic
LAM095-1	Bomb/clast	Plag, amph, qtz, oxides, rare biotite, rare epidote	Cg plag grains with amph inclusions. Clusters of mg qtz (recryst) and sometimes plag. Matrix is fg needles of green amph, rare fg brown biotite, rare epidote and recryst qtz. A plag grain appears broken. Amph grains and clusters are aligned -- foliated. Igneous texture well preserved.	Basaltic

Appendix A - Petrographic Description continued

Sample Number	Rock Type	Mineralogy	Description	Composition
Lithic tuff				
LAM096-1	Lithic tuff	Amph, plag, qtz, biotite, oxides	Abundant mg-cg, subidioblastic, colourless-green amph blades (porphs) in a matrix of granoblastic qtz and plag and fg, xeno biotite. Some areas of the thin section-possible clasts-- are fg, subidioblastic amph and cg oxides with minor fg qtz and biotite. Other areas are mg, xeno plag and qtz with abundant fg, xeno biotite and rare, mg-cg colourless amph. Some igneous texture preserved. foliated.	Andesitic-basaltic. Clasts are dacitic and basaltic.
LAM147-1	Mafic tuff	Amph, qtz, oxides, biotite, chlorite, epidote, carbonate	Blobs or densely matted chlorite-possible bombs? Most of the slide is mg-fg, xenoblastic, green amph blades with fg, brown, xeno biotite, fg, epidote and chlorite. Some areas have more qtz and less amph-- possibly bombs/clasts??	Basaltic

Appendix A - Petrographic Description continued

Sample Number	Rock Type	Mineralogy	Description	Composition
Lithic tuff				
LAM153-1	Clast + matrix (lithic tuff)	Matrix: amph, qtz, oxides. Clasts: qtz, amph, oxides, very rare biotite, rare plag, very rare epidote	Matric is fg needles of green-blue amph, and very minor qtz. Clasts are fg-mg recryst qtz, mg green-blue amph, fg epidote, rare fg plag, fg biotite. Strongly foliated.	Matrix: basaltic. Clasts:dacitic
LAM153-2	Bomb/clast	Amph, epidote, qrtz, oxides, plag	Cg plag grains, subhedral, with amph inclusions. Mg clusters of recryst qtz. Matrix is fg needles of green-blue amph, fg, xenoblastic epidote, fg recryst qtz. Foliated but igneous texture well preserved.	Basaltic
Sills/dykes in White Rock Formation				
LAM072A-1	Sill/dyke (WR) amphibolite?	Amph, chlorite, qtz, plag, oxides	Cg, subidioblastic blades of slightly poikiloblastic green amph. Matrix is mg-cg anhedral plag with very little grain size reduction or corrosion, mosaic qtz, fg chlorite.	Basaltic

Appendix A - Petrographic Description continued

Sample Number	Rock Type	Mineralogy	Description	Composition
Sills/dykes in White Rock Formation				
LAM094-1	Sill/dyke (WR)	Amph, chlorite, qtz, epidote, oxides, biotite, plag	Mg-fg, blue-green, acicular amph porphs; fg, xenoblastic brown biotite; fg, xenoblastic epidote in a matrix of recryst qtz and plag.	Andesitic-basaltic
LAM106-1	Sill/dyke (WR)	Amph, chorite, qtz, oxides	Vcg, subidioblastic, blades of poikiloblastic, green amph. Mg, acicular chlorite as well as plag pgrains replaced by chlorite? Lots of cryptocrystalline brown alteration. ~10 % matrix is recryst, mosaic qtz. Some amph grains replaced by chlorite. Some igneous texture preserved.	Basaltic
LAM107-1	Sill (WR)	Amph, biotite, chlorite, qtz, plag, oxides, epidote?	Vcg, subidioblastic, pale green, sheaf and needle amph porphs in a fg recryst qtz, plag, epidote, matrix.	Basaltic

Appendix A - Petrographic Description continued

Sample Number	Rock Type	Mineralogy	Description	Composition
Sills/dykes in White Rock Formation				
LAM108-1	Sill (WR)	Biotite, qtz, carbonate, rare amph, clinozoisite, sphene	Abundant mg, xeno-subidio, brown biotite porphs. Common, mg, xeno, colourless, clinozoisite; abundant, mg-fg xeno carbonate. Very rare, subidioblastic blades green amph. Common, xenoblastic, mg sphene? Matrix is fg, recryst, mosaic qtz and cryptocrystalline material and rare mg chlorite.	Granitic
LAM131-1	Sill/dyke (WR)	Amph, qtz, oxides, chlorite	Vcg, subidioblastic, poikiloblastic, blades of green amph. Matrix is recryst qtz and sericite. Slight foliation of the qtz but not of the amph?	Basaltic
LAM132-1	Dyke (WR)	Amph, biotite, chlorite, sericite, qtz, oxides	Vcg, feather-sheaf and blade green amph, poikiloblastic. Matrix is mg-fg, slightly recryst qtz, sericite, mg-fg brown biotite, mg chlorite.	Basaltic
LAM198-1	Dyke (WR)	Amph, biotite, oxides, qtz, epidote	Cg, blades of poikiloblastic green amph. Matrix fg-mg recryst qtz, fg brown biotite, fg-mg xenoblasts epidote.	Basaltic

Appendix A - Petrographic Description continued

Sample Number	Rock Type	Mineralogy	Description	Composition
Sills/dykes in White Rock Formation				
LAM199-1	Dyke margin(WR)	Garnet, biotite, chlorite, plag, qtz, oxides, rare amph	Vcg idioblastic, poikiloblastic pink garnet. Half of the garnet is inclusionless. Cg poikiloblastic brown biotite. Cg, poikiloblastic, xenoblastic plag. Mg xenoblastic undulose qtz.	?
LAM199-2	Dyke (WR)	Amph, biotite, qtz, oxides	Vcg, poikiloblastic, blades of green amph. Matrix is recryst qtz, fg, xenoblastic brown biotite	Basaltic
LAM200-1	Dyke (WR)	Amph, qtz, oxides, plag	Cg feather and sheaf, pale green amph, in an granoblastic, fg, plag and qtz matrix.	Basaltic
LAM205-1	Sill/dyke (Hfx) amphibolite?	Amph, plag, epidote, qtz, oxides, chlorite	No matrix in this sample. Mg-cg subhedral plag, with abundant included epidote, some corrosion and alteration. Porphs of mg, green amph, xeno-subidioblastic. Abundant porphs of mg-fg feathery chlorite. Qtz is very rare and vfg.	Basaltic

Appendix A - Petrographic Description continued

Sample Number	Rock Type	Mineralogy	Description	Composition
Sills/dykes in White Rock Formation				
LAM206-2	Sill (Hfx)	Amph, carbonate, qtz, oxides, epidote, chlorite	Cg poik, blades of blue-green amph, in a recryst, fg plag matrix with qtz, carbonate and fg epidote.	Basaltic
LAM206-3	Sill/dyke (Hfx) amphibolite?		Very similar to 205-1 but with more amph and qtz, much less plag	Basaltic
Sills/dykes in the Halifax Formation				
LAM202-1	Sill/dyke (Hfx) amphibolite	Amph, plag, qtz, oxides, chlorite, sphene, epidote?	Matrix is mg-cg subidioblastic plag, vfg epidote? Fg, subidioblastic sphene. Cg porphs of green, slightly poikiloblastic amph, subidio-xenoblastic and fg-mg subidioblastic porphs of chlorite.	Basaltic
LAM207-1	Sill/dyke (Hfx) amphibolite?		Very similar to 205-1 but with much more amph which is not as green and slightly poikiloblastic. Much less plag, more qtz, no apparent epidote. Sample has a matrix of plag and fg, acicular amph. Elongate grains are aligned -- foliation.	Basaltic

Appendix A - Petrographic Description continued

Sample Number	Rock Type	Mineralogy	Description	Composition
Mafic pegmatoid				
LAM049-9	Mafic pegmatite	Amph, epidote, chlorite, oxides, qtz, plag	Vcg, xeno-subidio, sheaf-like, blue-green amph porphs. Cg subhedral plag laths which are recryst, mg, xeno-subidioblastic epidote porphs. Matrix is recryst plag, fg xenoblastic brown biotite, fg epidote and fg amph needles and qtz. Igneous texture preserved.	Basaltic
LAM049-10A	Mafic pegmatite	same as 49-9	Same as 49-9 but much more biotite and coaser grain size.	Basaltic
LAM049-11	Mafic pegmatite	same as 49-9	Same as 49-9 but more biotite and matrix is more qtz-rich (less plag), more recrystallized and finer grained.	Basaltic
LAM049-12	Mafic pegmatite	same as 49-9	Same as 49-10A but less epidote and slightly less amph.	Basaltic
Granite				
LAM157-1	Granite	No garnet	Appears very recrystallized (grain size reduction) and more foliated/strained than 161 series.	
LAM158-1	Granite		Similar to 161 series	

Appendix A - Petrographic Description continued

Sample Number	Rock Type	Mineralogy	Description	Composition
Granite				
LAM159-1	Granite		Similar to 161 series but slightly more recryst (grain size reduction)	
LAM160-1	Granite		same as 159	
LAM161-1	Granite		Similar to 161 series	
LAM161A-1	Granite	Qtz, Kspar, plag, biotite, musc, zircon,garnet	Granular.Qtz and feldspar grains show consertal (interlocking-intergrowth) texture. Grains are mg-cg, subhedral. A micrographic texture between some qtz and alkali feldspar grains also present. Some cg musc appears intergrown with qtz and feldspar.	Monzogranite-syenogranite
LAM161B-1	Granite			
LAM161C-1	Granite			
LAM161D-1	Granite			
LAM161E-1	Granite			
LAM162-1	Granite	No garnet	similar to 159	
Amphibolite				
LAM081-1	Amphibolite	Amph, plag, qtz, epidote, carbonate, oxides, sphene	Vcg, xenoblastic flakes of blue-green amph, in a fg-mg matrix of plag, epidote and qtz. Qtz looks recryst. Carb appears to be infilling spaces.	Basaltic

Appendix A - Petrographic Description continued

Sample Number	Rock Type	Mineralogy	Description	Composition
Amphibolite				
LAM170-1	Amphibolite	Amph, oxides, plag, chlorite, qtz	Mg plag, minor qtz, matrix is granoblastic. Cg, xenoblastic, green amph is slightly poikiloblastic.	Basaltic
LAM172-1	Amphibolite	Amph, plag, qtz, oxides, chlorite	Cg, sheaf-like green, subidioblastic amph, slightly poikiloblastic in a matix of fg, recryst plag and qtz. Matrix appears granoblastic.	Basaltic
Metasedimentary rocks				
LAM014-1	Slate?	Qtz, biotite, musc, chlorite	Matrix is fg, recryst qtz, chlorite and musc. Clusters of mg qtz, mg chlorite blades and mg-cg, brown, poikiloblastic biotite in the centre of the cluster. Foliated.	
LAM114-1	Slate			
LAM175-1	Slate	Musc, qtz, oxides, garnet, chlorite, staurolite	Matrix is fg musc and recryst qtz. Strongly foliated and also crenulated. Vcg porphs (~1 cm) of idioblastic, poikiloblastic staurolite rimmed by chlorite. Cg, idioblastic, pink garnet. Clusters of mg qtz, musc and chlorite.	

Appendix A - Petrographic Description continued

Sample Number	Rock Type	Mineralogy	Description	Composition
Metasedimentary rocks				
LAM179-1	Musc biotite garnet schist	Biotite, musc, qtz, garnet, oxides	Matrix of recryst qtz and fg musc, Mg-cg subidio porphs of brown biotite and idioblastic pink garnet. Both are poikiloblastic. Strongly foliated.	
LAM183-1	Musc garnet biotite schist	Garnet, musc, biotite, qtz	Mg, subidio-idioblastic, slightly poikiloblastic pink garnet in a fg-mg matric of brown biotite, musc and recryst qtz. Strongly foliated.	
LAM183-4	Staurolite biotite schist	Staurolite, biotite, musc, chorite, qtz, oxides	Vvcg poikiloblastic porphs of subidioblastic brown biotite and idioblastic staurolite. Matrix is fg musc and recryst qtz. Large pressure shadows around the porphs which are qtz rich. Strongly foliated.	
LAM184-1	Staurolite garnet biotite schist	Garnet, plag (albite), biotite, staurolite, muscovite	Cg porphs of albite, staurolite, garnet and biotite in fg musc and plag matrix. Strongly foliated.	

Appendix A - Petrographic Description continued

Sample Number	Rock Type	Mineralogy	Description	Composition
Metasedimentary rocks				
LAM191-2	Tuffaceous sandstone	qtz, plag, kspar, biotite, epidote, sphene?	Fg partly recryst qtz, plag, Kspar, xenoblastic green biotite, xenoblastic epidote.	

APPENDIX B ANALYTICAL METHODS FOR ELECTRON MICROPROBE ANALYSIS

Analyses were obtained using JEOL 733 electron microprobe equiped with four wavelength dispersive spectrometers and an Oxford Link eXL energy dispersive system. Resolution of the energy dispersive detector was 137 ev at 5.9 Kev. Geological standards were used with 15 kV accelerating voltage and 15 nA beam current operating conditions. The accumulation time was 40 seconds and the probe spot was approximately 1 micron. Data were collected using the Oxford Link ZAF matrix correction program. Instrument calibration on cobalt metal was +/-0.5% at 1 standard deviation and accuracy for major elements was +/-1.5% to 2% relative. Detection limits for most elements range from approximately 0.1% to 0.3%.

Appendix B - Microprobe analyses of amphibole

Sample	075a-1-1	075a-1-2	075a-1-4	075a-1-5	075a-1-6	075a-1-7	075a-1-9
SiO_2	47.96	54.36	42.65	43.03	54.13	41.53	54.26
TiO_2	0.5	0.13	0.42	0.38	0	0.34	0.21
Al_2O_3	7.59	1.54	12.85	12.33	1.77	12.26	2.06
FeO	19.25	13.18	19.53	20.67	14.17	18.63	13.28
Cr_2O_3	0.02	0.04	0.2	0.16	0.04	0.21	0.24
MnO	0.47	0.24	0.2	0.24	0.38	0.31	0.23
MgO	12.43	17.02	8.97	8.52	16.53	8.71	16.51
CaO	9.59	12.6	11.43	11.7	11.8	11.01	12.3
Na_2O	1.04	0.38	1.7	1.52	0.5	1.89	0.36
K_2O	0.21	0	0.2	0.39	0.04	0.27	0.09
Cl	0.06	0.02	0	0.02	0.04	0	0.03
BaO	0	0	0	0.03	0.02	0	0
ZrO_2	0.09	0	0	0	0	0	0
NiO	0.18	0.25	0	0.01	0	0.12	0.11
La_2O_3	0.04	0.06	0	0.06	0.06	0	0
Total	99.43	99.91	98.2	99.03	99.49	95.38	99.81
Structural Formulae (based on 23 oxygens)							
Letters A,B,C and T refer to coordination sites in general formula $A_{0-1}B_2C_5T_8O_{22}(OH,F)_2$							
TSi	6.88	7.64	6.33	6.38	7.62	6.38	7.63
TAl	1.12	0.26	1.67	1.62	0.29	1.62	0.34
TFe^{3+}	0.00	0.11	0.00	0.00	0.09	0.00	0.04
Sum_T	8.00	8.00	8.00	8.00	8.00	8.00	8.00
CAl	0.17	0.00	0.58	0.53	0.00	0.60	0.01
CCr	0.00	0.00	0.02	0.02	0.00	0.03	0.03
CFe^{3+}	1.07	0.34	0.64	0.63	0.46	0.51	0.34
CTi	0.05	0.01	0.05	0.04	0.00	0.04	0.02
CMg	2.66	3.56	1.99	1.88	3.47	1.99	3.46
CFe^{2+}	1.02	1.06	1.72	1.88	1.04	1.82	1.14
CMn	0.03	0.01	0.01	0.02	0.02	0.02	0.01
Sum_C	5.00	5.00	5.00	5.00	5.00	5.00	5.00
BMg	0.00	0.00	0.00	0.00	0.00	0.00	0.00
BFe^{2+}	0.22	0.03	0.07	0.05	0.08	0.07	0.06
BMn	0.03	0.01	0.01	0.02	0.02	0.02	0.01
BCa	1.48	1.90	1.82	1.86	1.78	1.81	1.85
BNa	0.14	0.05	0.10	0.08	0.07	0.10	0.05
Sum_B	1.87	2.00	2.00	2.00	1.95	2.00	1.97
ANa	0.15	0.05	0.39	0.36	0.07	0.46	0.05
AK	0.04	0.00	0.04	0.07	0.01	0.05	0.02
Sum_A	0.19	0.05	0.43	0.44	0.08	0.52	0.07
Sum_cat	15.05	15.05	15.43	15.44	15.03	15.52	15.04
CCl	0.02	0.01	0.00	0.01	0.01	0.00	0.01
Sum_oxy	23.00	23.00	23.00	23.00	23.00	23.00	23.00

Appendix B - Microprobe analyses of amphibole continued

Sample	075a-1-10	075a-1-13	078-2-2	078-2-5	078-2-6	078-2-7	078-2-8
SiO_2	45.84	41.99	48.15	47.81	47.25	46.95	47.95
TiO_2	0.27	0.38	0.3	0.12	0.2	0.29	0.34
Al_2O_3	11.63	13.05	8.51	8.71	9.09	9.49	8.69
FeO	17.98	19.93	13.56	13.8	14.26	14.46	13.87
Cr_2O_3	0.04	0	0.07	0.04	0.09	0	0.05
MnO	0.25	0.34	0.34	0.25	0.45	0.29	0.34
MgO	9.67	8.43	15.05	14.51	14.09	14	14.51
CaO	11.27	11.85	12.07	12.02	12.14	12.24	12.24
Na_2O	2.03	1.63	1.51	1.26	1.57	1.42	1.51
K_2O	0.2	0.42	0.04	0.13	0.09	0.16	0.13
Cl	0.02	0	0.01	0	0	0.03	0.04
BaO	0.07	0	0	0	0.35	0	0
ZrO_2	0	0	0	0	0	0	0
NiO	0	0.16	0.05	0.02	0	0	0.05
La_2O_3	0.17	0	0	0	0.21	0	0
Total	99.53	98.26	99.77	98.72	99.99	99.38	99.72
Structural Formulae (based on 23 oxygens)							
TSi	6.72	6.29	6.81	6.83	6.75	6.70	6.81
TAl	1.28	1.72	1.19	1.17	1.25	1.30	1.19
TFe^{3+}	0.00	0.00	0.00	0.00	0.00	0.00	0.00
Sum_T	8.00	8.00	8.00	8.00	8.00	8.00	8.00
CAl	0.73	0.59	0.22	0.29	0.28	0.29	0.26
CCr	0.01	0.00	0.01	0.01	0.01	0.00	0.01
CFe^{3+}	0.25	0.60	0.66	0.65	0.62	0.66	0.56
CTi	0.03	0.04	0.03	0.01	0.02	0.03	0.04
CMg	2.11	1.88	3.17	3.09	3.00	2.98	3.07
CFe^{2+}	1.86	1.87	0.89	0.94	1.04	1.02	1.05
CMn	0.02	0.02	0.02	0.02	0.03	0.02	0.02
Sum_C	5.00	5.00	5.00	5.00	5.00	5.00	5.00
BMg	0.00	0.00	0.00	0.00	0.00	0.00	0.00
BFe^{2+}	0.09	0.03	0.06	0.06	0.04	0.04	0.04
BMn	0.02	0.02	0.02	0.02	0.03	0.02	0.02
BCa	1.77	1.90	1.83	1.84	1.86	1.87	1.86
BNa	0.12	0.05	0.09	0.09	0.08	0.07	0.07
Sum_B	2.00	2.00	2.00	2.00	2.00	2.00	2.00
ANa	0.45	0.42	0.32	0.26	0.36	0.32	0.34
AK	0.04	0.08	0.01	0.02	0.02	0.03	0.02
Sum_A	0.49	0.50	0.33	0.29	0.38	0.35	0.37
Sum_cat	15.49	15.50	15.33	15.29	15.38	15.35	15.37
CCl	0.01	0.00	0.00	0.00	0.00	0.01	0.01
Sum_oxy	23.06	23.00	23.00	23.00	23.00	23.00	23.00

Appendix B - Microprobe analyses of amphibole continued

Sample	078-2-9	078-2-14	133-1-3	133-1-4	133-1-5	133-1-7	133-1-8
SiO_2	45.14	46.3	45.85	48.06	47.87	47.67	45.1
TiO_2	0.42	0.32	0.39	0.42	0.41	0.32	0.47
Al_2O_3	10.37	9.85	10.75	8.86	9.15	9.13	11.22
FeO	15.11	14.63	12.78	11.76	12.95	12.91	13.76
Cr_2O_3	0	0.08	0	0.02	0	0	0.05
MnO	0.48	0.42	0.51	0.64	0.62	0.43	0.52
MgO	12.84	13.47	13.95	15.47	14.62	14.58	13.48
CaO	12.13	11.9	12.19	12.29	12.12	12.14	12.18
Na_2O	1.69	1.6	1.48	1.37	1.45	1.34	1.54
K_2O	0.21	0.17	0.15	0.11	0.12	0.16	0.29
Cl	0	0	0.01	0	0.01	0	0
BaO	0.02	0.18	0	0.17	0.09	0	0
ZrO_2	0	0	0	0	0	0	0
NiO	0.26	0.1	0.03	0	0	0	0.18
La_2O_3	0.11	0.07	0	0.14	0.14	0	0
Total	98.94	99.18	98.14	99.51	99.62	98.69	98.88
Structural Formulae (based on 23 oxygens)							
TSi	6.56	6.66	6.60	6.81	6.80	6.80	6.49
TAl	1.44	1.34	1.40	1.20	1.21	1.20	1.51
TFe^{3+}	0.00	0.00	0.00	0.00	0.00	0.00	0.00
Sum_T	8.00	8.00	8.00	8.00	8.00	8.00	8.00
CAl	0.33	0.33	0.42	0.28	0.32	0.34	0.39
CCr	0.00	0.01	0.00	0.00	0.00	0.00	0.01
CFe^{3+}	0.63	0.63	0.58	0.57	0.54	0.54	0.66
CTi	0.05	0.04	0.04	0.05	0.04	0.03	0.05
CMg	2.78	2.89	2.99	3.27	3.09	3.10	2.89
CFe^{2+}	1.19	1.08	0.93	0.80	0.96	0.96	0.97
CMn	0.03	0.03	0.03	0.04	0.04	0.03	0.03
Sum_C	5.00	5.00	5.00	5.00	5.00	5.00	5.00
BMg	0.00	0.00	0.00	0.00	0.00	0.00	0.00
BFe^{2+}	0.02	0.05	0.03	0.03	0.04	0.04	0.03
BMn	0.03	0.03	0.03	0.04	0.04	0.03	0.03
BCa	1.89	1.84	1.88	1.86	1.84	1.86	1.88
BNa	0.06	0.09	0.06	0.07	0.08	0.08	0.07
Sum_B	2.00	2.00	2.00	2.00	2.00	2.00	2.00
ANa	0.42	0.36	0.35	0.30	0.32	0.29	0.36
AK	0.04	0.03	0.03	0.02	0.02	0.03	0.05
Sum_A	0.46	0.39	0.38	0.32	0.34	0.32	0.42
Sum_cat	15.46	15.39	15.38	15.32	15.34	15.32	15.42
CCl	0.00	0.00	0.00	0.00	0.00	0.00	0.00
Sum_oxy	23.00	23.00	23.00	23.00	23.00	23.00	23.00

Appendix B - Microprobe analyses of amphibole continued

Sample	133-1-9	133-1-10	173-1-3	173-1-4	173-1-9	173-1-10	196-1-1
SiO_2	38.02	44.6	44.52	54.54	43.88	53.76	39.05
TiO_2	1.67	0.57	0.42	0.05	0.32	0.15	0.28
Al_2O_3	16.43	11.83	12.23	2.53	12.83	3.51	19.02
FeO	13.44	13.64	15.15	9.22	14.97	9.89	19.35
Cr_2O_3	0	0.11	0.17	0.02	0.09	0.09	0.18
MnO	0.02	0.46	0.22	0.3	0.26	0.11	0.27
MgO	16.22	12.99	12.17	18.87	12.02	18.5	6.48
CaO	0.07	12.19	12.1	13	11.81	12.72	10.95
Na_2O	0.29	1.55	1.91	0.46	1.99	0.7	1.38
K_2O	8.94	0.17	0.28	0	0.16	0	0.51
Cl	0	0.03	0	0	0.04	0	0.02
BaO	0.24	0.09	0	0	0	0	0.04
ZrO_2	0.14	0	0	0	0	0	0
NiO	0.1	0	0	0.05	0.06	0.04	0.14
La_2O_3	0	0.15	0	0	0	0.04	0
Total	95.58	98.38	99.22	99.04	98.43	99.51	97.71
Structural Formulae (based on 23 oxygens)							
TSi	5.66	6.45	6.43	7.59	6.38	7.46	5.83
TAl	2.31	1.55	1.57	0.41	1.62	0.54	2.17
TFe^{3+}	0.04	0.00	0.00	0.01	0.00	0.00	0.00
Sum_T	8.00	8.00	8.00	8.00	8.00	8.00	8.00
CAl	0.57	0.47	0.52	0.01	0.57	0.04	1.17
CCr	0.00	0.01	0.02	0.00	0.01	0.01	0.02
CFe^{3+}	0.74	0.59	0.49	0.33	0.55	0.39	0.68
CTi	0.19	0.06	0.05	0.01	0.04	0.02	0.03
CMg	3.50	2.80	2.62	3.91	2.60	3.83	1.44
CFe^{2+}	0.00	1.03	1.30	0.72	1.21	0.72	1.63
CMn	0.00	0.03	0.01	0.02	0.02	0.01	0.02
Sum_C	5.00	5.00	5.00	5.00	5.00	5.00	5.00
BMg	0.10	0.00	0.00	0.00	0.00	0.00	0.00
BFe^{2+}	0.90	0.02	0.05	0.01	0.06	0.04	0.10
BMn	0.00	0.03	0.01	0.02	0.02	0.01	0.02
BCa	0.01	1.89	1.87	1.94	1.84	1.89	1.75
BNa	0.04	0.06	0.07	0.03	0.09	0.06	0.13
Sum_B	1.04	2.00	2.00	2.00	2.00	2.00	2.00
ANa	0.05	0.38	0.47	0.09	0.48	0.13	0.27
AK	1.70	0.03	0.05	0.00	0.03	0.00	0.10
Sum_A	1.74	0.41	0.52	0.09	0.51	0.13	0.36
Sum_cat	15.79	15.41	15.52	15.09	15.51	15.13	15.36
CCl	0.00	0.01	0.00	0.00	0.01	0.00	0.01
Sum_oxy	22.57	23.00	23.00	23.00	23.00	23.00	23.00

Appendix B - Microprobe analyses of amphibole continued

Sample	196-1-2	196-1-4	205-1-8
SiO_2	39.53	40.19	49.82
TiO_2	0.34	0.48	0.19
Al_2O_3	18.01	18.57	5.1
FeO	17.64	19.99	16.46
Cr_2O_3	0	0.09	0.06
MnO	0.39	0.25	0.31
MgO	6.01	5.24	12.72
CaO	11.48	11.59	12.4
Na_2O	1.37	1.38	0.71
K_2O	0.43	0.43	0.06
Cl	0	0	0
BaO	0	0	0
ZrO_2	0	0.01	0
NiO	0	0	0.19
La_2O_3	0.17	0.07	0.02
Total	95.41	98.33	98.23
Structural Formulae (based on 23 oxygens)			
TSi	6.07	6.02	7.29
TAl	1.93	1.98	0.71
TFe^{3+}	0.00	0.00	0.00
Sum_T	8.00	8.00	8.00
CAl	1.32	1.30	0.17
CCr	0.00	0.01	0.01
CFe^{3+}	0.17	0.23	0.34
CTi	0.04	0.05	0.02
CMg	1.38	1.17	2.78
CFe^{2+}	2.07	2.22	1.67
CMn	0.03	0.02	0.02
Sum_C	5.00	5.00	5.00
BMg	0.00	0.00	0.00
BFe^{2+}	0.03	0.05	0.01
BMn	0.03	0.02	0.02
BCa	1.89	1.86	1.94
BNa	0.06	0.08	0.03
Sum_B	2.00	2.00	2.00
ANa	0.35	0.33	0.17
AK	0.08	0.08	0.01
Sum_A	0.43	0.41	0.18
Sum_cat	15.43	15.41	15.18
CCl	0.00	0.00	0.00
Sum_oxy	23.01	23.00	23.00

Appendix B - Microprobe analyses of biotite

Sample	011-1-3	011-1-5	011-1-13	078-2-3	133-1-1	133-1-2	133-1-6	161d-7c
SiO_2	36.05	36.28	36.13	38.44	37.59	37.93	37.94	35.24
TiO_2	2.64	2.37	2.26	1.5	1.72	1.7	1.56	3
Al_2O_3	17.61	16.93	16.75	15.82	16.63	16.22	16.31	16.84
FeO	17.87	19.66	18.75	15.22	14.47	13.95	13.98	28.38
MnO	0.63	0.66	0.39	0.09	0.09	0.14	0.02	0.55
MgO	11.05	11.41	11.18	16.09	16.31	16.29	15.92	1.98
CaO	0	0	0.03	0.01	0	0	0.05	0.01
Na_2O	0.33	0.19	0.24	0.23	0.45	0.23	0.29	0.09
K_2O	10.21	10.18	9.62	9.02	9.12	8.99	9.07	10.12
Cr_2O_3	0	0.02	0.01	0.05	0	0.09	0.12	0.01
NiO	0.34	0.16	0.02	0.22	0.17	0	0	0.1
P_2O_5	0	0.16	0.09	0	0.01	0.03	0.03	0.04
Cl	0	0.09	0	0.04	0.02	0.03	0	0.07
BaO	0	0	0	0.07	0.2	0.22	0.62	0.11
ZrO_2	0.06	0	0	0	0	0	0	0.03
La_2O_3	0	0	0	0.06	0	0.03	0.12	0.01
Total	96.8	98.13	95.46	96.87	96.78	95.84	96.02	96.6
Structural Formulae (based on 22 oxygen)								
Si	5.67	5.67	5.75	5.89	5.76	5.84	5.85	5.84
Al^{4+}	2.33	2.33	2.25	2.11	2.24	2.16	2.15	2.16
Al^{6+}	0.93	0.78	0.89	0.74	0.76	0.78	0.81	1.13
Ti	0.31	0.28	0.27	0.17	0.20	0.20	0.18	0.37
Fe^{2+}	2.35	2.57	2.50	1.95	1.85	1.80	1.80	3.94
Cr	0.00	0.00	0.00	0.01	0.00	0.01	0.02	0.00
Mn	0.08	0.09	0.05	0.01	0.01	0.02	0.00	0.08
Mg	2.59	2.66	2.65	3.67	3.72	3.74	3.66	0.49
Ba	0.00	0.00	0.00	0.00	0.01	0.01	0.04	0.01
Ca	0.00	0.00	0.01	0.00	0.00	0.00	0.01	0.00
Na	0.10	0.06	0.07	0.07	0.13	0.07	0.09	0.03
K	2.05	2.03	1.95	1.76	1.78	1.77	1.78	2.14

Appendix B - Microprobe analyses of biotite continued

Sample	161d-9g	161d-13	196-1-3	196-1-5	199-1-3	199-1-5	199-1-6	199-1-8
SiO_2	35.08	35.28	35.78	35.78	34.53	34.83	34.9	34.17
TiO_2	2.92	2.77	1.68	1.69	1.87	1.61	1.69	1.52
Al_2O_3	17.06	17.7	17.49	17.79	17.69	17.71	18.01	17.36
FeO	28.06	27.29	22.65	21.94	25.66	25.17	25.21	25.86
MnO	0.58	0.65	0.17	0.17	0.02	0.16	0.01	0.17
MgO	1.94	1.91	9.59	9.15	7.1	7.32	7.42	7.15
CaO	0.05	0	0.01	0.02	0.02	0	0.23	0.04
Na_2O	0.16	0.16	0.41	0.16	0.38	0.35	0.24	0.34
K_2O	10.05	10.14	9.69	9.78	9.49	9.39	9.08	9.64
Cr_2O_3	0	0	0.02	0.06	0	0.08	0	0
NiO	0.02	0.12	0.12	0.08	0.13	0.26	0.24	0
P_2O_5	0.13	0	0	0.01	0.02	0.04	0.01	0
Cl	0.08	0.06	0	0	0	0.04	0	0
BaO	0	0	0	0	0	0	0	0.23
ZrO_2	0	0.19	0.02	0	0	0.11	0	0.04
La_2O_3	0	0	0.03	0	0.02	0	0	0.03
Total	96.14	96.27	97.66	96.64	96.94	97.07	97.04	96.55
Structural Formulae (based on 22 oxygen)								
Si	5.83	5.83	5.67	5.70	5.60	5.63	5.62	5.60
Al^{4+}	2.17	2.17	2.33	2.30	2.40	2.37	2.38	2.40
Al^{6+}	1.16	1.28	0.93	1.04	0.98	1.00	1.04	0.95
Ti	0.37	0.34	0.20	0.20	0.23	0.20	0.21	0.19
Fe^{2+}	3.90	3.77	3.00	2.93	3.48	3.40	3.40	3.54
Cr	0.00	0.00	0.00	0.01	0.00	0.01	0.00	0.00
Mn	0.08	0.09	0.02	0.02	0.00	0.02	0.00	0.02
Mg	0.48	0.47	2.27	2.18	1.72	1.76	1.78	1.75
Ba	0.00	0.00	0.00	0.00	0.00	0.00	0.00	0.01
Ca	0.01	0.00	0.00	0.00	0.00	0.00	0.04	0.01
Na	0.05	0.05	0.13	0.05	0.12	0.11	0.08	0.11
K	2.13	2.14	1.96	1.99	1.96	1.94	1.87	2.01

Appendix B - Microprobe analyses of chlorite

Sample	004-1-1	075a-1-14	144-1-1	144-1-2	144-1-4	144-1-5	144-1-6	173-1-6	205-1-2	205-1-4	205-1-7
SiO_2	33.63	27.02	23.78	23.88	24.19	23.81	24.03	26.75	23.79	25.17	26.35
TiO_2	0	0.12	0.09	0	0	0.05	0	0.15	0	0.05	0.21
Al_2O_3	20.43	19.72	40.38	40.29	40.39	40.59	40.28	22.1	18.95	20.17	19.54
FeO	11.76	21.35	25.92	25.59	26.1	25.75	26.02	17.27	24.17	26.71	25.72
MnO	0	0.18	0.16	0.22	0.1	0.03	0.13	0.08	0.23	0.31	0.36
MgO	0.1	19.35	1.88	2	1.95	1.87	2.05	22.2	14.27	15.12	15.91
CaO	18.3	0.06	0	0	0	0	0.01	0.15	0	0	0.01
Na_2O	0.1	0.09	0	0.07	0.02	0.06	0.02	0.09	0.36	0.14	0.21
K_2O	0	0.02	0	0	0.04	0	0	0	0	0.02	0.14
NiO	0.08	0.15	0.14	0	0	0	0.16	0.11	0.12	0.01	0.16
P_2O_5	0	0.09	0	0.01	0	0	0	0	0.94	0.1	0.17
BaO	0	0	0.09	0.01	0.18	0	0	0.08	0	0	0
Cl	0.02	0.03	0	0	0	0	0.03	0.03	0.25	0	0
ZrO_2	0	0	0	0	0.06	0.05	0.04	0	0	0	0
La_2O_3	0	0	0.13	0.02	0.08	0.05	0	0.14	0	0	0
Total	84.42	88.17	92.56	92.18	93.09	92.27	92.85	89.24	84.79	87.82	88.87
Structural Formulae (based on 24 oxygen)											
Si	7.07	5.55	4.63	4.65	4.68	4.63	4.66	5.32	5.28	5.36	5.51
Al^{IV}	0.93	2.45	3.37	3.35	3.32	3.37	3.34	2.68	2.72	2.64	2.49
Al^{VI}	4.13	2.31	5.88	5.90	5.87	5.93	5.86	2.49	2.23	2.41	2.32
Ti	0.00	0.02	0.01	0.00	0.00	0.01	0.00	0.02	0.00	0.01	0.03
Fe^{2+}	2.07	3.67	4.22	4.17	4.22	4.19	4.22	2.87	4.49	4.75	4.50
Mn	0.00	0.03	0.03	0.04	0.02	0.01	0.02	0.01	0.04	0.06	0.06
Mg	0.03	5.92	0.55	0.58	0.56	0.54	0.59	6.58	4.72	4.80	4.96
Ca	4.12	0.01	0.00	0.00	0.00	0.00	0.00	0.03	0.00	0.00	0.00
Na	0.04	0.04	0.00	0.03	0.01	0.02	0.01	0.04	0.16	0.06	0.09
K	0.00	0.01	0.00	0.00	0.01	0.00	0.00	0.00	0.00	0.01	0.04

Appendix B - Microprobe analyses of epidote

Sample	004-1-5	004-1-6	004-1-11	011-1-1	011-1-2	011-1-9	075a-1-8	078-2-12	173-1-1	173-1-2	173-1-5	173-1-11
SiO_2	37.81	37.58	37.5	36.81	37.03	36.97	37.21	37.67	37.14	37.39	37.39	37.42
Al_2O_3	23.77	22.44	23.22	23.23	21.81	21.32	21.26	24.12	22.29	21.95	22.47	22.31
FeO	12.61	13.93	12.83	12.09	14.03	14.25	14.43	11.52	13.89	13.75	13.52	13.65
MgO	0.02	0	0.09	0.06	0.06	0.13	0.05	0.01	0	0	0.03	0.04
CaO	24.04	24.12	23.99	22.38	23.44	23.76	23.43	23.8	23.95	24.18	23.64	24.13
La_2O_3	0.28	0.15	0.03	0	0	0.01	0.09	0	0	0	0.06	0
K_2O	0	0	0.06	0.01	0	0.05	0	0	0.01	0	0	0
Cr_2O_3	0.03	0	0.16	0	0	0.04	0.04	0	0.2	0.16	0.06	0.01
NiO	0.03	0.26	0.06	0.03	0	0.18	0.28	0.03	0	0	0.15	0.16
P_2O_5	0	0.04	0.01	0	0.01	0	0	0	0.04	0.01	0	0
Cl	0.01	0	0.05	0.02	0.01	0.03	0.04	0	0	0	0	0
BaO	0.34	0.03	0.19	0.1	0	0.09	0.14	0	0	0.22	0.13	0
ZrO_2	0	0	0	0.03	0	0	0.15	0	0.05	0	0.1	0
SrO	0	0	0	0.42	0.11	0	0.13	0	0	0	0.06	0.01
Total	99.44	98.78	98.52	95.97	96.78	97.26	97.39	97.53	97.8	97.71	97.87	97.97
Structural Formulae												
Si	2.96	2.96	2.96	2.98	2.98	2.97	2.98	2.98	2.95	2.98	2.97	2.97
Al	2.19	2.08	2.16	2.22	2.07	2.02	2.01	2.25	2.09	2.06	2.10	2.09
Fe^{3+}	0.83	0.92	0.85	0.82	0.94	0.96	0.97	0.76	0.92	0.91	0.90	0.91
Mg	0.00	0.00	0.01	0.01	0.01	0.02	0.01	0.00	0.00	0.00	0.00	0.01
Ca	2.02	2.04	2.03	1.94	2.02	2.05	2.01	2.02	2.04	2.06	2.01	2.05
La	0.01	0.00	0.00	0.00	0.00	0.00	0.00	0.00	0.00	0.00	0.00	0.00
O	12.50	12.50	12.50	12.50	12.50	12.50	12.50	12.50	12.50	12.50	12.50	12.50

Appendix B - Microprobe analyses of garnet

Sample	175-1-6	175-1-7	175-1-8	175-1-9	196-1-6	199-1-1	199-1-2	199-1-4	199-1-9	199-1-11
SiO_2	36.43	36.72	36.61	36.55	37.04	36.42	36.49	36.71	36.55	36.5
TiO_2	0	0	0.08	0.05	0.22	0.1	0.09	0.14	0.17	0.01
Al_2O_3	21.01	20.9	21.08	20.98	21.22	20.52	20.77	20.72	20.76	20.83
Cr_2O_3	0.01	0	0	0.01	0.13	0.06	0	0.03	0.03	0.04
FeO	31.48	34.73	33.84	34.45	30.96	33.95	34.82	31.9	33.55	32.39
MnO	8.21	6	6.68	6.32	5.51	3.39	2.14	5.24	3.53	5.36
MgO	1.6	1.64	1.66	1.65	1.38	1.08	1.13	1.09	1.19	1.1
CaO	1.67	1.7	1.57	1.59	5.18	4.92	5.91	5.44	5.51	4.87
Na_2O	0.15	0.06	0	0	0	0.09	0	0.01	0.04	0
K_2O	0	0	0.02	0	0.02	0.03	0.03	0	0.01	0
NiO	0	0	0.18	0.25	0.13	0	0.03	0.17	0.02	0.05
P_2O_5	0	0.09	0.13	0.16	0	0.03	0.1	0	0.1	0.15
BaO	0	0.22	0.09	0	0	0.23	0	0	0	0.24
ZrO_2	0	0	0	0	0.14	0	0	0	0	0
Total	100.59	102.32	102.05	102.01	101.94	100.96	101.52	101.46	101.48	101.67
Structural Formulae (based on 24 oxygens)										
TSi	2.95	2.94	2.94	2.94	2.95	2.94	2.92	2.94	2.93	2.93
TAl	0.05	0.06	0.06	0.07	0.05	0.06	0.08	0.06	0.08	0.07
Sum_T	3.00	3.00	3.00	3.00	3.00	3.00	3.00	3.00	3.00	3.00
Al^{6+}	1.95	1.91	1.93	1.92	1.94	1.89	1.88	1.90	1.88	1.90
Ti	0.00	0.00	0.01	0.00	0.01	0.01	0.01	0.01	0.01	0.00
Cr	0.00	0.00	0.00	0.00	0.01	0.00	0.00	0.00	0.00	0.00
Sum_A	1.95	1.91	1.94	1.92	1.96	1.90	1.88	1.91	1.89	1.91
Fe^{2+}	2.13	2.33	2.27	2.31	2.06	2.29	2.33	2.14	2.25	2.18
Mg	0.19	0.20	0.20	0.20	0.16	0.13	0.14	0.13	0.14	0.13
Mn	0.56	0.41	0.45	0.43	0.37	0.23	0.15	0.36	0.24	0.37
Ca	0.15	0.15	0.14	0.14	0.44	0.43	0.51	0.47	0.47	0.42
Na	0.02	0.01	0.00	0.00	0.00	0.01	0.00	0.00	0.01	0.00
Sum_B	3.05	3.09	3.06	3.08	3.04	3.10	3.12	3.09	3.11	3.09
Sum_cat	8.00	8.00	8.00	8.00	8.00	8.00	8.00	8.00	8.00	8.00
Alm	60.93	66.32	65.10	65.91	57.98	73.17	64.59	67.57	61.97	59.85
Gross	6.24	6.56	5.98	6.06	18.47	14.30	22.81	15.80	20.92	18.22
Pyrope	8.37	8.81	8.80	8.81	7.04	4.43	6.07	4.43	6.32	5.78
Spess	24.41	18.31	20.12	19.18	15.98	7.90	6.53	12.10	10.66	15.99
Uvaro	0.04	0.00	0.00	0.04	0.53	0.20	0.00	0.10	0.13	0.17

Appendix B - Microprobe analyses of K-feldspar

Sample	004-1-2	004-1-12	004-1-14	004-1-15	161d-11g	161d-14	161d-15
SiO_2	64.6	65.62	64.91	64.64	64.69	65.01	64.92
TiO_2	0.04	0.06	0.08	0	0	0	0.02
Al_2O_3	18.62	19	18.61	18.82	18.5	18.7	18.64
FeO	0	0.08	0	0.12	0.17	0.17	0.06
MnO	0.11	0	0	0	0	0.11	0.01
MgO	0.05	0.01	0	0.04	0.01	0.05	0.01
CaO	0.02	0	0.05	0	0	0	0
Na_2O	0.38	0.59	0.4	0.35	0.87	1.12	0.54
K_2O	16.94	17.08	17.31	17.38	16.59	16.17	16.8
NiO	0	0.14	0	0.12	0.03	0.06	0.08
P_2O_5	0	0	0.09	0	0	0.1	0.1
BaO	0.21	0.49	0.37	0.16	0.02	0.09	0.14
La_2O_3	0.09	0.12	0.21	0.05	0	0	0.02
Cr_2O_3	0.05	0.07	0	0.06	0	0	0.04
Total	101.12	103.26	102.07	101.88	100.89	101.59	101.4
Structural Formulae (based on 32 oxygen)							
Si	11.90	11.87	11.88	11.85	11.92	11.88	11.90
Al	4.04	4.05	4.01	4.06	4.01	4.03	4.03
Ti	0.01	0.01	0.01	0.00	0.00	0.00	0.00
Fe^{3+}	0.00	0.01	0.00	0.02	0.03	0.03	0.01
Mn	0.02	0.00	0.00	0.00	0.00	0.02	0.00
Mg	0.01	0.00	0.00	0.01	0.00	0.01	0.00
Ca	0.00	0.00	0.01	0.00	0.00	0.00	0.00
Na	0.14	0.21	0.14	0.12	0.31	0.40	0.19
K	3.98	3.94	4.04	4.07	3.90	3.77	3.93
Ab	3.30	5.00	3.40	3.00	7.40	9.50	4.70
An	0.10	0.00	0.20	0.00	0.00	0.00	0.00
Or	96.60	95.00	96.40	97.00	92.60	90.50	95.30

Appendix B - Microprobe analyses of muscovite

Sample	011-1-4	011-1-8	161d-8c	161d-10g
SiO2	45.4	44.88	46.89	47.54
TiO2	0.89	0.75	0.74	0.88
Al2O3	30.45	31.29	30.17	30.2
Fe2O3				
FeO	4.76	5.52	6.35	6.82
MnO	0.15	0.09	0.08	0.03
MgO	1.62	1.29	0.98	0.97
CaO	0	0	0	0
Na2O	0.31	0.29	0.28	0.21
K2O	10.98	10.3	8.6	9.27
F				
Cl	0.03	0	0	0
Cr2O3	0	0.15	0.02	0
NiO	0.17	0.05	0.08	0.03
BaO	0.65	0.62	0.03	0.1
ZrO2	0	0	0	0.01
La2O3	0	0	0.03	0.14
Total	95.56	95.36	94.29	96.19
Structural Formulae				
Si	6.24	6.17	6.41	6.41
Al^{IV}	1.77	1.84	1.59	1.59
Al^{VI}	3.16	3.23	3.27	3.20
Ti	0.09	0.08	0.08	0.09
Fe^{3+}	0.00	0.00	0.00	0.00
Fe^{2+}	0.55	0.63	0.73	0.77
Mn	0.02	0.01	0.01	0.00
Mg	0.33	0.26	0.20	0.20
Ca	0.00	0.00	0.00	0.00
Na	0.08	0.08	0.07	0.06
K	1.92	1.81	1.50	1.59
Cations	14.16	14.10	13.85	13.91
CCl	0.01	0.00	0.00	0.00
O	24.00	24.00	24.00	24.00

Appendix B - Microprobe analyses of plagioclase

Sample	004-1-3	004-1-4r	004-1-6a	004-1-8	004-1-9	004-1-13	011-1-6	011-1-7	011-1-10	011-1-11	011-1-12	075a-1-3	075a-1-11
SiO_2	69.4	68.69	65.89	68.01	68.47	65.12	67.84	67.74	67.47	66.72	67.12	68.19	67.81
TiO_2	0	0	0	0	0.02	0.07	0	0.02	0	0.05	0.03	0	0.04
Al_2O_3	20.25	19.99	22.75	20.26	20.39	22.11	20.28	19.93	20.01	20.06	20.03	20.29	20.76
FeO	0	0.08	0.37	0	0.14	0.03	0.16	0	0.02	0.18	0.06	0.13	0.04
MnO	0.07	0.11	0.04	0	0	0.01	0	0	0.07	0	0.03	0	0.02
MgO	0.08	0.14	0.08	0.04	0.11	0.11	0.15	0.09	0.18	0	0.09	0.06	0.05
CaO	0.41	0.42	0.67	0.55	0.48	3.16	0.71	0.54	0.43	0.75	0.71	0.52	1.34
Na_2O	9.88	10.55	7.79	11.78	11.78	9.19	10.58	11.2	10.73	10.57	10.85	10.32	10.03
K_2O	0.04	0.02	1.66	0.05	0	0.1	0.03	0	0.05	0.04	0	0.05	0
NiO	0.18	0	0.11	0	0.14	0.05	0.09	0.02	0.15	0	0	0.03	0.07
P_2O_5	0.17	0.07	0.12	0.17	0.19	0.19	0.03	0.16	0.18	0.09	0.05	0	0.19
BaO	0	0.05	0.06	0	0.14	0	0.14	0.06	0	0.01	0	0.16	0
La_2O_3	0	0	0.02	0.08	0.12	0	0.03	0	0	0.03	0	0.09	0.16
Cr_2O_3	0	0	0	0.15	0.05	0.04	0.01	0.1	0	0	0.03	0.01	0
Total	100.49	100.12	99.54	101.1	102.05	100.21	100.07	99.86	99.3	98.48	99	99.88	100.51
Structural Formulae (based on 32 oxygen)													
Si	11.98	11.95	11.57	11.79	11.78	11.42	11.85	11.86	11.86	11.83	11.85	11.91	11.78
Al	4.12	4.10	4.71	4.14	4.13	4.57	4.17	4.11	4.14	4.19	4.16	4.17	4.25
Ti	0.00	0.00	0.00	0.00	0.00	0.01	0.00	0.00	0.00	0.01	0.00	0.00	0.01
Fe^{3+}	0.00	0.01	0.05	0.00	0.02	0.00	0.02	0.00	0.00	0.03	0.01	0.02	0.01
Mn	0.01	0.02	0.01	0.00	0.00	0.00	0.00	0.00	0.01	0.00	0.00	0.00	0.00
Mg	0.02	0.04	0.02	0.01	0.03	0.03	0.04	0.02	0.05	0.00	0.02	0.02	0.01
Ca	0.08	0.08	0.13	0.10	0.09	0.59	0.13	0.10	0.08	0.14	0.13	0.10	0.25
Na	3.31	3.56	2.65	3.96	3.93	3.13	3.58	3.80	3.66	3.64	3.71	3.50	3.38
K	0.01	0.00	0.37	0.01	0.00	0.02	0.01	0.00	0.01	0.01	0.00	0.01	0.00
Ab	97.50	97.70	84.20	97.20	97.80	83.50	96.20	97.40	97.50	96.00	96.50	97.00	93.10
An	2.20	2.10	4.00	2.50	2.20	15.90	3.60	2.60	2.20	3.80	3.50	2.70	6.90
Or	0.30	0.10	11.80	0.30	0.00	0.60	0.20	0.00	0.30	0.20	0.00	0.30	0.00

Appendix B - Microprobe analyses of plagioclase continued

Sample	075a-1-12	078-2-1	078-2-4	078-2-10	161d-3c	161d-3r	161d-4c	161d-12	173-1-7	173-1-8	173-1-12	199-1-10	205-1-1
SiO_2	68.15	66.72	68.76	66.84	65.94	66.29	66.52	54.6	62.12	62.58	62.05	59.52	67.05
TiO_2	0.02	0	0.02	0	0	0	0	0.06	0.02	0.02	0	0	0.08
Al_2O_3	20.74	20.43	20.16	21.22	21.26	21.47	21.1	23.72	24.42	24.42	23.93	25.97	20.42
FeO	0.02	0	0	0.12	0.07	0	0	0.03	0.19	0.1	0.04	0	0.06
MnO	0.04	0	0	0.07	0	0	0.03	0	0	0	0.1	0.07	0.07
MgO	0.05	0.04	0.18	0.04	0.03	0.05	0	0.09	0.07	0	0	0.09	0
CaO	1.11	1.03	0.41	1.65	2.23	2.32	1.82	12.49	5.44	5.48	5.29	7.59	1.16
Na_2O	10.21	11.36	10.18	10.87	10.2	10.12	9.89	8.28	8.66	8.71	8.47	7.04	11.28
K_2O	0.01	0.01	0.02	0.06	0.16	0.17	0.16	0.03	0.02	0.03	0.06	0.06	0.06
NiO	0.03	0.08	0.06	0.04	0.16	0	0.03	0.01	0.12	0.08	0.08	0.1	0
P_2O_5	0.15	0.06	0.08	0.2	0.06	0.14	0.11	0.07	0	0.03	0.03	0	0.04
BaO	0	0.15	0	0.03	0.08	0.07	0	0	0.02	0	0.11	0	0
La_2O_3	0	0	0	0.02	0.08	0.02	0.01	0	0	0	0.03	0.08	0
Cr_2O_3	0	0.06	0.06	0	0	0.06	0	0	0.15	0.02	0.04	0	0.06
Total	100.57	99.96	99.94	101.17	100.26	100.72	99.68	99.38	101.32	101.51	100.25	100.51	100.33
Structural Formulae (based on 32 oxygen)													
Si	11.82	11.73	11.95	11.61	11.58	11.56	11.68	10.10	10.90	10.94	10.99	10.57	11.74
Al	4.24	4.23	4.13	4.34	4.40	4.41	4.36	5.17	5.05	5.03	4.99	5.43	4.21
Ti	0.00	0.00	0.00	0.00	0.00	0.00	0.00	0.01	0.00	0.00	0.00	0.00	0.01
Fe^{3+}	0.00	0.00	0.00	0.02	0.01	0.00	0.00	0.01	0.03	0.02	0.01	0.00	0.01
Mn	0.01	0.00	0.00	0.01	0.00	0.00	0.00	0.00	0.00	0.00	0.02	0.01	0.01
Mg	0.01	0.01	0.05	0.01	0.01	0.01	0.00	0.03	0.02	0.00	0.00	0.02	0.00
Ca	0.21	0.19	0.08	0.31	0.42	0.43	0.34	2.48	1.02	1.03	1.00	1.44	0.22
Na	3.43	3.87	3.43	3.66	3.47	3.42	3.37	2.97	2.95	2.95	2.91	2.42	3.83
K	0.00	0.00	0.00	0.01	0.04	0.04	0.04	0.01	0.00	0.01	0.01	0.01	0.01
Ab	94.30	95.20	97.70	92.00	88.40	87.90	89.90	54.50	74.20	74.10	74.10	62.40	94.30
An	5.70	4.80	2.20	7.70	10.70	11.10	9.10	45.40	25.70	25.80	25.60	37.20	5.40
Or	0.10	0.00	0.10	0.30	0.90	1.00	1.00	0.10	0.10	0.20	0.40	0.40	0.30

Appendix B - Microprobe analyses of plagioclase continued

Sample	205-1-3	205-1-6	205-1-10	205-1-12	205-1-13
SiO_2	67.78	68.17	66.69	67.47	67.82
TiO_2	0	0.07	0	0.05	0.03
Al_2O_3	20.27	20.05	21.24	20.74	20.19
FeO	0.07	0.31	0.21	0.2	0.14
MnO	0.03	0	0	0	0.01
MgO	0.01	0	0.06	0.08	0.06
CaO	0.52	0.51	1.84	1.14	0.67
Na_2O	11.58	11.43	10.46	10	11.33
K_2O	0.03	0	0.02	0	0
NiO	0.02	0.24	0.03	0.02	0.02
P_2O_5	0.09	0.11	0.15	0.02	0.16
BaO	0.28	0	0.09	0.09	0
La_2O_3	0.17	0	0.04	0	0
Cr_2O_3	0	0.01	0	0.07	0.07
Total	100.86	100.9	100.83	99.91	100.49
Structural Formulae (based on 32 oxygen)					
Si	11.81	11.84	11.62	11.79	11.81
Al	4.16	4.10	4.36	4.27	4.14
Ti	0.00	0.01	0.00	0.01	0.00
Fe^{3+}	0.01	0.05	0.03	0.03	0.02
Mn	0.00	0.00	0.00	0.00	0.00
Mg	0.00	0.00	0.02	0.02	0.02
Ca	0.10	0.10	0.34	0.21	0.13
Na	3.91	3.85	3.53	3.39	3.83
K	0.01	0.00	0.00	0.00	0.00
Ab	97.40	97.60	91.10	94.10	96.80
An	2.40	2.40	8.80	5.90	3.20
Or	0.20	0.00	0.10	0.00	0.00

Appendix B - Microprobe analysis of staurolite

Sample	175-1-3	175-1-4
SiO_2	27.71	27.33
TiO_2	0.34	0.34
Al_2O_3	55.54	55.89
FeO	12.00	12.38
MnO	0.25	0.24
MgO	1.14	1.14
CaO	0.00	0.01
Na_2O	0.31	0.29
K_2O	0.00	0.03
Cr_2O_3	0.06	0.00
NiO	0.20	0.11
P_2O_5	0.09	0.00
Cl	0.00	0.00
BaO	0.00	0.00
SrO	0.00	0.00
ZrO_2	0.00	0.09
La_2O_3	0.02	0.00
Total	97.66	97.84

APPENDIX C ANALYTICAL METHODS FOR X-RAY FLUORESCENCE ANALYSIS

Samples were analyzed with the Philips PW2400 X-ray spectrometer with a Philips PW2510 102-position sample changer at the Regional Geochemical Centre, St. Mary's University, Halifax, Nova Scotia. Major element oxides and some trace elements (V, Cr, Sc, Ce, Ba, Pb, Ni, Zn, Ga, and Co) were measured on fused beads. Other trace elements were measured on pressed powder pellets. Loss on Ignition (LOI) was measured by calculating the diference in sample weight before and after heating to 300^0 C for 90 minutes and 1000^0C for 150 minutes. The relative accuracy for SiO_2 is about 0.5%. The relative accuracy for other major elements measured as oxides is about 0.01% and is about 5% for trace elements. Detection limits for TiO_2, MnO, and Na_2O are 0.005%, 0.003% and 0.02%, respectively. All other major oxides have a limit of detection of about 0.01%. Detection limits for trace elements are 1 ppm, except for Sc (16 ppm), V (12 ppm), Cr (12 ppm), Ba (39 ppm) and Ce (66 ppm).

Appendix C - Major and trace element geochemistry

SAMPLE	LAM002-1	LAM004-1	LAM009-1	LAM071A-1	LAM072A-1
Major elements (wt.%)					
SiO_2	47.77	71.17	61.16	48.15	45.26
TiO_2	2.55	0.36	0.87	1.98	4.06
Al_2O_3	15.06	14.30	18.29	11.34	15.35
Fe_2O_3	14.34	2.85	6.45	12.97	18.11
MnO	0.20	0.04	0.06	0.20	0.23
MgO	7.55	0.50	1.13	13.57	6.26
CaO	4.64	0.96	1.52	7.19	7.03
Na_2O	3.50	3.03	8.71	0.93	2.69
K_2O	1.82	6.43	1.40	0.32	0.29
P_2O_5	0.40	0.09	0.27	0.27	0.56
LOI	0.89	0.60	0.29	3.49	1.42
Trace elements (ppm)					
Sc	19	34	19	10	25
V	282	22	65	259	447
Cr	283	0	0	601	51
Co	69	36	30	81	78
Zr	205	254	771	139	264
Ba	326	396	14	0	181
La	30	40	83	13	25
Ce	44	107	103	17	71
Nd	32	24	70	7	49
Ni	142	0	0	267	30
Cu	16	6	47	46	26
Zn	105	64	57	96	152
Ga	18	26	23	16	27
Rb	37	235	57	20	10
Sr	378	143	284	134	564
Y	33	45	34	26	39
Nb	20	29	93	15	20
Sn	2	5	7	3	2
Pb	10	28	16	4	16
Th	1	21	14	0	1
U	2	4	4	2	2

Appendix C - Major and trace element geochemistry continued

SAMPLE	LAM075-4	LAM075A-1	LAM078-2	LAM079-1	LAM080-1
Major elements (wt.%)					
SiO2	46.58	45.55	52.40	46.18	48.03
TiO2	2.91	3.48	2.33	3.43	3.49
Al2O3	15.45	15.55	19.04	14.29	13.51
Fe2O3	15.14	16.97	11.00	17.94	15.94
MnO	0.21	0.23	0.14	0.30	0.21
MgO	6.49	5.88	2.81	3.66	5.23
CaO	10.51	6.34	4.58	8.95	10.81
Na2O	2.35	4.32	6.56	4.18	2.39
K2O	0.30	0.38	0.78	0.44	0.44
P2O5	0.36	0.49	0.54	1.07	0.47
LOI	0.82	1.10	1.00	0.10	0.29
Trace elements (ppm)					
Sc	0	43	31	0	17
V	346	362	215	218	411
Cr	72	70	14	0	78
Co	69	83	50	74	66
Zr	201	193	361	327	203
Ba	0	40	140	0	0
La	23	33	41	23	19
Ce	50	102	137	148	10
Nd	22	22	54	48	34
Ni	75	60	15	0	50
Cu	49	47	72	3	39
Zn	112	109	131	165	122
Ga	24	22	23	31	18
Rb	11	12	29	8	10
Sr	487	480	670	418	464
Y	33	37	33	46	35
Nb	17	19	39	29	17
Sn	2	2	0	3	3
Pb	4	0	7	2	9
Th	0	1	5	1	1
U	2	2	2	2	2

Appendix C - Major and trace element geochemistry continued

SAMPLE	LAM081-1	LAM084-1	LAM085-3	LAM094-1	LAM095-1
Major elements (wt.%)					
SiO2	47.49	47.32	46.65	47.99	46.29
TiO2	2.03	3.77	3.65	3.12	3.59
Al2O3	16.18	15.50	16.47	14.77	16.49
Fe2O3	10.98	15.38	15.56	15.71	14.07
MnO	0.14	0.18	0.22	0.23	0.20
MgO	7.51	5.11	4.31	3.90	4.97
CaO	11.18	7.16	6.72	6.89	9.35
Na2O	3.19	3.00	3.38	4.83	3.46
K2O	0.45	1.79	0.95	1.62	0.61
P2O5	0.23	0.67	0.76	1.48	0.73
LOI	1.92	0.91	2.48	0.49	0.30
Trace elements (ppm)					
Sc	15	1	21	17	30
V	253	304	270	199	297
Cr	370	0	0	0	0
Co	56	63	63	58	57
Zr	152	343	353	487	327
Ba	187	659	297	1543	125
La	21	34	41	60	48
Ce	36	72	118	105	51
Nd	10	36	37	62	44
Ni	140	27	0	0	11
Cu	74	21	31	12	4
Zn	87	146	168	184	136
Ga	24	26	31	29	31
Rb	16	29	17	20	14
Sr	570	872	841	1548	882
Y	23	34	34	38	31
Nb	14	30	32	35	24
Sn	3	2	3	3	2
Pb	0	2	11	12	1
Th	0	1	1	3	0
U	2	2	2	2	3

Appendix C - Major and trace element geochemistry continued

SAMPLE	LAM106-1	LAM131-1	LAM133-1	LAM147-1	LAM148-1
Major elements (wt.%)					
SiO2	42.56	48.02	46.04	44.15	43.01
TiO2	3.84	2.44	3.98	3.07	1.14
Al2O3	17.94	15.82	15.30	11.87	11.52
Fe2O3	17.51	13.98	16.64	15.85	15.77
MnO	0.50	0.21	0.25	0.18	0.21
MgO	4.65	6.96	4.72	11.52	15.96
CaO	9.34	9.27	6.04	8.55	7.13
Na2O	0.88	0.89	4.42	2.39	1.48
K2O	1.13	1.45	1.16	0.74	0.09
P2O5	0.99	0.33	0.70	0.48	0.10
LOI	1.82	1.31	1.76	1.08	4.01
Trace elements (ppm)					
Sc	11	18	35	27	5
V	270	298	339	292	180
Cr	0	82	3	361	805
Co	66	64	68	84	101
Zr	381	155	316	259	55
Ba	0	0	290	114	89
La	72	32	34	15	13
Ce	143	22	130	124	0
Nd	61	27	53	41	4
Ni	10	72	16	344	618
Cu	1	2	13	49	28
Zn	268	118	168	140	146
Ga	35	21	31	22	19
Rb	21	30	20	20	10
Sr	200	117	560	459	88
Y	42	32	35	33	25
Nb	35	16	31	22	8
Sn	3	6	2	4	2
Pb	5	4	2	5	3
Th	2	0	1	1	0
U	2	2	3	2	2

Appendix C - Major and trace element geochemistry continued

SAMPLE	LAM153-2	LAM157-1	LAM158-1	LAM159-1	LAM160-1
Major elements (wt.%)					
SiO2	46.77	77.44	77.48	76.84	75.56
TiO2	3.53	0.13	0.15	0.13	0.22
Al2O3	15.23	12.40	12.50	12.06	13.22
Fe2O3	15.18	1.21	1.37	1.36	1.71
MnO	0.20	0.02	0.02	0.03	0.01
MgO	5.39	0.05	0.06	0.05	0.12
CaO	9.38	0.29	0.36	0.31	0.53
Na2O	3.36	3.03	2.92	2.72	3.18
K2O	0.19	5.43	5.58	5.52	5.32
P2O5	0.67	0.08	0.05	0.03	0.12
LOI	0.10	0.60	0.58	0.38	0.47
Trace elements (ppm)					
Sc	0	34	37	37	49
V	364	8	1	4	1
Cr	32	0	0	0	0
Co	65	44	47	57	38
Zr	326	78	117	95	215
Ba	30	260	127	0	593
La	35	0	15	2	43
Ce	75	13	30	36	360
Nd	43	22	3	15	42
Ni	35	0	0	0	0
Cu	48	3	4	7	5
Zn	134	52	60	61	50
Ga	24	28	29	28	27
Rb	9	233	253	277	248
Sr	1097	34	36	19	62
Y	31	42	43	39	52
Nb	24	52	45	50	49
Sn	3	12	9	11	10
Pb	12	30	37	33	27
Th	2	9	13	11	19
U	2	2	2	1	3

Appendix C - Major and trace element geochemistry continued

SAMPLE	LAM161-1	LAM161A-1	LAM161B-1	LAM161C-1
Major elements (wt.%)				
SiO2	76.83	76.86	76.94	76.16
TiO2	0.15	0.14	0.14	0.14
Al2O3	12.57	12.56	12.46	12.66
Fe2O3	1.45	1.37	1.42	1.40
MnO	0.03	0.03	0.04	0.03
MgO	0.07	0.08	0.06	0.06
CaO	0.48	0.54	0.52	0.53
Na2O	3.09	3.09	3.27	3.23
K2O	5.37	5.40	4.86	5.21
P2O5	0.05	0.05	0.05	0.05
LOI	0.18	0.56	0.70	0.27
Trace elements (ppm)				
Sc	42	15	36	49
V	10	0	12	5
Cr	0	0	0	0
Co	51	49	51	39
Zr	127	117	116	117
Ba	281	235	361	190
La	20	41	18	39
Ce	96	95	30	72
Nd	42	35	29	26
Ni	0	0	0	10
Cu	3	3	3	0
Zn	50	57	65	56
Ga	24	25	24	26
Rb	262	264	275	275
Sr	42	37	35	34
Y	54	52	50	54
Nb	46	42	49	45
Sn	13	15	25	13
Pb	27	28	23	21
Th	19	19	18	19
U	3	3	2	2

Appendix C - Major and traceelement geochemistry continued

SAMPLE	LAM161D-1	LAM161E-1	LAM162-1	LAM165-1	LAM170-1
Major elements (wt.%)					
SiO2	76.46	75.57	74.78	49.71	46.33
TiO2	0.17	0.15	0.21	2.74	1.92
Al2O3	12.53	12.47	13.03	11.64	16.09
Fe2O3	1.65	1.42	1.82	11.03	14.45
MnO	0.03	0.03	0.03	0.21	0.20
MgO	0.08	0.08	0.15	5.42	7.03
CaO	0.56	0.55	0.55	12.51	10.07
Na2O	3.03	3.02	3.08	2.76	2.53
K2O	5.49	5.39	5.48	0.13	0.18
P2O5	0.05	0.05	0.08	0.48	0.25
LOI	0.34	0.27	0.20	3.01	0.56
Trace elements (ppm)					
Sc	22	27	21	0	23
V	0	7	9	290	321
Cr	0	0	0	293	268
Co	24	47	35	52	61
Zr	168	121	199	219	173
Ba	289	365	575	330	0
La	31	31	34	28	19
Ce	57	57	97	31	104
Nd	32	34	37	34	25
Ni	0	0	0	162	50
Cu	1	0	2	17	21
Zn	65	56	63	87	124
Ga	26	27	27	19	25
Rb	247	235	205	12	10
Sr	34	35	71	674	1183
Y	59	54	31	24	29
Nb	49	44	44	34	12
Sn	14	11	10	5	0
Pb	28	22	30	5	21
Th	22	19	16	1	1
U	3	3	3	2	3

Appendix C - Major and trace element geochemistry continued

SAMPLE	LAM172-1	LAM173-1	LAM199-2	LAM202-1	LAM205-1
Major elements (wt.%)					
SiO2	49.64	44.93	50.80	50.12	48.17
TiO2	2.96	3.16	3.23	1.67	2.87
Al2O3	15.68	13.56	13.06	15.16	16.50
Fe2O3	13.68	15.48	18.65	13.97	13.49
MnO	0.19	0.23	0.31	0.19	0.22
MgO	5.44	8.81	3.48	6.45	5.09
CaO	6.95	9.86	8.07	10.44	7.06
Na2O	4.25	2.93	0.82	2.35	4.19
K2O	0.07	0.17	0.90	0.15	0.12
P2O5	0.39	0.42	1.07	0.15	0.38
LOI	0.48	1.01	0.00	0.89	2.53
Trace elements (ppm)					
Sc	36	4	19	0	15
V	353	369	309	307	352
Cr	82	352	11	277	89
Co	61	73	65	66	63
Zr	273	217	353	91	190
Ba	0	0	85	0	0
La	14	26	52	0	20
Ce	62	80	153	20	9
Nd	25	24	38	8	32
Ni	44	215	4	43	5
Cu	38	46	1	33	29
Zn	106	111	182	109	157
Ga	25	22	29	21	27
Rb	12	9	23	10	12
Sr	646	419	111	303	484
Y	32	34	44	29	32
Nb	18	19	22	10	22
Sn	3	3	3	3	2
Pb	12	2	9	13	7
Th	1	0	2	0	0
U	2	2	2	2	2

Appendix C - Major and trace element geochemistry continued

SAMPLE	LAM206-3	LAM207-1
Major elements (wt.%)		
SiO2	45.87	48.71
TiO2	3.88	3.20
Al2O3	15.24	14.15
Fe2O3	15.47	15.40
MnO	0.21	0.21
MgO	6.07	5.93
CaO	9.61	11.32
Na2O	2.89	0.69
K2O	0.19	0.12
P2O5	0.51	0.40
LOI	0.96	1.11
Trace elements (ppm)		
Sc	21	0
V	437	388
Cr	138	72
Co	67	66
Zr	316	166
Ba	0	0
La	35	23
Ce	127	20
Nd	30	23
Ni	53	56
Cu	21	31
Zn	120	124
Ga	24	25
Rb	10	9
Sr	647	225
Y	38	34
Nb	22	16
Sn	4	2
Pb	12	17
Th	1	1
U	2	2

APPENDIX D ANALYTICAL METHODS FOR ICP-MS ANALYSIS

Samples were analyzed by inductively coupled plasma-mass spectrometry at Memorial University, St. John's Newfoundland using a pure quartz reagent blank and one or more certified reference standards such as gabbro MRG-1 (CCRMP) and basalt BR-688 (NIST SM 688). Analytical procedure for rare earth elements includes (1) sintering of a 0.2 g samples aliquot with sodium peroxide, (2) dissolution of the sinter cake, separation and dissolution of precipitate, and (3) analysis by ICP-MS using the method of internal standardization to correct for matrix and drift effects. Elements Zr, Nb, Ba, Hf, and Ta were analyzed by the digestion procedure and results are semi-quantitative.

Appendix D -ICP-MS Chemical data

Sample	LAM002-1	LAM004-1	LAM075A-1	LAM085-3	LAM131-1	LAM161D-1	LAM205-1
ppm							
Y	20.57	33.82	28.64	26.65	19.96	47.23	26.19
Zr	217.17	229.61	263.16	367.16	181.44	136.08	182.16
Nb	35.62	29.79	39.02	61.64	27.70	14.91	33.74
Ba	288.75	439.99	134.59	394.19	36.26	200.05	21.94
La	22.09	41.95	23.43	39.06	23.71	35.54	22.14
Ce	49.29	82.93	54.49	86.68	50.73	77.00	48.61
Pr	6.26	9.24	7.21	11.03	6.43	9.19	6.21
Nd	26.31	33.44	31.39	46.07	26.82	33.77	26.85
Sm	5.91	6.55	7.26	9.90	6.03	8.09	6.39
Eu	1.96	0.67	2.39	3.16	2.11	0.61	1.93
Gd	5.60	5.83	7.23	8.71	5.67	7.93	6.46
Tb	0.79	0.93	1.04	1.15	0.78	1.38	0.94
Dy	4.50	6.01	6.10	6.18	4.40	8.88	5.49
Ho	0.85	1.25	1.15	1.08	0.81	1.79	1.05
Er	2.19	3.76	3.03	2.65	2.09	5.05	2.80
Tm	0.29	0.56	0.41	0.34	0.28	0.74	0.38
Yb	1.78	3.58	2.46	1.95	1.64	4.69	2.34
Lu	0.25	0.50	0.35	0.28	0.24	0.65	0.33
Hf	4.99	5.92	6.11	8.08	4.18	4.00	4.54
Ta	1.43	2.72	1.51	2.48	1.33	2.35	1.40
Th	2.36	16.14	2.36	3.55	1.49	14.49	3.11

APPENDIX E ANALYTICAL METHODS FOR SM-ND ISOTOPIC ANALYSIS

All analysis were conducted at Memorial University, St. John's, Newfoundland. Concentration data are standard ICP-MS trace element analyses and are precise to ± 5 % (2σ) (Longerich et al. 1990). $^{147}Sm/^{144}Nd$ ratios were measured directly by high-precision ICP-MS with an estimated precision of ± 5 % (2σ). $^{143}Nd/^{144}Nd$ ratios were determined by thermal ionization mass spectrometry using a VG Micromass 30B spectrometer or Finnegan MAT 262 spectrometer and normalized to a $^{146}Nd/^{144}Nd$ ratio of 0.7219 with an estimated error of ± 0.000030 (2σ). The isotopic data were corrected to LaJolla value of 0.511850. All epsilon Nd values were calculated with respect to CHUR, assuming a present day $^{147}Sm/^{144}Nd$ ratio of 0.196593 and a $^{143}Nd/^{144}Nd$ ratio of 0.512638.

Appendix E - Sm-Nd isotopic analysis

Sample #	LAM004-1
$^{143}Nd/^{144}Nd$	0.512601
2 Sigma	0.000056
$^{147}Sm/^{144}Nd$	0.1593
2 Sigma	0.00002
ug/g Nd	29.00
ug/g Sm	7.48
Age	440
ND (UR)	1.37
T (CHUR)	152.2
ND (dm)	-9.93
T (DM)	1209